2021

Nebulizer-based Systems to Improve Pharmaceutical Aerosol Delivery to the Lungs

Benjamin M. Spence
Virginia Commonwealth University

Nebulizer-based Systems to Improve Pharmaceutical Aerosol Delivery to the Lungs

A dissertation submitted in partial fulfillment of the requirements for the degree of Doctor of Philosophy at Virginia Commonwealth University

By

BENJAMIN MICHAEL SPENCE

Advisory Committee:

Dr. P. Worth Longest

Dr. Michael Hindle

Dr. Laleh Golshahi

Dr. Wei-Ning Wang

Dr. Ram Gupta

Virginia Commonwealth University

Richmond, Virginia, USA

December, 2021

Acknowledgements and Disclosures

I stand on the shoulders of giants who worked in this research laboratory before I arrived. I especially want to acknowledge my long-time mentor and friend, Dr. Landon Holbrook. You have provided helpful guidance and support as I, at times quite literally, follow in your footsteps. I also thank Dr. Dale Farkas and Dr. Karl Bass for the years of daily collaboration and friendly competition.

Research reported in this publication was supported by the National Heart, Lung and Blood Institute of the National Institutes of Health under Award Number R01HL107333. The content is solely the responsibility of the authors and does not necessarily represent the official views of the National Institutes of Health.

Virginia Commonwealth University is currently pursuing patent protection of devices and methods described in this study, which if licensed and commercialized, may provide a future financial interest to the author

Table of Contents

List of Tables

List of Figures

Executive Summary

This document presents research conducted by Benjamin Spence over the past several years at VCU for the Aerosols In Medicine laboratory in the area of mesh nebulized aerosols. It is submitted together with a presentation as the dissertation defense for doctoral degree at Virginia Commonwealth University in the Department of Mechanical and Nuclear Engineering. The first and second chapters set the research goals, provide the context of the research, and present basic subject matter knowledge in the area of mesh nebulized aerosols. Next, Chapters 3-6 cover research and development of medical device technologies for nebulizer-based pharmaceutical aerosol therapies concurrent with continuous flow breathing support. Then, Chapters 7 and 8 present a shift of the nebulizer-based pharmaceutical delivery technologies focused on high efficiency delivery to the lungs during oral inhalation while limiting fugitive aerosol emissions. Subsequently, Chapters 9 and 10 document the technology development, experimentation, and process methodology for improving the spray drying process with mesh nebulizers to produce dry powder pharmaceutical aerosols. Chapter 11 summarizes the knowledge gained and lessons learned to provide a set of scientific outcomes and insight into future projects stemming from this research. Lastly, the final two chapters, presented as appendices, describe additional technical and administrative details related to the preparation, approval, execution, analysis, and archiving of the research projects. At the time of dissertation submission, the findings in many of these chapters have already been published in various forms within the scientific community.

Abstract

Combining vibrating mesh nebulizers with additional new technologies leads to substantial improvements in pharmaceutical aerosol delivery to the lungs across therapeutic administration methods. In this dissertation, streamlined components, aerosol administration synchronization, and/or Excipient Enhanced Growth (EEG) technologies were utilized to develop and test several novel devices and aerosol delivery systems. The first focus of this work was to improve the poor delivery efficiency, e.g., 3.6% of nominal dose (Dugernier et al. 2017), of aerosolized medication administration to adult human subjects concurrent with high flow nasal cannula (HFNC) therapy, a form of continuous-flow non-invasive ventilation (NIV). The developed Low-Volume Mixer-Heater (LVMH) system delivered 71.6% of the nebulized dose to the tracheal filter of adult simulated subjects (Table 4.5) and successfully passed an initial human subject safety study. A second focus created a Heated Dryer System (HDS) from similar concepts as the LVMH but designed for unsteady flows such as direct oral breathing. System aerosol delivery efficiency of approximately 90% to the tracheal filter of a simulated adult subject was found for the HDS (Table 8.2). A jump in high-performance liquid chromatography (HPLC) recovery from ~85% for the LVMH to near total recovery of the nebulized dose for the HDS suggest a limited production of fugitive aerosol emission from the filtered HDS flow pathway (Tables 4.5 and 8.2). A third segment of work focused specifically on the production of EEG powders with vibrating mesh nebulizers for use in dry powder inhalers (DPIs). The developed VCU Small Particle Spray Dryer achieved production of powders with similar performance in a novel DPI as powders produced in a commercial lab-scale spray drying system (Table 9.4). Notably, the developed spray dryer was a fraction of the cost and contained expandable capacity for future experimental needs.

Chapter 1: Specific Aims

The overarching goal of this dissertation is the development of multiple nebulizer-based systems to improve the drug targeting of pharmaceutical aerosols to and within the lungs. In each of the new systems developed, vibrating mesh nebulizers are implemented together with different secondary devices and technologies. In the 1st system, mesh nebulizer technology is used to form a new combination mixer-heater device for the administration of high flow nasal cannula (HFNC) therapy together with the efficient administration of pharmaceutical aerosols, when desired, through the nose-to-lung (N2L) route. This new adult mixer-heater device is optimized for efficient delivery of the aerosol to the lungs using highly realistic *in vitro* airway models. Moreover, testing of device actuation during inhalation is evaluated in human subjects through an Institutional Review Board (IRB)-approved protocol. Supplemental investigations of the adult mixer-heater for combined HFNC therapy and on-demand pharmaceutical aerosol delivery redefine the size and operating parameters for applications with infants. As a 2nd nebulizer-based system, aspects of the adult mixer-heater are translated to create a new Heated Dryer System (HDS) for direct oral inhalation of high-dose nebulized aerosols and expired breath filtration. This new HDS was developed in response to the COVID-19 pandemic, in which HFNC therapy was initially viewed (although now debunked) as a substantial source of virus transmission, and was developed to filter all expired breath. A leading application of the new HDS, highlighted by the COVID-19 pandemic, is the administration of high-dose nebulized antivirals for deep lung delivery. Additionally, isolating the high efficiency delivery from the HFNC therapy support greatly reduces the system setup and operation burden. The 3rd nebulizer-based system involves the use of mesh nebulizers as the aerosol formation units in a modified spray dryer system developed to form highly dispersible powders for application in dry powder

inhalers (DPIs). Key areas of focus are optimization of the spray dryer conditions, in a way that avoids flash evaporation of small droplets; integration of measurement procedures into the production process, in a way that allows comparison between batches; and improvement of the collection mechanism for dried particles, in a way that potentially avoids static charging. The aerosolization performance of these spray-dried powders is then tested in state-of-the-art high efficiency DPIs, and compared with powders from a commercial spray dryer.

The nebulizer-based systems developed in this research combined with pharmaceutical agents (mucus clearing agents, surfactants, steroids, antibiotics, anti-virals, and anti-inflammatories) could eventually be used to treat patients suffering from cystic fibrosis (CF), chronic obstructive pulmonary disease (COPD), asthma, bacterial & viral pneumonias, and a myriad of other diseases. A key enabling technologic method underpinning these systems is the use of excipient enhanced growth (EEG) particles in multiple inhalations methods. The concept of inhalation therapy using EEG particles was developed through a collaboration of the engineering and pharmacy departments at VCU (Hindle and Longest 2012). EEG technology implements small hygroscopic aerosols, for decreased delivery losses, that then grow in size within the humid lungs to target the region of aerosol deposition (Hindle and Longest 2012). Developed systems operate independently or concurrent with gas inhalation therapies to deliver pharmaceuticals at much greater efficiencies than current systems.

Commonly used non-invasive ventilation (NIV) provides breathing support to individuals and presents a convenient opportunity for pharmaceutical treatment. However, integration of pharmaceutical aerosol devices into preexisting NIV systems leads to exceptionally low

efficiency N2L aerosol delivery (Dugernier et al. 2017). Considering design parameter criteria for enhanced pharmaceutical aerosol delivery, such as streamlined components and EEG formulations, during initial design phases has potential to greatly increase N2L delivery efficiency of dual NIV/N2L systems. For example, Golshahi et al (2014) developed a mixer-heater device capable of delivering EEG particles with an emitted dose of 92% of the nebulized dose. Longest et al (2015) developed an inline DPI emitting 1.4 μm particles with an emitted dose, defined as exiting the cannula, of 67% loaded dose during NIV. These systems achieved high estimated lung dose in laboratory benchtop settings; however, multiple barriers exist before these systems can be implemented in a clinical setting. Specifically, the liquid formulation nebulizer-based systems of Golshahi et al (2014) required large breathing volumes to empty the aerosol from the device and lacked mechanisms for real-time synchronization of delivery to unknown inhalation waveforms. The dry powder formulation air-jet DPI systems of Farkas et al (2018) required substantial prescreening of the loaded highly dispersible powders produced with laboratory-scale spray drying equipment to ensure consistent powder aerosolization.

Cross-department collaboration at VCU has and continues to facilitate high efficiency aerosol delivery system development via analytical calculations, computer simulations, experimental validations, and human subject testing. This multi-pronged dissertation project utilizes the VCU Team to develop new vibrating mesh nebulizer (VMN) based delivery platforms and to improve the performance of spray-dried powders produced using a VMN. The three objectives of this dissertation provide four or more unique deliverable components for increased efficiency N2L aerosol delivery. The first component, the low volume mixer heater (LVMH) system, has the distinct ability to provide N2L high efficiency delivery concurrent with

NIV to adults. A high level of collaboration was needed with this device to develop the system from an analytical concept to an experimentally tested and computer optimized 3D printed model; to a system for a human subject safety study; and to a system for a human subject lung deposition study. The LVMH is expected to demonstrate that well engineered systems utilizing EEG aerosols can deliver greater than 70% of nebulized dose to the human lungs during HFNC therapy across different breathing profiles. The second component, the infant low volume mixer heater (iLVMH), is intended to function similarly to the first component but with applications to infants. In future studies, the iLVMH system will be tested in highly realistic *in vitro* models and is expected to demonstrate an order of magnitude increase in estimated lung delivery dosage compared to standard of care mask systems for aerosol delivery to infants. The third component, a Heated Dryer System (HDS) shares some features of the LVMH system but is re-engineered for use as a stand-alone aerosol source for inhalation testing of EEG aerosols. HDS designs will be evaluated with laboratory flow tests and pharmaceutical drug deposition experiments. The fourth component, a Small-Particle Spray Dryer, focuses on production enhancements of dry powder drug formulations for use in DPIs for both adults and infants. Powder generation enhancements by the implemented modifications will be evaluated based on powder output and dosage variability when used with aerosolization devices developed by the VCU Team. In addition to the expected efficiency increases in pharmaceutical aerosol delivery, work completed in this proposal lays the groundwork for additional human subjects testing by the VCU aerosol research group.

Objective 1: Development of a combination device for high flow nasal cannula (HFNC) therapy and high efficiency pharmaceutical aerosol delivery for adults and recommendations on design modifications for infants.

Rationale

High flow nasal cannula (HFNC) therapy is an increasingly popular form of non-invasive ventilation (NIV) for both adult and pediatric patients with respiratory failure or insufficiency (Lee et al. 2013, Ward 2013, Haq et al. 2014, Nishimura 2015). Subjects receiving HFNC therapy often have underlying lung conditions that may benefit from treatment with inhaled pharmaceutical aerosols (Ari and Fink 2012, Hess 2015). As with other forms of NIV, a convenient approach is to add the inhaled medication directly to the inspired gas stream (Dhand 2007, Hess 2015). However, lung delivery efficiency of pharmaceutical aerosols is low during all forms of NIV (Ari and Fink 2012, Dhand 2012), and is reported to be especially low during HFNC therapy (Perry et al. 2013, Hess 2015, Dugernier et al. 2017). For example, Perry et al. (2013) reported ex-cannula aerosol dose was <0.4% of the nominal dose at typical adult HFNC flow rates of 20 L/min (LPM) and above. Positioning a mesh nebulizer upstream of the HFNC humidity unit, Reminiac et al. (2016) achieved 2 to 10% of nebulized dose downstream of an *in vitro* nasal model. It is expected that these low lung delivery efficiencies are due to HFNC systems that were not originally designed for the administration of pharmaceutical aerosols. By developing a combination HFNC and pharmaceutical aerosol device, it is expected that high efficiency lung delivery can be achieved.

Methods

It is proposed that HFNC heat and humidity can be provided by the heated evaporation of isotonic saline droplets from the incorporated aerosol source. The new mixer heater system will therefore employ separate humidity (isotonic saline) and drug mesh nebulizers to provide continuously humidified airflow, while pharmaceutical aerosols are delivered only during a portion of inhalation. This approach avoids the need for temperature cycling in the heating section. Furthermore, a device providing humidity from isotonic saline droplets is currently not available and has the potential to be less irritating to the lungs compared with 100% pure water vapor (Anderson and Smith 1991). Additionally, it is proposed that nebulization of excipient enhanced growth (EEG) formulations (Hindle and Longest 2012) can be synchronized to a subject's inhalation via backpressure sensing of the HFNC airflow. Laboratory development, testing, and validation will occur in both the VCU School of Pharmacy and College of Engineering. Human subject testing for safety, system tolerability, and function will be conducted at the VCU Medical Center with assistance from the VCU Johnson Center for Critical Care and Pulmonary Research.

Tasks

Task 1.1: Design Low Volume Mixer Heater (LVMH) Unit and Control System

- Status: Study complete, presented at ISAM conference, and journal article published (Spence et al. 2019)

Task 1.2: Synchronization Method Development and Optimization

- Status: Study complete, presented at RDD 2020 conference, and published with RDD Online

Task 1.3: Extend LVMH to Human Safety Study at VCU Medical Center

- Status: Study complete, presented at RDD 2020 conference, and published with RDD Online

Task 1.4: Recommendations on Extending to Infant Device

- Status: Studies completed, presented by Team members at RDD 2017, ISAM 2017, and RDD Asia 2018 conferences; published with RDD Online

Outcomes

Work completed in Objective 1 yielded a novel system for administering aerosolized pharmaceuticals via the N2L route while simultaneously evaluating performance of the previously developed EEG aerosol strategy. The delivery system flow path and control system subcomponents provided a platform for future research within this dissertation project and to others on the VCU Team of aerosol researchers. Additionally, patent protection for the system has been granted. Knowledge and techniques developed during synchronization development provide the research group with precision digital tracking for experimental conditions. Completion of a human safety study was a first for this lab group and will be a benefit to future studies.

Objective 2: Development of a patient-inhalation driven nebulizer-based device for high-efficiency EEG aerosol delivery by oral inhalation that can safely be used during the ongoing COVID-19 pandemic.

Rationale

A clinical safety test of the LVMH device of Objective 1 was conducted during autumn 2019 with plans for running additional tests in 2020. However, continuing human subjects experiments presented significant and unexpected challenges due to COVID-19. In March of 2020, VCU ended all human subjects experiments not directly related to COVID-19 research. The large quantity of uncontrolled ventilation gas released during HFNC therapy was initially expected to contribute to the spread of virus laden aerosols. However, these concerns have recently been disproven with the combination of HFNC and a simple filter mask. Although varied throughout the world, recommendations in early 2020 for COVID-19 respiratory therapy were the use of full facemask and filter during Continuous Positive Air Pressure (CPAP) and Noninvasive Positive Pressure Ventilation (NPPV) or the use of Invasive Mechanical Ventilation (IMV) in severe cases. Overall, the LVMH still has high potential for further development and testing. Additionally, the goal of creating a testing platform for EEG aerosol delivery remains. However, this objective pivoted to a high-dose nebulization device that allowed for oral inhalation delivery and filtered exhalation gases. Advantages of this approach include the delivery of medications that require high dosages, that benefit from extended delivery durations, that do not have dry powder formulations, or that are site specific within the lungs.

Methods

Methodology for tracking deposition within the respiratory tract has not shifted; however, the system for production and inhalation must change for continued testing. Therefore, it is proposed that the development of a passive-flow stand-alone nebulized high-efficiency EEG aerosol delivery platform inspired from the LVMH can serve this purpose with multiple application advantages over currently marketed devices. Advantages include: hands-free administration assisting with high dose or long duration medicines, compatibility with early clinical pharmaceuticals which are developed as liquid formulations before spray-dried powders are available, and a more direct path to human subject testing. This system has applications for use with both therapeutics requiring long uniform delivery windows such as antivirals, antibiotics, and lung pH control and therapeutics requiring targeted delivery such as high-cost or side-effect prone medications. One significant difference from the HFNC system is that the interface positioned in the mouth or nose is now creating an airtight seal and enabling the subject to inhale through the device and exhale through a filter. Oral, nasal, and oro-nasal interfaces are envisioned with oral interfaces developed initially in this work.

Tasks

Task 2.1: Design and Evaluation of Heated Dryer System (HDS) Unit and Control System

- Status: Study complete, presented at ISAM conference, and combined journal article of Task 2.1 & Task 2.2 in progress

Task 2.2: In vitro Testing of HDS Interfaces in a MT Model

- Status: Study complete, and combined article of Task 2.1 & 2.2 in progress

Outcomes

Work completed in Objective 2 yielded a novel system for administering aerosolized pharmaceuticals via the oral route while simultaneously evaluating performance of the previously developed EEG aerosol technology. This system could then be used for additional human subjects studies at VCU. Additionally, this system provided development of an advanced heating region that could be incorporated into the LVMH at a later date.

Objective 3: Create an in-house small-particle spray dryer with enhanced instrumentation and control systems.

Rationale

Aerosolizing liquid drug formulations in suspension, colloid, or solution, then evaporating excess liquid to form dry particles (simply called spray drying) was utilized in the previous two objectives. These systems directly administer aerosol to subjects without an intermediate particle storage phase. Spray drying is also one of multiple methods to manufacture powders for administration with dry powder inhalers (DPIs). Pharmaceutical powder production via a spray dyer is applicable to many drug substances and provides adjustable powder characteristics (Weers and Miller 2015). The manipulation and control of process variables generates engineered particles with tunable radial composition, improved bioavailability and efficacy, and enhanced aerosol dispersion characteristics (Vicente et al. 2013). VCU Pharmacy department purchased a Buchi Nano Spray Dryer B-90 (Buchi Laboratory-Techniques, Flawil, Switzerland) system with key features for generating engineered particles including: bottle gas or ambient air source, temperature controlled preheating inlet unifier, multiple spray configurations, two evaporation chamber lengths, and an electrostatic powder collection system. Powder produced in the B-90 was utilized for testing of the VCU Team's laboratory DPIs during development. Computational Fluid Dynamics (CFD) simulations of the B-90, developed by Longest et al (2020), link dryer maximum instantaneous drying rate (κ_{max}) and the dispersibility of powders. It is expected that the process of Quantitative Analysis and Design (QAD) and CFD first applied to inhaler mouthpieces (Longest and Hindle 2009) can also benefit the spray drying process by decreasing κ_{max}. Additionally, experimental observations of collected powders from the B-90 show residual charges on power particles, which likely produce decreased device

performance. Removal of particles from airflows has been heavily researched, and several alternatives to electrostatic collection exist. Perhaps alternative collection methods can achieve powder collection with higher dispersibility. However, implementation of new collection methods requires accurate, repeatable, and controllable spray processes to ensure an isolated comparison of collection devices.

Methods

This large group project utilized QAD for the systematic exploration of new high-performance powders. The B-90 CFD model, developed by Dr. Longest, was redeveloped for additional trials of various internal conditions and simulated top performance powders were recommended for experimental production at pharmacy. Subsequently, the VCU Small Particle Spray Dryer target operational conditions were changed to reproduce these highest performance powders. Re-evaluation of the CFD and experimental data fed into additional rounds of testing and recommendations for the selections of mesh spray heads, intake air properties, and internal conditions.

In order to develop and test new powders, spray drying system knowledge and capabilities of both in-house and external resources were utilized. The newly designed in-house system, developed in the first task of this objective, mimicked the commercial system and provided a testing apparatus for system improvements without removing the commercial system from operation. Once in-house spray drying became operational, it was clear the unified operation monitoring system of the second task was needed for reference back to both the CFD and other spray dried powders. The control system, built upon a collection of existing pre-fabricated electronic components, prioritized functionally over miniaturization, internal error

handling, external troubleshooting, and expandability. Post-production aerosolization testing of powders was conducted in novel high performance DPIs dispensing powder into a Next Generation Impactor (NGI) for Aerodynamic Particle Size Distribution (APSD) information and *in-vitro* infant models for deposition information.

Tasks

Task 3.1: Build Spray Dryer and Test Powder Aerosolization in VCU Devices

- Status: Study complete; separate journal article focused on mesh head selection in-progress

Task 3.2: Quantify and Catalogue Spray Drying Operation Metrics

- Status: Study complete; control system tested and additional operators trained

Outcomes

Objective 3 developed and implemented several components in an in-house small particle spray dryer with the intention of improved aerosol performance in novel DPIs. The process offered the opportunity to learn and work in a similar but uniquely challenging aerosol field while implementing knowledge gained from past research for solving complex problems. The components produced for the system enhanced and augmented the measurement and production capabilities which ultimately led to powder production with increased performance in DPIs.

Chapter 2: Background

2.1 Objective 1: Develop Combination Device

2.1.1 Task 1.1 HFNC Combo Device Background

High Flow Nasal Cannula (HFNC) therapy is an established form of non-invasive ventilation for use in both adults and pediatric patients (Lee et al. 2013, Ward 2013). Multiple commercially available HFNC systems have been developed (See Figure 2.1). The VCU Team of researchers has previously developed and tested a large volume mixer-heater system for high efficiency aerosol delivery while providing options for breath support (Golshahi et al. 2014) (See Figure 2.2). In addition to elevating the inhalation gas from room temperature, the heating region counters the cooling effect of the introduced aerosol. Although other heating methods were explored (Longest et al. 2012), the previously developed large volume mixer-heater system ultimately utilized electrically heated metal plates for the transfer of heat into the flow path. The large volume mixing reservoir allowed continuous nebulization with minimal wall deposition, thereby performing well during steady-state experiments (Golshahi et al. 2013). However, the large reservoir volume resulted in poor emptying on low-normal volume breaths when operated under unsteady air flow environments. This device could be configured and integrated into a system for combined HFNC therapy and high efficiency delivery but was unable to provide true HFNC breathing support on its own. Dual therapy required both large amount of space and large number of individual custom components bordering on impracticality for real-world, non-laboratory applications.

Clinical staff have various commercial options for the application of HFNC therapy including the ability to connect drug nebulizers into the system. Unfortunately, these efforts have been found minimally efficient at depositing the loaded drug for nebulization into the patient's

lungs (Dugernier et al. 2017). Administration of a radiolabeled drug phantom during HFNC therapy was found to have single digit deposition efficiency to the lungs (Dugernier et al. 2017). Commercial HFNC therapy systems were designed for delivery of near body temperature gas at near saturated conditions and not for aerosol drug delivery. Therefore, inefficient delivery of inhaled pharmaceutical aerosols through these systems is not unexpected. Complicating matters, respiratory therapist have multiple placement options depending on the specific nebulizer and HFNC system combination. Even on similar system technologies designed by the same company, such as the Fisher & Paykel MR850 and the AIRVO2 systems, the recommended vibrating mesh nebulizer locations are different. Both these systems and the Vapotherm systems utilize pure water as the humidity source to prevent lung drying at high flows which could be irritating to the lung if an osmolarity imbalance of sodium chloride occurs. Nebulized solutions of hypertonic saline have been implemented for the stimulation of cough and the encouragement of lung secretion movement (Eschenbacher et al. 1984, Lowry et al. 1988). Nebulized isotonic saline has been regularly administered to patients as a carrier fluid for many pharmaceutical aerosols. However, few if any studies have implemented nebulized isotonic saline, the balance between pure water and hypertonic saline, as a long-term humidity source.

2.1.2 Task 1.2 Synchronization Background

Synchronization, as related to this field of study, broadly covers the linking of pharmaceutical aerosol delivery with the inhalation phase of a subject's breathing profile. High efficiency aerosol delivery targeting the lungs requires correctly timing an aerosol reaching the patient interface with continuing inhalation flow (See Figure 2.3). The synchronization of aerosol delivery has been implemented to various extents and effectiveness in DPI's, MDIs, and

nebulizers both directly and with secondary devices (Longest et al. 2019). Depending on design, these units offer synchronization initiated by the user or inherent in the system. Breath enhanced nebulizers have an increased output during inhalation periods; however, they do not stop production during exhalation, which limits their overall efficiency. The I-neb handheld device for oral inhalation has successfully implemented tracking of inhalation and delivering aerosol during an adjusting window of inhalation (Nikander et al. 2010). Matching of aerosol delivery to a breathing pattern generally adds complexity to systems, but has been achieved in both laboratory and commercial devices.

While synchronization has improved respiratory drug delivery, results remain suboptimal. MDI inhalers with mechanical auto-actuators might not fire if insufficient inhalation power is exerted by the user. Newer electronic MDI units have incorporated monitoring and flow sensors to increase synchronization of the dose to inhalation. Synchronization benefits of the Aerogen Ultra valved holding chamber connected to a constantly producing Aerogen Solo mesh nebulizer have been reported when utilizing the system as a face mask aerosol delivery device (Bennett et al. 2019). However, the connection of supplemental oxygen flow directly to the mask, similar in purpose to low-flow nasal cannula oxygen therapy, lowers synchronization benefits (Sarhan et al. 2019). Suboptimal results occur in the VCU large volume mixer-heater, specifically designed for high efficiency delivery, during *in-vitro* situations of low inhalation volume. One area that may especially benefit from aerosol synchronization is administration during HFNC therapy. However, this has not been attempted prior to our work with the large-volume mixer-heater.

HFNC therapy continuously administers airflow at a steady rate; therefore, additional information above and beyond direct HFNC equipment is needed to synchronize aerosol therapy

to inhalation. Standardized information exchange pathways between breath sensing systems and drug delivery systems have not been commercially developed to date. Additionally, knowledge of the HFNC therapy induced travel delay from aerosol production location to user interface must be accounted for in synchronization calculations. Since inhalation effort is not the same for each breath, a well-defined criterion for defining inhalation starting point determination is required for consistently synchronizing delivery. The Low-Volume Mixer-Heater (LVMH) combination device developed in Task 1.1 utilized the lung simulator signaling mechanism for data collection. Initial device prototypes included electromechanical components for sensing the decreased backpressure during the inhalation phase of the breath pattern. These components were limited in continuous adaptation to the overall system pressure, but were able to provide proof of concept. The synchronization work in Task 1.2 tests the function of updated components to achieve reliable breath sensing during system use with simulated subjects breathing a variable pattern during the administration period.

2.1.3 Task 1.3 Human Safety Study Background

Conducting the human subject studies for testing technology developed in the area of high efficiency aerosol delivery during high-flow nasal cannula therapy branched into two phases. These phases were; (i) testing the safety and comfort of the device and (ii) testing the lung delivery efficiency of the therapy device. The first phase establishes testing procedures by evaluating synchronization functionality in a human subject and evaluating the safety and comfort of human subjects receiving isotonic saline sourced humidity during HFNC therapy from the LVMH (See Figure 2.4). Task 1.2 of phase 1 worked exclusively with realistic *in-vitro* airway systems for the development of heating control and aerosol synchronization. The second

phase was intended to establish lung delivery efficiency metrics by adapting standard deposition testing techniques into the device testing routine developed in the first phase. This second phase entailed realistic *in-vitro* testing followed by planned *in-vivo* standard deposition tests involving inhalation of a radiolabeled drug for gamma scintigraphy image capture. In addition to lung deposition, this method would quantify auxiliary deposition in the device and interface.

Planned utilization of SPECT gamma scintigraphy imaging in the second study phase guides the setup of the first phase. The selected gamma emitter, Technetium-99m (^{99m}TC), is routinely utilized in medical diagnostics and has been utilized by multiple aerosol research facilities around the world for deposition studies (Ditcham et al. 2014, Bennett et al. 2015, Dugernier et al. 2017). However, due to the expected increase in lung deposition efficiency, a short delivery duration was planned to ensure quality pictures without undue radiation exposure to the human subjects. Unavoidable radiation exposure occurs during testing; however, exposure dose levels of inhalation studies are generally considered low enough for subjects to participate in multiple studies per year (Corcoran 2015). By nature, inhalation studies utilize relatively low overall activity, plus the expected high delivery efficiency of this system means minimal extraneous deposition outside the lung region. Expected treatment time to achieve required Technetium-99m dose for quality images is approximately five minutes with the main gamma scintigraphy images captured just after the end of drug nebulization.

2.1.4 Task 1.4 Infant Delivery System Background

Efficient nasal delivery of aerosolized drugs to infant populations suffers from similar obstacles that the adult system was designed to overcome. Utilization and investigation of nasal inhalation for aerosol therapy are important for this population of preferential nasal breathers

(DiBlasi 2015). However, delivery efficiency of aerosol to the lungs is reported to be in the low single digit percentage of the nominal dose (El Taoum et al. 2015). Although similar, this low efficiency delivery problem is multi-faceted with additional difficulties over the adult system. In the infant population, small tidal volumes, rapid breaths, high airway resistance, small interface requirements, and ethical concerns have limited the successful implementation of high efficiency systems (DiBlasi 2015). The technological capability of the LVMH to create excipient enhanced growth (EEG) aerosols for direct inhalation opened the door to possible efficiency increases in this population (Spence et al. 2019). Concept testing was carried out by Virginia Commonwealth University's Aerosols In Medicine and Aerosol Research Group (VCU's AIM and ARG labs of the Mechanical and Nuclear Engineering and Pharmaceutics Departments respectively) lab groups to evaluate baseline depositional characteristics utilizing EEG aerosol treatment within an infant experimental setup. This promising work confirmed the expected boost in lung delivery efficiency from using the LVMH technology to treat the infant population. However, this exploratory work glossed over several factors that would be at play outside the controlled laboratory environment. First, the timing of aerosol administration to a specific breath was not able to occur without prior knowledge of the programmed breathing profile. Second, aerosol transport and nasal interface systems were not evaluated for tolerability nor resiliency. Therefore, a need exists for the development of a system suitable for aerosol delivery to infants in an experimental system mimicking the real world to a higher degree. Several members of our lab groups continue to address this need of delivery efficiency in a realistic model through multiple different strategies, approaches, and devices. Project work related to and presented in this dissertation topic involved the creation of devices for testing by collaborators in additional studies.

2.2 Objective 2: HDS Development

2.2.1 Task 2.1 Design of HDS Device and Control Background

The LVMH device developed in Objective 1 successfully underwent a human subjects safety study in preparation to test radiolabeled Excipient Enhanced Growth (EEG) formulations in human subjects (Spence et al. 2020). Unfortunately, these deposition studies were put on hold due to the global pandemic of 2020. However, the demonstrated promise of EEG drug delivery in laboratory studies needed to be evaluated in human subjects. Therefore, a goal was set to develop a stand-alone device for high efficiency drug delivery with highly automated delivery and tracking. This oral inhalation device with filtered outflow was also viewed as applicable to the COVID-19 pandemic for the administration of high dose nebulized medications like antivirals. Additionally, functionality of device was desired to be similar to the LVMH for future support of human studies on EEG aerosol delivery. For the purpose of this study, DPIs are disregarded due to their dissimilarities to the LVMH platform, but they might serve as an alternative EEG testing platform. Evaluation of novel DPIs for EEG delivery are currently under investigation within our lab group (Howe et al. 2021) and Objective 3 covers supporting work for these devices.

Direct testing of nebulizer-based EEG particle forming technology in already successful inhalation devices is not possible, but aspects of these devices can be translated into the new system. For example, the iNeb device's lack of heating and limited control system accessibility hinder direct technology translation into this device. However, the iNeb operation does include adaptation of the nebulization duration which could provide increased efficiency based on errors

seen in Task 1.3 (Nikander et al. 2010, Spence et al. 2020). Integration of one-way valves into the mouthpiece, like the Pari nebulizer delivery systems, would limit the exhalation dead volume of the device. Considering the volume of the LVMH, evaluation of directly integrating the Pari mouthpieces into the newly developed system could prove beneficial in limiting rebreathed air. The LVMH determination of breathing by analysis of system pressure functioned reasonably well for a system with a moving target inherent with the system (Spence et al. 2020). Simplification of the LVMH programing for breath detection and data output structuring could reasonably be applied to the HDS system to achieve delivery goals. Transitioning the active flow driven LVMH device into the passively driven HDS decreases the complexity of breath detection for synchronization; but it adds new complexity of user interface and unsteady aerosol post-production travel timing.

2.2.2 Task 2.2 In-vitro Testing of HDS in MT Model Background

Main design and development of the HDS was successfully completed in Task 2.1 resulting in a device capable of producing one micrometer aerosol for inhalation and tracheal filter deposition efficiency of approximately 85 percent (Spence et al. 2021). The developed device utilized oral delivery; however, it was tested in a model similar to the LVMH tests which lacked a realistic oral cavity (See Figure 2.5). Device outlet characteristics of the HDS matching the LVMH suggest minimal deposition in the extra-thoracic region due to small particle size; therefore, the lack of detail was considered unimportant for initial studies. That model functioned for proof of concept testing, initial data collection, and comparison to the LVMH studies; however, future IRB approval would likely require testing in a highly realistic model of the oral region similar to models already used in oral studies at VCU (Hosseini 2021). Mouthpiece

designs fitting into these new models have not been investigated in respect to use with the HDS; however, mouthpiece design has been heavily investigated for other applications (Hindle and Longest 2013, Dionisio et al. 2018). Previous tasks utilized breathing patterns setup developed assuming ventilation support of HFNC therapy and not passive breathing through a device restricted by filters. Therefore, additional investigation and programming of a situationally relevant and realistic breathing pattern is suggested. Overall, this task's detailed testing of the HDS in airway models fills several holes in the previous studies when considering the specific parameters of the subject inhalation driven aerosol delivery system.

2.3 Objective 3: Spray Dryer

2.3.1 Task 3.1 Build Dryer and Test Powder Aerosolization Background

Laboratory-scale production of spray dried powder is a capability of the VCU research group via commercially developed systems. The Buchi Nano B-90 Spray Dryer consists of multiple components and configurations to support the controlled aerosolization, drying, and collection of liquid solutions. The lab currently implements a specific subset of these components and procedures for the purpose of producing high-performance powders for our devices (See Figure 2.6). For example, the Buchi B-90 was typically configured for open loop air flow with an aspirator, full length drying, and recirculating nebulizer solution during production of powders for DPI testing by Farkas et al. (2018). Characteristics of a high-performance powder often include: low density with surface roughness, uniform primary particle size, high fine particle fraction (FPF) less than 1 μm, FPF less than 5 μm, high dispersibility, and high stability. The commercial system provides batches of high-quality powders for device testing and is

regularly being utilized for experimental powder production. Increased testing capabilities and increased production consistency, along with the high cost of a new commercial system drives the need for creating a secondary laboratory scale production system for the VCU research group.

This task requires developing a system similar to the Buchi B-90 but with higher degree of flexibility for future studies. Future investigations of drying tower inlet conditions, collection methods, and spray head configurations are planned for minimizing variability among individual aerosol droplets. Therefore, the developed system design should prioritize increased modularity and reconfiguration over compact and well presenting layout. Evaporation rate, which were found to be in an extremely broad range, can directly change particle morphology, causing changes in powder characteristics and aerosol deposition (Longest et al. 2020). Future experimental reconfigurations of the inlet airflow are planned to address evaporation rate spikes. In preparation for these experiments, separation of the heating from the tower inlet unifier is a requirement for this new system. Additionally, multiple sensor and sampling ports are expected to be needed in future systems. Therefore, construction materials should be relatively easy to re-manufacture, adjust, and mount additional components. Device construction documented in this task enables new tools for the group through the redesign of and modifications to the commercial system.

2.3.2 Task 3.2 Quantify and Catalogue Spray Drying Operation Metrics Background

Through the comparison of data collected from experiments and CFD simulations, the importance of accurately accounting for experimental conditions became apparent. In CFD simulations, the spray rate is set to a specific value and remains constant for each particular run

of simulation parameters (Longest et al. 2020). However, in experimentation, spray rates on the Buchi B-90 are adjusted during the run to achieve the specified value. These adjustments occur over long timescales due to the current bulk volumetric measurement method which leads to considerable amounts of wasted time and material. In the Buchi B-90 system, the approximate scales of the nebulized liquid flows are 0.6 mL/min spray rate, 12 mL/min pump flow rate, and a 1000 mL starting bulk volume. Spray rate controls are limited to an electrical signal percentage range and measured as a post-hoc average. However, actual spray rate varies by mesh type, age, cleanliness, mesh size, solution viscosity, temperature, and electrical signal. Experimental logs and experience enable estimation of spray rate before experimental completion, but the values are not immediately known. Developing accurate and quick spray rate operation control is an important factor in the control system design.

Measurement and control of the air parameters used for aerosol droplet evaporation during experiments was also identified as important for further investigations. The complex and two-way-coupled aerosol flow in the upper section of the dryer forms eddies and can lead to flash evaporation of aerosol sections which leave the main central core (Longest et al. 2020). Possible ideas to mitigate flash evaporation include: redesigned mixing at of inlet air and aerosol flows, spray head design changes, and manipulating the drying air water content. Therefore, control and logging of the inlet air water content during the system process is an important aspect of this task. Spray dryer sensors must handle typical operation where air sourced at atmospheric pressure and approximately 22 degrees Celsius is heated to 120 degrees Celsius at around 120 Liters per minute. During initial operational tests, inlet air water content was manually controlled and adjusted throughout the process to provide reasonably stable input condition with constant monitoring.

2.4 Figures

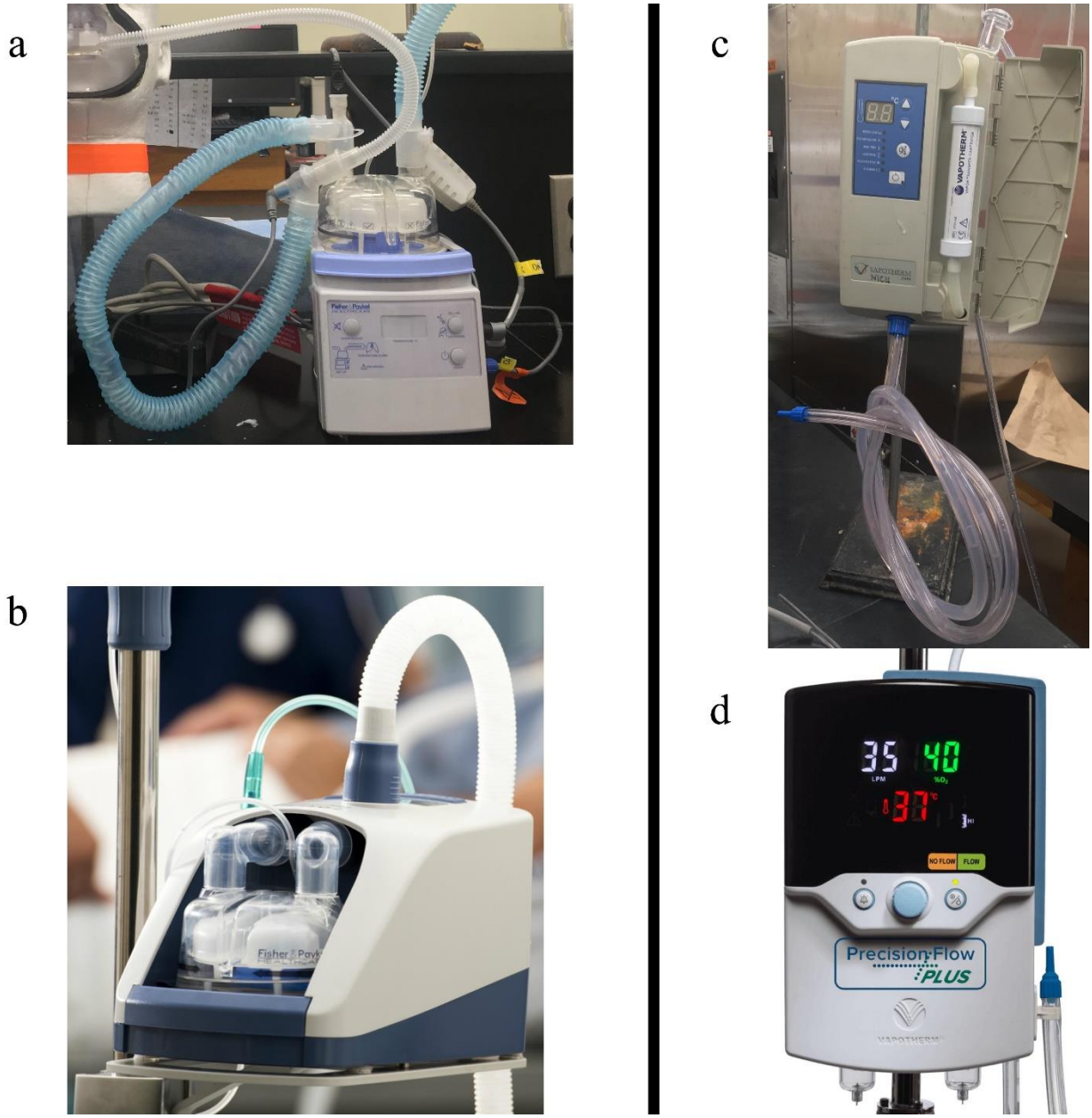

Figure 2.1: High Flow Nasal Cannula (HFNC) Therapy Commercial Systems

The central units of the **(a)** Fisher & Paykel MR850, **(b)** Fisher & Paykel Airvo 2, **(c)** Vapotherm 2000i, and **(d)** Vapotherm Precision Flow systems.

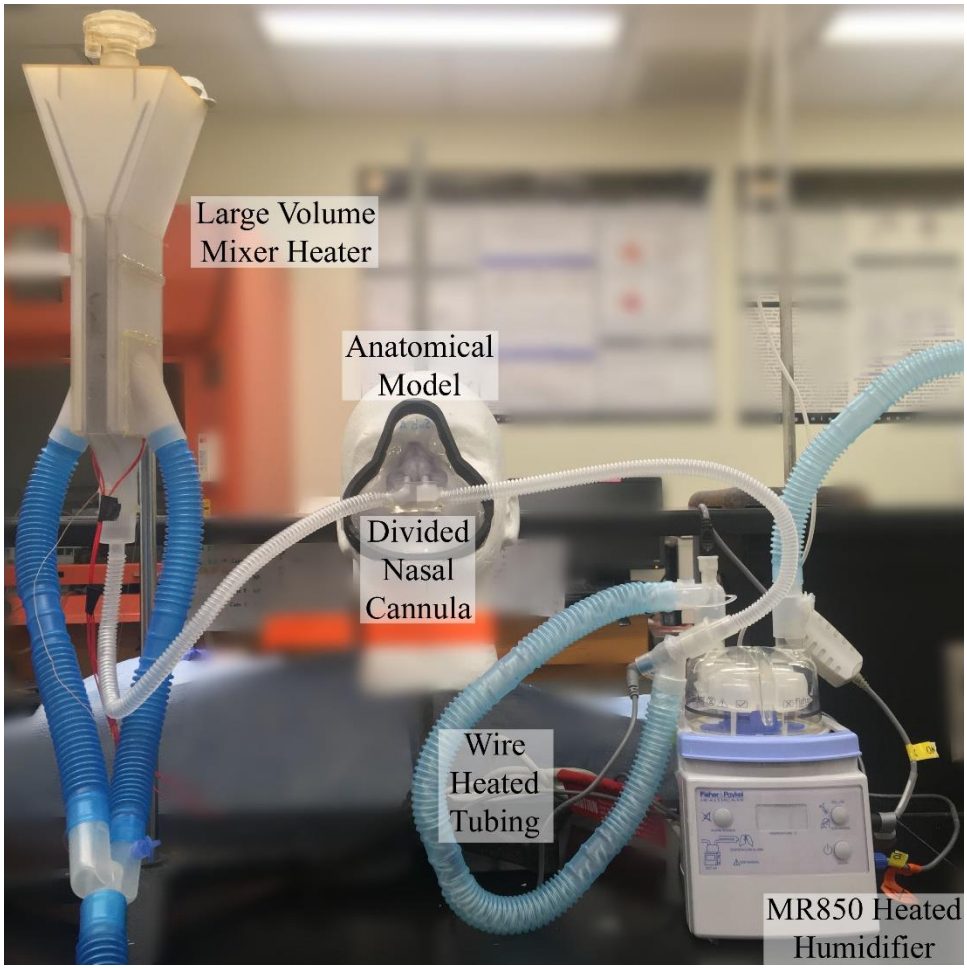

Figure 2.2: Large-Volume Mixer-Heater Unit Previously Developed at VCU

Example system setup for combined HFNC therapy from commercial system and drug delivery using a divided cannula.

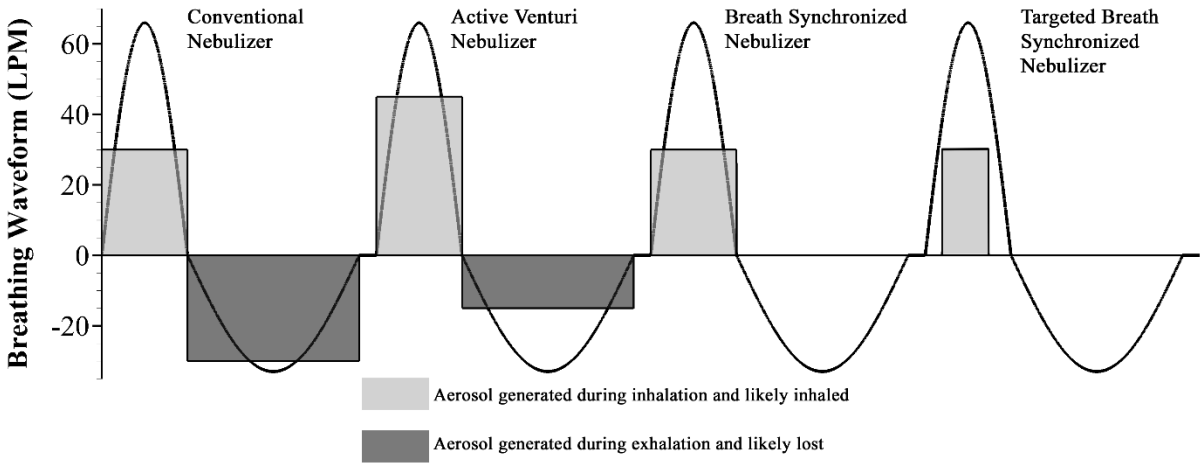

Figure 2.3: Multiple forms of aerosol generation synchronized to a breathing profile.

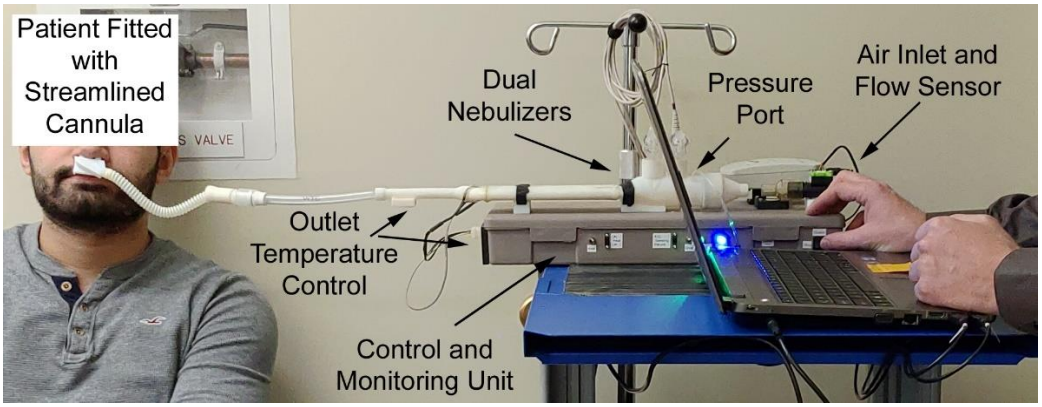

Figure 2.4: Low-Volume Mixer-Heater (LVMH) system developed for human subject safety testing at VCU

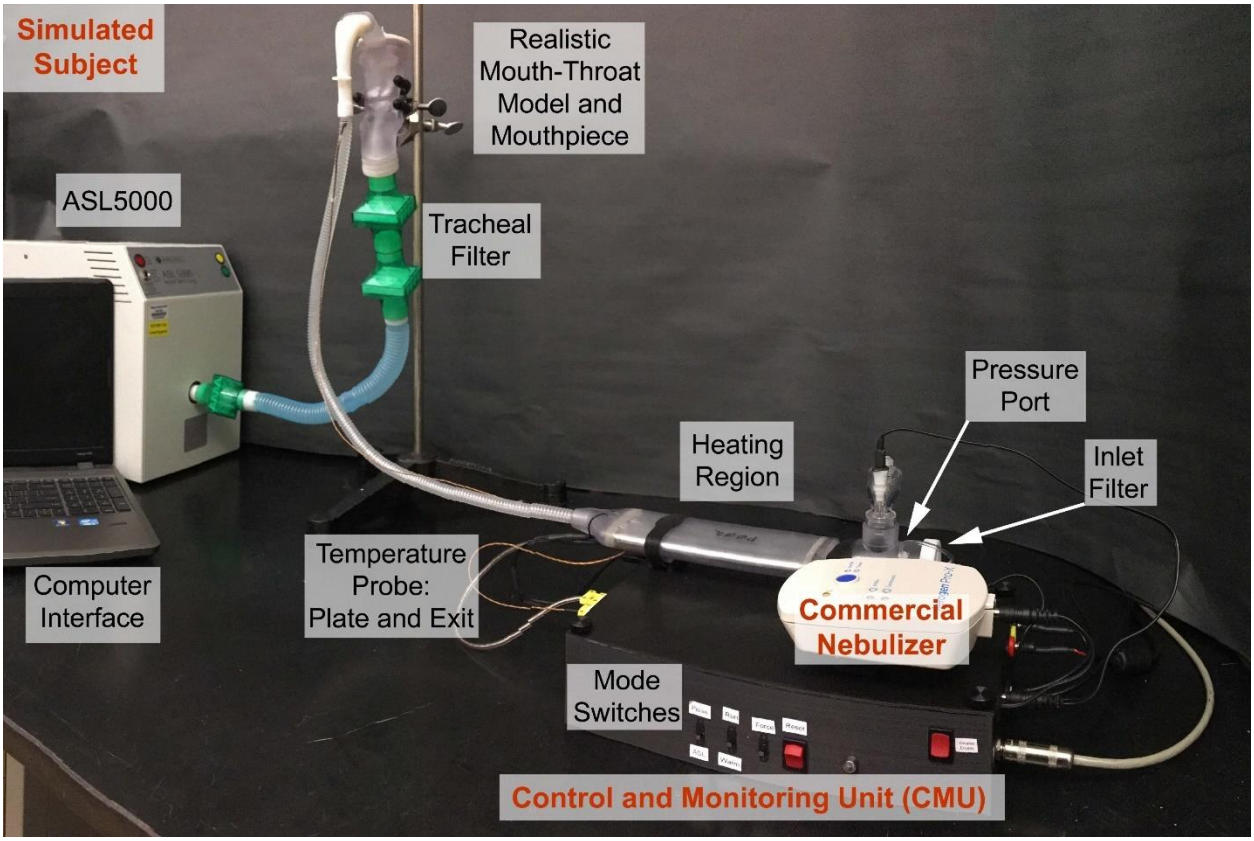

Figure 2.5: Heated Dryer System (HDS) with Basic Elements Labeled

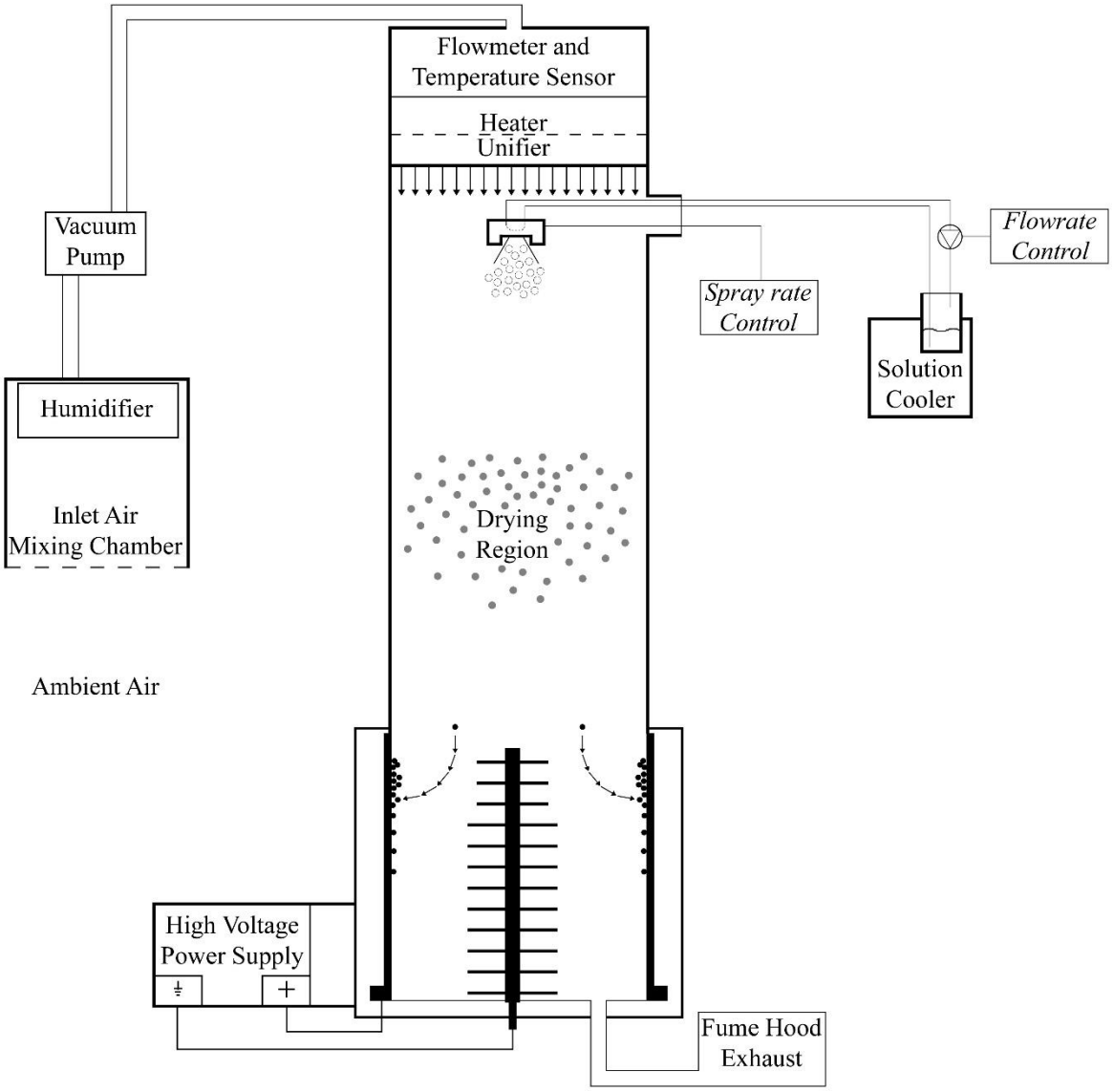

Figure 2.6: Schematic or Rendering of Buchi-B90 with Key Elements

Chapter 3: LVMH Combination Device

3.1 Introduction

High flow nasal cannula (HFNC) therapy is an increasingly popular form of non-invasive ventilation for both adult and pediatric patients with respiratory failure or insufficiency (Lee et al. 2013, Ward 2013, Haq et al. 2014, Nishimura 2015). Subjects receiving HFNC therapy often have underlying lung conditions that may benefit from treatment with inhaled pharmaceutical aerosols (Ari and Fink 2012, Hess 2015). As with other forms of non-invasive ventilation (NIV), a convenient approach is to add the inhaled medication directly to the inspired gas stream (Dhand 2007, Hess 2015). However, lung delivery efficiency of pharmaceutical aerosols is low during all forms of NIV (Ari and Fink 2012, Dhand 2012), and is reported to be especially low during HFNC therapy (Perry et al. 2013, Hess 2015, Dugernier et al. 2017). For example, Perry et al. (2013) reported ex-cannula aerosol dose was <0.4% of the nominal dose at typical adult HFNC flow rates of 20 L/min (LPM) and above. Positioning a mesh nebulizer upstream of the HFNC humidity unit, Reminiac et al. (2016) achieved 2 to 10% of nebulized dose downstream of an *in vitro* nasal model. It is expected that these low lung delivery efficiencies are due to HFNC systems that were not originally designed for the administration of pharmaceutical aerosols.

It is observed that a new system is needed that can provide HFNC therapy together with on-demand pharmaceutical aerosols at a high lung delivery efficiency. By developing a combination HFNC and pharmaceutical aerosol device, it is expected that high efficiency lung delivery of the pharmaceutical aerosol can be achieved. Moreover, it is proposed that humidity can be provided by the evaporation of isotonic saline droplets, which should help preserve the ionic balance of the lungs. The new mixer-heater system will therefore employ separate humidity (isotonic saline) and drug mesh nebulizers to provide continuously humidified airflow, while

pharmaceutical aerosols are delivered only during a portion of inhalation. This approach avoids the need for temperature cycling in the heating section. Furthermore, a device providing humidity from isotonic saline droplets is currently not available and has the potential to be less irritating to the lungs compared with 100% pure water vapor (Anderson and Smith 1991).

The objective of this study is to develop a new device based on vibrating mesh nebulizers that can provide continuously heated and humidified high-flow nasal cannula therapy as well as on-demand pharmaceutical aerosols delivered with high efficiency, using the nose-to-lung route. To develop this device, a concurrent analytical, *in vitro*, and CFD approach (Longest and Hindle 2009, Hindle and Longest 2013) will be used along with 3D printing of rapid prototyped physical models. Based on past experience and analytical analysis, an initial mixer-heater is first proposed that uses a small-volume design and synchronized actuation of the nebulizers instead of actuation of the airflow. This initial design is assessed with analytical calculations, CFD, and *in vitro* analysis. Comparisons of these three methods leads to a validated CFD model that is used to better understand device performance. The validated CFD model and *in vitro* experiments are then used to develop new designs to achieve low aerosol loss within the device, as well as targeted outlet temperature and RH conditions. Using this concurrent analytical, *in vitro*, and CFD approach, the goal of this study is to develop a combination device that achieves a high transmission efficiency of the nebulized aerosol ($\geq$ 90%) when operated cyclically, produces a small particle aerosol (with a mean particle diameter of approximately 1 μm), and can administer the inhaled medication simultaneously with HFNC therapy.

3.2 Materials and Methods

3.2.1 Mixer Heater Design

In this study, a new small-volume mixer-heater design is proposed and evaluated that takes advantage of mesh nebulizer actuation synchronized with the breathing cycle. A primary characteristic of this design is a minimized size of the mixing region, which will improve emptying of the aerosol from the device. This improved emptying will reduce spread of the aerosol bolus over time compared with the larger mixing region that was included in the previous mixer-heater design (Longest et al. 2013). Improved emptying should also minimize the time delay between when the aerosol is generated and when it reaches the patient, thereby enhancing the lung delivery benefits of synchronization. For adults, passive inhalation durations are typically 1.5 s or greater (ICRP 1994). As a target, the mixer-heater should empty within 20% of this inhalation duration, providing an emptying time of approximately 0.3 s. To achieve this emptying time at a HFNC flow rate of 20 LPM (or 333.3 cm^3/s), the system volume including connective outlet tubing should be approximately 100 ml or less. Similarly at 30 LPM (or 500 cm^3/s), an emptying time of 0.3 s can be achieved with a system volume of approximately 150 ml or less. While reducing the system volume appears beneficial from an emptying standpoint, it is noted that the aerosol leaving the mesh nebulizer has observable momentum due to two-way momentum coupling. Therefore, walls of the mixing region should remain sufficiently far from the mesh nebulizer in order to minimize deposition.

A second primary characteristic of the small-volume mixer-heater is the use of two vibrating mesh nebulizers. A first nebulizer provides isotonic saline droplets used to humidify the airflow while maintaining ionic balance in the lungs, and a second nebulizer provides a pharmaceutical aerosol when needed (i.e., on-demand). In a *continuous mode* of operation, the

humidity nebulizer runs continually and the drug nebulizer is actuated when needed during a portion of the inspiration. In *alternating mode* operation, the humidity nebulizer is paused when the drug nebulizer is actuated during a portion of each inhaled breath. While the humidity nebulizer is off, water in the drug formulation is used to humidify the airstream. Based on analytic estimates in the Results, the nebulizers in this study are operated in alternating mode for the aerosol drug delivery experiments described below.

Based on our previous studies (Longest et al. 2012, Longest et al. 2013), it was determined that a heating section with a rectangular (or elliptical) cross section was ideal for warming and evaporating a nebulized aerosol. Tubular heating configurations required unreasonable lengths, resulting in increased volume and aerosol deposition. The rectangular cross section design slows the airflow and simultaneously provides a large surface area for heat transfer. Based on the results of Longest et al. (2013), a channel height (minimum dimension) and length (in the direction of flow) of 0.7 and 12 cm may be acceptable for pharmaceutical vibrating mesh nebulizers with liquid outputs in the range of 0.2 to 0.4 ml/min. However, a longer heating section may be required to ensure full evaporation of the aerosol.

The initial small-volume mixer-heater prototype was based on previous studies, and is shown in Figure 3.1a with a 12 cm long heating section (Design 1). The mixing section was based on the streamlined T-connector developed by Longest et al., (2013) which reduced depositional loss for an Aeroneb Lab mesh nebulizer (Aerogen Limited, Galway, Ireland) from 30.6 to 5.7% when operated at a flow rate of 30 LPM. This design includes a perforated plate near the 1.0 cm ventilation gas inlet to help unify the incoming airflow (but does not require that the aerosol pass through the porous plate). As with the streamlined T-connector, the exit of the mixing region extends along the top of the device, which was found to provide a minor reduction

in depositional loss. The bore diameter of the initial mixing region was 2.4 cm to be consistent with the T-connector of Longest et al. (2013). As described above, the heating section had an elliptical cross-section with a height of 0.7 cm, width of 5 cm, and length of 12 cm and ended with a streamlined taper leading to outlet tubing with a diameter of 0.635 cm. The approximate volume of the device starting at the center of the drug nebulizer was 19 ml for the remainder of the mixing section and 40 ml for the heating section including the taper. Including an outlet tubing length of 50 cm, the total mixer-heater volume traversed by the aerosol is 75.0 ml, which is smaller than the 100 ml target volume.

Additional mixer-heaters considered in this study include an improved design with a circular inlet (Design 2) and a vertical design (Design 3), both with 16 cm heater lengths (Figures 3.1 b and c). As described in the Results, these designs are based on CFD and experimental analysis of the Design 1 case. Characteristics of Design 2 include a uniform inlet velocity profile, larger 3.5 cm internal diameter mixing region and longer (16 cm) heating section. To further reduce mixer-heater depositional loss, Design 3 was also considered, which includes a 2.5 cm by 4.4 cm mixing region and a 90-degree rotation of the heating section. This arrangement is expected to minimize changes in aerosol direction prior to evaporation in the heating section. In contrast, the horizontal mixer-heater is expected to improve spreading of the aerosol over the heating channel.

The mixer-heater designs were produced using 3D printing as shown for Design 1 in Figure 3.2 with Aerogen Solo mesh nebulizers used as the separate humidity and drug sources. Specifically, the rapid prototypes were produced using an Objet®24™ printer (Stratasys Inc, Eden Prairie, MN, USA) and VeroWhite^{TM} (Stratasys Inc.) material. For cases where higher heat

resistance was required, the heating section was rapid prototyped via selective laser sintering in a heat resistant nylon material, DuraForm® PA (3D Systems, Rock Hill, SC, USA).

3.2.2 Nebulizer Control and Heating System

Actuation of the nebulizers and heating of the airstream were managed with a control unit (See Appendix Computer Code: Development Triggering from ASL) Considering nebulizer actuation, a standard Aeroneb Solo driving signal was alternated between the humidity and drug nebulizers with the switching triggered by a 50 ms 5V TTL pulse from the ASL 5000 Breathing Simulator (IngMar Medical, Pittsburgh, PA, USA) at the start of each inhalation to initiate drug nebulization. In this study, the nebulizers were actuated for set time periods to capture any potential transient effects of nebulizer cycling over multiple breaths. To capture a wide range of potential adult breathing conditions (ICRP 1994), the drug nebulizer was actuated for a period of 1.5 s (approximate inhalation phase) followed by a 6 s pause in which the humidity nebulizer was actuated (approximate exhalation phase). As with conventional HFNC therapy, a constant flow rate of 20 or 30 LPM was passed through the system at all times.

The outer shell of the heating section, which is constructed of 3D printed material, contains parallel aluminum heating plates, which are heated by Kapton® (Polyimide Film) heaters (KHLV-105/5 Omega Engineering, Norwalk, CT, USA). The two heating plates are in direct contact with the ventilation gas flow path with the heaters positioned on the back side of the plates next to the 3D printed material, forming an insulating layer. Approximately 1 cm from the end of the lower plate, a K-type thermocouple (SA1-XL-K Omega Engineering) is adhered to the metal and is connected to a temperature controller (TA4 MYPIN, Guangdong, China). The temperature controller regulates the heater power to attain the set-point temperature at the

location of the thermocouple. A majority of the supplied energy goes into evaporating the aerosol due to the high heat of vaporization of water (~16 W) with much less energy required to heat the airstream (~5 W). Because either the humidity or drug nebulizer is active at all times, wide temperature swings in the system are avoided as the drug nebulizer cycles on and off, and the system can rapidly attain the thermocouple set-point temperature in a stable manner. Preliminary experiments indicated that the initial VeroWhite^{TM} material could maintain a thermocouple set-point temperature up to 60 °C, but not higher due to heat damage.

3.2.3 Targeted Delivery Conditions

As described in several recent reviews, HFNC therapy consists of air or blended oxygen delivered at a constant flow rate above 6 LPM and typically greater than 20 LPM in adults (Lee et al. 2013, Ward 2013). All modern HFNC systems heat and humidify the gas to improve patient comfort and reduce thermodynamic burden on the lungs (Ward 2013). While it is well known that heating and humidifying the airstream is required for effective HFNC therapy, the level of heat and humidity has not been objectively assessed. Lindemann et al.(2002) reported human *in vivo* nasal mucosal surface temperatures measured using a rapid response miniature thermocouple at different nasal locations during inspiration and expiration. Surface temperature varied at different locations and with the breathing cycle. The most relevant region for considering gas exposure from a nasal cannula is likely the nasal valve and anterior turbinate area. In these regions, Lindemann et al.(2002) report instantaneous temperature profiles in the range of 28 to 32 °C with mean (time-averaged) values of 30 to 32 °C. Effective HFNC therapy is intended to deliver warmed and humidified gas to the patient. Therefore, a reasonable delivery

temperature consistent with the anterior nasal temperature to maintain patient comfort and provide warmed respiratory gas is assumed to be 32 ± 2 °C for this study.

Little is known regarding appropriate humidity values during forms of NIV in which airflow does not bypass the nose. Recommendations for invasive mechanical ventilation where the nose is bypassed are for 100% RH and 37 °C, which is equivalent to 44 mg H_2O / liter of air (mg/L) (Restrepo and Walsh 2012). However, these delivery conditions are known to cause condensation and liquid pooling, especially in the nasal cannula and cooler (~30 °C) anterior nasal regions (DiBlasi 2015). For NIV flows, ASTM International recommends at minimum 10 mg/L of water (2004). Therefore, a reasonable goal for HFNC humidity is 10 mg/L of water vapor and above. At temperatures of 30, 32 and 34 °C, 10 mg/L of water vapor at a flow rate of 30 LPM produces RH values of 32.8, 29.5, and 26.5 %, respectively. Therefore, our targeted RH range for HFNC therapy is approximately >30%, which provides >10 mg/L of water vapor and is larger than the ASTM International minimum required value. For perspective, 10 mg/L of water vapor delivered at 30 LPM at a room temperature of 21 °C produces a RH of 55%.

In previous studies at steady state operation and with cyclic breathing, the reservoir-based mixer-heater emitted 70 to 80% of the nebulized drug dose out of the cannula (Golshahi et al. 2013, Golshahi et al. 2014). With the advantages of the small-volume design, it is expected the new system can achieve <10% system depositional drug loss. Optimized synchronization should enable >80% ex-cannula drug dose. It is noted mesh nebulizers are expected to lose ~5% of the nebulized dose in the outlet skirt of the nebulizer device, which will not be altered in this study to retain the FDA approved commercial nebulizer. Therefore, the mixer-heater device should produce approximately 5% or less depositional loss (based on the nebulized drug dose) to meet the <10% system depositional loss target.

3.2.4 Analytical Analysis

An analytical analysis was used to calculate exit RH at specific airflow rates and temperatures, as well as nebulizer solution concentration vs. monodisperse dried particle size. Calculation of exit RH at full droplet evaporation requires knowledge of water vapor mass fraction (Y_v) and saturated mass fraction ($Y_{v,sat}$). The water vapor mass fraction was calculated as

$$Y_v = \frac{\dot{m}_l}{\dot{m}_l + \dot{m}_{air}} \qquad \text{(eq 3.1)}$$

where $\dot{m}_l$ and $\dot{m}_{air}$ are the mass flow rates (g/s) of liquid water from the nebulizer and input HFNC ventilation gas, respectively. Inlet ventilation gas was at 0% RH. $Y_{v,sat}$ was determined from the Antoine equation and ideal gas law, as described by Longest et al. (2012). The resulting RH at a specific temperature is then calculated as

$$RH = \frac{Y_v}{Y_{v,sat}} \times 100\% \qquad \text{(eq 3.2)}$$

The fully dried final geometric particle diameter (d_{final}) based on an initial droplet diameter ($d_{initial}$) is predicted as

$$d_{final} = d_{initial}\left(Y_{initial}\frac{\rho_{initial}}{\rho_{final}}\right)^{1/3} \qquad \text{(eq 3.3)}$$

where $Y_{initial}$ is the initial total mass fraction of solutes in the nebulizer solution and ρ represents initial and final densities of the droplet or particle. In this expression, the mass fraction of drug in the solution ($Y_{initial}$) can be converted to an initial w/v ($\bar{\rho}_{initial}$) typically used in preparing formulations as

$$\bar{\rho}_{initial} = Y_{initial} \times \rho_{initial} \qquad \text{(eq 3.4)}$$

where the density is entered in g/cm^3 and is assumed to be 1 g/cm^3 in this study due to the very low initial solute concentration values.

The final density (ρ_{final}) of the dried particle is calculated as

$$\rho_{final} = (m_w + m_{drug} + m_{ex})\left(\frac{\rho_w}{m+\frac{m_{drug}\rho_w}{\rho_{drug}}+\frac{m_{ex}\rho_w}{\rho_{ex}}}\right) \qquad \text{(eq 3.5)}$$

In this expression, m and ρ are the masses and densities of water (w), drug, and hygroscopic excipient (ex). The drug and model excipient considered in this study were albuterol sulfate (AS; ρ_{drug} = 1.340 g/m^3) and sodium chloride (NaCl; ρ_{ex} = 2.160 g/m^3). The nebulized formulation was prepared with 0.5% w/v combined solutes (solids) with a 50:50 NaCl to AS weight ratio. It is noted that the analytically predicted dried particle diameter is not intended to exactly match the CFD predictions or *in vitro* measurements of final size, but instead provides a theoretical minimum size that can be achieved if full drying of the aerosol occurs.

3.2.5 Computational Fluid Dynamics (CFD)

Computational fluid dynamics (CFD) simulations were used to analyze the initial small-volume mixer-heater design and to develop improved versions. For the CFD simulations, a steady state flow rate of 30 LPM through the system was considered, which is consistent with HFNC therapy in adults. At this flow rate, the Reynolds number range within the initial geometry is 300 to 4060, indicating laminar, transitional, and turbulent flows. The simulations captured the flow field, heat transfer from the heating plates, mass transfer of water vapor, droplet transport and evaporation with a hygroscopic solute, and droplet/particle deposition. Droplet evaporation was limited by the amount of available heat and air, making two-way coupled simulations necessary (Finlay 1998, Longest and Hindle 2012). The equations governing mass, momentum and energy conservation including the effects of turbulence and two-way

coupling are available in previous studies (Longest and Xi 2008, Longest and Hindle 2010, Longest et al. 2012). To model turbulence, the Reynolds-averaged two-equation low Reynolds number (LRN) k-ω model with shear flow corrections was implemented (Wilcox 1998).

Droplet and particle transport was simulated using the Lagrangian tracking approach and included terms for discrete element drag, sedimentation and buoyancy (Crowe et al. 1998). Droplet evaporation included the effect of the solute on the droplet surface mass fraction of liquid. A complete description of droplet transport and evaporation is provided in our previous studies (Longest and Hindle 2012, Longest et al. 2012). Previous studies describing two-way coupled simulations of droplet evaporation and condensation include Longest et al. (Longest and Hindle 2011, Longest and Hindle 2012, Longest et al. 2013). In these studies, an iterative approach is used between the flow solver and discrete element solver until convergence of the two-way coupling is achieved. However, in the current system, the use of completely dry inlet gas caused the two-way coupling to become unstable. As a result, the droplet tracking algorithm was updated to limit the evaporation in each CFD control volume to the amount of water vapor the control volume could hold. This approach dramatically improved stability and convergence of the two-way coupling approach. Turbulent dispersion of droplets was predicted using an eddy interaction model. Anisotropic corrections for near-wall turbulence were employed as previously described (Longest et al. 2008, Longest et al. 2012).

The commercial CFD package Fluent 16 (ANSYS, Inc.) was employed to solve the governing equations in all cases considered. User-supplied Fortran and C programs were implemented for the calculation of initial flow and droplet profiles, hygroscopic droplet evaporation, near-wall anisotropic turbulence approximations, near-wall particle interpolation (Longest and Xi 2007), as well as heat and mass sources and sinks during two-way coupling.

CFD best practices were employed including the use of second or higher order discretization, hexahedral grids (Vinchurkar and Longest 2008), and double precision calculations. Grid converged results based on negligible change in the velocity and temperature fields (< 1% relative error) as well as negligible differences in the outlet droplet size (< 5%) and deposition (<5%) were established for meshes consisting of approximately 760,300 to 840,000 hexahedral control volumes for the small-volume mixer-heater geometries.

Inlet velocity profiles, in each of the prototypes considered, were consistent with a 30 LPM steady state flow rate. Initial *in vitro* measurements confirmed that the incoming ventilation gas (medical grade air) entered the mixer-heater at approximately 24 °C and 0% RH. In the mesh nebulizer, droplets are emitted from a 4 mm diameter mesh at a rate of approximately 0.4 ml/min. The resulting high concentration droplet stream affects the momentum of the surrounding gas creating a two-way momentum coupled system. Simulating two-way momentum coupling is extremely time intensive (Longest and Hindle 2009). As a previously developed approximation (Longest and Hindle 2009), a small amount of air was injected at the 4 mm mesh within the nebulizer to approximate this momentum coupling effect. The injected air had a temperature of 21 °C and RH of 100%, which are typical conditions in areas of high droplet concentration and largely eliminate the thermodynamic effect of the injected air. The injected air velocity was based on high speed video images of the aerosol plume exiting the mesh nebulizer, as reported in the Results. The quality of this approximation will be assessed through comparison of the CFD result with *in vitro* experiments for droplet deposition, evaporation and exiting thermodynamic conditions.

Walls of the mixer-heater geometry, not including the heating surfaces, were assumed to be insulated (zero heat flux) and dry (zero water vapor mass flux). The heating surfaces were set

to a constant temperature based on the assumption that the aluminum plates evenly distributed the energy from the film heaters.

3.2.6 In Vitro - General

In vitro experiments were used to evaluate both the initial and improved small-volume mixer-heater designs at flow rates of 20 and 30 LPM. These experiments included determination of outlet temperature and RH during cyclic operation of the device, determination of aerosol depositional drug loss within the device, and determination of the outlet aerosol particle size distribution at the exit of the mixer-heater. A rapid prototyped version of the initial mixer-heater (Design 1) is provided in Figure 3.2, which shows the humidity and drug nebulizers. The drug nebulizer is positioned nearest the heating section to minimize aerosol travel distance (device volume) and therefore maximize delivery of the more valuable medication. In all cases, the drug nebulizer was filled with a 0.25 %w/v albuterol sulfate and 0.25 %w/v sodium chloride in water (0.5%w/v total solute concentration) nebulizer formulation. The humidity nebulizer was filled with isotonic saline (0.9% w/v NaCl in water). The system was typically operated with the humidity nebulizer on for 3 minutes to allow for heater warm-up and stabilization. After the 3 minute warm-up period, the system was operated in alternating mode with the drug nebulizer actuated for 1.5 second increments followed by 6.0 second increments of the humidity nebulizer.

3.2.7 In Vitro – Gas Temperature and RH

Ventilation gas temperature (T) and RH were measured at the outlet of the mixer-heater for the alternating operation mode at flow rates of 20 and 30 LPM. To capture exiting energy and humidity, a custom shell was prototyped to fit around the temperature and humidity probe tip

(HM70 Vaisala, Woburn, Massachusetts) and the shell positioned the probe tip parallel with the outlet of the mixer-heater. Temperature and RH measurements were recorded over a 5 minute period after the initial 3 minute startup period and time-averaged values were calculated.

3.2.8 In Vitro – Depositional Drug Loss and Aerosol Particle Size Distribution

Both the depositional drug loss within the mixer-heater and aerodynamic particle size distribution of drug aerosols at the outlet were determined using the alternating mode at system flow rates of 20 and 30 LPM. The drug deposition study was performed with a low-resistance filter (Pulmoguard II^{TM}, Queset Medical, North Easton, MA, USA) positioned at the exit of the mixer-heater which was connected to a vacuum pump (30 LPM) to allow for total capture of the emitted aerosol for mass balance purposes. The aerodynamic particle size distribution was measured by replacing the filter with an Andersen Cascade Impactor (ACI, Nottingham, United Kingdom) operated at 30 LPM. Particle sizing experiments were performed in a controlled temperature and humidity environment to prevent evaporation or condensation of the emitted aerosol prior to sizing in the impactor. The impactor was placed in a controlled temperature and humidity chamber and allowed to equilibrate prior to each experiment. The environmental conditions were set to the measured equilibrium temperature and humidity of the emitted aerosol (determined above and shown in Table 3.5). In both studies, the drug nebulizer was actuated 60 times to ensure reliable dose collection. The apparatus was dissembled after each run and albuterol sulfate was collected by rinsing the outlet skirt of the drug nebulizer, mixer-heater, and filter or ACI plates with known amounts of deionized water. The drug nebulizer was weighed before and after the experiment to calculate the nominal delivered dose. Samples were analyzed with a validated HPLC method.

3.2.9 In Vitro – Inlet Velocity and Heating Plate Temperature Measurements

Mixer-heater inlet velocity was obtained using a custom-made pitot tube assembly to relate differential pressure to air velocity. A 14-gauge needle, attached to the high-side port of a Sensirion SDP600-500Pa pressure sensor, was placed parallel to the flow direction and was attached to a linear traversing system for positioning. Needle tip positions for the different diameter inlets (2.4 vs. 3.5 cm) were calculated based on a 6-point log-tchebycheff method of air flow testing. The inlet sections for Designs 1 and 2 were printed to the start of the vertical plane at the beginning of the first nebulizer to allow for pitot tube positioning. Pressure readings were taken every 0.016 seconds at each point over an approximate 4 second window before moving to the next location. The average differential pressure readings at each location were used to calculate the local inlet velocity.

During device development, the heating region was thermally imaged and monitored with a Fluke Ti25 handheld infrared camera and Smartview 4.3 analysis software (Everett, WA, USA). Heating units used for thermal imaging had rectangular sections of the 3D printed shell removed for direct imaging of the heater plate metal surface.

3.2.10 Methods Summary

Figure 3.3 provides an overview of the three assessment methods that were employed (analytical, *in vitro*, and CFD) and highlights the characterization metrics from each method. Metrics that were assessed from multiple methods are shown in the overlap regions and are compared in the Results. The three assessment methods were first applied to Design 1 (initial design), which was developed based on insights from previous studies. Knowledge gained from

this analysis was then used to develop Designs 2 and 3, which, in combination with heating modifications to Design 1, were then analyzed using *in vitro* experiments and CFD simulations.

3.3 Results

3.3.1 Preliminary Experimental Data

Preliminary experiments were conducted to collect necessary data for the initial analytical and CFD analyses. Liquid nebulization rates of three new Aeroneb Solo nebulizers, tested three times each, were determined on a gravimetric basis. The nebulizers were filled with 2 ml of a 0.9% w/v NaCl in water solution and operated for 5 minutes. The mean (standard deviation; SD) liquid nebulization rate was 0.4 (0.02) mL/min. The speed of the aerosol plume exiting the Aeroneb Solo device at a position approximately 2 cm from the mesh (just below the nebulizer outlet flange) was determined using high speed video recordings. The aerosol plume velocity was approximately 3.8 m/s; however, establishing variability was difficult due to inherent transient oscillations. The droplet diameter exiting the Aeroneb Solo device was predicted using the ACI operating with near 100% RH air to prevent droplet evaporation, as previously described (Longest et al. 2013). The resulting mean mass median aerodynamic diameter (MMAD) of the initial Aeroneb Solo aerosol was 5.3 (0.1) μm with a geometric standard deviation (GSD) of 2.2 (0.4) μm.

3.3.2 Analytical Analysis

Table 3.1 provides analytically predicted outlet RH values assuming full evaporation of the aerosol and no depositional loss for specified outlet temperatures based on eqs. 3.1 & 3.2. As

described, the target outlet thermodynamic conditions for the mixer-heater are 32 ± 2 °C with RH values greater than 30%. Actuation of one nebulizer is consistent with alternating mode delivery, and actuation of two nebulizers is consistent with continuous mode delivery during the period when both nebulizers are operating. For all cases considered, the targeted RH condition of >30% is achieved (Table 3.1). Lowest RH conditions occur for alternating delivery at 30 LPM, and were in the range of 35% to 50%. Continuous operation at 20 LPM leads to fully saturated conditions (RH = 100%), indicating that the droplets would not completely evaporate. In contrast, RH in the range of 70% to 97% can be achieved with two nebulizers (continuous mode) operating at 30 LPM. As a result, the system is capable of providing a range of RH conditions for patient comfort and can easily attain the minimum requirement of >30% RH. Operating at an outlet temperature of 32 °C in alternating mode appears ideal with measured RH conditions at 58.6% and 39.3%, under flow conditions of 20 and 30 LPM respectively. As a result, analysis in the remainder of this study will focus on alternating mode operation of the nebulizers. Furthermore, a wide range of RH conditions can be achieved with the two-nebulizer design if higher RH values are required in future applications.

Estimates of the fully dried (final) geometric and aerodynamic particle diameters are presented in Table 3.2, based on an initially measured droplet MMAD of 5.3 μm, over a range of drug nebulizer formulation total solute concentrations containing a 50:50 mixture of AS:NaCl. With the 0.5% w/v solute concentration used in the experiments, complete drying of the droplets will result in a final geometric diameter of 0.77 μm, which equates to a final aerodynamic diameter of approximately 1 μm (calculated particle density of 1.650 g/m^3).

3.3.3 CFD Analysis of the Initial Design

CFD simulations of the initial small-volume mixer-heater design are shown in Figure 3.4 for a gas flow rate of 30 LPM and heating plate temperature of 60 °C, which was the maximum allowed for Design 1 constructed in VeroWhite^{TM} material. To match the measured aerosol inlet velocity at the outlet of the nebulizer, a 3.8 m/s inlet velocity with 100% RH air stream was applied to the 4 mm diameter nebulizer mesh. Applying the injected air velocity over the 4 mm mesh resulted in an additional flow of 2.9 LPM through the system, which is <10% of the total flow for the CFD simulation (30 LPM ventilation gas inlet) and is not sufficient to appreciably change the heat transfer characteristics of the downstream region. Midplane and cross sectional contours of velocity and velocity stream traces indicate non-uniform flow in the mixing region that is initiated at the porous inlet plate (Figure 3.4a). Recirculation is observed to occur in the nebulizer body and downstream of the junction between the drug nebulizer and mixer-heater. Temperature contours indicate rapid heating of the inlet 24 °C air; however, the mixer-heater outlet temperature of 29 °C is lower than the targeted value of 32 °C (Figure 3.4b) at the initial maximum plate temperature of 60 °C. Particle trajectories do not sufficiently spread over the heating channel (laterally normal to the direction of flow); however, near full evaporation of the aerosol is achieved with an outlet MMAD of 0.9 μm (Figure 3.4c). Predicted total aerosol particle deposition within the nebulizer skirt and mixer-heater was 20.2% of the nebulized dose, with significant concentrations of deposited drug particles in the transition region at the heater inlet and near the heater outlet (Figure 3.4d). Based on the approximate inlet condition used to capture momentum from the mesh nebulizer, it was not possible to accurately differentiate between deposition in the nebulizer skirt and mixer-heater.

Contours of RH including the effect of the evaporating aerosol on the thermodynamics of the gas stream (with two-way temperature and mass coupling) are shown in Figure 3.5. At 30 LPM, the mass-flow-weighted average RH of 42% at 29 °C is similar to the analytically predicted range in Table 3.1, giving confidence in the CFD model predictions. However, the CFD predicted value is approximately 10% (relative difference) lower than the analytical prediction due to some aerosol depositional loss occurring in the model when unevaporated droplets hit the geometry walls. In the CFD calculations, particles are removed from the flow field at the time of particle-to-wall contact and further contribution of water vapor mass to the flow field is not considered.

3.3.4 In Vitro Analysis of the Initial Prototype

Experimentally measured temperature and RH values for Design 1 with a 60 °C thermocouple temperature are shown in Table 3.3 for alternating mode delivery. Measured RH values at 20 and 30 LPM are approximately 10% (relative difference) below analytically predicted values, likely because of aerosol depositional loss occurring with the experimental system. Agreement between the experimental and CFD predicted values at 30 LPM is excellent for both temperature (28.7 vs. 29.0 °C) and RH (40.3 vs. 42.0%). As observed with the CFD analysis, the desired outlet temperature of 32 °C was not attained in the experiments with a plate thermocouple temperature of 60 °C. With Design 1 and VeroWhite^{TM} material, increasing the thermocouple temperature above 60 °C resulted in heat damage to the system.

Experimentally measured aerosol deposition fractions (as a percent of nebulized dose) and the MMAD exiting the mixer-heater for Design 1 with a 60 °C plate temperature are reported in Table 3.4. Experimental determinations of depositional loss in the mixer-heater at

both flow rates are approximately 11%. Combining the nebulizer and mixer-heater deposition fractions at 20 and 30 LPM, respectively, results in total depositional loss values of 19.3% and 17.3%. In comparison, the combined DF from CFD at 30 LPM was 20.2%, indicating good agreement with the experimental system. As described, depositional drug losses in the mixer-heater are considerably higher than the desired 5% or less target values. Moreover, the experimental measurements also indicate incomplete evaporation of the aerosol, with an exit MMAD of 1.7 μm at 20 LPM and 1.6 μm at 30 LPM. The CFD model underpredicted the exiting aerosol size in comparison with the experiments.

3.3.5 In Vitro Optimization and Design Improvements

Both CFD simulations and experiments identified shortcomings of Design 1 to be low exit temperature and depositional drug loss that was higher than targeted. Depositional losses in the mixing region were associated with non-uniform inlet flow and disturbed flow patterns. It was expected that these flow patterns and associated depositional drug losses could be reduced by (i) unifying the inlet flow and (ii) increasing the mixing region diameter to 3.5 cm.

To improve the inlet flow profile, a flow unifier was developed as described below. In order to verify non-uniform inlet flow as observed with CFD, the pitot tube velocity measurement probe tip was traversed across the inlet porous plate of Design 1 at an offset distance 1.4 cm corresponding to immediately upstream of the humidity nebulizer. Sample velocity traces in Design 1 operated at 30 LPM are shown in Figure 3.6a with maximum and minimum flow rate differing by a ratio of 15.5-to-1. These velocity traces were taken on horizontal and vertical lines (with respect to gravity) on the same axial plane. In order to unify the inlet velocity profile within a compact volume, a 3D mesh of rods was developed (Figure

3.6b). The rods had a diameter of 1.75 mm with an in-plane gap distance of 1.0 mm and were contained centrally on 2 mm thick circular inserts with each insert rotated by 90 degrees. Six circular inserts ending in a filter media insert (Pulmoguard II™, Queset Medical, North Easton, MA) were used to construct the flow unifier. As shown in Figure 3.6a, the flow unifier reduced maximum to minimum inlet velocity difference ratios to a value of 1.9-to-1. As shown in Figure 3.6c the filter smoothed the temporal variation of measured pressure at any given position.

The limitations of low exit temperature and incomplete aerosol evaporation are interconnected and may be the result of poor aerosol spreading over the heating section. To improve heat transfer, the heating section length was increased to 16 cm. Furthermore, it was not clear how the thermocouple temperature differed from the plate temperature field under flow conditions. A thermal image of the heating section for Design 1 with the plate operated at a thermocouple temperature of 60 °C and flow rate of 30 LPM is shown in Figure 3.7. The heated plate is observed to have a highly variable temperature profile with visible temperatures ranging from 59 to 73 °C.

To improve the heating conditions, two approaches were taken. First, the heating section was constructed from a heat resistant nylon material (DuraForm® PA, 3D Systems) that could withstand the higher operating temperatures near the heater strips. Second, the thermocouple temperature was considered to be an adaptable set-point for each mixer-heater to achieve the desired outlet temperature of 32 ± 2 °C. Based on experimental measurements, the thermocouple set-points to achieve steady state outlet temperatures of 32 ± 2 °C for Design 1, Design 2, and Design 3 were 93, 110, 134 °C, respectively for 30 LPM airflow. It is noted that these set-point thermocouple temperatures are related to the position of the thermocouple on the heating plate as

well as design of the heating plates. Therefore, the set point temperatures do not necessarily represent the average plate temperature.

3.3.6 CFD Development and Analysis of the Improved Mixer Heater Design

CFD analysis of the Design 2 mixer-heater is shown in Figure 3.8. Velocity fields and stream traces show significantly less recirculation in the mixing region, as expected, together with enhanced transport toward the lower heating plate (Figure 3.8a). Uniform inlet flow and the increased heating length improve effectiveness of the heating region resulting in an outlet temperature of 32.4 °C for a uniform wall temperature of 55 °C. Surprisingly, Design 2 spreads the aerosol over the entire width of the heating section resulting in full evaporation of the aerosol and an outlet MMAD of 1.0 μm (Figure 3.8c). The associated CFD-predicted total depositional loss (nebulizer and mixer-heater) is 10.6%, which is just above the 10% total target, but could potentially be even lower if deposition in the transition between the mixer and heater regions was reduced (Figure 3.8d).

To further reduce depositional loss, Design 3 was developed as shown in Figure 3.9. A flow unifier was also developed for Design 3 such that the CFD boundary condition was again uniform inlet flow. While streamlines are highly linear, the heat transfer region was less effective with a 60 °C constant wall temperature required to produce an outlet temperature of 31.5 °C (Figure 3.9b). Trajectories illustrate a concentration of the aerosol along the top half of the vertical heating region resulting in incomplete evaporation (MMAD = 1.1; Figure 3.9c). However, the CFD-predicted total depositional loss (nebulizer and mixer-heater) was further decreased to 9.9%.

As described, all three geometries have volumes below the 100 ml target (including 50 cm of outlet tubing). However, trajectories and turbulence result in different mean droplet transit times through the mixer-heater, as shown in Figure 3.10. Each design has a mean transit time of <0.3 s, as desired. Design 2 increases droplet transit time from 0.23 s to 0.27 s. However, due to flow streaming through the middle and top half as well as reduced turbulence, Design 3 has the fastest average droplet transit time (t_{exit} = 0.18 s; Figure 3.10c).

3.3.7 Experimental Analysis of Improved Designs

For experimental testing, the heating sections of all three designs were produced in heat resistant DuraForm^{TM} nylon resin. Set point temperatures of the heating plates in each design were adjusted to achieve an outlet temperature of 32 ± 2 °C after the three-minute warm-up period. Experimentally measured temperature and RH conditions at the outlet of each heater system are reported in Table 3.5. In all cases, the target outlet temperature of 32 ± 2 °C was achieved. Measured RH conditions were consistently lower than predicted with the analytical model. Specifically, at 20 and 30 LPM, measured RH was 40 and 20% below (relative difference) analytically predicted values, respectively. Furthermore, measured RH conditions were similar between 20 and 30 LPM cases. Theoretically, RH conditions at 20 LPM should be larger than at 30 LPM by a factor of 1.5 fold assuming similar depositional losses among the cases. As a final observation, RH values are expected to be similar between designs at a constant flow rate assuming similar depositional losses, as was seen at 30 LPM. However, larger variations in RH values are observed at 20 LPM, with Design 2 having the highest RH and Design 1 having the lowest RH. These unexpected RH findings may arise from difficulty in

measuring water vapor content in a fast moving heated gas stream that also contains a hygroscopic aerosol, which may potentially deposit and collect on the RH probe.

Experimentally determined deposition fractions and MMADs of the aerosols exiting the three systems are reported in Table 3.6. Depositional loss was reasonably consistent between 20 and 30 LPM, allowing for a focus on conditions at the higher flow rate. Considering the mixer-heater, approximately 10% deposition in Design 1 was reduced to ~5% loss with Design 2 and <5% with Design 3. However, in all cases, aerosol deposition in the skirt of the nebulizer was approximately 10%, making it not possible to achieve <10% total deposition in the system. Combining the nebulizer and mixer-heater depositional losses at a flow rate of 30 LPM, as with the CFD calculations, the system with the lowest total loss was Design 2 (11.5%) followed by Design 3 (13.3%) and then Design 1 (20.2%). A similar rank order in total depositional loss is observed at 20 LPM, but with both Design 2 and 3 having a total loss of approximately 13%. In all cases, the measured MMAD was within the range of 1.1-1.3 μm with a very small standard deviation (SD) range (0 – 0.2) (Table 3.6).

3.3.8 Verification of CFD Results in Improved Designs

System depositional losses (nebulizer and mixer-heater) are compared between the experimental measurements and CFD predictions in Figure 3.11 with a targeted 32 °C outlet temperature. In all cases, the CFD predictions fall within +/- 1 SD of the mean experimental values. As described, the CFD model could not capture the distribution of aerosol deposition between the nebulizer and mixer-heater. Nevertheless, the CFD predictions accurately captured mean total depositional loss in the system, which implies accurate predictions of system emitted

dose. In all cases, CFD-predicted MMAD values of approximately 1 μm were close to the measured values of 1.1 – 1.3 μm.

3.4 Discussion

The improved mixer-heater prototypes, Designs 2 and 3, both met the primary challenge of 5% or less depositional loss. Surprisingly, the Aeroneb Solo mesh nebulizer had approximately 10% depositional loss in the nebulizer skirt region, which was higher than previously observed in other systems using the Aeroneb Lab and Pro nebulizers (Golshahi et al. 2013, Longest et al. 2013, Longest et al. 2013, Longest et al. 2014). It is not clear if this increase in depositional loss is due to the nebulizer device or circulating airflow patterns arising from the cross-flow design of the mixing region. At the primary flow rate of interest (30 LPM), Designs 2 and 3 had total depositional losses (nebulizer and mixer-heater) of 11.5 and 13.3% of the nebulized dose, respectively, which is acceptably close to the target of 10% system deposition. Reducing the system flow rate to 20 LPM did not appreciably change performance. Both devices provided adequate evaporation of the aerosol, with Design 3 producing slightly more drying potential than Design 2. However, Design 3 had a substantially faster aerosol clearance time compared with Design 2. As a result, both Designs 2 and 3 performed well with respect to aerosol delivery and should be considered further in future realistic aerosol delivery testing.

Considering device outlet temperature and RH measurements, producing the heating section in heat resistant material enabled all designs to achieve the targeted temperature range of 32 ± 2 °C during aerosol production within the first three minutes of operation. As described, the RH results are less clear. Consistency was observed between RH measurements, analytical

calculations and the CFD predictions for the initial system (Design 1) with a plate temperature of 60 °C. However, measured RH conditions were substantially lower with increased outlet temperatures, did not agree with the analytic calculations, and were not consistent with thermodynamic concepts. It is expected that the current measurement setup may not be able to capture the complete RH of the small diameter (~ 0.7 cm) aerosol and gas stream exiting the mixer heater. Still, measured RH values achieved the 30% target value.

For high efficiency trans-nasal (i.e., nose-to-lung) aerosol delivery, the mixer-heater is intended to evaporate a majority of the liquid from the droplets producing an aerosol size of approximately 1 μm or below. These values were observed to be close to the experimentally measured MMAD values exiting the heater section that were approximately 1.1 – 1.3 μm. Based on the validated CFD predictions of Walenga et al. (2014), at this aerosol size, depositional loss of approximately 7% is expected in a streamlined nasal cannula and average adult nasal airway combined. Similarly, CFD predictions indicate a fully dried aerosol with an MMAD of ~1 μm at the device outlet, which produces <4% depositional loss in the same streamlined nasal cannula and nasal model. The CFD predictions were based on an initial monodisperse aerosol size, but were similar when simulating the full polydisperse initial aerosol distribution. Both the experimental measurements and CFD predictions satisfy the requirement of a small aerosol with relatively little expected depositional loss.

It is noted that the analytical estimates of particle size represent a minimum that can only be achieved if complete drying of the aerosol droplets into particles occurs. Partial evaporation of the aerosol is viewed as a less controlled and likely unstable state that will be associated with low gas stream temperatures, on the order of approximately 21 °C; therefore, full evaporation of the aerosol is desired. However, if partial evaporation of the aerosol is to be predicted

analytically, then more advanced models of evaporation (Finlay 1998, Longest and Hindle 2011) that include two-way coupling are needed.

A primary advantage of using mesh nebulizers to provide both the humidity source and drug aerosol is that one constant temperature heating region can be implemented. This approach simplifies the heating control, better evaporates the aerosol, and helps to maintain a safe targeted inhalation temperature. For example, if the HFNC gas was composed of water vapor and air (or an oxygen mixture), as with all current commercial systems, approximately 5 Watts (W) of power would be required to heat the flow stream from 24 to 32 °C. However, during periods when the drug nebulizer is actuated, a total 21 W of power is required to evaporate the aerosol and heat the flow stream, due to the high latent heat of vaporization of water. To provide this additional power input, the heating section would need to cycle temperature up very quickly during periods of nebulizer actuation to provide 21 W and then cycle temperature back down to provide 5 W. Considering that the drug nebulizer is only actuated for a portion of the inhalation period, which may be under 1 s, the temperature cycling of the heating section becomes difficult to control; and it will likely under evaporate the aerosol at the start of drug nebulization and then overheat the airstream at the end of nebulization. If 21 W of power, which is required when the nebulizer is actuated, is applied to a gas stream of air and water vapor without aerosol droplets, the outlet temperature will become approximately 60 °C (140 °F), which is not safe for direct inhalation. In contrast, the alternating nebulizer design in which both nebulizers deliver the same liquid flow rate and only one nebulizer fires at a time, allows the single heating section to remain at one constant temperature with a constant power input of approximately 21 W.

In developing a high efficiency aerosol administration system, it is also important to consider the drug formulation delivery rate. The Aeroneb Solo mesh nebulizer was found to

nebulize an aqueous low concentration formulation at a rate of approximately 0.4 ml/min. In this study, the drug aerosol nebulizer was only actuated 20% of the time (with the humidity nebulizer actuated the remaining 80% of the time). Considering the estimated 90% aerosol delivery efficiency, the resulting delivery rate of the drug formulation out of the combination device was 0.072 ml/min. During deep inspiration, the drug delivery time may be increased to approximately 50%, resulting in a maximum drug formulation delivery rate (assuming 90% delivery efficiency) of 0.18 ml/min. Increases in the nebulization rate are also allowable by as much as 2-fold considering that the RH of the heated aerosol stream was approximately 30% at a flow rate of 30 LPM.

A number of other studies have evaluated aerosol delivery efficiency during high flow nasal cannula therapy. Using commercial components and Aerogen mesh nebulizers, estimated lung doses are typically either less than approximately 5% for small diameter nasal cannula (Perry et al. 2013, Sunbul et al. 2014, Bennett et al. 2018) or less than approximately 15% for larger diameter adult nasal cannula (Reminiac et al. 2016, Dailey et al. 2018). These previous studies have seldom reported depositional losses in the delivery system separate from lung delivery efficiency. One exception is the *in vivo* study of Dugernier et al. (2017), who considered mesh nebulizer aerosol delivery during HFNC therapy using single-photon emission computed tomography (SPECT) in humans. Total depositional loss in the delivery system was 58.2% of the nebulized dose with only 3.6% reaching the lungs. Assuming small tubing and nasal cannula deposition, based on small particles and streamlined designs (Walenga et al. 2014), the mixer-heater in the current system is approximately 5-6 times more efficient than the commercial system evaluated by Durgernier et al. (2017).

The trans-nasal aerosol delivery device (tPAD) considered by Zeman et al. (2017) does not report device delivery efficiency, but includes a “spacer” to selectively filter larger droplets from an Aerogen Pro mesh nebulizer, with an estimated delivery rate of 0.4 ml/min (Longest et al. 2012) when actuated continuously. From the reported ex-device delivery rate of 2 ml/hr (or 0.033 ml/min) (Zeman et al. 2017), it can be estimated that the tPAD device has a delivery efficiency of approximately 8% of the nebulized dose. Hence, the mixer-heater device developed in this study is significantly more efficient than commercial and other experimental systems, and it produces a significantly higher drug formulation delivery rate.

In this study, an EEG formulation of 50:50 AS and NaCl was employed as a test aerosol based on its safety profile and well-developed characterization methods. As described in our previous work, the EEG approach delivers a small particle aerosol that is composed of an inhaled medication and hygroscopic excipient (Hindle and Longest 2012) (Longest et al. 2012). The small initial size of the aerosol provides for low depositional loss in the delivery system and extrathoracic airways. Once inside the lungs, the presence of the hygroscopic excipient causes the particles to take up water, increase in size, and deposit. The amount and type of hygroscopic excipient, initial aerosol size, and inhaled air conditions can all be used to control the rate of particle size increase and, together with inhalation rate, can be used to target the region of deposition (Longest and Hindle 2011, Tian et al. 2013, Tian et al. 2014). Considering AS and other bronchodilators delivered during NIV, clinical benefit is frequently reported even though the lung delivery efficiency is low (typically <10%) and intersubject variability is high for conventional delivery systems (Hess 2007, Ari and Fink 2012, Dhand 2012, Hess 2015, Walenga et al. 2017). This is generally considered acceptable because AS has a wide therapeutic window, relatively mild side effects, and is relatively in-expensive. Nevertheless, improved knowledge of

the delivered dose may help to lessen the potential beta-agonist side effects of atrial and ventricular arrhythmias and tachycardia (Higgins et al. 1987, Küng et al. 1987, Dhand 2007), especially when these medications are delivered in very high doses as with acute severe asthma.

Beyond the administration of bronchodilators, we envision the combination delivery device to be useful for respiratory drug delivery in cases involving (*i*) high dose nebulized medications, (*ii*) drugs with rapid absorption where continuous delivery is beneficial, (*iii*) medications that require uniform concentration in airway surface liquid, (*iv*) therapeutics targeted to specific lung regions such as the tracheobronchial or alveolar airways. One potential sample application that could benefit from the combination delivery system and the EEG strategy is the administration of nebulized antibiotics, which may require high doses and would likely benefit from uniform surface concentration throughout the lungs. At the current nebulized solution concentration of 0.5%, the combination device delivers approximately 0.9 mg/min of drug (with deep inspiration at a liquid delivery rate of 0.18 ml/min). Increasing the solute concentration to 3% would further increase the drug delivery rate to 5.4 mg/min and would produce an approximately 1.9 μm (aerodynamic diameter) aerosol, which is still expected to have low extrathoracic depositional loss. Tian et al. (2014) previously considered N2L delivery of 1 μm EEG particles using a complete-airway CFD model. Compared with conventional static particle sizes, the EEG approach increased small tracheobronchial airway deposition by a factor of approximately 35-fold (Tian et al. 2014). This increase is approaching what is required to achieve uniform concentration in airway surface liquid (μg of drug / ml of liquid) based on initial particle deposition site.

A second application of the combination device may be continuous or long-term administration of inhaled medications, perhaps during sleep. As described by Geller (2009),

beta-lactam antibiotics are effective based on the duration of time the drug concentration remains above the minimum inhibitory concentration (MIC) of the bacteria, in comparison with other concentration-dependent antibiotics. The long-term administration of beta-lactams simultaneously with HFNC or other forms of NIV may provide another option for the treatment of respiratory infections that is not currently available. Zeman et al. (2017) describe the tPAD device for administration of hypertonic saline to improve airway clearance in cystic fibrosis (CF) subjects. However, clinical trials did not indicate an improvement in clearance rate associated with overnight administration of hypertonic saline (Corcoran et al. 2017), which was likely due to an insufficient delivery rate (Corcoran et al. 2017). Based on hypertonic saline oral inhalation studies, a target delivery rate for effective improvement in clearance may be closer to 5.0 mg/min (Corcoran et al. 2017), whereas the tPAD device delivered 1.3 mg/min or less using a 7% saline formulation (Corcoran et al. 2017). For NaCl as the therapeutic molecule in the combination device, increasing the concentration to 3% will increase the drug delivery rate to 5.4 mg/min and the dried aerodynamic particle diameter to 1.9 μm. The increase in dried hygroscopic particle size would likely be effective in targeting the tracheobronchial region and especially the lower tracheobronchial airways. However, it is not clear if delivering dried particles with humidity, which then re-hydrate before deposition, will be more or less effective compared with nebulizer delivery of standard 7% hypertonic saline for improving airway clearance. Considering a third application, the dual nebulizer setup may be useful for the administration of different therapies simultaneously, potentially targeting different regions of the lungs based on nebulizer timing, in an effort to reduce treatment time and burden for subjects with complex inhalation regimes, as with CF.

Several study limitations should be noted and addressed before advancement of the combination device to human subjects testing. In this evaluation, the system lacked a nasal cannula interface, which when included will result in additional depositional losses. However, in multiple previous studies we have described the development of streamlined nasal cannula interfaces (Longest et al. 2013, Longest et al. 2013, Farkas et al. 2018) that are designed for aerosol administration and have very low depositional losses (<1% for nebulized aerosol based on *in vitro* experiments (Longest et al. 2013)) when delivering particles on the scale of ~1 μm at flow rates of approximately 30 LPM. Compared with other HFNC systems, we propose that RH values >30% (and in the range of 40-60%) are acceptable for HFNC therapy, based on ASTM standards for NIV (ASTM_International 2004). Moreover, by using a RH condition that is below 100%, common HFNC problems of liquid sputtering (DiBlasi 2015) and nose drippage may be avoided. The use of nebulized isotonic saline is currently untested as a means to humidify the airways on a long-term basis. We contend that delivering isotonic saline will help to maintain the correct osmotic gradient in the lungs, compared with the common practice of delivering humidity from pure water vapor. Furthermore, the salt concentration can be increased to enable simultaneous hypertonic saline administration, which is a known therapy for improving airway clearance (Daviskas and Anderson 2006). In this study, alternating actuation of the nebulizers was simply cycled with an expected inhalation time course. In future studies (See Chapter 4), breath monitoring will be added to the system to enable active synchronization of the aerosol during a portion of inhalation. It is expected that maximum delivery efficiency can be achieved when the subject can execute a “slow and deep” inhalation together with active synchronization of the aerosol delivery. Future *in vitro* studies will be conducted with variable breathing scenarios to test the ability to sense flow and synchronize actuation for a variety of nasal

anatomies. *In vitro* studies are also in progress to further test safety and reliability of the heating system. Upon in vitro testing and development of the combination system with synchronized delivery, studies to determine the synchronization performance (See Chapter 5), and to determine the lung deposition of radiolabeled aerosol in human subjects are planned.

In conclusion, multiple approaches (analytical, *in vitro* experimental and CFD) were used concurrently to develop a new combination device for administering HFNC therapy and simultaneous 'on-demand' pharmaceutical aerosols to the lungs with high efficiency. Designs 2 and 3 both satisfied the 5% or less mixer-heater depositional loss requirement and produced small particle aerosols with expected subsequent low depositional losses. Based on CFD and *in vitro* assessment of an initial design, the validated CFD model was used to guide development of the improved designs and achieve the specified performance metrics. Rapid prototyping and experimental testing of the improved designs confirmed improved aerosol and outlet temperature performance. Potential limitations of each approach were overcome with comparisons to the other methods. Further studies are needed to verify the expected analytical predictions of RH in all cases and resolve differences between predicted and measured outlet particle size. A system for synchronizing alternating actuation of the nebulizers with inspiration is currently in development. Subsequent studies will consider lung delivery efficiency during cyclic respiration using realistic *in vitro* airway models and then human subjects testing.

3.5 Tables

Table 3.1: Analytical predictions of Relative Humidity (%) if all nebulized liquid is evaporated for specified outlet temperatures, number of nebulizers and system airflow rates

Outlet Temperature (°C)	Number of Nebulizers	20 LPM % RH	30 LPM % RH
28	1 (Alternating)	73	49
30	1 (Alternating)	65	44
32	1 (Alternating)	59	39
34	1 (Alternating)	53	35
28	2 (Continuous)	100[a]	97
30	2 (Continuous)	100[a]	86
32	2 (Continuous)	100[a]	78
34	2 (Continuous)	100[a]	70

[a]Values limited to 100% indicate the occurrence of a partially evaporated aerosol

LPM, liters per minute; RH, relative humidity

Table 3.2: Solute concentrations (% w/v) for the 50:50 drug nebulizer mixture of AS:NaCl vs. dried particle size and drug (AS) delivery rate for initial monodisperse 5.3 µm nebulized droplets.

Solute Concentration (w/v) %	**Initial Droplet Diameter ($d_{initial}$; µm)**	**Final Geometric Diameter (d_{geo}; µm)**	**Final Aerodynamic Diameter (d_{ae}; µm)**	**Drug Mass Delivery Rate (µg/min)**
0.001	5.3	0.10	0.12	2
0.005	5.3	0.17	0.21	10
0.01	5.3	0.21	0.27	20
0.05	5.3	0.36	0.46	100
0.1	5.3	0.45	0.58	200
0.5	5.3	0.77	0.99	1000
1	5.3	0.97	1.24	2000
5	5.3	1.65	2.13	10000

AS, albuterol sulfate; NaCl, sodium chloride

Table 3.3: Table Experimentally measured mean (standard deviation) temperature and relative humidity values for Design 1 with a 60°C thermocouple temperature operating in alternating mode

Initial_12cm		**20 LPM**	**30 LPM**
	T (°C)	26.6 (0.1)	28.7 (0.2)
	RH (%)	61.3 (0.6)	40.3 (0.8)

Table 3.4: Experimentally determined mean (standard deviation) aerosol deposition fraction (% of nebulized dose) in different regions for Design 1 with a 60°C thermocouple temperature and mean (standard deviation) mass median aerodynamic diameter of the outlet aerosol

Design 1		**20 LPM**	**30 LPM**
	Nebulizer (%)	8.1 (0.2)	6.1 (0.8)
	Mixer-heater (%)	11.2 (0.6)	11.2 (1.5)
	Outlet filter (%)	78.0 (1.9)	76.6 (0.4)
	MMAD (μm)	1.7 (0.1)	1.6 (0.0)

Table 3.5: Experimentally measured mean (standard deviation) temperature and relative humidity values for all mixer heater designs with a targeted 32°C outlet temperature operating in alternating mode

		20 LPM	**30 LPM**
Design 1	**T (**°C**)**	32.7 (0.5)	32.2 (0.6)
	RH (%)	33.4 (2.1)	31.7 (1.7)
Design 2	**T (**°C**)**	32.8 (0.5)	32.7 (1.1)
	RH (%)	39.2 (1.1)	21.2 (3.9)
Design 3	**T (**°C**)**	32.7 (0.3)	32.4 (0.5)
	RH (%)	35.2 (0.6)	29.6 (1.1)

Table 3.6: Experimentally determined mean (standard deviation) aerosol deposition fraction (% of nebulized dose) in different regions of all mixer-heater designs with a targeted 32°C outlet temperature and mean (standard deviation) mass median aerodynamic diameter of the outlet aerosol

		20 LPM	**30 LPM**
Design 1	**Nebulizer (%)**	7.0 (0.7)	9.1 (0.7)
	Mixer-heater (%)	11.4 (1.2)	11.1 (0.6)
	Outlet filter (%)	71.1 (2.4)	71.2 (0.4)
	MMAD (µm)	1.6 (0.0)	1.5 (0.0)
Design 2	**Nebulizer (%)**	7.2 (0.7)	7.0 (1.4)
	Mixer-heater (%)	6.2 (1.6)	4.5 (1.6)
	Outlet filter (%)	79.2 (4.1)	80.2 (3.4)
	MMAD (µm)	1.6 (0.0)	1.5 (0.0)
Design 3	**Nebulizer (%)**	9.3 (1.6)	9.2 (3.9)
	Mixer-heater (%)	4.4 (1.8)	4.1 (2.4)
	Outlet filter (%)	80.5 (1.1)	85.5 (4.7)
	MMAD (µm)	1.6 (0.0)	1.6 (0.1)

3.6 Figures

Figure 3

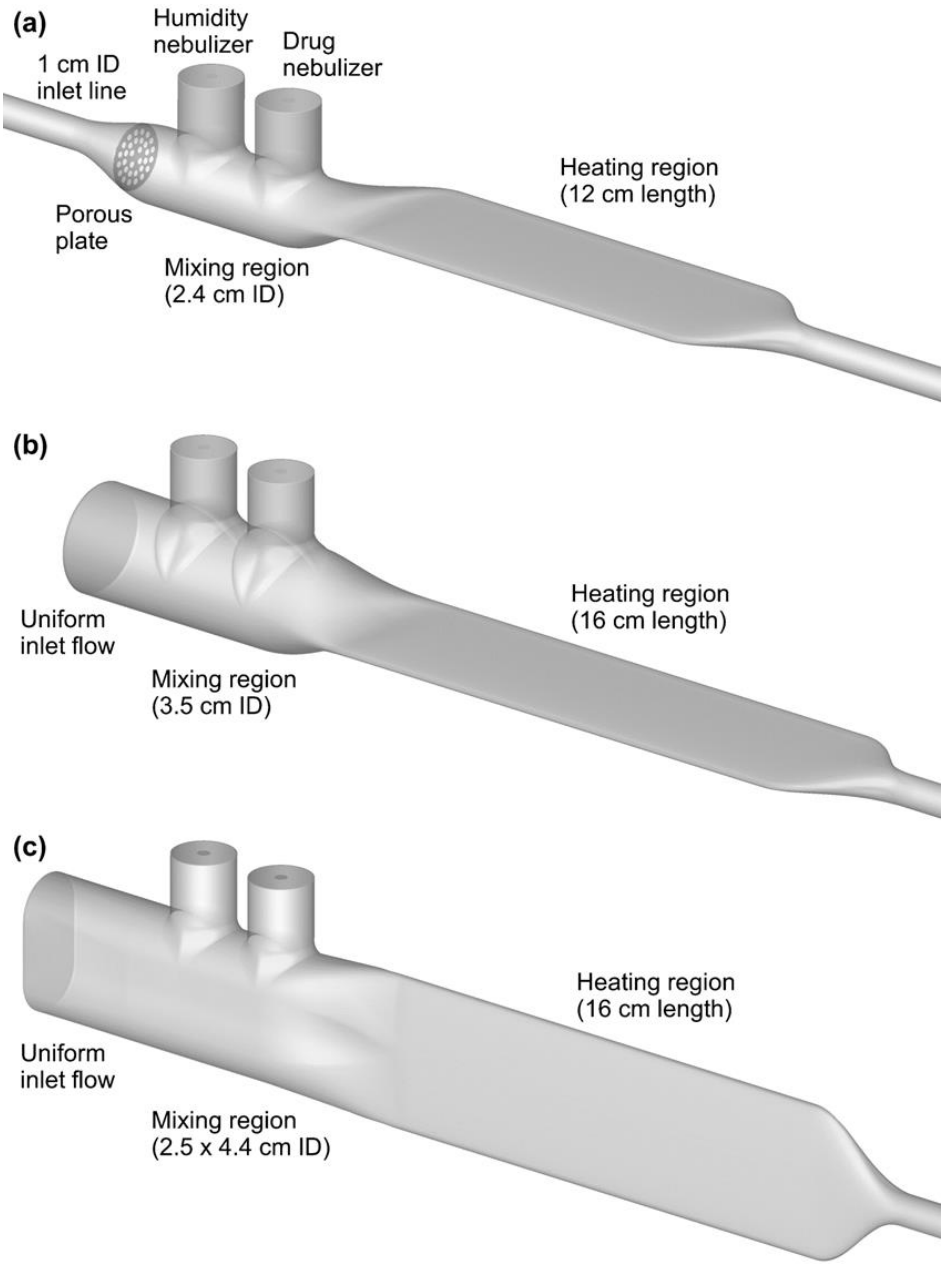

Figure 3.1: Surface models of the mixer-heater portion of the combination HFNC and pharmaceutical aerosol device (combination device) denoted as **(a)** Design 1, **(b)** Design 2, and **(c)** Design 3. The mixer-heater is intended to produce <5% depositional loss of the nebulized dose and fully evaporate the aerosol into dried particles.

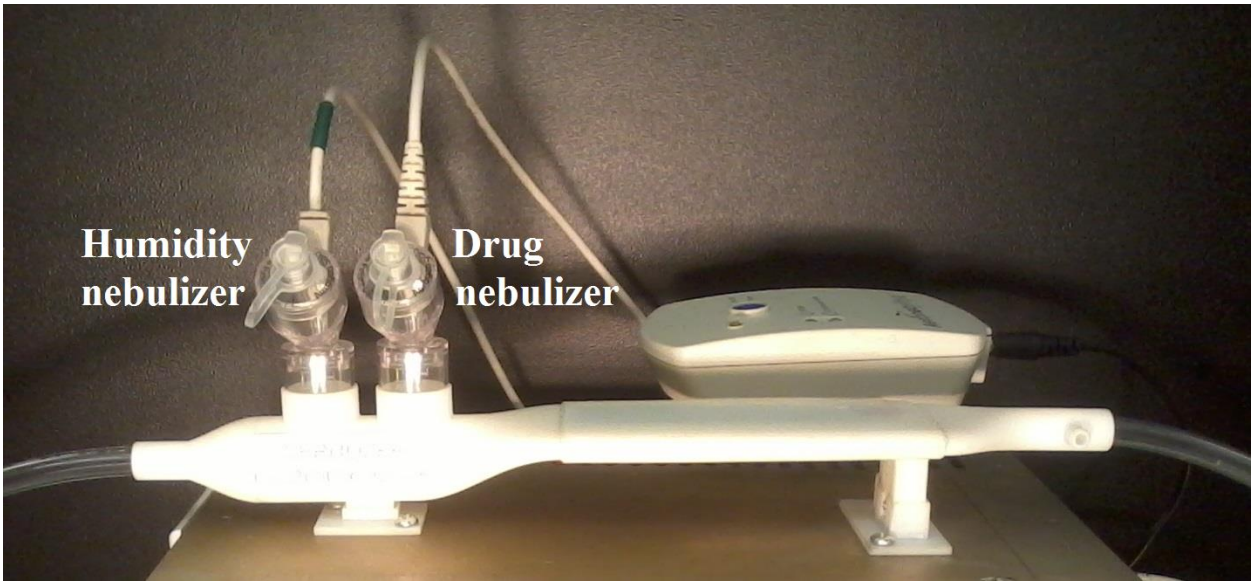

Figure 3.2: Mixer-heater device (Design 1) produced with 3D printing and positioned on top of the nebulization and heating control unit. Separate nebulizers are used for humidifying the airstream (humidity nebulizer) and providing pharmaceutical aerosol when needed (drug nebulizer).

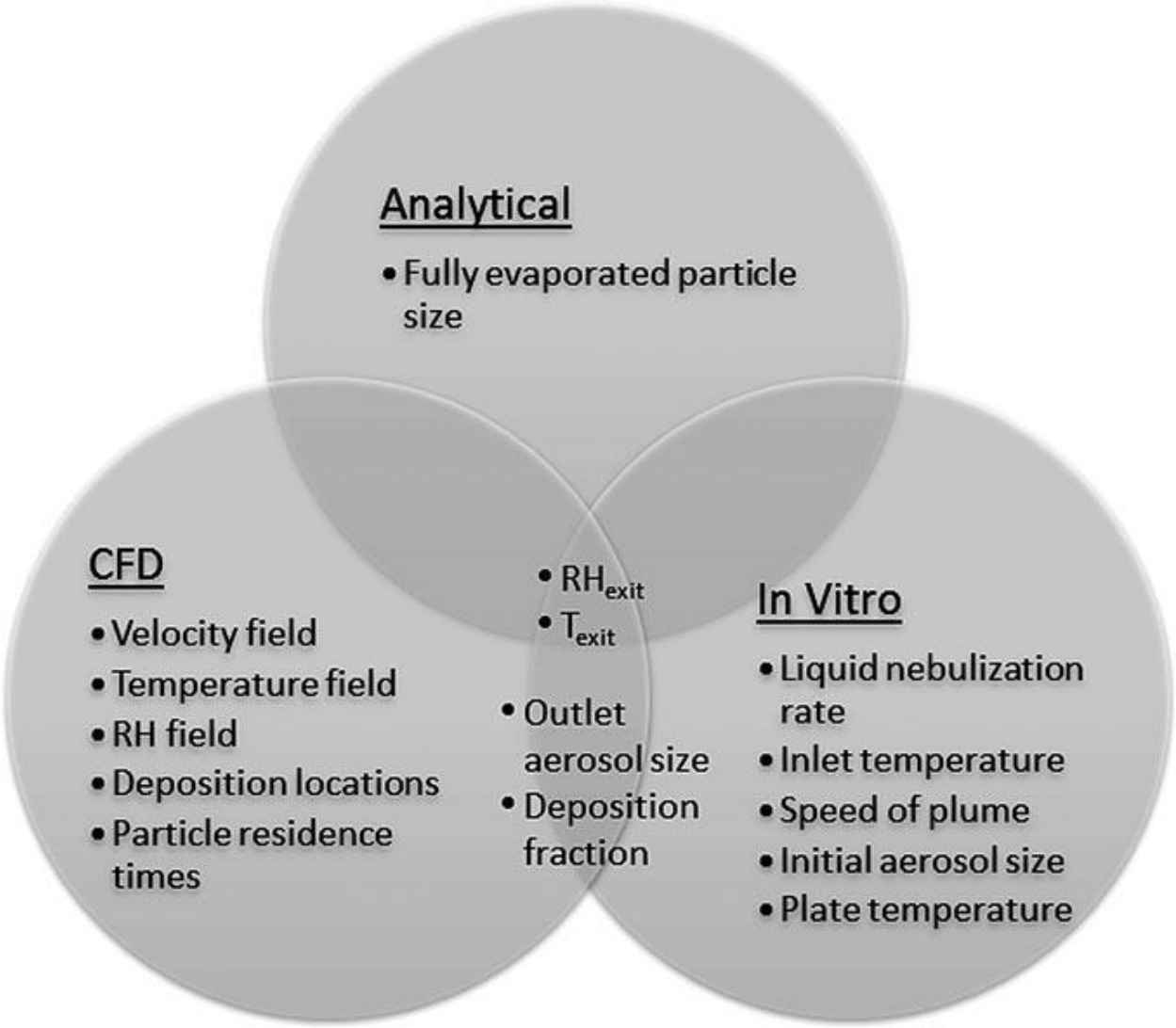

Figure 3.3: Diagram illustrating the three assessment methods (analytical, CFD, and in vitro experiments), characterization metrics (e.g., outlet aerosol size), and overlap among the methods. Characterization metrics arising from more than one method (e.g., RH_{exit}) are compared in the Results section.

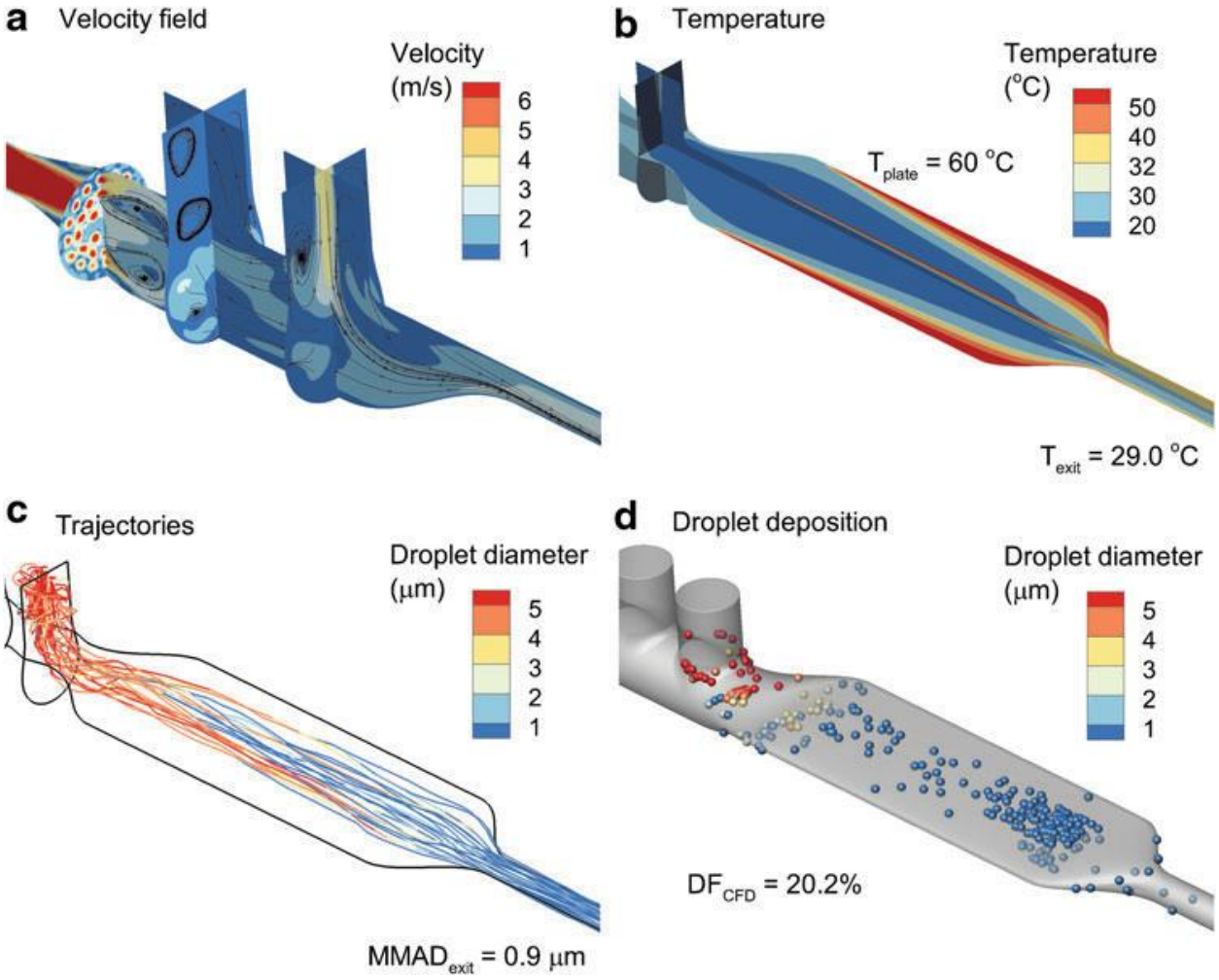

Figure 3.4: CFD analysis of Design 1 operated at 30 LPM with a constant plate temperature of 60°C, including **(a)** surface contours and stream traces of the velocity field, **(b)** contours of the temperature field, **(c)** droplet trajectories with an initial size of 5.3 μm and colored based on geometric diameter, and **(d)** droplet deposition locations, including the size of the droplets/particles at the point of deposition.

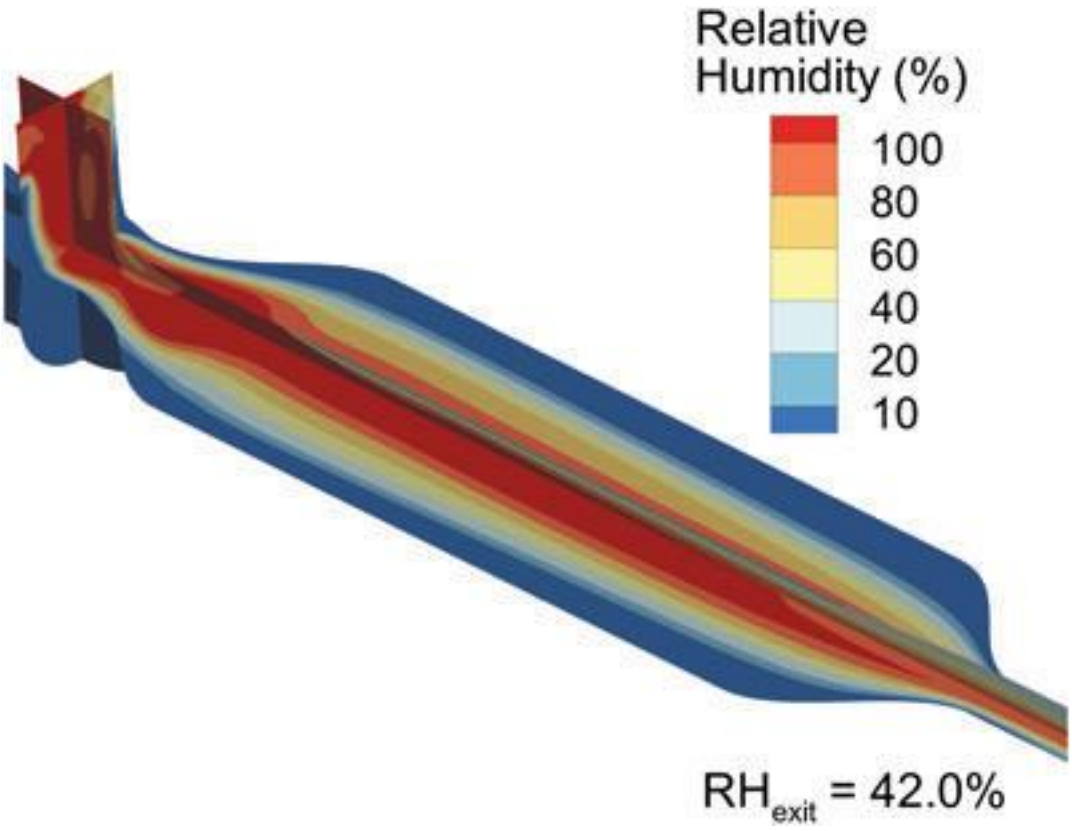

Figure 3.5: RH field of Design 1 producing an outlet RH of 42% with an outlet temperature of 29°C.

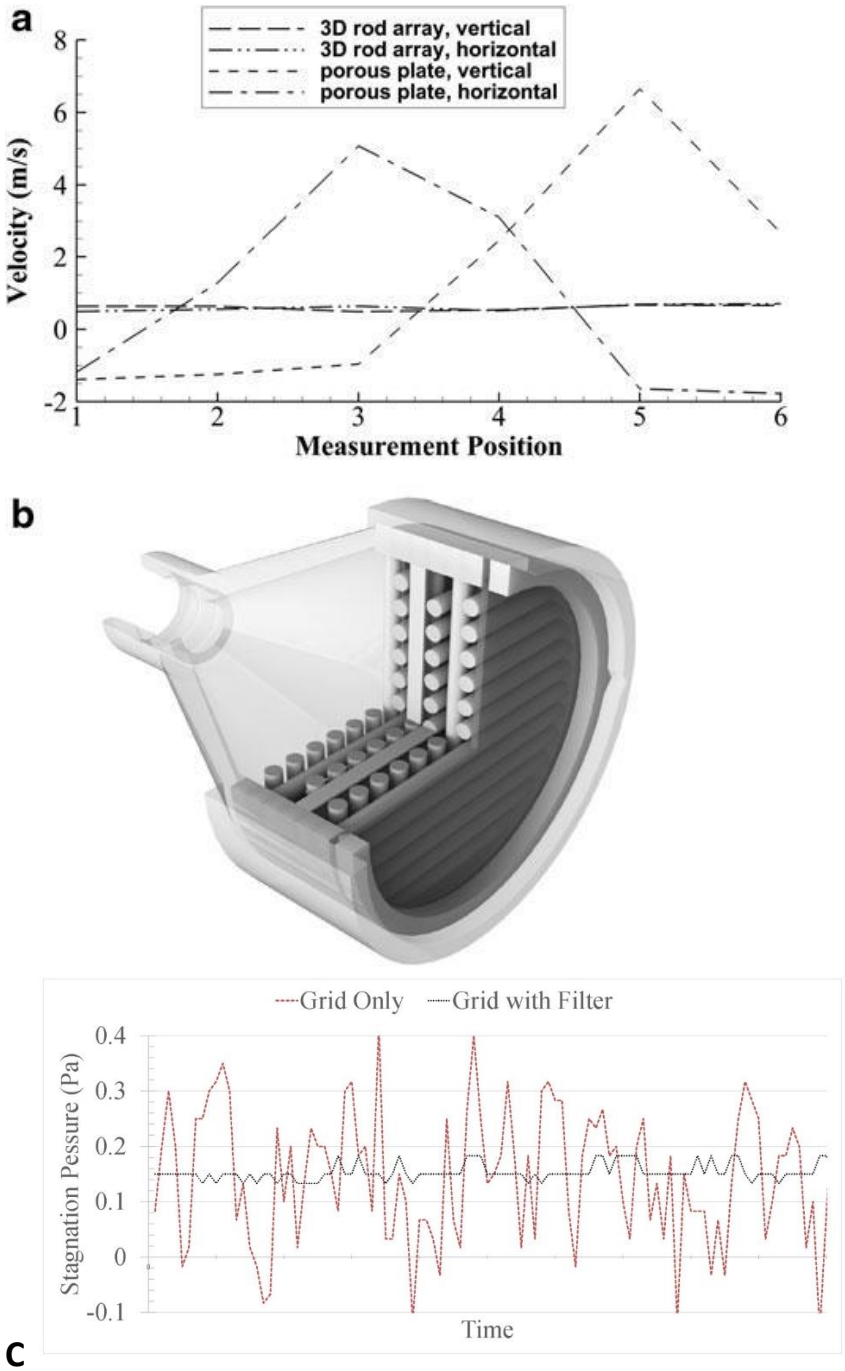

Figure 3.6: Development of the inlet flow unifier device, including **(a)** sample inlet velocity profiles in the horizontal and vertical directions without (Design 1) and with (Design 2) the flow unifier, **(b)** assembled Design 2 flow unifier, including a Pulmoguard II™ (Queset Medical, North Easton, MA) filter at the outlet. **(c)** Sample plot of pitot tube readings at a single point through time with and without a filter

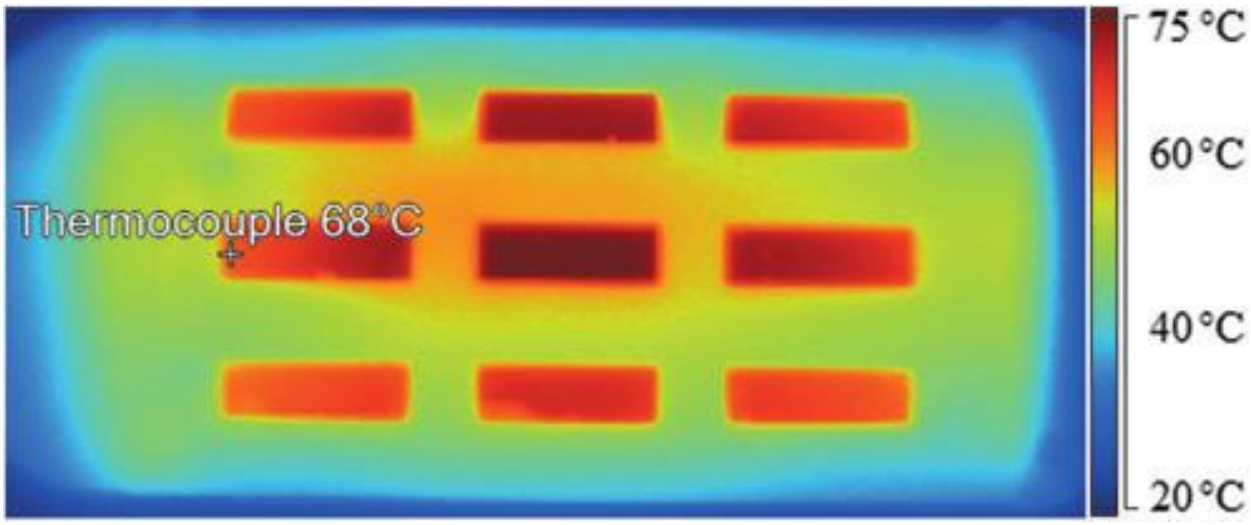

Figure 3.7: Thermal image of the heating plate taken with the rectangular sections of the outer nylon shell removed for the Design 1 mixer-heater operated at 30 LPM with a thermocouple set point of 60°C. Approximate thermocouple location marked and labeled with software-determined temperature.

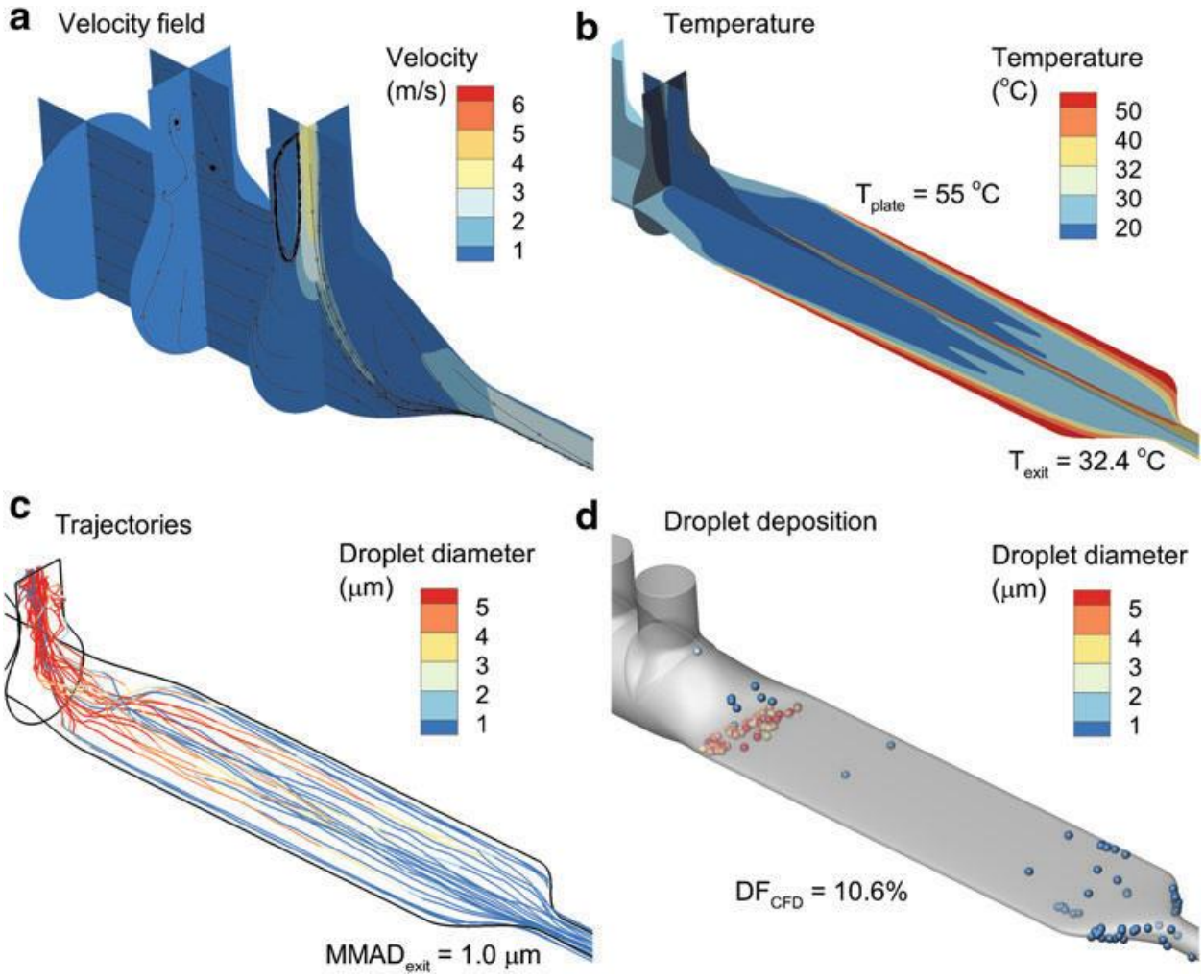

Figure 3.8: CFD analysis of Design 2 operated at 30 LPM with a constant plate temperature of 55°C, including **(a)** surface contours and stream traces of the velocity field, **(b)** contours of the temperature field, **(c)** droplet trajectories with an initial size of 5.3 μm and colored based on geometric diameter, and **(d)** droplet deposition locations, including the size of the droplets/particles at the point of deposition.

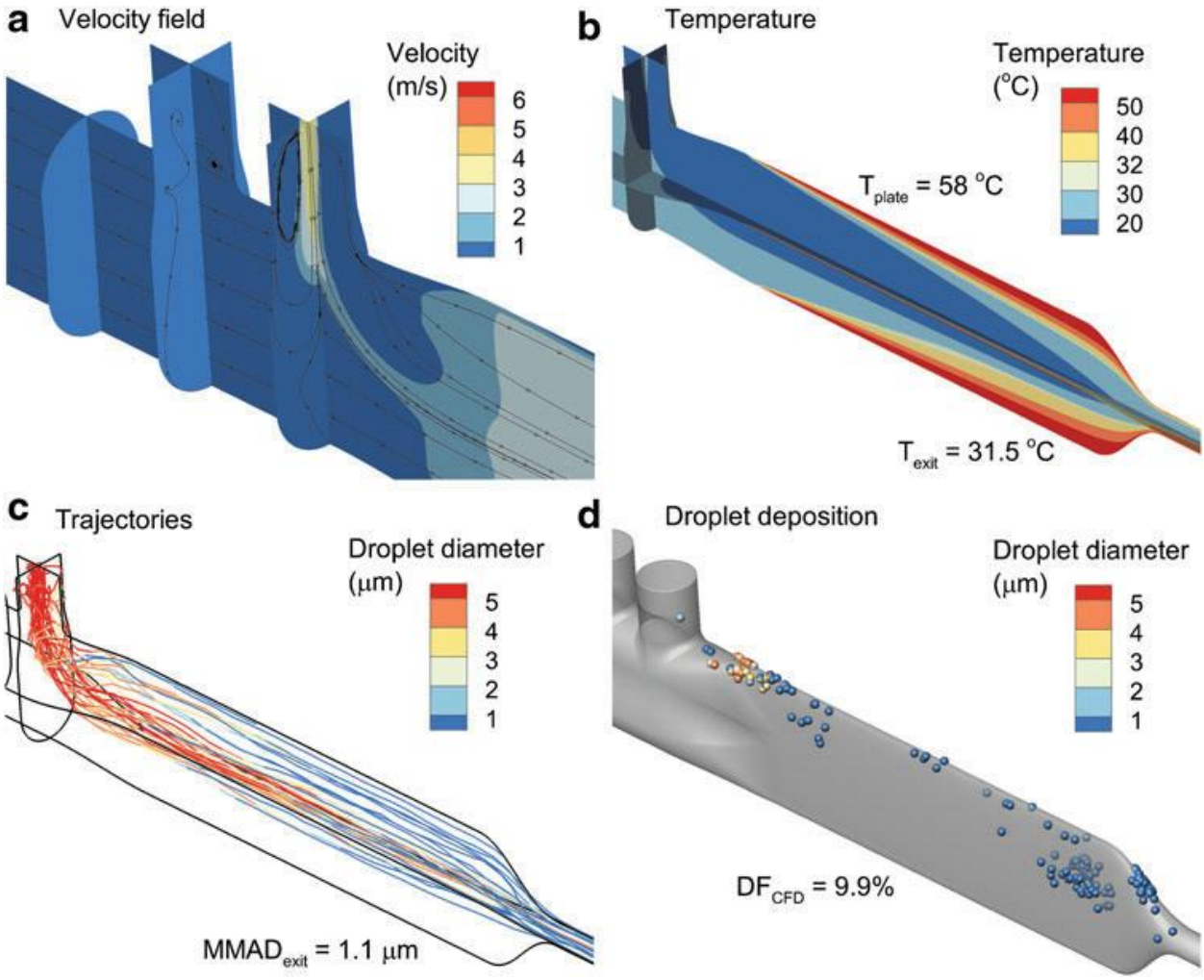

Figure 3.9: CFD analysis of Design 3 operated at 30 LPM with a constant plate temperature of 60°C, including **(a)** surface contours and stream traces of the velocity field, **(b)** contours of the temperature field, **(c)** droplet trajectories with an initial size of 5.3 μm and colored based on geometric diameter, and **(d)** droplet deposition locations, including the size of the droplets/particles at the point of deposition

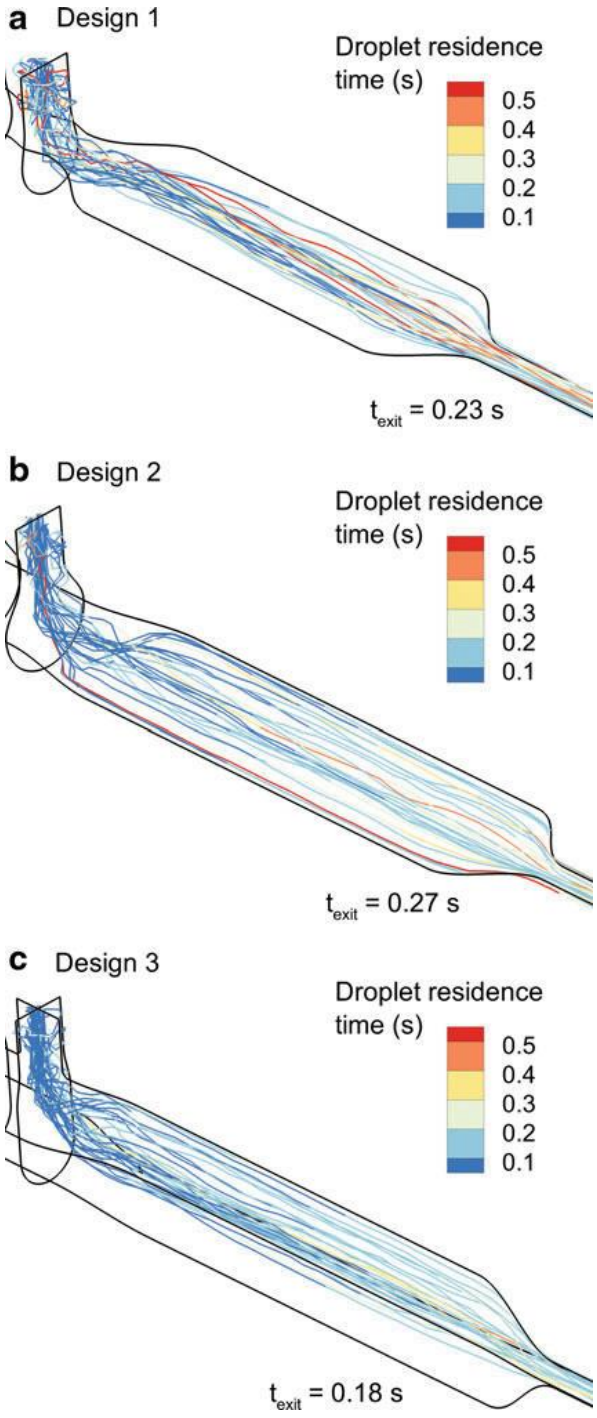

Figure 3.10: Droplet trajectories contoured by mixer-heater residence time (starting at the point of injection from the drug nebulizer) for **(a)** Design 1, **(b)** Design 2, and **(c)** Design 3.

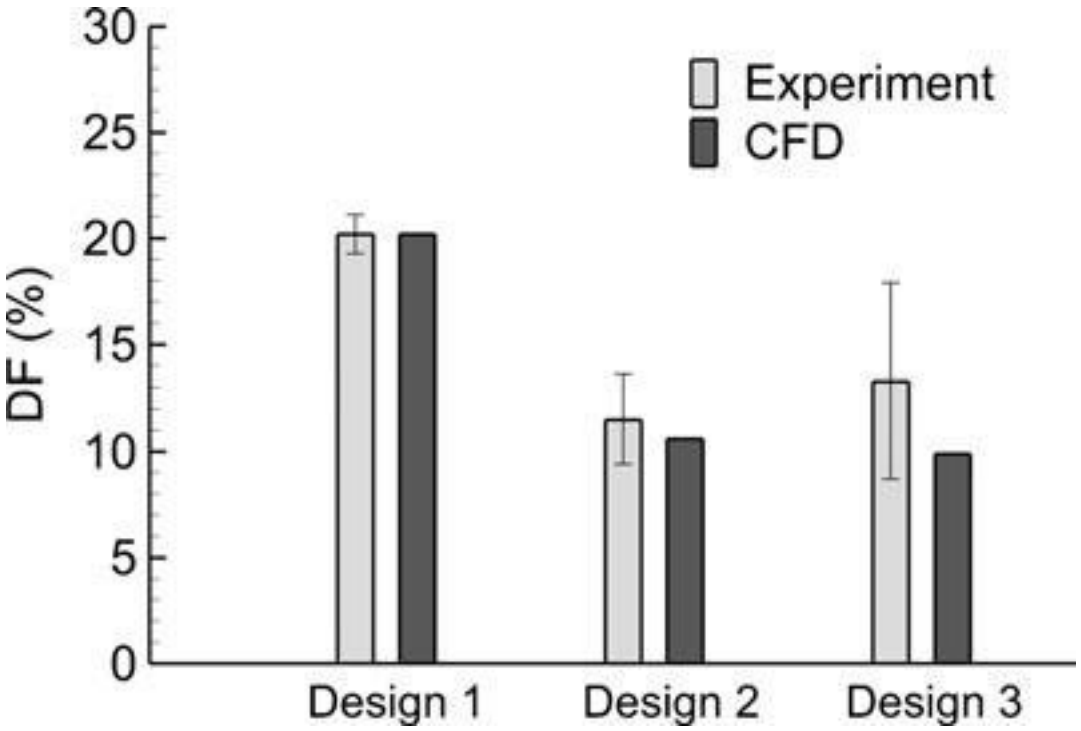

Figure 3.11: Comparison of total deposition fractions (as a percentage of nebulized dose) within the nebulizer and mixer-heater based on experimental data and CFD predictions. Three trials of each experiment were conducted (*n=3*) and error bars denoted ±1 standard deviation of the experimental data.

Chapter 4: Matching Aerosol Delivery to Breathing Profile in Real-Time

4.1 Introduction

High flow nasal cannula (HFNC) therapy is a form of non-invasive positive pressure ventilation (NPPV) in which a continuous flow of ventilation gas, typically at or above 20 LPM, is administered to subjects via a nasal cannula interface. When pharmaceutical aerosols are needed, delivering them simultaneously with HFNC therapy through the nasal cannula interface is convenient and allows the patient to remain connected to the ventilation support. Despite this convenience, aerosol delivery to the lungs through HFNC systems is reported to be highly inefficient, with a recent *in vivo* study reporting that only 1–4% of a nebulized dose deposited in the lungs of human subjects (Dugernier et al. 2017).

Spence *et al.* (2019) developed a combination device for simultaneously administering HFNC therapy and on-demand pharmaceutical aerosols that included streamlined low-volume mixing and heating regions totaling less than 100 milliliters (mL) for adults. The device implements separate nebulizers to humidify the gas stream and to deliver the on-demand pharmaceutical aerosols synchronized with inhalation. During a period of pharmaceutical aerosol delivery, the heating passage reduces the aerosol size and provides a convenient source of excipient enhanced growth particles for direct inhalation (Golshahi et al. 2014). Advancing previous mixer-heater designs, the resulting combination device for high flow therapy and high efficiency pharmaceutical aerosol delivery developed by Spence *et al.* (2019) is referred to as the Low Volume Mixer Heater (LVMH).

A significant challenge in the advancement of the LVMH is identifying the period of patient inhalation for the delivery of the pharmaceutical aerosol. This breath sensing is complicated by the continuous flow of HFNC gas at a typical rate of 30 LPM. For optimal

aerosol delivery, the start of inhalation should be identified as closely as possible using a pressure sensor. After a specified time-delay, the device control unit then triggers the drug nebulization for a set time period (e.g. 1 sec) leading to inhalation synchronized aerosol administration. The overarching objectives of this study were to develop a method for synchronizing drug delivery with simulated patient inhalation and to develop validated administration procedures for use in a future human subjects study. This chapter focuses on presenting representative data from a subset of experiments considering multiple realistic human airway models, breathing conditions, and nasal cannulae.

4.2 Materials and Methods

Experimental work and device development explored the interaction among the four subsystems: Simulated Subject, Control and Monitoring Unit (CMU), Commercial Nebulizer System, and LVMH Flow Path. An information flow schematic of the subsystems and components is presented in Figure 4.1. Three individual airway geometries were extracted from CT scans processed in the study of Walenga *et al* (2017) and 3D printed to create nose-mouth-throat (NMT) airway models. Naming conventions of these airway geometries for the various studies are presented in Table 4.1. Medical air from a pressurized tank was supplied at 30 LPM through the LVMH device and delivered to the NMT model via a nasal cannula interface. To estimate the aerosol drug mass reaching the lungs, filters were placed at the end of the laryngeal region, which were then connected to a breathing simulator (ASL 5000, IngMar Medical; Pittsburgh, PA). The ASL 5000 was programmed with differing breathing patterns as device experimentation progressed. Experimentation was split into cases depending on the programmed

breathing pattern and LVMH system operation (See Table 4.2). Focusing on the final experimental setup of Case 3, the lung simulator was programmed with a randomized variable pattern based on deep nasal inhalations. In this randomized sinusoidal breath pattern the tidal volume was a consistent 1225 mL; however, the breath length was randomly varied from 5.25 to 9.75 seconds with an inhalation-to-exhalation ratio range of 1:2 through 1:3 (See Table 4.3 for additional numerical details). From the 42 possible breath parameter combinations, a randomized string of 60 breaths was selected to create the pattern that was saved and implemented for each run. A custom routine was created in Mathematica for this process. The future custom routine version used to create a Case 5 pattern is presented in the Appendix 13.1.3 ASL Routine Creation. The ASL 5000 communication firmware was configured to output a low voltage signal during inhalation that was read by the Control and Monitoring Unit (CMU). The CMU controlled all aspects of the LVMH system operation including receiving and interpreting the signal from an integrated pressure measurement sensor, actuating the drug nebulizer (which may alternate with the humidity nebulizer), providing feedback control of the heating section to achieve a 32°C humidified gas temperature delivered to the patient, and system shutdown in the event of a malfunction. The CMU was developed around an Arduino Uno microcontroller (Arduino, Somerville, MA) and custom-developed code. Updated versions of this code were used in later studies which utilized the code presented in Appendix 13.1.1.

During Case 3 experiments, the CMU software received and logged the inhalation signal from the ASL 5000 (*actual-inhalation-start-time*). However, the *predicted-inhalation-start-time* was based on comparison of the critical pressure value to the current system pressure as measured by a Sensirion SDP800 sensor placed upstream of the nebulizers, as is the intended device operation. The critical pressure value changed over time based on historic maximum and

minimum pressures. The CMU software logged the resulting *predicted-inhalation-start-time* and *drug-nebulization-start-time* for later analysis. Based on the expected transport delay of aerosol through the system and flow conditions of the standard deep nasal inhalation breathing pattern, the *drug-nebulization-start-time* was set to occur 0.25 seconds after the *predicted-inhalation-start-time*. Drug nebulization was set to last one second but was ended early if exhalation occurred during the nebulization period. Data presented in this chapter include three nasal geometries tested with two different interface setups. The first setup (I2) used a commercially available Optiflow500 series nasal cannula (Fisher & Paykel Healthcare, Auckland, New Zealand). The other setup (I3) used a customized 3D printed streamlined (Longest et al. 2013) nasal cannula redesigned for this specific application.

After warm-up and stabilization, the drug nebulizer was activated to aerosolize a model drug solution containing 0.25% albuterol sulfate for 60 breaths. Finite volumes of deionized water were used to individually wash all system components downstream of the drug nebulizer to determine drug deposition using high performance liquid chromatography (HPLC) quantitative analysis. Total recovery was calculated as the sum of deposition on all components including the tracheal filter. Cannula prong emitted percentages were calculated as 100% minus deposition in the LVMH device, connective tubing, and cannula.

Microcontroller event logs from each run were analyzed and the difference between *predicted-inhalation-start-time* (based on sensor readings) and *actual-inhalation-start-time* (based on ASL signal) was calculated to obtain a time differential value for each breath (TDB). Negative TDB values indicated the software sensed inhalation before it actually started. Averaging over each run of 60 breaths, the mean and standard deviation of the 60 individual TDB values were calculated and defined as mean-time-differential (MTD) and time-differential-

standard-deviation (TDSD) for each airway model. Therefore, MTD values quantify the accuracy of the breath prediction software within each particular 60 breath run. Similarly, TDSD values quantify the consistency of the breath prediction software within each particular 60 breath run. Replicate runs were performed and the descriptive statistics of mean and standard deviation were also calculated to determine the system prediction software consistency over multiple treatments in the same NMT model.

4.3 Results

Pressure sensor placement and control were critical issues in system performance. Degradation over time of the pressure sensor information positioned at the original location prompted investigation and eventual movement of the measurement location upstream. Pressure sensor degradation was overlooked during initial runs due to the successfulness of the CMU algorithm. The CMU adaptive system for setting the critical pressure value compensated for sensor drift. However, when plotted over time (See Figure 4.2:) the downward trend became evident and the issue was fixed to achieve a relatively stable critical pressure value. Of note, the numerically higher sensed pressure values of the second location presented in the plot are arbitrary due to the physical design of the pressure sensing flow circuit, which includes a needle valve for fine tuning of sensor flow.

Table 4.4: presents each model's mean and standard deviation values of the MTD and TDSD for the three replicate runs. Note that although time is required for aerosolized drug to travel through the device, there is also a delay from the actual inhalation start to when the cyclic inhalation waveform equals the 30 LPM HFNC therapy flow rate. Therefore, based on system

design, the expected ideal MTD is positive (~250 milliseconds) with low variability. Low TDSD values, relative to the inhalation duration, indicated good system ability to adapt to the variable breathing profile. Combined data from all nose-mouth-throat (NMT) models is presented in the last row of the table. MTD values serve as a predictor link to the run's total drug recovery resulting from the expected exhalation losses due to timing mismatch. The variability in both MTD and TDSD between the nasal airway models and the cannulae indicated hundreds of milliseconds variability in breath sensing by the device.

Drug recovery percentages from the total system and selected areas are presented in Table 4.5: . High emitted dose from the cannula prongs with mean values greater than 85% indicated that, despite breath sensing variability, the LVMH device delivered drug to the NMT models with high efficiency. Furthermore, total system recovery averaging greater than 80% nebulized dose signifies that little drug was lost to the environment during exhalation indicating well timed drug delivery pulses synchronized with inhalation. The link between synchronization and recovery was evident in Case 3 runs for both cannula styles; however, it was not seen in Case 2 data (See Figure 4.3:). LVMH estimated lung delivery efficiency, as determined by approximately 70% of the nebulized dose depositing on the tracheal filter, represents an order of magnitude increase from the 3.6% lung delivery efficiency seen in human subjects by Dugernier *et al*. (2017). Low variability was found in the deposition of drug within individual NMT models; however, a wide range of NMT deposition fractions (3.5% to 14.2%) was found between models. It was noticed that in certain positions, the cannula exits created jets aimed at the model walls creating increased nasal deposition. For consistent high efficiency delivery, care should be taken in the positioning and sizing of the nasal cannula.

4.4 Discussion

This study developed and demonstrated a method to detect breathing and to provide pharmaceutical aerosol delivery synchronized with breathing during HFNC therapy directly from upstream measurements of system backpressure. Removing the need for additional external breath sensing equipment, such as a respiratory inductance plethysmography system, reduced clinical setup burden. The developed system functioned in multiple *in vitro* patient nasal anatomies and breathing patterns. Additionally, these multiple anatomies required different cannula sizes for testing while still allowing for efficient delivery. The high estimated lung delivery efficiency achieved in this study suggests that the variability in the synchronizing algorithm is low enough to provide substantially higher aerosol lung delivery efficiency than standard of care methods used with HFNC therapy.

In considering the HPLC deposition results in combination with general experimental observations, several conclusions for discussion were made. Continued functionality with decreased losses within the mixer heater region compared to previous versions of the device signaled improved device mechanical robustness. This experiment used two Pulmoguard II filters placed sequentially for substantial capture of aerosol with minimal flow resistance, instead of a single higher capture efficiency filter such as the Pall BB-50T. Demers et al. (2016) demonstrated filter bypass occurs in respiratory line filters, however filter bypass in our experiment would lead to under prediction of the actual tracheal aerosol dose. HPLC recovery below 100% was mainly a result of aerosol loss to the environment due to the inherent HFNC therapy system leak at the nasal interface. Standard of care systems lose large portions of drug at

the interface; but in this study, synchronizing aerosol generation with inhalation lowered exhalation losses substantially.

This study utilized a complex and randomized deep nasal inhalation pattern for testing the synchronization capability of the system under anticipated operation. However, the question of realism still remains as a possible weakness of this study. This pattern provided a variety of pressure change rates and time scales stemming from randomly generated deviations around a preset base breath pattern in the hope of capturing the challenges of a yet unknown pattern. Unfortunately, truly natural breath patterns are not random and mathematical models can predict the upcoming breath based on information of the preceding breaths (Benchetrit 2000). As a check on the randomized DNI pattern realism, several overall statics were calculated and compared positively to literature reported values. The programmed breath pattern timing Coefficient of Variation (CV) calculated at 19.7% fell well within published findings. Tobin *et al.* (1988) found at rest breath-to-breath CV frequency of 20.8 ± 11.5% and tidal volume of 33 ± 12.6% in healthy adults. These measurements were recorded using inductive plethysmography; a technique using electronic bands to measure volume changes of the chest cavity and explained in detail by Tobin *et al.* (1983). Although the addition of HFNC therapy could alter mean frequency and tidal volume values, minimal impact on the breath-to-breath CV values are expected. Therefore, it was concluded that the pattern contained right amount of variability for a realistic testing routine. The impressive results of this synchronization study are expected to be verified in future human subject studies, and adjustments to the adaptive critical pressure algorithm will be performed if necessary.

4.5 Tables

Table 4.1: Model Naming and Sources

Walenga et al. (2014) Name	**Walenga et al. (2017) Name**	**This Study Name**
Open model	Open model	Open model
Constricted 2	Subject A	Subject A
Not used	Subject B – New Data	Subject B

Table 4.2: System Variable Case ID

	Drug Trigger	**Breathing Pattern**	**Reason**	**Cannula Tested**
Case 1	ASL	Repeated DNI Unmodified	Comparison to previous studies and evaluation of MH design modification	Optiflow
Case 2	CMU	Repeated DNI Unmodified	Baseline functionality and consistency of breath sensing design	Optiflow and Streamlined
Case 3	CMU	Randomized Modified DNI	Higher realism of breath patterns	Optiflow and Streamlined

Table 4.3: DNI Parameters for Breath Cases

Item	Repeated Deep Nasal Inhalation	Randomized Deep Nasal Inhalation
V_T (ml)	1750	1225
Breath Length (sec)	7.5	5.25 – 9.75 5.25, 6.00, 6.75, 7.50, 8.25, 9.00, 9.75
I:E (Ratio of inhalation length to exhalation length)	1:2	1:2 – 1:3 1:2, 1:2.2, 1:2.4, 1:2.6, 1:2.8, 1:3.0
t_{travel} (sec) [a]	0.270	0.270
t_1 (sec) [b]	0.245	0.145 – 1.041
t_2 (sec) [c]	2.3	1.168 – 2.201
t_3 (sec) [d]	2.1	1.023 – 1.375
Required nebulizer start time for exit at inhalation greater than 30 LPM	-0.025	-0.122

a Transit time through the HFNC delivery system for a flow rate of 30 LPM and system volume of ~100 mL
b Intersection of breathing flow and HFNC 30 LPM flow rate – falling pressure
c Intersection of breathing flow and HFNC 30 LPM flow rate – rising pressure
d Time duration that HFNC 30 LPM flow rate is less than breathing flow rate

Table 4.4: Timing differentials of the *actual-inhalation-start-time* and *drug-nebulization-start-time* for each of the nose-mouth-throat (NMT) models.

NMT Model	MTD (milliseconds) (Mean ± SD)		TDSD (milliseconds) (Mean ± SD)	
	Optiflow500 Cannula (I2)	Streamlined Cannula (I3)	Optiflow500 Cannula (I2)	Streamlined Cannula (I3)
Open	591 ± 270	266 ± 54	475 ± 31	565 ± 45
Sub A	262 ± 20	-37 ± 73	163 ± 16	391 ± 83
Sub B	3 ± 69	65 ± 113	438 ± 66	298 ± 30
All	302 ±279	98 ± 152	359 ± 139	418 ± 128

Table 4.5: Aerosol depositional data obtained from HPLC analysis for each of the nose-mouth-throat (NMT) models

NMT Model	Total Recovery (% Nebulized) (Mean ± SD)		Tracheal Filter (% Nebulized) (Mean ± SD)		NMT (% Nebulized) (Mean ± SD)		Emitted Prongs (% Nebulized) (Mean ± SD)	
	I2	I3	I2	I3	I2	I3	I2	I3
Open	78.6 ± 10.5	84.3 ± 3.6	61.4 ± 9.9	72.0 ± 3.0	5.7 ± 1.1	5.2 ± 0.5	87.2 ± 1.0	92.1 ± 0.8
Sub A	84.9 ± 3.0	89.4 ± 4.4	68.1 ± 2.9	78.4 ± 3.7	4.2 ± 0.4	3.5 ± 0.3	86.8 ± 1.2	92.2 ± 0.6
Sub B	88.8 ± 5.3	90.4 ± 4.5	67.8 ± 4.4	64.3 ± 6.9	7.6 ± 0.7	14.2 ± 2.3	85.8 ± 2.7	86.6 ± 1.0
All	83.6 ± 7.7	88.0 ± 4.6	65.4 ± 6.7	71.6 ± 7.4	4.9 ± 1.4	6.6 ± 4.6	87.9 ± 4.1	90.3 ± 2.8

4.6 Figures

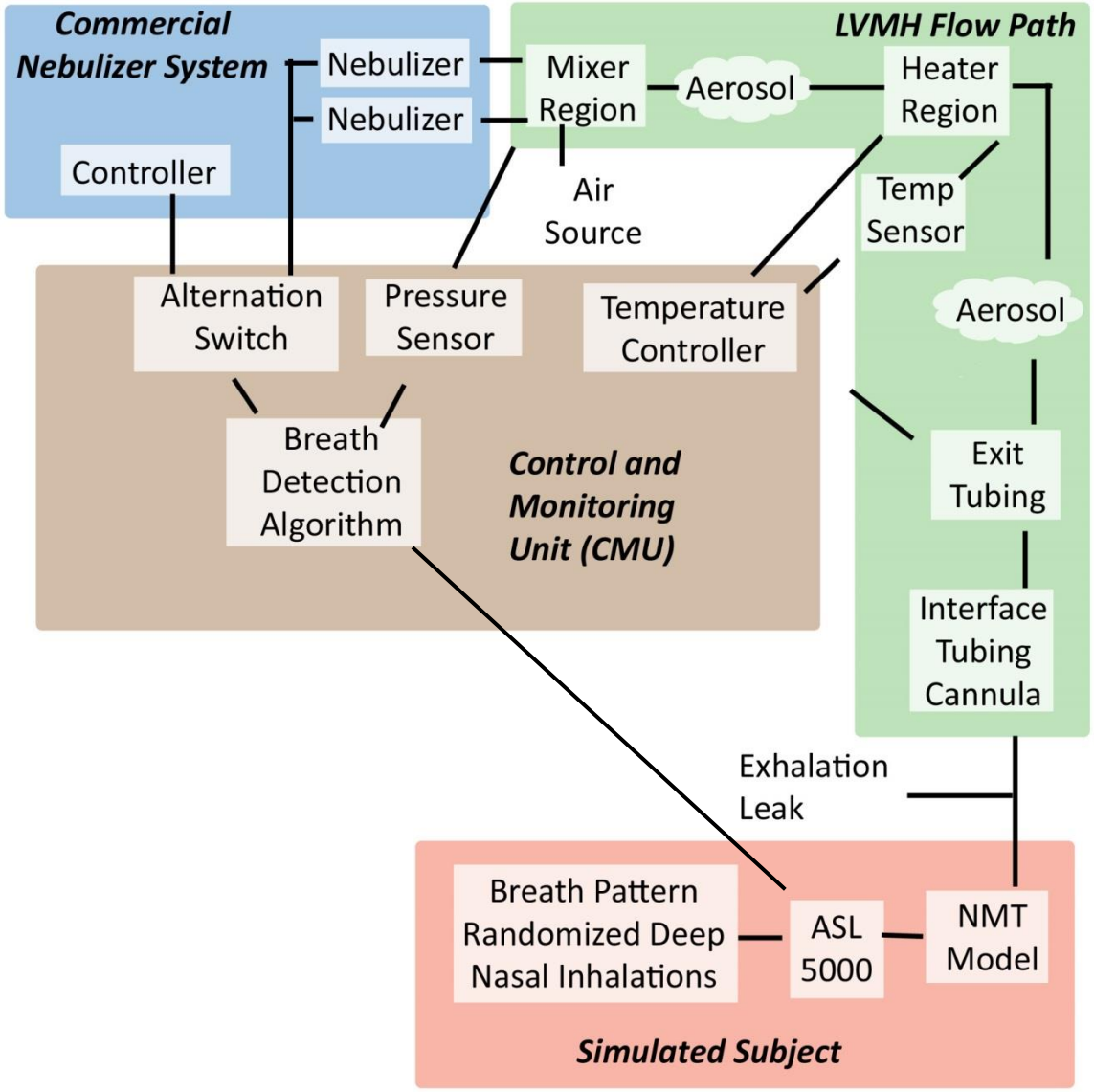

Figure 4.1: Experimental system setup diagram for synchronization testing.

a

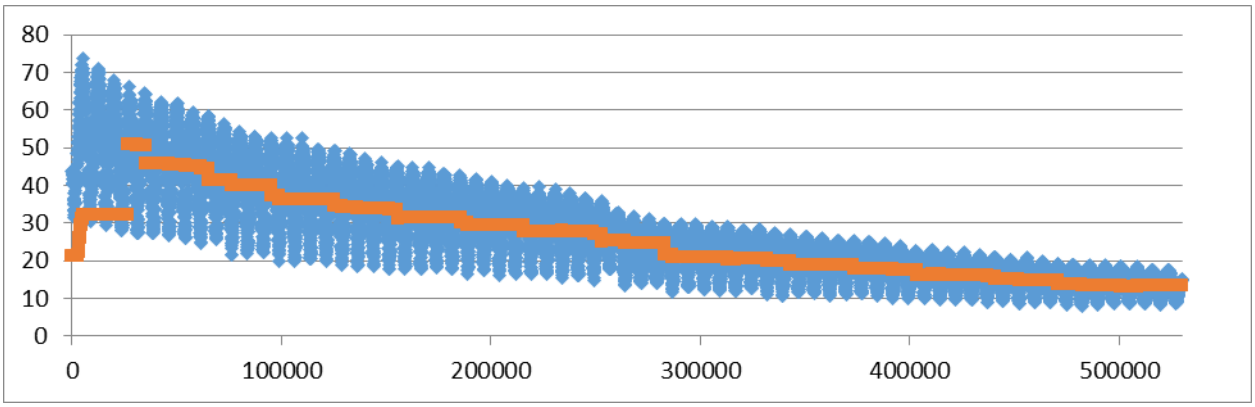

b

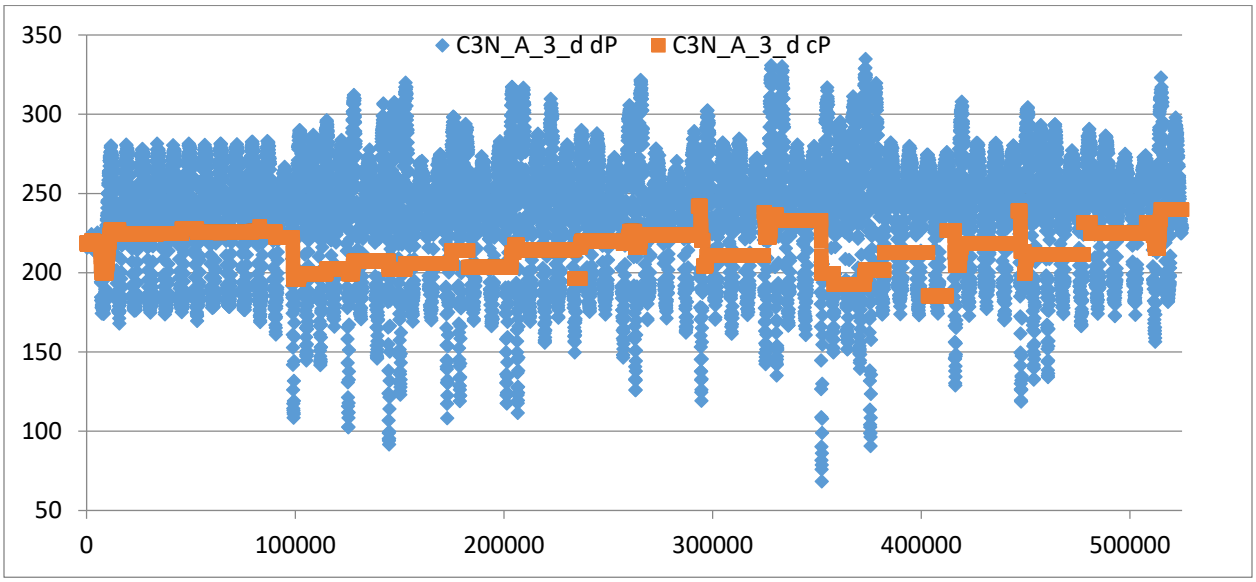

Figure 4.2: Time series chart of sensed backpressure (blue) and resetting of calculated critical pressure (orange)

at a) initial location with continuously degrading sensor resetting and b) revised location with stable sensor resetting.

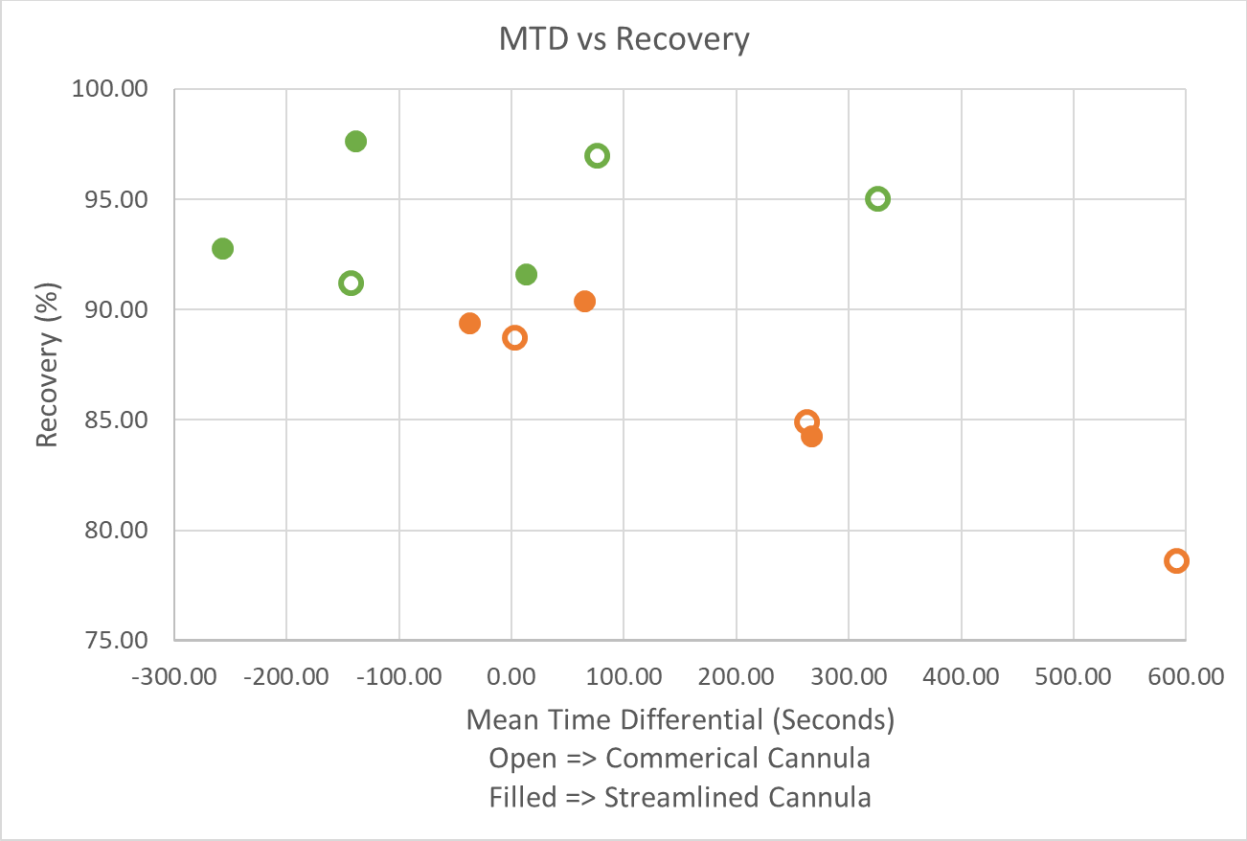

Figure 4.3: Mean Time Differential (MTD) versus total recovery for cases 2 and 3.

Downward trend in Case 3 (orange); however, no trend in Case 2 (green) tests.

Chapter 5: LVMH Human Safety Study

5.1 Introduction

Current systems for aerosol drug delivery to the lungs during high flow nasal cannula (HFNC) therapy are not efficient. Dugernier et al. (2017) reported that only 1-4% of the nebulized dose deposited in the lungs when using a jet or mesh nebulizer placed inline with a HFNC system. This study extended the Low Volume Mixer Heater (LVMH) device, previously developed for laboratory use by Spence et al. (2019), into a clinical testing environment. The LVMH device used in this study for combined HFNC therapy and high efficiency aerosol delivery included two vibrating mesh nebulizers to provide both HFNC airflow humidification and inhalation synchronized drug delivery, when desired. The system calculated drug delivery timing based on backpressure against the HFNC therapy airflow created by the subject's breathing profile, thus allowing drug nebulization to be synchronized to inhalation. This study's objectives were to perform a safety and tolerability study of the LVMH system in human subjects and to make an initial assessment of performance before a subsequent study on aerosol delivery efficiency to the lungs in human subjects.

5.2 Material and Methods

The data collection portion of this Human Safety Study was conducted at the VCU Medical Center North Hospital building over two days in December 2019. Prior to subject arrival all major equipment was organized within the room as shown in Figure 5.1 for efficient utilization of room space and subject time. Experimental equipment included, but was not limited to: vitals test cart, LVMH test cart, cannula fitting table, subject and facilitator chairs,

and a cleaning sink. Due to the multi-day experiment, project-specific supplies were organized on the LVMH test cart and stored in the hospital floor's equipment closet overnight. Data analysis of collected data occurred in multiple areas across campus, depending on equipment requirements while taking appropriate measures to protect subject privacy. For example, the post-study timing analysis of the breath profile characteristic points was performed on the campus library's 4K gaming monitor for better data visualization; but data was stripped of all identifying information.

Through the guidance, expertise, and substantial work of the staff at the VCU Johnson Center for Critical Care and Pulmonary Research, five healthy participants were enrolled and provided informed consent to participate in this study under Institutional Review Board (IRB) study number HM20016743. All subjects were prescreened for any exclusion criteria and were found eligible to enroll. The voluntary informed consent process was handled by the study facilitating nurse with the experimenter available to answer any specific questions. Due to monetary compensation for the study, participants were required to provide their Social Security Number or Tax Payer ID information, which was also handled by the facilitating nursing staff. The onsite nurse from the Johnson Center for Critical Care and Pulmonary Research performed all measurements and analysis of subject temperature, blood pressure, and blood oxygen saturation during the study.

The experimental test procedure, starting after informed consent, consisted of four main segments: cannula fitting, HFNC therapy demonstration, HFNC therapy with combined placebo drug treatment, and post-treatment observation. The cannula fitting segment involved using an in-house template to determine a matching interface with correct cannula prong diameter and prong spacing distance. Once this nasal interface was selected, cannula assembly and HFNC

therapy device warmup were performed simultaneously. Cannula assembly involved removing and swapping-in the chosen nasal interface in place of the prongs and cannula adapter from an Optiflow Nasal Cannula MR850 (OPT542, Fisher & Paykel Healthcare, New Zealand). Once the HFNC therapy device achieved stable operation, the temporary outlet filter was removed and the subject was connected to the therapy device. After one minute of therapy demonstration, combined therapy and placebo drug delivery operation was run for five minutes. This five-minute window was defined and analyzed post data collection and used for performance calculations. At the end of combination therapy, subjects were monitored for 15 minutes while the system was shutdown, cleaned, and reset. To help ensure experimental run timing and consistency, a reminder list, shown below, was printed and adhered to the test cart.

- Turn on air @ 30 LPM
- Turn on device and enable heat **3 min warmup**
- Start flow logging software
- Add saline to humidity nebulizer
- Start humidity nebulizer
- Record temperatures at 3 min mark
- Monitor temps for **5 min stabilization**
- Remind patient to breathe deeply
- Add saline to drug nebulizer
- Connect patient to airflow **1 min device adjustment**
- Flip switch to Enable **5 min saline delivery from drug nebulizer**
- Refill both nebulizers
- Disconnect patient from airflow **15 min monitor**
- Disconnect and stop recorders
- Turn off nebulizers and heat
- Save recorded output data
- Turn off airflow

To fulfill this study's objectives of testing safety and tolerability of LVMH and assessing performance before a subsequent study, multiple system variables were catalogued and monitored, including: Cannula Size, Subject Comfort, Subject Vitals, Breath Rate, Breath I:E

Ratio, Pressure Sensor Profile, and Nebulizer Actuation. Cannula fit had an important role in HFNC therapy, as it affects the system pressure. Therefore, one of nine different custom developed cannulae sizes was selected which provided approximately 50% open area within the subject's nostril and had prong centerlines matching the subject's nares centerlines. All nine cannulae were developed with identical tubing and rubber strap connections. The custom rubber straps were molded from Dragon Skin ™ (Smooth-On, Macungie, PA, USA) silicone rubber with end connections for the commercial fabric headband to hold the cannula to the subject. Subjects were asked about cannula comfort during the fitting process and were given the option to try another size if uncomfortable. Subjects were asked about system therapy comfort post testing and comments were noted in experimental notes. At any point the subject was able to remove themselves from the system in the event of discomfort. The subject's vitals of temperature, blood pressure, and oxygen saturation where measured at multiple points and served as an indicator of device safety. The developed system Control and Monitor Unit (CMU) recorded nebulizer actuation and pressure sensor values throughout the entire system operation. Figure 5.2 provides an image of the CMU and LVMH system on the experimental cart. For detailed CMU operation see Chapter 4.2 Materials and Methods pertaining to the laboratory experimental device validation work. See Figure 5.3 for the experimental device schematic depicting the CMU's connection and role of nebulizer and temperature control of the system. Post experimental determination and analysis of breath rate, I:E ratio, and actuation of drug nebulizer required more processing than benchtop experiments of previous studies, due to the lack of direct electronic feedback from the therapy subject regarding inhalation state.

During the experiment, the CMU interpreted and recorded the LVMH system airflow backpressure to determine inhalation start for drug delivery timing and to later assess the system

operation. During post-processing, each subject's breath timing information was found via transcription of the pressure data into a list of inhalation and exhalation start points. The raw timing data was organized such that the start of each drug nebulization pulse was associated with an inhalation and assigned a Time Differential (TD) value based on the time from its associated inhalation start point. Next, a breath-by-breath performance evaluation of the drug delivery system was conducted for each subject. A breath with Correct Delivery (CD) was defined as a single one second pulse of the drug nebulizer timed such that drug would fully exit the nasal cannula prongs only during the first 90% of the subject's inhalation time. The CD delivery timeframe was reduced by 10% of the entire inhalation duration to account for HFNC therapy airflow mismatch and expected sufficient time for deposition in the lungs. See Figure 5.4 for a labeled example of a CD breath system response. For each subject, the number of breaths containing a CD was tallied and divided by the total number of breaths to determine a Correct Delivery Ratio. Breaths without a CD were identified, grouped by error type, tallied, and converted to percentage ratios based on the total number of incorrect deliveries. Error types were set as: Multiple Delivery (MUD) error in which multiple pulses of drug nebulization occurred; Missed Delivery (MID) error in which a single pulse of drug nebulization occurred but was timed such that some drug reached the subject outside the first 90% of inhalation time; and No Drug Delivery (NDD) error in which a drug nebulization did not occur during the breath. See Figure 5.5 and Figure 5.6 for labeled diagrams of MUD and MID errors, respectively.

5.3 Results

All five enrolled volunteers completed the experimental study and showed no significant adverse effects nor significant discomfort. Subject vital signs, recorded during the experiment, were as expected and are listed in Table 5.1, organized by subject identification number. Breathing frequency and I:E ratio, calculated after the experiments from pressure readings, are presented in Table 5.2 along with device performance metrics. Among the enrolled subjects there was a range of breathing frequency, 3.5–10.4 breathes per minute, which provided a realistic challenge for the device timing algorithm. The breath pattern variability for each subject, as measured by the coefficient of variance (CV), was highest in Subject D at 38.7%, and this subject also had the lowest CD ratio of 11.8%. However, the lowest breath frequency CV of 15.9% in Subject E did not correspond to the highest CD ratio of 86.4% in patient B. Subject E's low CD was mainly due to the control algorithm's method for handling pressure spikes which caused several breaths to go undetected. In respect to high efficiency delivery, NDD error is least concerning due to the lack of drug waste. However, it does increase treatment time to achieve the full prescribed nebulized dose. Considering the overall type of delivery error experienced during experiments, most (57.7%) were due to missing the defined window of delivery. These MID errors result in reduced drug delivery efficiency due to exhalation losses. A large portion of these errors were associated with Subject C who had the largest breathing frequency, therefore shortest breath length and smallest interval for CD. Approximately one third of the overall errors across subjects were MUD errors. During the experimental treatment procedure, MUD error only slightly decreased drug delivery efficiency because most of these errors still contained a one-second nebulization period correctly timed plus an additional short burst of nebulization incorrectly timed due to the CMU falsely determining the inhalation start point.

5.4 Discussion

This study successfully tested a device that was tolerable and safe for additional human subject studies and it brought to light additional challenges that need to be addressed for additional predictability among subjects. The breath algorithm self-adjusted to nebulize drug for 94.8% of the 191 breaths taken by the five subjects; however, only 45.5% of all administrations were delivered without error. Caution should be taken when evaluating the sensing algorithm based solely on the concept of "Correct Delivery" and error type as defined by this study. There is currently no data directly linking the "Correct Delivery" criteria to high nor low delivery efficiency. Additional software improvements would decrease the required treatment time and increase delivery efficiency for individual subjects with lowest device performance. Possible software improvements include: pulse length variability, increased data refresh rate, and inhalation prediction algorithm adjustments. Data recorded from this study can be used to test performance during development of new breath sensing codes. Although breathing time parameters were able to be determined, future studies would benefit from the inclusion of airflow volume data collection for additional data verification. Besides code improvements for increased efficiency, future study subjects should be reminded to concentrate on breathing steadily and not talking nor laughing during the period of pharmaceutical aerosol administration, possibly helped by mentally counting during each inhalation and exhalation cycle.

The cannula fitting and assembly process, which used the developed template to help determine size, went relatively smoothly. The template eliminated most of the guess-and-check selection process used in pre-study simulations. The cannula strapping system connectors failed

during the sizing of an individual but functioned correctly once properly adjusted. These connections were developed for direct integration into the now-discontinued OPT54X series nasal cannula head straps. The newer OPT94X series head straps are redesigned and could provide more reliable function during setup conditions. However, the OPT94X series also contains a redesigned inlet tubing connector requiring a new tubing adapter design. The time intensive cannula setup process caught the attention of medical staff as an area of possible concern for future clinical application. Future cannula design considerations include limiting the number of available sizes and preassembly of the cannula unit.

5.5 Tables

Table 5.1: Subject Vitals

ID	Temp (ºC)			Blood Pressure (mmHg)			SpO_2 (%)		
	Base	**1 Min**	**5 Min**	**Base**	**1 Min**	**5 Min**	**Base**	**1 Min**	**5 Min**
1	37.1	36.9	36.9	123/83	134/75	131/79	98	98	96
2	36.5	36.5	36.5	133/78	123/79	136/66	96	96	97
3	37.0	37.0	37.0	122/79	111/77	117/86	96	96	96
4	36.6	36.5	36.7	117/68	106/85	109/72	98	98	98
5	36.7	36.5	36.9	133/83	129/77	120/78	99	99	97

Table 5.2: Subject breathing characteristics and device performance

Subject	Breath Freq per min (Mean±SD)	Breath Freq CV	I:E Ratio 1:X (Mean±SD)	I:E Ratio CV	Correct Delivery (%)	Multiple Delivery Error (%)	Missed Delivery Error (%)	No Drug Delivery Error (%)
A	5.8±1.3	21.7	2.5±0.6	23.8	84.6	50	50	0
B	3.5±0.7	18.9	3.8±0.8	21.7	86.4	0	33	67
C	10.4±2.5	24.2	2.3±0.6	26.0	24.7	16	78	5
D	8.6±3.3	38.7	3.5±1.6	45.2	11.8	63	33	3
E	4.1±0.7	15.9	4.2±0.9	21.2	56.5	30	30	40

5.6 Figures

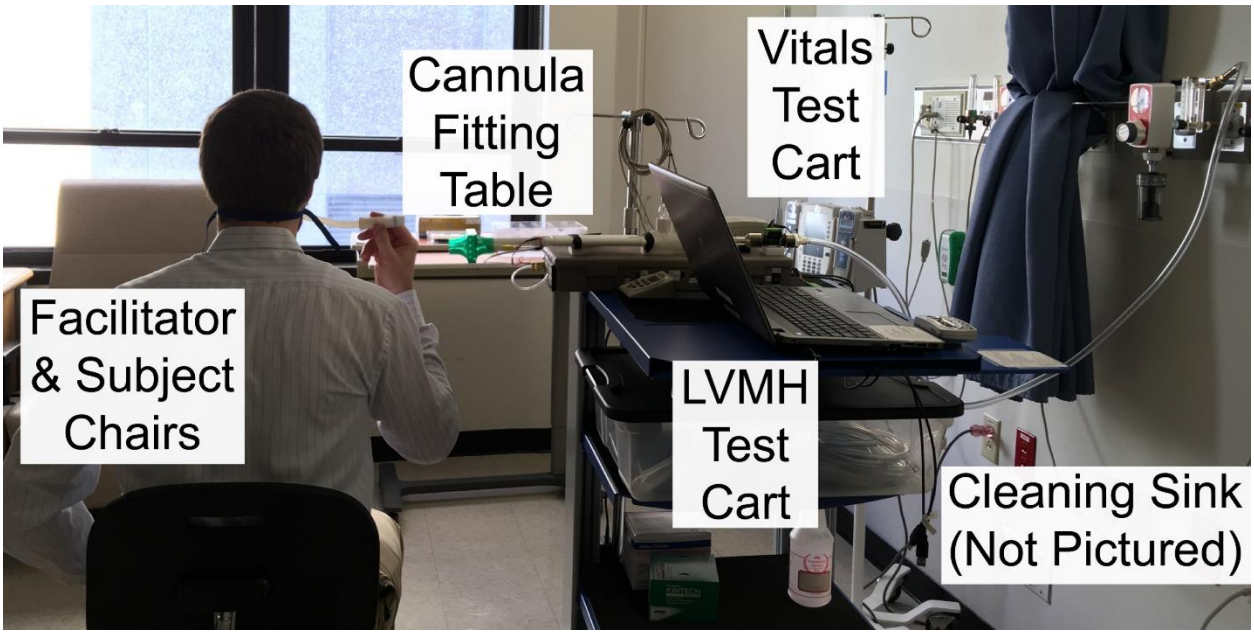

Figure 5.1: Room layout for conducting human subject study

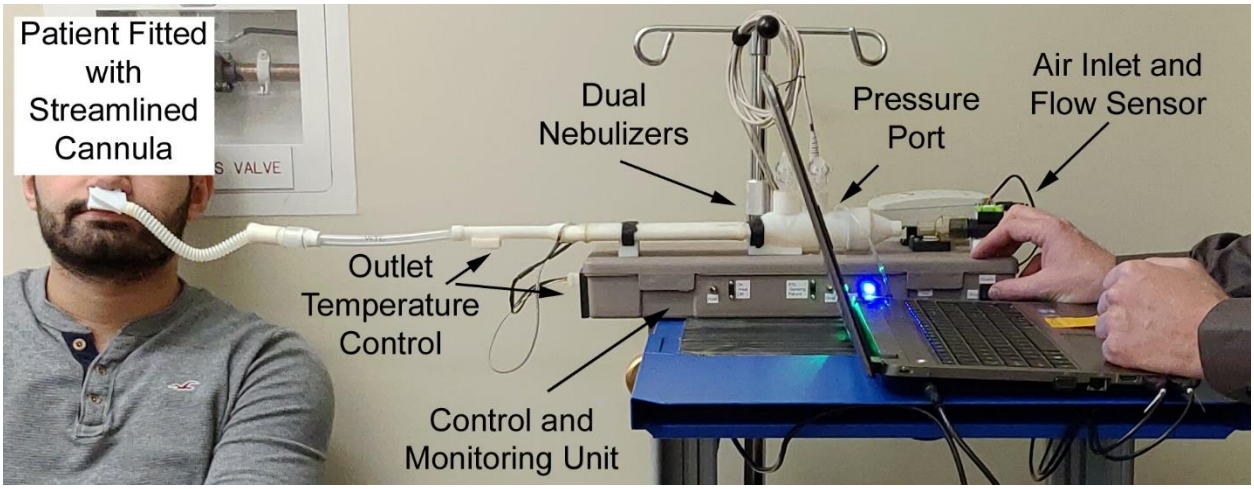

Figure 5.2: Experimental setup with example subject connected to LVMH

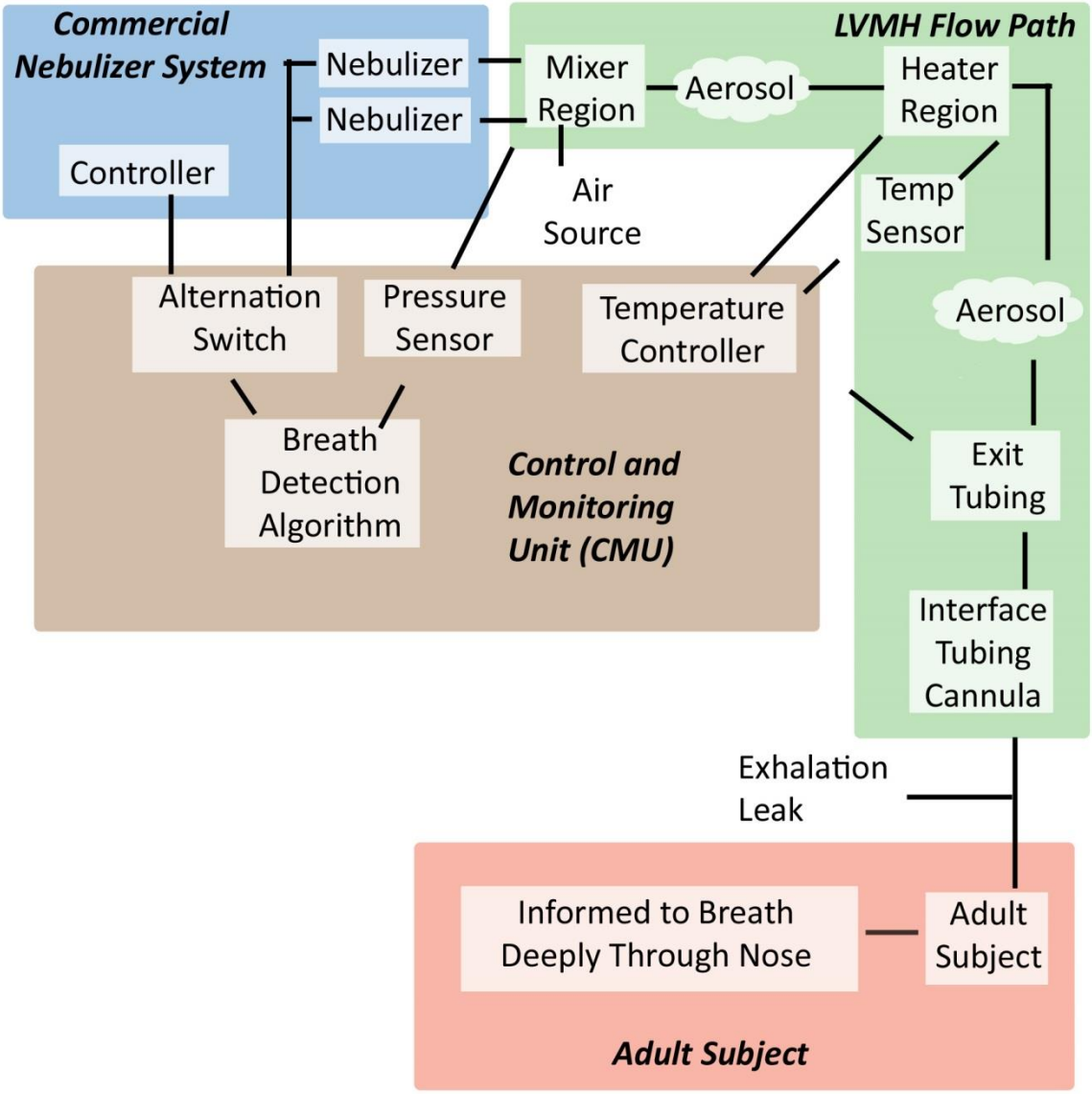

Figure 5.3: Experimental system setup diagram for human safety study

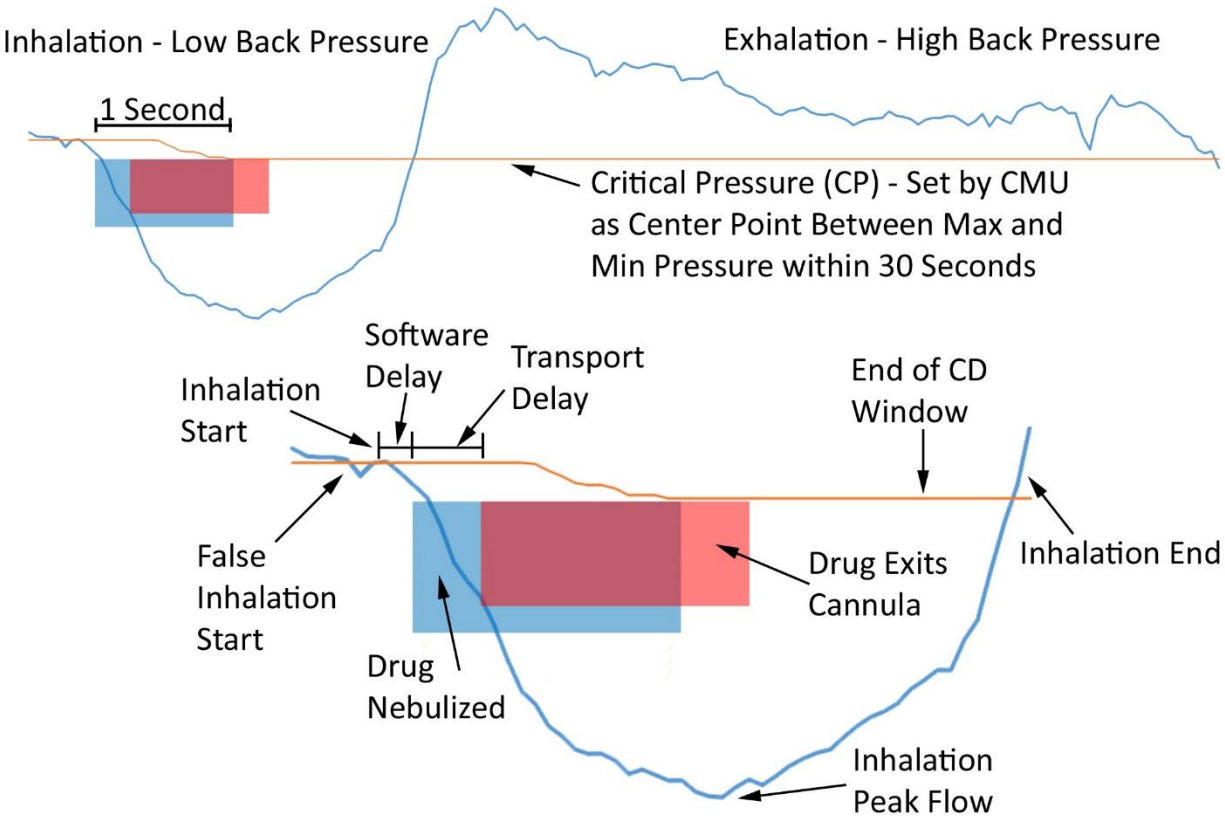

Figure 5.4: Correct Delivery (CD) monitored breath pressure profile example

Drug nebulization (blue box) starts after a short software delay and last for 1 second. Drug exits the cannula (red box) after traveling through the device.

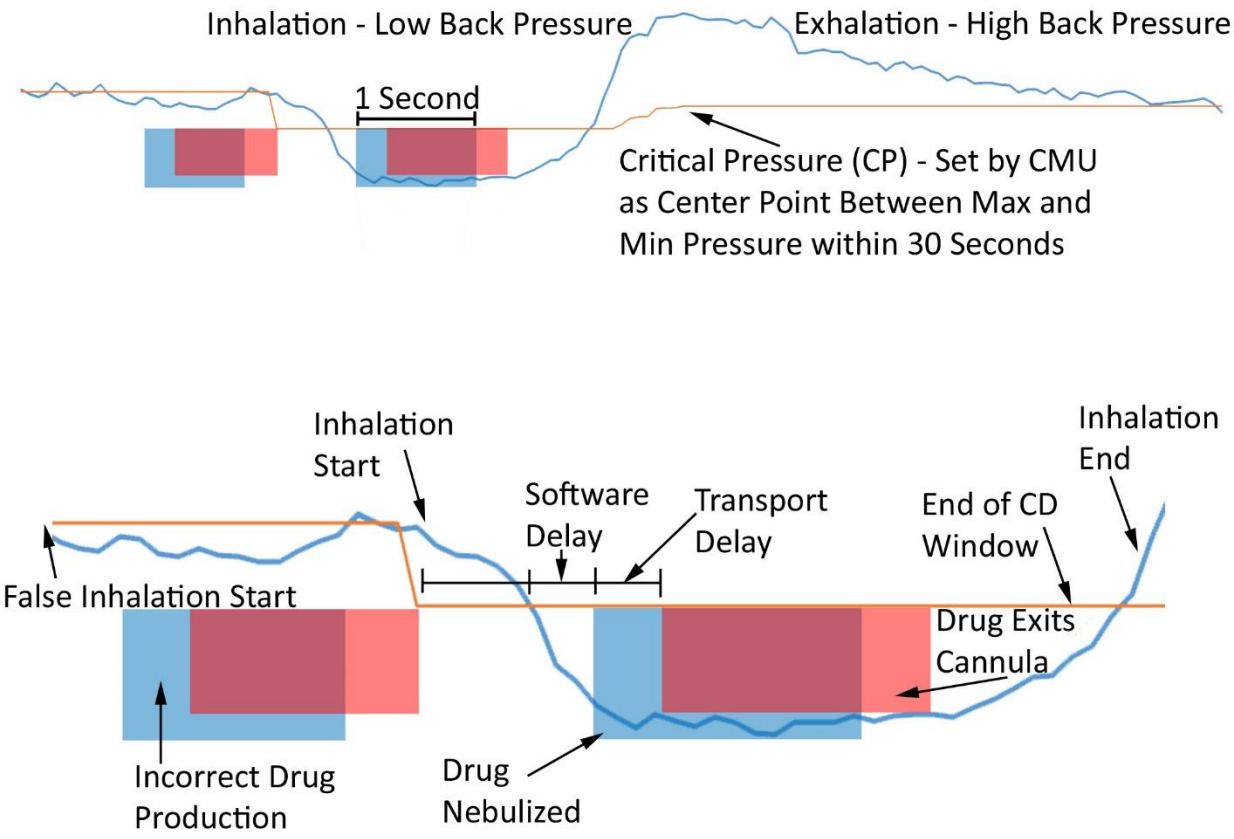

Figure 5.5: Multiple Delivery (MUD) error monitored breath pressure profile example

Drug nebulization (blue box) starts after a short software delay and last for 1 second.

Drug exits the cannula (red box) after traveling through the device.

MUD errors have an additional incorrect drug production associated with the breath.

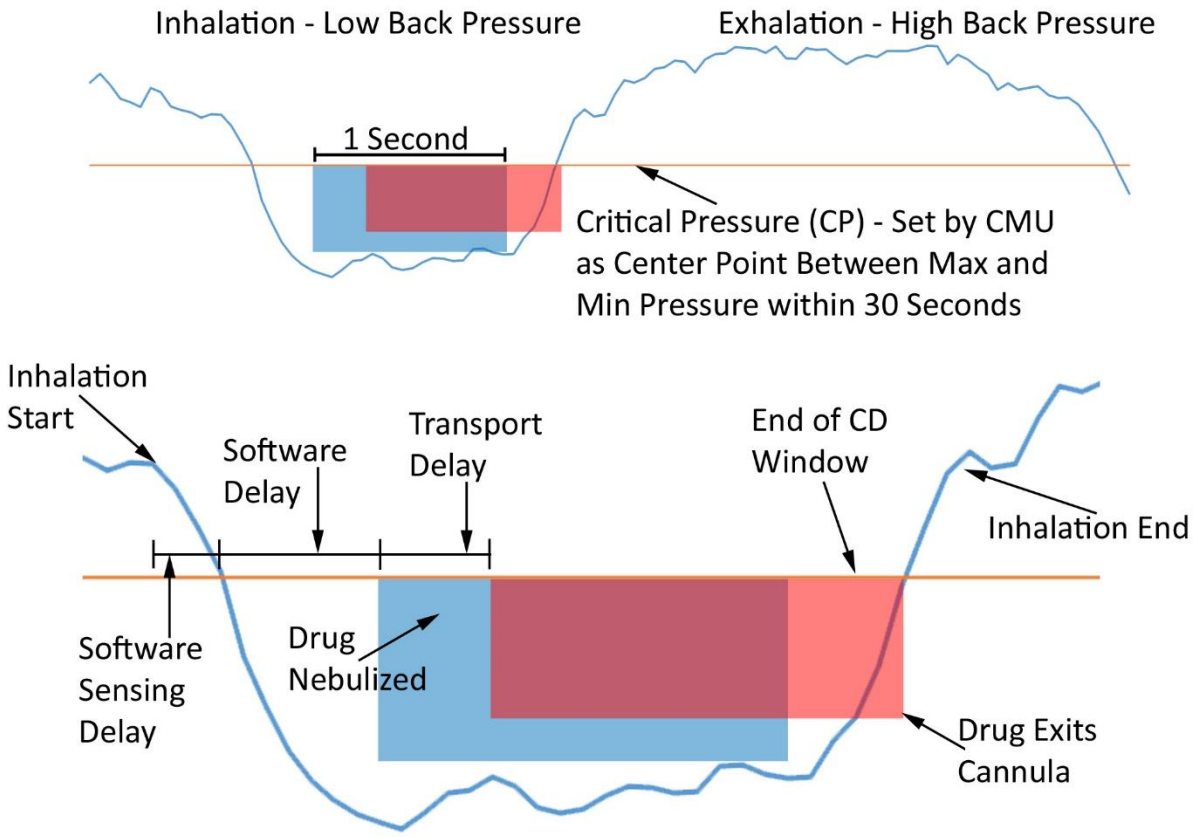

Figure 5.6: Missed Delivery (MID) error monitored breath pressure profile example

Drug nebulization (blue box) starts after a short software delay and last for 1 second.

Drug exits the cannula (red box) after traveling through the device.

MID errors have drug exiting cannula after the end of CD window.

Chapter 6: Applying Lessons Learned to Infant Subjects – The iLVMH

6.1 Introduction

Efficient nose-to-lung delivery of aerosols to pediatric and especially infant subjects is a complex and challenging research field. DiBlasi (2015) offers a comprehensive review commentary on the struggles facing researchers and clinicians attempting to administer pharmaceutical aerosols to infants. One challenge is the small passageways of the pediatric and infant lungs. The Low Volume Mixer Heater (LVMH) was designed for delivery of particles through the small and turbulent nasal region of adults (Spence et al. 2019). Boc et al. (2017) tested a modified adult LVMH system delivering nebulized albuterol sulfate solution to an infant *in vitro* nose-throat model created by Bass et al. (2019). The exploratory study of Boc et al. (2017) achieved significantly larger estimated lung dose during steady-state inhalation with the modified adult LVMH (76%) compared to a standard-of-care front-loaded mask (14%) and prompted continued research. However, this study made several assumptions to reduce the real-world complex system such as interface shape tolerability and system flow characteristics. Specifically, two breath patterns were utilized, steady state and a sinusoidal profile, with drug delivery initiated from the lung simulation machine timing information and not pressure sensing. Additionally, this study assumed no movement of the nasal interface and utilized rigid cannula prongs for consistent curvature. Although high lung delivery efficiency estimates were found, the small infant tidal volumes, as compared to the adult LVMH system volume, caused poor emptying and unrealistic timing challenges.

Aerosol particle size is a large determinate of deposition location during inhalation with smaller sizes generally depositing deeper. Modifications to the Aerogen Solo nebulizer system led to a decrease in aerosol MMAD to 3.8 (0.6) μm as measured on an Andersen Cascade

Impactor (ACI, Nottingham, United Kingdom) operated at 30 LPM (Boc et al. 2017). Both decreased post-production coalescing and decreased extrusion momentum could have led to a reduction in observed sizing, however the exact mechanisms were not investigated. These modifications which decreased initial particle size not only benefited particle transport but also reduced drug mass production rate, possibly lengthening therapy times.

The objective of this study was to apply lessons learned from creation of the LVMH into an EEG delivery system for infant subjects. Key attributes of these systems include continuous nasal cannula therapy airflow, heated airflow delivery, modifications to commercial aerosol production devices, and custom flow pathway designs.

6.2 System Methods and Materials

This section summarizes three designs that were tested and subsequently revised to address specific shortcomings in the previous infant LVMH design. The systems were designed through a series of prototype iterations utilizing CFD and reworking technology to address the unique requirements of infant populations. In short, multiple devices were developed, jointly tested experimentally with various methods, analyzed, and remade to overcome shortcomings. Design, construction, and initial testing were performed for this dissertation; however, the additional experimental work and CFD concept testing were performed by other individuals on the VCU research team.

6.2.1 Infant Design Criteria Goals

Numerical targets for this population differed drastically from the adult system. The High Flow Nasal Cannula (HFNC) airflow target was reduced to 5 LPM at a temperature of 32 °C ± 2 °C with 30% relative humidity. Stock aerosol production rates of the Aerogen Solo nebulizers would oversaturate the airflow with water vapor preventing droplet evaporation at these airflow rates and therefore required reduction. A new target of 0.04 mL/min from the nebulizer was specified based on thermodynamic calculations. Newborn infant tidal volumes of approximately 30 mL factored into the decision to set a post-drug-production device volume goal of approximately 5 mL; however, tidal volumes for this population span a wide range and are heavily influenced by age and weight. The system would also need to be able to handle inhalation times as short as 0.5 seconds. Not all goals were achieved by each device iteration; however, these challenging goals were imposed with the realization that pediatric application design specifications could be much easier achieved.

6.2.2 Initial iLVMH with Preheating

A preheated design was developed to position the nebulizer very close to the subject and move the high temperature heating element away from the subject. The separate and independent heating system built for this system was capable of heating 5 LPM of air from a pressurized cylinder to 43 °C with adjustment to other outlet temperatures as needed. Heating beyond the target inhalation temperature of 32 °C was required due to the cooling associated with the evaporation of the liquid droplets. The separate temperature control unit and heater element were housed in a box and were powered from a standard 120VAC outlet. In this version of the iLVMH, aerosol mixed into the heated air stream leading to both evaporative cooling to the

design criteria temperature of 32 °C and RH goals (30%) and EEG dry particle formation. Analytically calculating the energy available and the energy required for the evaporation of liquid from the droplets, nebulization rates on the low side of 0.033 – 0.07 mL/min were first proposed. The rate was eventually set to 0.04 mL/min. The body of the iLVMH was 3D printed to include an inlet unifier, nebulizer ports, and tapered mixing region with internal dimensions of approximately 5mm x 15mm x 50mm (See Figure 6.1). The device outlet connected to 4mm tubing for use with previously developed streamlined infant nasal cannula and nose-throat model (Bass et al. 2019). Estimated volume of this device downstream of the drug nebulizer was approximately 5 mL, not including cannula tubing.

6.2.3 Initial iLVMH with Single Channel Downstream Heating

A scaled down version of the LVMH was developed using a rectangular vertical heating region with various construction techniques. The upper portion of Figure 6.2a shows an intermediate design construction method including integrated nebulizer mesh holders and side-slide style insertion of heating elements. Final heater construction of this single channel design mimicked the wrapped heater style of the LVMH, but at a smaller scale, using the 3D printed jigs shown in the lower portion of Figure 6.2a. Slots to assist in assembly and allow more direct thermal imaging were placed in the heating region outer shell. Nebulizer ports were utilized for aerosol injection into the vertical mixing region. Inlet and outlet 4mm tubing connected via a press fit into the device for experimental delivery to pre-existing models. Device CAD was created for 3D printing and Figure 6.2a presents a labeled rendering of the developed and produced singled channel iLVMH. The system was designed to fit onto and to be controlled by the LVMH CMU, with simple adjustments to code setpoints. Combined dead space of the unit

was still higher than desired for infant spontaneous breath sensing applications and aerosol delivery with a 30 mL tidal volume. Experimental testing of this device was conducted by collaborators at the VCU School of Pharmacy.

6.2.4 Revised iLVMH with Dual Channel Downstream Heating

The final revision of the iLVMH utilized a dual channel heating section between the nebulizer and outlet. CFD simulations performed by Dr. Longest suggested incorporation of a 10 cm dual channel heating region with heat input from all sides for additional experimentation. This system, referred to as Design 18 in the CFD work, split the flow into two 5 mm square channels for heating and utilized a 28.7 cm section of 4 mm ID tubing for aerosol transport and subject interface. This nasopharyngeal tubing was modeled with a specific curvature and meant to insert approximately 7 cm into the nasal passage as a nasopharyngeal tube. The CFD simulations predicted nominal particle residence time of Design 18 through exit of the tube was 0.09 seconds at expected operating conditions. The CFD simulated Design 18 had the drug nebulizer central axis 5 mm from the beginning of the metal heating region and mesh surface level with the mixing region's upper wall. Iterative CFD and experimental work led to the fabrication of Design 18 for experimental testing.

Experimental construction of the dual channel iLVMH, referred to in prototyping and experimental work as D18, mimicked CFD closely while balancing realistically feasible device construction. Lack of readily available dual square 5 mm channel tubing meant that two square tubes were connected together thereby increasing the separation distance of the channels. The two pieces of approximately 5 mm x 5 mm internal dimension aluminum tubing were brazed together and then excess brazing material removed to form smooth surfaces (See center-right

side of Figure 6.3b). Flat Kapton-covered electrical resistance heaters where applied with thermally conductive grease to the upper and lower outer surfaces. A thermocouple was also applied to the bottom surface before an aluminum wrapping was applied to the heating unit to secure components and dissipate heat to all parts of the metal channel. This heating subsystem was inserted into the 3D printed flow path and components were epoxied together. The mixing region contained an inlet unifier and tapered outlet connected to tubing which was secured to a positioning guide and inserted into the nose-throat model (See Figure 6.3b). New modifications to the 6-month-old nose-throat model, originally created by Dr. Bass (Bass et al. 2019), were made to accept the nasopharyngeal tube insertion. The tracheal filter at the model outlet was connected to the lung simulator. The iLVMH device was able to be connected to the LVMH CMU for experimental operation with nebulization triggered by the lung simulator. For intended performance with pressure sensing nebulization triggering, the Dual Channel iLVMH needed advanced controls with faster response times for experimental testing.

6.2.5 Aerogen Solo Nebulizer Modification

Modifications to both the physical form and electrical control of the commercially available Aerogen Solo nebulizer were required for application in these studies. Physical changes to the vibrating mesh holding structure brought the mesh output surface closer to the flow path. The blue Kobalt round hook tool found in our lab easily disengaged the tabs of the mesh retainer structure for removal from the lower structure. A Dremel attachment was designed for easy alignment and cutting off of the lower 15.0 mm of the Solo outlet skirt (See left side of Figure 6.3a). Once the structures were cut, cleaned, and beveled, the pieces were superglued together for original functionally simply without the lower section of outlet skirt. Electrical control

changes were implemented to reduce liquid output rate and droplet exit velocity for the Aerogen nebulizers. Specifically, the normal Aerogen ProX Controller was removed from the system and replaced by a signal generator plus an amplifier to provide $87V_{PP}$ (~$24V_{RMS}$) to the nebulizer (See Figure 6.4). The Rigol DG10220 Waveform Generator supplied a sinusoidal signal to the TS200 Modulated Power Supply which supplied the necessary voltage and current boost to drive the piezoelectric element attached to the nebulizer mesh. Through the variable voltage input of the signal generator, production rates ranging up to approximately 0.55 mL/min were achieved (See Figure 6.5).

6.2.6 Control System Details

Infant breathing rates of 60 breaths per minute are much higher than the adult breathing rates for which the original LVMH CMU was designed to operate. Estimated inhalation period in an infant is 0.5 seconds equating to 500 milliseconds (ms), leading to errors when directly using the original CMU. Nyquist's theorem suggests the sampling of the system pressure must occur at least every 250 ms to accurately reconstruction the breathing pattern. However, due to the CMU operational programming code design, sampling must be much faster than 250 ms for the system to function properly. Original microcontroller loop times were 20 ms when operating nebulizer control from ASL5000 signals and 110 ms when checking the pressure sensor for nebulizer control. A major reason for this loop time increase was the required minimal 45 ms delay when using the *single-pressure-reading* call-function. The Sensirion sensor had capability for down to 0.5 ms reads when using *continuous-pressure-reading* call-functions, but this feature was not implemented because the workload of additional coding was outside the parameters of the adult LVMH studies. A Honeywell pressure sensor used in our research group had similar continuous

read speeds (~0.5 ms) and was implemented into new CMUs. Quick temporal response from the pressure sensor moved the bulk of the computational time to data processing and decision making. Updated control system components implemented in later studies (See Chapter 7) could control the iLVMH systems with minimal modifications.

6.2.7 CFD Simulations of Nasopharyngeal Interface

The tight aerosol administration timeline forced by infant breathing rates presents a challenging hurdle for drug delivery. CFD work performed by members of the VCU research team focused on steady-state simulations in initial design stages. A priority of this work was the system development for production of EEG aerosols with outlet conditions within design specifications. Adding the more invasive (but commonly used for resuscitation) nasopharyngeal tube potentially decreases drug depositional losses in the nasal region and increases the window for synchronized delivery. CFD simulation utilized a specific curvature within the delivery tubing, and the experimental setup mimicked this closely. Exact curvature within the model was modified and followed an expected path based on the actual model geometry. The intermediate tube section was positioned via a guide based on CFD simulation geometry and experimental insertion depth. Of note, neither the CFD simulation nor the experimental nasopharyngeal tubes contained outlet modifications, such as angled cuts or dual openings, found on some commercial tubes for reducing risk of tube occlusion during treatment. This assumption of a simple straight cut was justifiable due to the controlled testing conditions with lack of movement from a model subject.

6.3 Results and Discussion of Future Applications

It was hypothesized that moving to pre-heated mixing air would drastically reduce device volume between the nebulization and subject while still retaining aerosol evaporation capabilities. The reduction in nebulizer output meant that the energy in a pre-heated stream of air was theoretically enough to fully evaporate excess water from the aerosol thus enabling this heating design change. Unfortunately, evaporation performance was not as high as expected; possibly due to inadequate turbulent mixing in the device. Further lowering of the nebulization rate would have even more severely limited the deliverable drug mass capability. However, reducing nebulizer-to-subject device volume greatly benefited aerosol synchronization timing in regards to travel time. Additionally, separation of the heat source and associated wires from the downstream side reduced heat-injury risk, clutter, and device bulk at the face. Overall, the preheat design failed to meet expectations of the hypothesize and design changes were considered.

The single channel downstream heating system (heater placed between the nebulizer and subject) was found to successfully reach outlet conditions and sizing goals. This experimental system produced an aerosol of 0.7 μm MMAD (Dhapare et al. 2018). Working on the setup of this study highlighted the lack of temporal resolution in the adult LVMH CMU that was supporting the iLVMH testing. Using control signals from the ASL5000 for breath synchronization, Dhapare et al. (2018) achieved 65% peak estimated lung dose, starting nebulization 0.2 seconds before *actual-inhalation-start-time*; with lower lung does on either side of this timing mark. The estimated lung doses of this novel delivery system in preemptively-triggered delivery tests were extremely high compared to the single digit efficiency found during *in vivo* tests of commercial delivery systems (Fok et al. 1996, El Taoum et al. 2015).

Further wholistic analysis of the system moved the interface design from a dual pronged nasal cannula to a nasopharyngeal tube. Combined with the new dual-channel lower-volume mixing region, the D18 version of the iLVMH system can potentially achieve correct outlet conditions and timing characteristics suitable for spontaneous inhalation aerosol delivery. Unfortunately, this design was never fully tested due to various delays and external factors. Although the single channel metal tubes were readily available, sourcing a dual channel tube delayed the project. Additionally, software development for increased sensor speed added unforeseen delays. Uncertainty and difficulties surrounding physical insertion of the nasopharyngeal tubing into the developed model added to poor project timing. These delays eventually lead to the project falling behind while development of the new HDS for delivering COVID-19 therapies took precedence.

For infants, developmental resources were strategically moved away from the iLVMH project towards alternative in-house dry powder devices showing excellent delivery performance of EEG aerosols. Externally, Aerogen developed and has been running human subjects trials of nebulized aerosol treatment strategies for infants. Their system utilizes a new mesh head design with a decreased droplet size compared to the Solo's mesh head. This new mesh does not produce EEG particles; but, the reduction in particles size, due to the new design, likely benefits the system's deliverable lung dose. The aerosol production occurs very close to the non-invasive ventilation nasal cannula for minimal volume and increased synchronization benefit. Perhaps successful Aerogen clinical trials and successful LVMH *in vivo* preclinical trials will spur increased motivation for addressing the final major challenges of the iLVMH system.

Work related to the iLVMH projects was a useful exploration and investment by the VCU research teams. The iLVMH served as an additional testing grounds for laboratory

technology. Direct integration of the Aerogen Vibrionic mesh unit into our laboratory's devices was first explored and implemented in the single channel postheat iLVMH device. Our lab has recently developed a functional holding structure for the Solo piezo mesh element for use in separate projects. Operation and testing requirements for the iLVMH population stretched and enhanced the control system knowledge base for later use in multiple projects. Additionally, multiple heat path development technologies placed in the LVMH were originally investigated in iLVMH prototypes. Although additional iLVMH development was paused, multiple useful engineering concepts were explored during experiments.

6.4 Figures

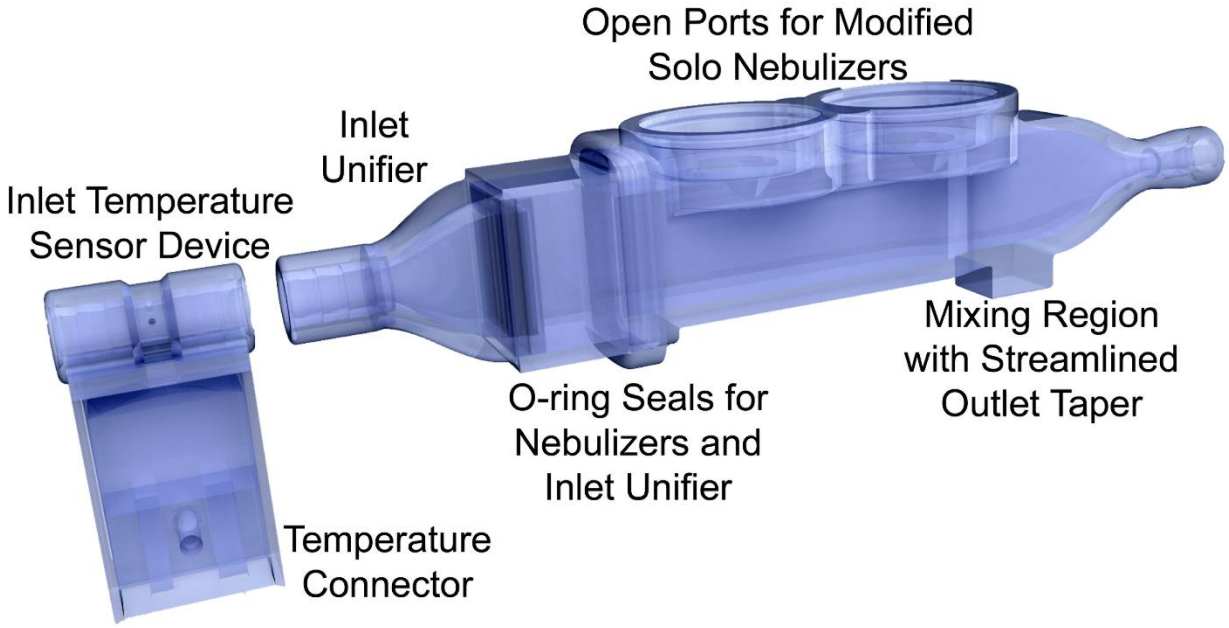

Figure 6.1: Pre-heating configuration of iLVMH

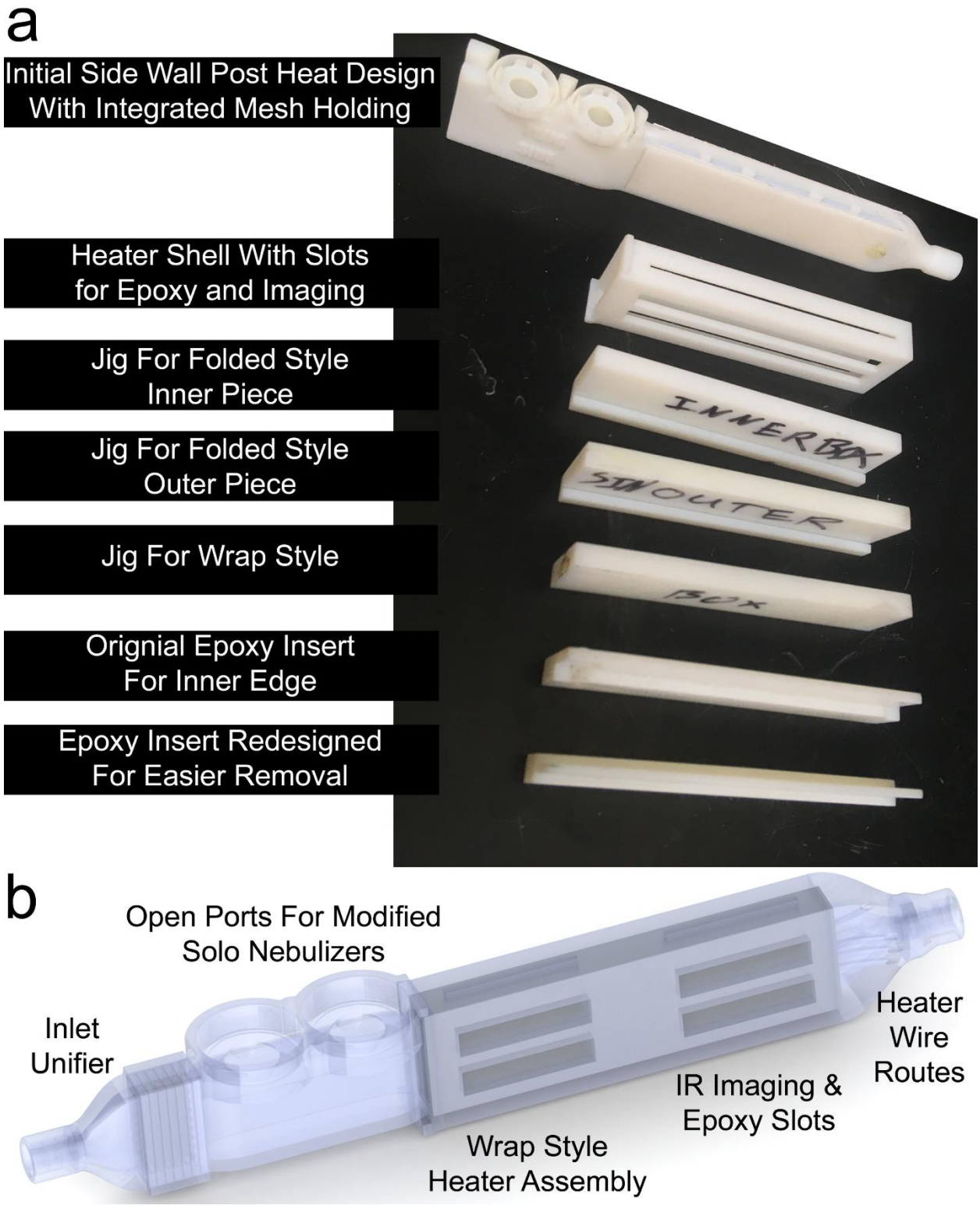

Figure 6.2: Post-heating **(a)** construction elements and **(b)** configuration of the iLVMH

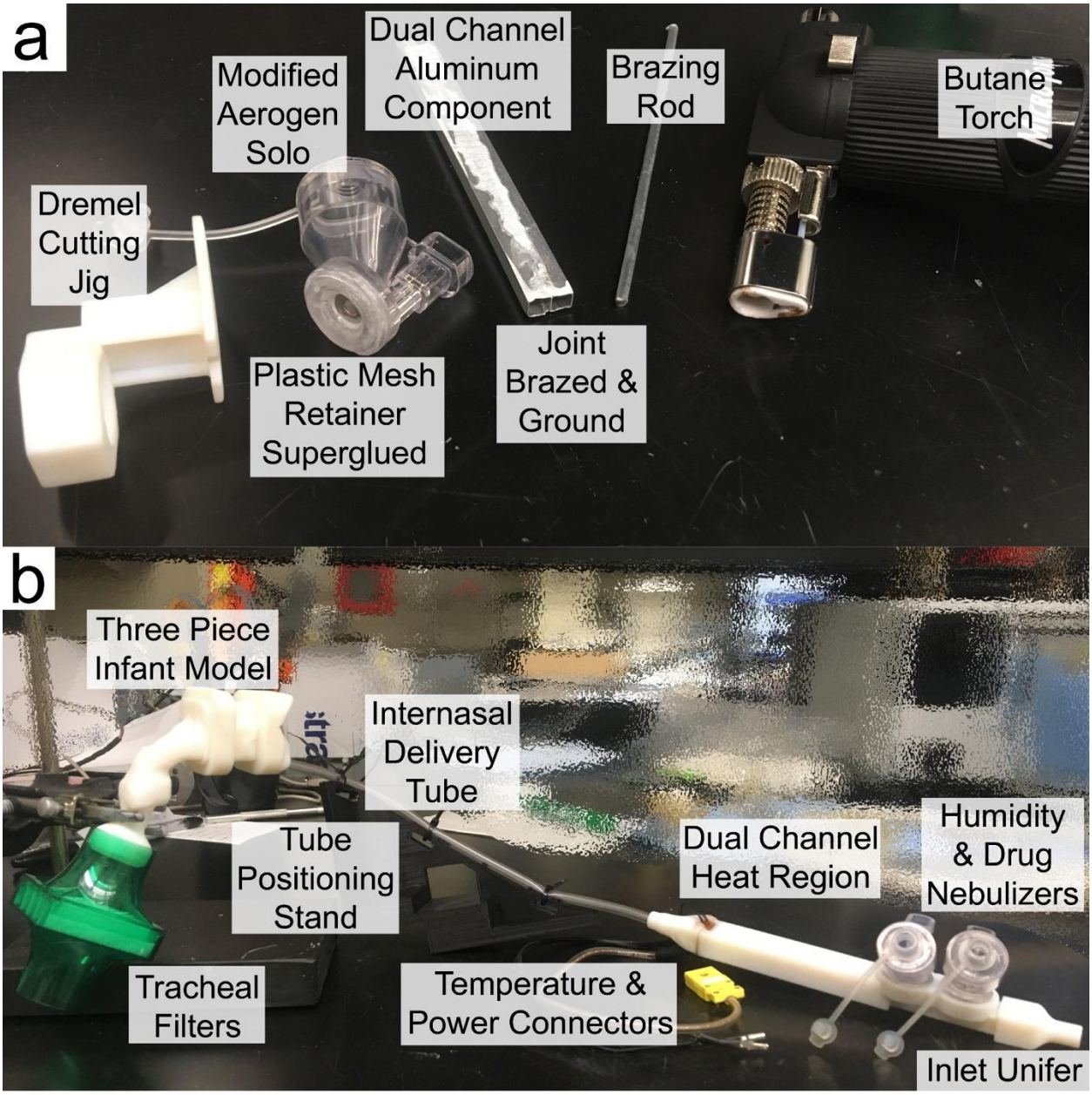

Figure 6.3: Post-heating dual channel nasal tube device version **(a)** construction elements and **(b)** experimental configuration of the iLVMH Dual Channel version

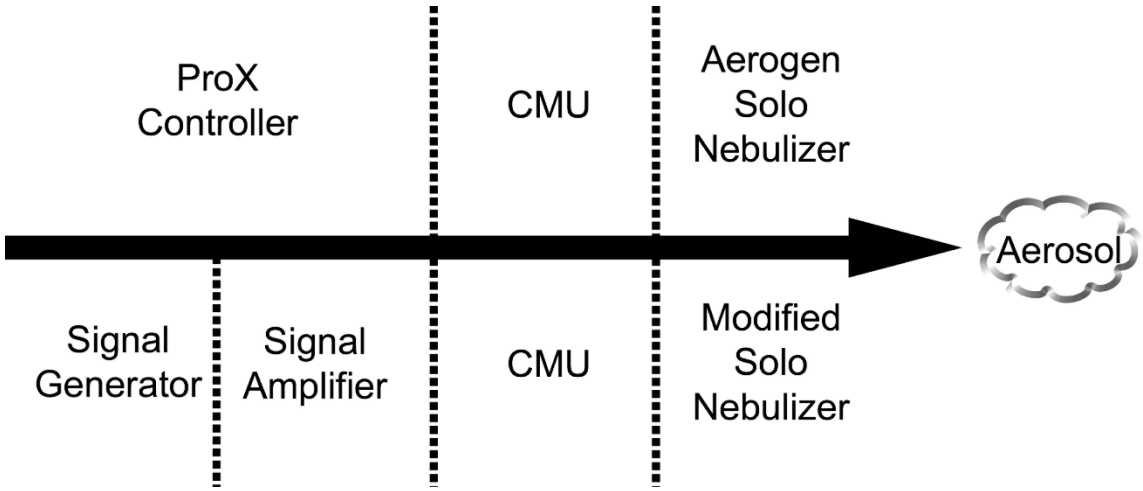

Figure 6.4: Aerogen Solo modifications with upper half showing adult information flow and lower half showing infant information

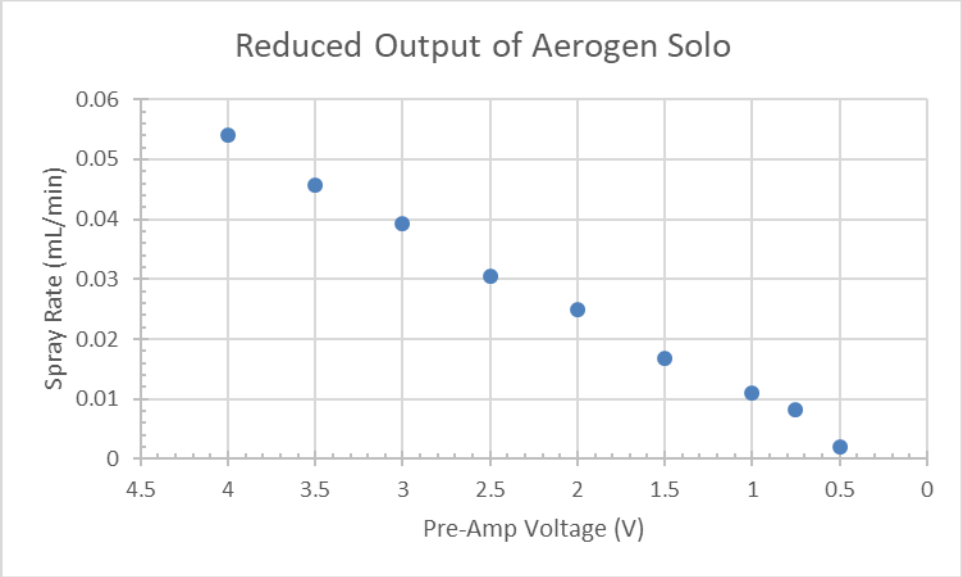

Figure 6.5: Graph of the modified Aerogen Solo nebulizer output rate when using the modified electronic control system leading to overall reduction in output.

Chapter 7: Development of an HDS Platform for High Efficiency Administration of Nebulized Aerosol

7.1 Introduction

Many available nebulizer-based inhalation devices waste a large portion of the aerosolized drug leading to low and highly-variable lung delivery efficiency. Three major elements driving low delivery efficiency are poorly timed aerosol production with respect to the inhalation cycle, device losses, and extrathoracic deposition. Simple device spacers, a passive method of aerosol timing, have been implemented for many years and have been shown to increase the efficacy of nebulizers (Pitance et al. 2010), but they also increase overall device losses. Active methods of aerosol synchronization have been implemented in devices to reduce or eliminate aerosol production during exhalation (Nikander et al. 2010), however many devices lack the ability to integrate with breathing support therapy. Devices that combine multiple approaches to increase delivery efficiency achieve the most substantial improvements in lung delivery efficiency (Longest et al. 2019). Commercially available devices fail to address all three aspects adequately and none can directly produce Excipient Enhanced Growth (EEG) aerosols for inhalation.

Previous work developed and tested a combination device for high flow nasal cannula (HFNC) therapy and EEG aerosol production (Spence et al. 2019, Spence et al. 2020, Spence et al. 2020). This chapter's study utilized key components and underlining technologies of this previous work to develop a stand-alone heated dryer system (HDS) for high efficiency and high dose EEG aerosol administration to human subjects through oral inhalation. HFNC therapy breathing support has grown in popularity over the years and has several advantages over invasive mechanical ventilation. However, the onset of the coronavirus global pandemic greatly

complicated the use of this therapy. Additionally, the pandemic complicated the human subject testing of devices, especially ones that might increase the spread of bioaerosols. Therefore, the HDS does not incorporate the continuous high flow air support for the transport of aerosol to the subject. In intended operation of the HDS, the subject draws breathing air from the environment through a device filter into a mixing region. Aerosolized drug droplets from a single nebulizer combine with the inhalation air and travel through the heating region forming an aerosol of EEG particles that continues towards the subject via flexible tubing and an attached mouthpiece (See Figure 7.1). The subject's exhalation air travels the reverse route leaving through the device filter to capture remaining drug aerosol and potential exhaled droplets. The HDS flow path is attached on top of the Control and Monitoring Unit (CMU) that manages aerosol administration, heating input, and operational interface. The specific timing of aerosol administration is informed by the sensing of the internal device pressure. This internal device pressure is physically linked to the movement of air through the unit. The HDS was developed for aerosol inhalation therapy that would last approximately 5-10 minutes; but treatments can be administered for longer time periods, equating to higher nebulized volumes, without any device software adjustments. The objective of this chapter was to develop an HDS platform for testing high efficiency nebulized aerosol administration. Key attributes of the platform include: capacity to produce EEG aerosols, filtered inlet and outlet air, oral delivery, and electronic monitoring.

7.2 Design, Methods, and Materials

7.2.1 Experimental Setup Overview

Initial device prototypes were developed with a combination of computational fluid dynamics (CFD) and past knowledge in an iterative process to achieve the published HDS unit prototype. Laboratory testing of the HDS mimicked the intended operation but was adjusted where needed to acquire data. Aerosol sizing was determined by an Anderson Cascade Impactor (ACI, Nottingham, United Kingdom) operated in an environmental chamber set to the approximate outlet conditions of the HDS system to prevent particle size change during measurement. A vacuum pump connected at the ACI outlet pulled a steady 30 LPM of air through the impactor which had a 3D printed inlet adapter to position the HDS tubing centrally while allowing environmental chamber air into the impactor. During sizing experiments and system warmup, a fan driven constant flow rate of 29LPM was forced through the HDS and a timer initiated cyclic 1 second pulses of the nebulizer. This flow rate of 29 LPM was chosen due to the flow requirements of the ACI and similarity to the LVMH flow rate. Deposition experiments used an Advanced Servo Lung 5000 (ASL5000, IngMar Medical, Pittsburgh, PA, USA) programmed with user-created breathing profiles and connected to a 3D printed mouth-throat geometry for testing of the device under expected realistic flow conditions. Determination of albuterol sulfate (AS) drug mass on each impactor stage and device component was determined with validated high-performance liquid chromatography (HPLC) methodology. The main outcomes of this study were production of the HDS unit, aerodynamic particle size distribution (APSD) data of the inhalation aerosol, and regional depositional data within the delivery system and mouth-throat geometry.

7.2.2 Breathing Interface Design

Due to the subject's breathing as the driving force of air flow, a well-sealed device and interface were required to ensure all breathing air passed through the device. Several conforming-seal nasal and oral-nasal interfaces with exhalation ports were initially proposed for this device to allow for the comparison of EEG aerosol delivery with direct nebulizer approaches and to allow for the ability of subjects to still orally communicate during treatment. However, it was determined that a simpler and potentially more efficient device could be achieved by passing all inhalation and exhalation air through the same filter located behind the nebulizer (See Figure 7.1). This design increases the amount of re-breathed gas adding the requirement to maintain a dead space volume below that which would led to hypoxic conditions for a specific tidal volume. For this study we assumed the device volume of approximately 250 mL can be cleared with standard adult ventilation volumes. This 250 mL volume is sufficiently large for timing considerations, and additional dead-volume is undesirable. Interface sealing was important for this design due to the need for filtration of the exhalation air to help prevent the spread of undeposited drug and spread of SARS-CoV-2 through bioaerosol exhalation.

This study utilized a realistic idealization of the mouth-throat-mouthpiece sub-system developed from previous work. The newly designed interface mouthpiece outlet size and profile were similar to the Pari eRapid mouthpiece (Midlothian, VA; Part Number 22F3050) but contained a streamlined downward direction change and connection to the HDS flexible tubing. The internal anatomy geometry of the throat model was developed from data of Guilmette (1989) and a 3D printable model version was created by Ross Walgena (2014) referred to as the Open Model. Subsequently, several versions of this Open Model were utilized in multiple studies (Farkas et al. 2018, Spence et al. 2020) with simple modification for study specific needs.

Modification for this study included the removal/blockage of the nasal region and reshaping of the throat loft cross-section from oval to a rounded slot matching the mouthpiece (See Figure 7.2). The removal of the nasal region was deemed a reasonable step due to expected lack of nasal airflow from closing of the nasopharynx or the use of a nasal clip during future human subjects testing. Removable sealed connections among the mouth-throat-mouthpiece components were obtained with O-ring and parafilm wrap that were replaced with each experimental run. The simplified components of the breathing interface were considered sufficient for first pass development work of the HDS system without being overly complex.

7.2.3 Heating System Operation

The primary goal of the heating region was the addition of thermal energy such that the temperature of the inhaled evaporated aerosol stream was raised to a constant 30°C and that the nebulized droplets dried into EEG particles. The constructed sub-system contained a metal heat transfer region, multiple thermocouples, and an Arduino Uno microcontroller running custom temperature control code. The heating controller code processed temperature inputs from the mouthpiece and metal heat transfer regions along with airflow information to switch the heater input power among Full-Power, Half-Power, and No-Power states (See Appendix 13.1.2). During operation, the heater power state regularly switches due to the challenging steady temperature output goal under cyclic input heating requirements arising from discontinuous aerosol generation and the subject's changes in breathing airflow. Analytical analysis of the LVMH found system operation requirements of a consistent power input of ~16 watts utilized for aerosol evaporation and ~5 watts utilized for heating of the air flow (Spence et al. 2019). Identical power requirements apply for aerosol evaporation in the HDS and similar power

requirement for heating of the air during the drug nebulization period of inhalation. Theoretical power requirements during inhalation without nebulization and during exhalation drop to near 5 watts. The cyclic heating requirement of an ideal system was dealt with by utilizing a large thermal mass heat transfer region and loosening the inhalation temperature goal to allow for variations of a few degrees around 30 °C. Additionally, temperature spikes at the start of inhalation are avoided due to the movement of air through the heating region during exhalation. Assessment of the heating system was achieved by measuring outlet particle size and reviewing controller data logs.

System heating only occurs within the heating region although the aerosol still travels through outlet tubing to reach the subject. In previous studies (Longest et al. 2012) and in commercial high flow nasal canal delivery systems such as the Airvo (Fisher&Paykel Healthcare), engineers embed heating elements within transport tubing. The HDS design utilizes standard tubing and overheating of the aerosol stream at the heating region outlet such that the correct temperature occurs at the downstream outlet interface. Analytical estimates, based on fully developed flow in a 61cm length of smooth wall 10mm diameter tube with previously investigated 42 °C inlet, found temperature drop of approximately 5 °C at 30 LPM air flow. The HDS uses 60 cm of 10 mm inner diameter smoothbore spiral ventilator tubing (KC-048-5N, Instrumentation Industries) positioned in an arc from heating region exit to mouthpiece. Analytical estimates exclude additional temperature drop due to incomplete evaporation of the aerosol. When considering the wide range of reasonably expected operating temperature (16 °C – 32 °C) and relative humidity (10 – 90 %) at the future end user location, the unknown room operating temperature and humidity complicated heating requirements. As a simplification, all deposition testing was performed in Richmond, Virginia, USA, inside a commercially climate-

controlled building with consistent temperature and humidity among tests. Tubing outlet temperature was utilized as the main temperature feedback for heating system operation to accommodate heat loss during aerosol transport.

7.2.4 Heating Region Structure and Construction

Computational fluid dynamics simulations were utilized to improve the performance of the HDS heating region over the LVMH heating region. Design of the heating region required balancing increasing surface area and flow mixing for better heat transfer with decreasing surface area and turbulence for lower particle deposition losses. The CFD simulations performed by Dr. Rabijit Dutta investigated several configurations for the addition of fins and channels into the heating region. Modeling work suggested the heat exchanger incorporate three vertical thin walls extending the length of the heater to split the region into 4 separate channels. Simulated 2-fin-3-channel design had uneven aerosol concentrations among channels which provided undesirable spikes in deposition and heater temperatures. Additionally, the uneven heating causes incomplete evaporation of total aerosol at heater exit. The CFD also suggested chamfering the leading and trailing edges and chamfering the connection between the thin walls and outer surfaces.

Incorporating the CFD suggestion, the designed multi-channel metal heat exchanger was 3D printed in aluminum using Direct Metal Printing technique with surface finish selected as "Unfinished Ra 4-7μm" by 3D Systems Incorporated. This design production method was able to achieve fin thicknesses of 1.25mm with channel surface roughness similar to cast aluminum (See Figure 7.3). Total metal length was 163mm with an airflow cross-sectional area of 261.3mm^2, matching closely to the LVMH's cross-sectional area of approximately 270mm^2. The

cross-sections of the outer two channels are slanted and rounded to the edge but the center two channel were shaped to ensure a flat outer surface to mount the heaters. A thin layer of high thermal conductivity paste was applied to the rectangular Kapton heaters (KHLVA-105/5 Omega Engineering) before placing on the heat exchanger and wrapping the assembly with aluminum tape. To sense heating plate temperature, a type-K thermocouple (SA1XL-K, Omega Engineering) was attached to the center outer underside of the heat exchanger approximately 1 cm from the exit end before the aluminum wrap was applied. The HDS flow path CAD was built from scratch using Solidworks modeling software (Dassault Systèmes, France) such that the model could be streamlined to match the new heating region shape and fin placements. Heating region and device assembly continued with the metal heating section first attached to the exit region which provided cable stabilization and routing. Lastly, the entrance region and outer shell was slid over wrapped metal unit and attached, leaving an air-gap between the metal and plastic outer surfaces (See Figure 7.3). The heating region combined with the entrance and mixing regions form what is referred to as the main HDS flow path.

7.2.5 Breathing Waveforms

Study experimentation was split into two cases (see Table 7.1) based on breathing profiles created to mimic an adult subject orally breathing through the HDS device. The sinusoidal breathing pattern for Case 7.1 closely matched the Randomized Deep Nasal Inhalation used in development of the LVMH (Spence et al. 2019) but with a reduced tidal volume of 600 mL and modified I:E ratio range. Inductance plethysmography performed by Dugernier et al. (2017) found the median tidal volume of six healthy male subjects was 774 mL during high-flow nasal cannula therapy. Reduction of tidal volume for this study was implemented to account for

lack of additional therapy breathing support. Based on the underlying breathing parameters, the Case 7.1 pattern was also referred to as Sinusoidal Resting Adult Male (SRAM) during experimentation. The trapezoidal breathing pattern for Case 7.2 resembled pattern characteristics observed during device utilization in initial device development. Further supporting a trapezoidal pattern, Biswas et al. (2017) found trapezoidal inspiratory waveforms during MDI use in asthmatic and COPD subjects with large tidal volumes. The steep, flat-top flow profiles seen in early device testing and modeled by Case 7.2 had tidal volumes near 900 mL and a more even and narrow I:E ratio than previous test patterns. From the underlying breathing parameters used for programing the breathing pattern, Case 7.2 was also referred to as Trapezoidal Conscious Adult Male (TCAM) during experimentation.

Breath patterns produced by the ASL were scripted in Mathematica (Wolfram, Champaign, IL) building from the code previously used in Chapter 4 (See Appendix 13.1.3 ASL Routine for code and waveform details). Briefly, the Mathematica Notebook creates the supporting files and instructions for the ASL to produce a starting zero flow pause, 10 breaths of a median characteristic profile, 60 pseudo-randomly chosen breathes of testing breathing profile, 1 breath of a median characteristic profile, and an ending zero flow pause. The first 10 breathes bring the system to equilibrium with no drug administered, and then the middle 60 breaths administer drug based on the selected nebulizer control scheme. The main outputs of the Mathematica Notebook to the working file directory were text files containing ASL settings, flowrate values, and sequencing instructions. Updates to the Mathematica file over Chapter 4 include both increased automation and inclusion of additional profile shapes.

7.2.6 Nebulizer Operation Parameters

The HDS utilized the Aerogen Solo vibrating mesh nebulizer and ProX Controller (Aerogen Limited, Galway, Ireland) for the aerosolization of a model drug solution. No internal modifications were made to the commercial system components; however, the CMU was plugged in between the ProX Controller and Solo nebulizer to specify the start and stop of nebulization. The nebulization solution for this experiment contained 0.25% albuterol sulfate (AS) and 0.25% sodium chloride (NaCl) in water. A typical solution volume of 750µL was pipetted into the nebulizer reservoir just before starting the breath patterns. The subtraction of the remaining drug mass in the reservoir at the end of the run, as determined by HPLC, was used to calculate nebulized dosage.

Study experimentation of Case 7.1 and Case 7.2 were further split into 2 nebulization stoppage timing decision processes (see Table 7.1) identified as Critical Pressure Stoppage (CPS) and Informed Duration Stoppage (IDS). Both operation modes utilized a differential pressure sensor (Honeywell SSCDLNN060MDSA5) with the high side connected at the mixing region to identify subject inhalations and subsequently nebulization start timing. To prevent most false positive inhalation identification, the controller defined inhalation start at -5 pascals, not just any negative pressure in the device. After nebulization start, the controller continues to loop through the system code up to every 10ms checking to see if a stoppage criterion has been met.

In either decision method, nebulization ended if subject was determined to be exhaling, i.e., the measured pressure is greater than -5 pascals. When set in CPS mode, nebulization stoppage occurs when measured pressure difference drops below 30 pascals. This estimated value corresponds to the flow rate cutoff for which remaining inhalation volume equals that of the mixer heater when considering a median Case 7.1 breath. When set in IDS mode, the

nebulization stoppage occurs at a pre-defined time equal to one-third of the subject's average inhalation duration. This value was selected to prioritize high efficiency delivery by ensuring substantial time for aerosol to travel from origin to the lung filters. For Case 7.1 and Case 7.2, the microcontroller was pre-informed that the average inhalation time was 2.025 second and 2.325 second, thus nebulization stoppage criteria were 0.675 second and 0.775 second, respectively. Values used for stoppage decision process for each case are tabulated in Table 7.1 plus further coding details are in Appendix 13.1.2 Heated Dryer System.

7.2.7 Control and Monitoring Unit

The Control and Monitoring Unit (CMU) not only contains the microcontrollers coordinating nebulizer and heater operations but also serves as interface holder for the other system components. Therapy power source requirements have been simplified over the LVMH by now requiring only a 24VDC 5A input provided by a single repurposed 120VAC laptop charger. Heater power is drawn directly from the 24VDC input but the microcontrollers draw power through a prefabbed 12VDC converter. The commercial nebulizer controller sources power through a TO-220 packaged 9VDC linear voltage regulator (L7809CV, STMicroelectronics; Switzerland) circuited with noise filtration capacitors. Heater and nebulizer power interface via opposite gender barrel style connectors of different sizes positioned on opposite sides of the device to avoid incorrect user connections. Temperature sensing capability was integrated into the microcontroller, thereby removing the previous additional 120VAC power requirements of the LVMH's CMU. This design change led to visual temperature monitoring available only from the data logging laptop via microcontroller serial output. However, microcontroller capacity remains for direct visual display of temperature on future

CMU iterations. With the HDS flow path strapped on its pedestal atop the CMU, the centrally located pressure port tubing easily connected to the barb fitting at the mixing region. Due to a different sensor design, no bulk flow occurs through the Honeywell differential pressure sensor, therefore limiting contamination during subject exhalation. Both the temperature and pressure PCBs communicate new data when triggered every approximately 50 and 10 milliseconds via SPI protocol by their respective microcontrollers.

7.3 Experimental Results

The HDS development process entailed multiple stages of experiments. The initial stage concept feasibility experiments where performed *in silico* and *in vitro* to develop and prototype system sub-components. Once a functioning experimental prototype system was obtained, *in vitro* testing was split into two main stages. Device outlet aerosol sizing experiments were conducted first to verify operation. Then, realistic *in vitro* deposition experiments were conducted attempting to capture realistic in-use system performance. The following Experimental Results sections are organized into these three experimental stages of feasibility, sizing, and deposition.

7.3.1 Feasibility Experiments

Experimental determination of the pressure difference across the inlet filter region found flow rates up to 50 LPM resulted in less than 120 pascals of pressure at the mixing region sensor. From Figure 7.4: the selected critical pressure value of 30 pascals corresponds to approximately 15 LPM of device flow. Inclusion of an inlet flow meter desired for experiments, but not

intended for end use, was found to have negligible effect on microcontroller breath sensing capabilities. Device utilization of an SSC series Honeywell differential pressure sensor greatly reduced HDS CMU loop times compared to the LVMH CMU. Sub-microsecond sensor timing was achieved; however, continuous loop time lagged noticeably after an initial burst of speed. Utilizing artificial delay, a steady microcontroller loop time of 10 ms was achieved for the control and logging of data to an external Windows OS laptop computer with a 40 ms time stamping interval.

7.3.2 Sizing Experiments

Impactor testing found the device produced aerosol particles with an MMAD of 1.0 μm under experimental conditions with a loaded nebulizer solution of 0.25% AS and 0.25% NaCl. HDS outlet temperature measurements fluctuated in the range of 32°C – 37°C following the unsteady operation of the nebulizer. Numerical results are tabulated in Table 7.2: Aerosol Sizing Parameters.

7.3.3 Deposition Experiments

Using realistic *in-vitro* testing methods, greater than 80% of the nebulized dose deposited on a tracheal filter during electronically controlled timed nebulization. For Case 1, the tracheal filter captured 60% for CPS control and 85% for IDS control of the nebulized dose. Similarly in Case 2, the tracheal filter captured 58% and 86% respectively. This study was conducted with room conditions of 22°C and 23% relative humidity. Tracheal and Inlet Filter deposition were highly sensitive to nebulizer stoppage criteria, but not mouth-throat deposition. The pressure stoppage scheme (CPS) reduced tracheal filter dose to 60% of the nebulized dose, due to

inability for some droplets to reach the tracheal filter before exhalation. Numerical results are tabulated in Table 7.3: .

Data logs from the HDS indicate satisfactory performance of the developed control system. Graphical representation of the temperature system operation spanning several typical breaths of a Case 2 IDS run is depicted in Figure 7.5: . The upper panel illustrates heat exchanger plate temperature achieved the dynamic setpoint of 78°C. The middle panel displays the system operation states during same set of breaths. The lower panel contains temperature data from the tubing outlet during heater operation. Overall, typical tubing outlet temperatures ranged from 25°C to 34°C. Isolating segments of interests, an outlet temperature range of 29°C to 32°C was achieved during aerosol production, with minimal temperature spikes, during non-nebulization inhalation periods. Determination of inhalation start via the device internal static pressure at the inlet filter aligned well with the actual ASL5000 inhalation start time. Data logs showed high levels of agreement between the *actual-inhalation-start-time* and *pressure-determined-inhalation-start-time*.

7.4 Discussion

The Heated Dryer System was found to be capable of delivering orally inhaled medications efficiently with pressure sensing control. The two tested breathing profile cases were found to have little effect on tracheal filter deposition when considering a specific control scheme. Lung delivery efficiency, as estimated by drug deposition on the tracheal filter, was found to be sensitive to the nebulizer stoppage timing. Considering just the two tested nebulizer stoppage methods, this study suggests usage of a pre-informed timing criterion over a critical

pressure criterion. With additional coding, critical pressure value determination improvements are possible. However, the flow length and shape remaining after reaching critical pressure would still be ambiguous. Suggested additional coding would dynamically adjust timing to reduce the system setup burden on the device end user. Future ideal control schemes should utilize both pressure and temporal data, forming a critical volume value that dynamically updates and assumes a breath tidal volume dynamically responding to the subject's history. Technology to create such a control system is achievable, but has not yet been applied to this form of breathing therapy. Considering the mid 80% tracheal filter deposition for both breathing cases running the Informed Duration Stoppage code, the HDS control system performs exemplarily for future experiments without immediate additional coding requirements. Tracheal delivery of previously developed HFNC combination device (Spence et al. 2019) matches the current study results of approximately 85% of the nebulized dose. Although the HDS CMU design shares and improves certain aspects of the LVMH CMU design, the system should not be construed as intending to supersede the previous unit. The particulars of the different therapy design parameters separate the two control systems at this stage in development.

The experimentally determined aerosol MMAD of 1.0 μm leaving the outlet tubing aligns directly with data from the similarly designed LVMH (Spence et al. 2019) . Although the HDS device operates with variable flowrates, sizing was measured at a single flow rate of 30 liters per minute. This discrepancy appears minor, considering once excess aerosol liquid evaporates, the fully dried particles have little size change. Therefore, aerosol MMAD reaching the subject is expected to be consistent throughout most of the subject's inhalation period. The experimental model and the ASL simulator mimic *in-vivo* flow characteristics; however, they both lack the capability to supply heat addition to the system. Minimal effect on particle deposition is expected

from the lack of heating. During intended operation with a human subject, exhalation temperatures would be above the supplied inhalation temperature and near body temperature. Therefore, by design, the current control system ignored values from the outlet tubing sensor during exhalation. The inhalation temperature goal of approximately 32°C was reached without the addition of exhalated heat, and it is expected to be achievable with human subjects. System operation at 22°C and 23% RH room conditions without insulated heated tubing did not cause excessive moisture formulation within the experimental system. However, substantive tests were not performed at lower temperature nor higher humidity environments that the system would also be reasonably exposed to during operation.

Deposition experiments utilizing established HPLC methods found high recovery as expected for this fully contained system. This high recovery suggests the HDS released a lower amount of fugitive aerosols than the LVMH which had recovery values in the range of 80 % (See Table 4.5:). The calculated recovery values greater than 100% found in a few experimental runs do not greatly affect the overall trend of the deposition data. The most likely reason for the elevated recovery values was incomplete solvent washing of the HPLC column after injections of the high concentration solutions found in the preceding sample.

Differences in the inlet and tracheal filters support the continued use of the Informed Duration Stoppage scheme with the HDS system. The majority of the IDS inlet filter deposition reduction led to the increase of tracheal filter deposition as the remaining regions experienced minimal deposition change. Visual monitoring at the start of exhalation of a trapped aerosol cloud traveling from nebulizer skirt to inlet filter accounts for a portion of the 1% inlet filter deposition. As noted in previous work, this skirt could be removed by modifying the commercial system to eliminate the recirculation area without hindering aerosolization performance of the

device. Additional unseen exhaled aerosol deposited on the inlet filter. But, once deposited on the filter exhaled aerosol dose became indistinguishable from the trapped cloud source. Notably, higher drug deposition percentages on the tracheal filter was not indicative of higher drug mass on the filter, but instead a higher delivery efficiency of the nebulized drug. Exact nebulization rates for each run were unable to be calculated due to instances of the nebulizer running dry before the end of the experimental run. However, AS delivery to the tracheal filter on the order of 0.15 mg/min was achieved by the HDS device operating with IDS nebulization control, 900mL tidal volume breathing, and a 0.25%w/v nebulization drug solution.

7.5 Tables

Table 7.1: Breathing and Nebulizer Control Parameters

Item	Case 7.1	Case 7.2
Alternative Name	SRAM	TCAM
Waveform Shape	Sinusoidal	Trapezoidal
Volume Tidal (mL)	600	900
Breath Length (sec)	4.2 – 7.8	4.2 – 7.8
I:E Ratio	1:1.5 – 1:2.5	1:1.3 – 1:1.8
Inhalation Length (sec)	1.2 – 3.12	1.50 – 3.39
Min – Max Inhalation Peak Flow (L/min)	18.12 – 47.12	19.60 – 44.31
Inhalation Peak Flow Length (sec)	----------	0.94 – 2.12 5/8 of Inhalation Length
Critical Inhalation Pressure (Pascal)	-5	-5
Critical Nebulization Stoppage Pressure (Pascal)	-30	-30
Informed Delivery Length (sec)	0.675	0.775

Table 7.2: Aerosol Sizing Parameters

Item	Value
Room Inlet Air	26.0°C 44.7%RH
Nominal Device Flow Rate	29 LPM
Nominal Plate Setpoint	64°C
Outlet Temperature Range	32°C -37°C
Environmental Chamber	34°C 30%RH
Nominal ACI Flow Rate	30 LPM
MMAD	1.03 µm
Aqueous Nebulizer Solution	0.25% Albuterol Sulfate 0.25% Sodium Chloride

Table 7.3: Drug deposition (mean and standard deviation) for two control schemes and two breathing patterns

	Case 7.1		**Case 7.2**	
Stoppage	**CPS**	**IDS**	**CPS**	**IDS**
	$\mu \pm \sigma$	$\mu \pm \sigma$	$\mu \pm \sigma$	$\mu \pm \sigma$
Neb Skirt	1.47 ± 1.86	1.06 ± 0.42	5.39 ± 2.58	1.17 ± 0.73
Inlet Filter	28.39 ± 0.92	3.86 ± 0.63	20.26 ± 0.36	1.79 ± 0.44
Mixer Heater	3.30 ± 1.86	4.27 ± 0.70	3.96 ± 0.12	1.82 ± 0.51
Tubing	5.37 ± 2.57	7.75 ± 0.28	10.25 ± 1.09	7.04 ± 1.23
Mouthpiece	0.65 ± 0.15	1.03 ± 0.26	0.88 ± 0.15	1.00 ± 0.07
Model	1.14 ± 0.03	1.22 ± 0.44	0.72 ± 0.08	1.01 ± 0.36
Tracheal Filter	59.29 ± 4.46	85.34 ± 1.12	58.36 ± 3.61	86.00 ± 2.23
Recovery	99.62 ± 2.40	104.53 ± 2.01	99.83 ± 1.18	99.84 ± 3.14
Device Total	10.79 ± 6.28	14.11 ± 1.08	20.49 ± 3.72	11.04 ± 1.81
Distal Filter Mass (µg)	1130.28 ± 214.96	805.26 ± 9.66	1146.92 ± 71.16	994.19 ± 20.36

All values are expressed as a percentage of nebulized, except for Distal Filter Mass in µg. All values are based on triple replicates except Case 7.1 CPS Distal Filter Mass which only represents data from two runs.

7.6 Figures

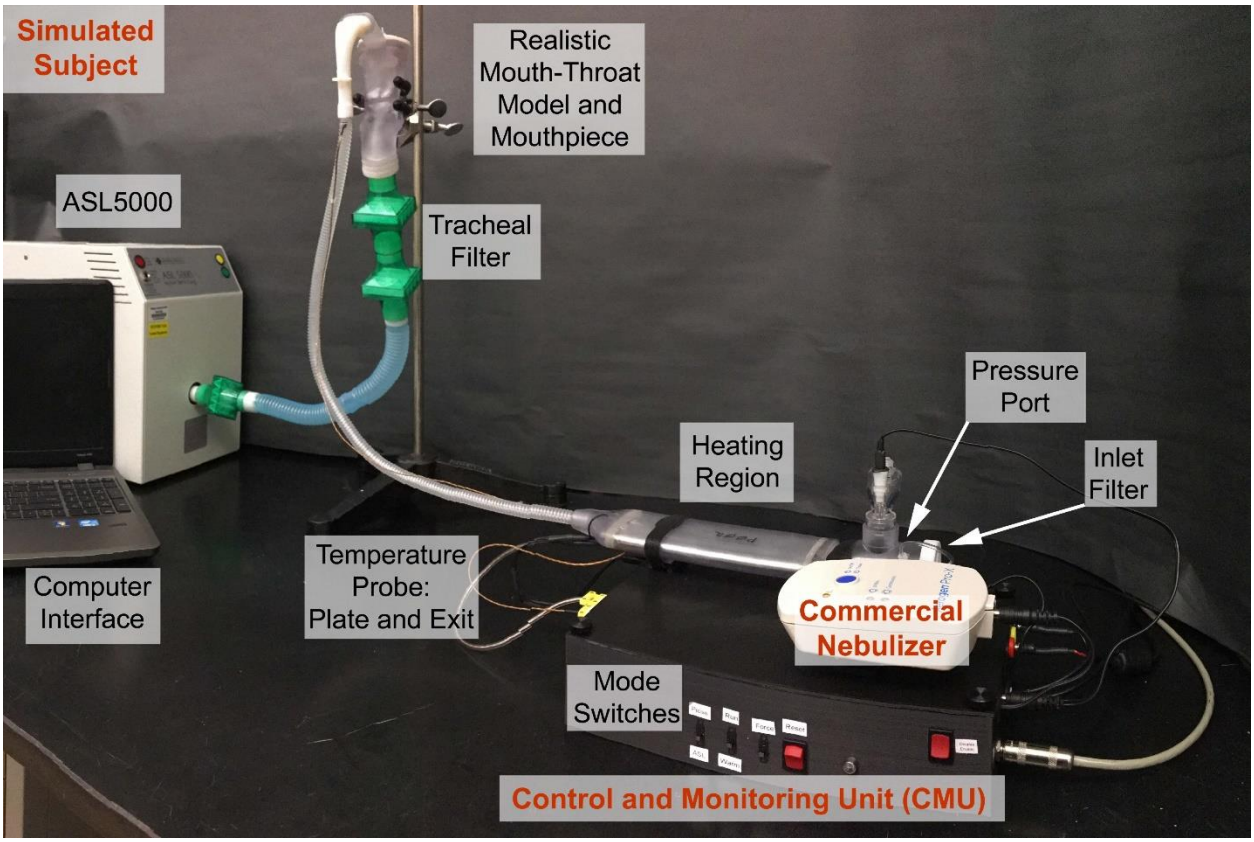

Figure 7.1: Heated Dryer System device experimental setup

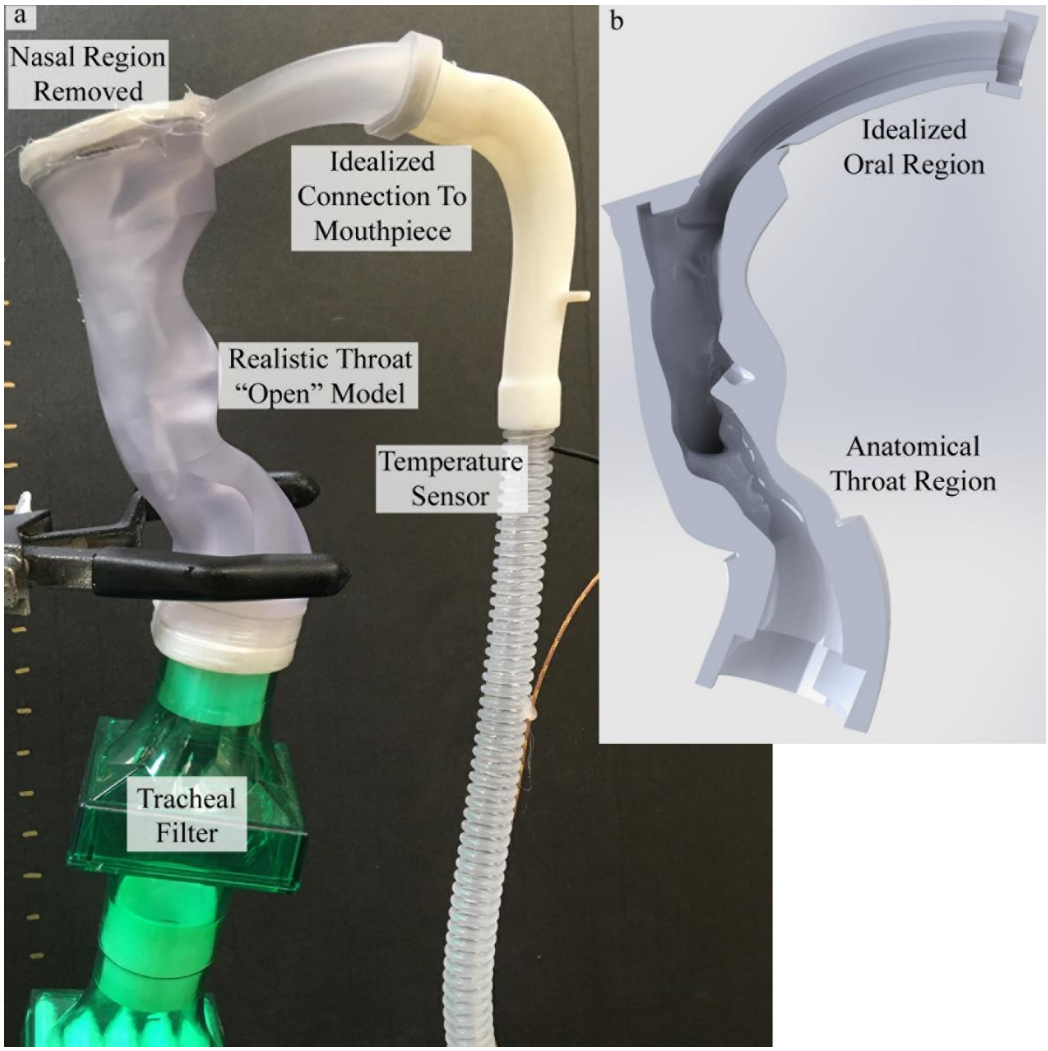

Figure 7.2: Mouth-Throat (MT) model and mouthpiece interface of the Open model. **(a)** Open model containing new mouth transition loft, streamlined mouthpiece, and dual tracheal filters as setup for experimental testing. **(b)** Representative cross-section illustrating the anatomically correct throat region and the computer-generated oral region lofted connection.

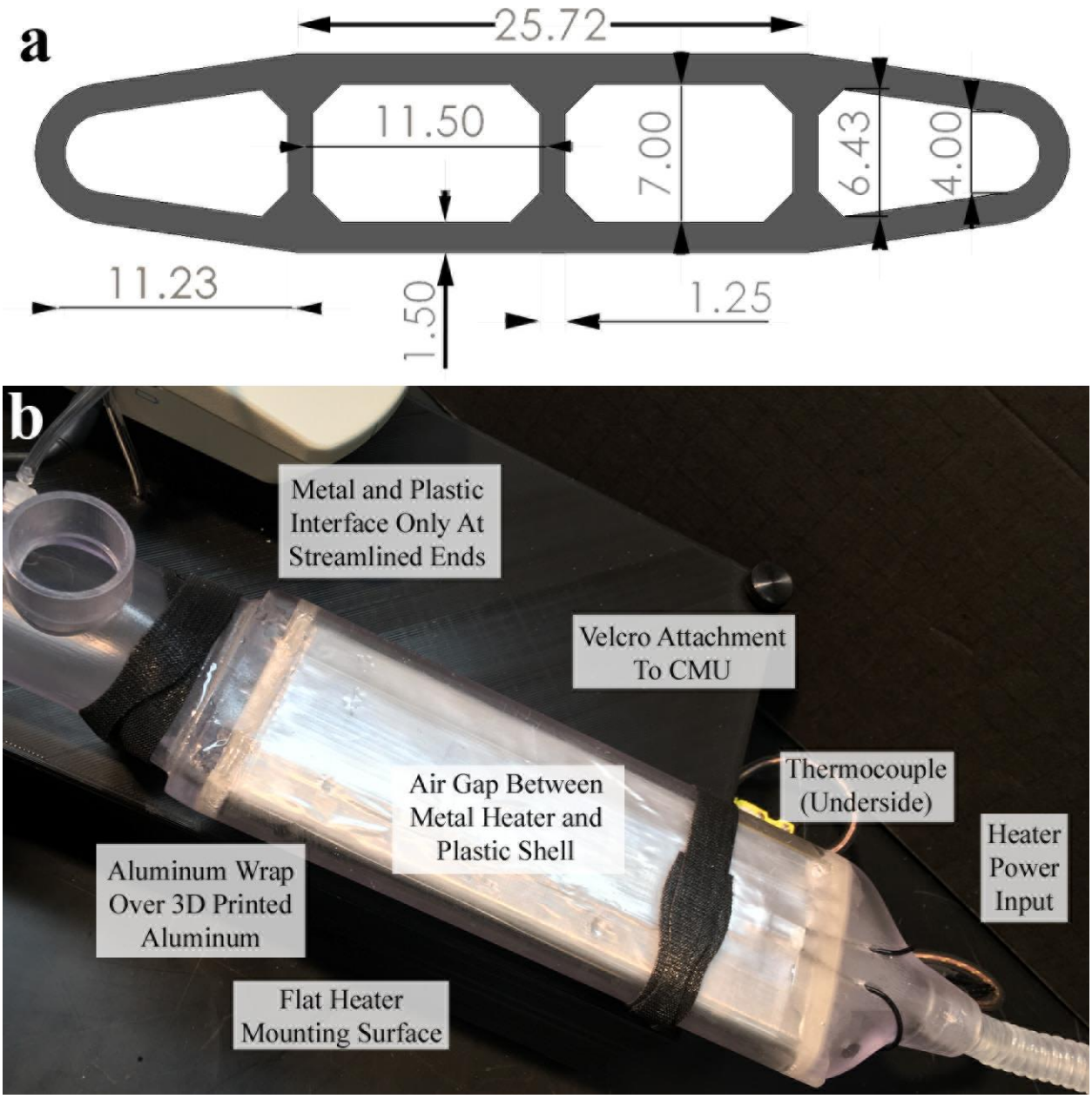

Figure 7.3: HDS metal heat transfer region with 3 fins and 4 channels

(a) cross section detail and **(b)** labeled heating region

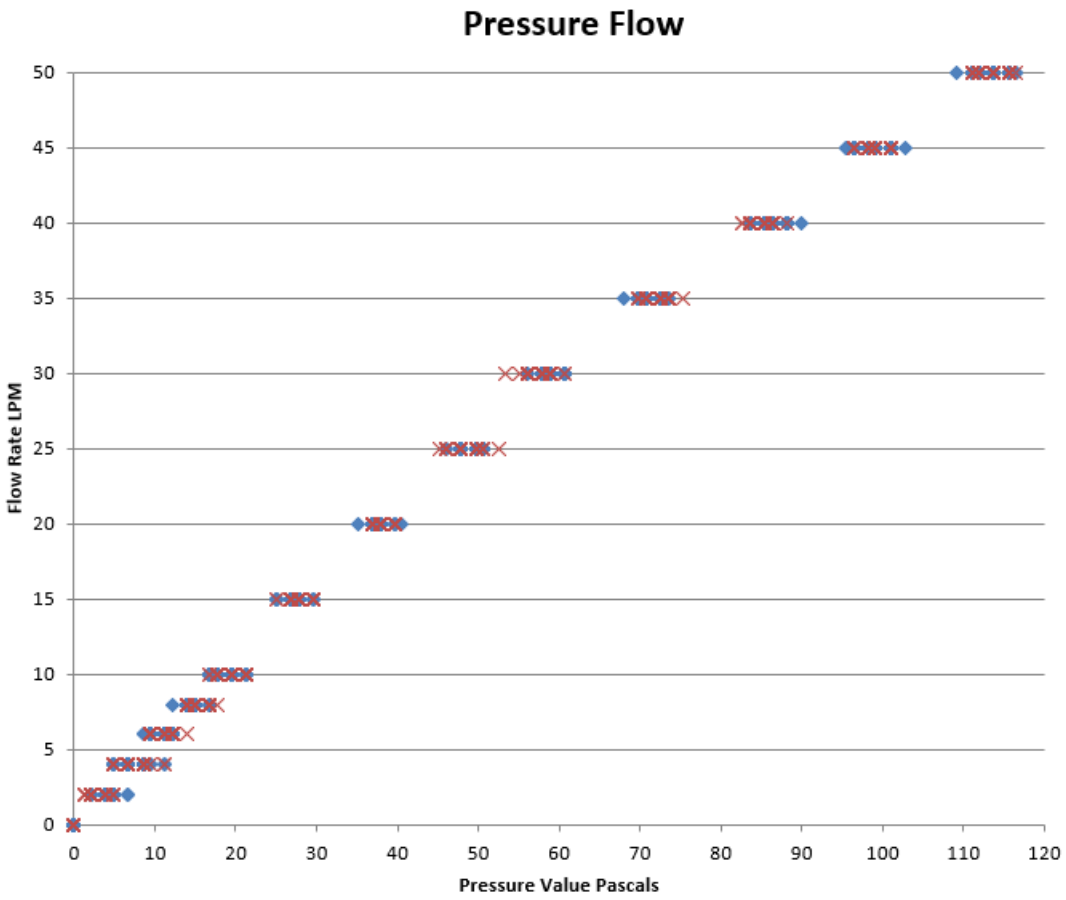

Figure 7.4: Observed pressure drop across the inlet filter at flow rates up to 50 LPM. Two sets of measurements recorded over approximately 4 seconds once system had stabilized.

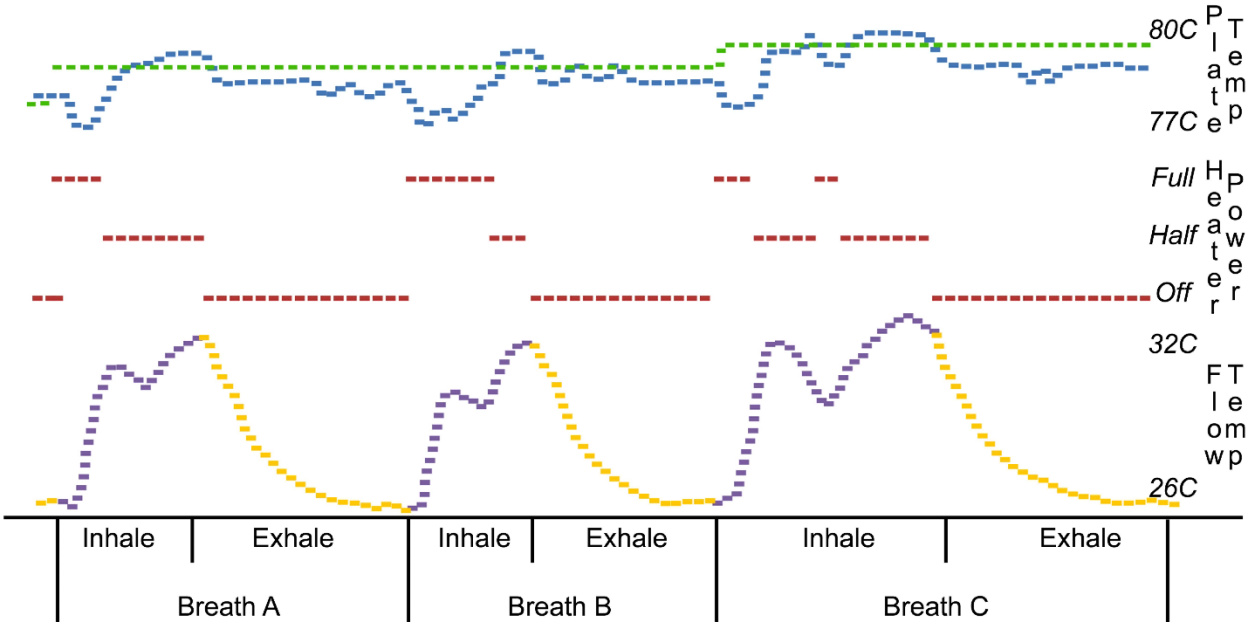

Figure 7.5: Graphical representation of CMU data output CMU during three breaths.

Image Color Key: **Top** → plate temperature (blue) achieves variable set point (green) of approximately 78 °C; **Middle** → unit state/heater power (red); **Lower** → outlet tube temperature 29 °C - 33 °C during inhalation (purple) and exhalation (yellow)

Chapter 8: Heated Dryer System (HDS) Testing in a Realistic Mouth-Throat (MT) Model

8.1 Introduction

The Heated Dryer System (HDS) achieves high efficiency aerosol delivery to the lungs through synchronizing aerosol administration to the inhalation cycle, limiting device losses, and achieving low extrathoracic deposition. Developmental experimentation, presented in Chapter 7 and at the International Society for Aerosols in Medicine (ISAM) 2021 Congress, focused on synchronization while utilizing a mouthpiece and extrathoracic model of limited geometric realism (Spence et al. 2021). Aerosol particles reaching the mouthpiece had an MMAD of nearly 1 μm, at steady state, (See Table 7.2) and therefore relatively low deposition would be expected in the upper airway under normal breathing conditions (Hinds 1999, Finlay 2001). However, it was hypothesized that oral deposition is a factor in real-world usage of the HDS due to mouthpiece alignment and positioning of the tongue. The objective of this chapter was to develop and test additional oral interfaces for the Heated Dryer System with a more realistic mouth-throat (MT) geometry. Key challenges of this experiment were adaptation of an anatomically detailed oral model and development of mouthpiece designs considering tongue position.

8.2 Design, Methods, and Materials

8.2.1 Experimental Setup Overview

The Heated Dryer System (HDS) developed previously in Chapter 7 served as the center point of this experimental setup developed for the testing of three mouthpiece designs integrated

into a highly realistic simulated subject oral model (See Figure 8.1 and Figure 8.2). First, mouthpiece designs were developed which incorporated streamlined interior flow paths, temperature sensors, external connectors, and outlet shape modifications. Second, an anatomic model of the mouth-throat region was created for each mouthpiece design (See Figure 8.3 to Figure 8.5). Laboratory deposition testing of the HDS used an Advanced Servo Lung 5000 (ASL5000, IngMar Medical, Pittsburgh, PA, USA) programmed with user-created breathing profiles enabling realistic flows through the models. Determination of albuterol sulfate (AS) drug mass deposition on each device component was accomplished by analysis of washing liquid with validated high-performance liquid chromatography (HPLC) methodology.

8.2.2 Mouthpiece Design

The three mouthpiece designs were developed and tested in order to provide a minimal particle loss transition from the HDS tubing to the oral cavity. All designs contained similarly streamlined interior flow paths curved from the near vertical 9.5mm ID tubing to the 26mm wide x 9mm tall rounded slot cross-sectional profile entering into the mouth (See Figure 8.4). This outlet slot size was based off the Pari eRapid mouthpiece (Midlothian, VA; Part Number 22F3050) dimensions. Mouthpiece designs attempted to minimize oral deposition with three different outlet configurations. The first mouthpiece, Simple Curve (SC), utilized 1 mm thick walls at the outlet and directed aerosol over the tongue. The second mouthpiece, Tongue Block (TB), attempted to decrease oral deposition by forcing the mouth open wider, thereby lowering the tongue surface relative to the mouthpiece outlet flow. The TB mouthpiece had 1 mm upper and side wall thickness but 4.2 mm lower wall thickness. The third mouthpiece, Tongue Depressor (TD), utilized uniform 1 mm wall thickness but extended the lower wall along the

flow path. This extension was intended to route the aerosol flow path up and over the tongue. Mouthpieces were 3D printed in Accura Clearvue for experimental testing of their ability to efficiently direct the HDS aerosol flow with minimal particle deposition.

8.2.3 Human Anatomy Model

The replica human mouth-throat models tested in this study were printed in Accura Clearvue by 3D Systems Inc. The base anatomical model, referred to as Subject 5, was originally converted to a solid model by Dr. Sana Hosseini from medical scans of a 55-year-old male and was utilized for deposition studies (Hosseini 2021). The detailed model extends into the trachea and includes geometric structures of the lips, teeth, tongue, uvula, and larynx. Changes to the model outlet and inlet connections were made for this experiment. First, the model outlet was sized to fit into a low resistance filter (Pulmoguard II^{TM}, Queset Medical, North Easton, MA, USA) without changing the internal flow path geometry. Second, the base model's mouth opening, approximately 3 mm (distance measured between upper and lower teeth tips near mouth centerline) during the original medical scans, was widened to approximately 10 mm and 14 mm to fit the mouthpieces for this study. Opening of the mouth required minor changes to the flow path as stated in the following paragraph.

Modifications to the oral region of Subject 5 and integration of the designed mouthpieces were performed mainly in Solidworks. The Subject 5 model was split 50 mm posterior to the inner edge of the upper central incisor teeth and no modification were performed on the posterior section (See Figure 8.3 and Figure 8.5). The anterior section was further split into a superior and inferior region following the model geometry. The inferior region was then rotated downward in a similar manner as opening the jaw, such that the study mouthpieces were able to fit in between

the teeth. Material was then judiciously added to rejoin the oral geometry similar to the stretching of the cheeks. To smooth sharp and jagged edges, the modified anterior oral cavities were re-meshed in Meshmixer and then re-imported into Solidworks. The study mouthpieces were then placed into the models and additional material added to mimic the sealing of lips around the mouthpieces. To facilitate measurement of regional deposition, the mouthpiece was made removable from the mouth model. A rubber seal was added around the mouthpiece surface and the anterior left quadrant of the mouth was made removable to allow insertion of the mouthpiece. Flat clamping surfaces were created to secure the model pieces together. Lastly, the posterior and anterior sections were rejoined to form the complete models. The SC and TD mouthpieces utilized the same Subject 5-10mm model, while the TB mouthpiece used the Subject 5-14mm model. These newly developed models mimicked the original Subject 5 geometry except with the mouth opening widened to 10 mm and 14 mm, respectively.

8.2.4 Breathing Waveform and Nebulization Control Scheme

This study utilized the Case 7.2 Trapezoidal Conscious Adult Male (TCAM) breathing waveform (See Appendix 13.1.3 ASL Routine) and Informed Duration Stoppage (IDS) control scheme developed in Study 2.1 and detailed in Sections 7.3.5 and 7.3.6. Briefly, each run consisted of 71 trapezoidal shaped breaths of 900mL tidal volume with nebulization over 60 breaths. For the first ten and last one breaths, all parameters were held constant with no nebulization to provide system stabilization and reference data. The central 60 breaths were varied in their specific parameters with an average inhalation length of 2.325 seconds. Per the IDS scheme, nebulization duration was set to one-third the inhalation length equating to 0.775 seconds per breath. This combination of pattern and stoppage method was chosen because not

only did it provide more efficient delivery than previous tests, but it also delivered a more predictable dosage, thus making mouthpiece comparisons easier.

8.2.5 HPLC Deposition Testing

For system deposition testing, 1000 µL of aqueous 0.25% AS and 0.25% NaCl formulation was loaded into the nebulizer. After the simulated treatment period, system components were washed with known quantities of deionized water (See Table 8.1). The concentration of AS in the washing fluid was determined by a validated HPLC methodology to quantify the deposition within the washed region. Nebulized dose was calculated as a subtraction of loaded concentration minus remaining concentration after the run. Initial tests used a total of ten samples with the removable lower quadrant of the mouth-throat model washed separately from the rest of the mouth-throat model. However, low deposition in this region led to combined washing of the mouth-throat regions as one item. In continued experimental runs, Sample ID 8 (previously the removable lower quadrant) was left blank. This blank was kept to prevent errors in the developed spreadsheet data analysis automation code developed for the original sample size of ten. Drug concentrations (µg/mL), found by the HPLC readout, were entered into the spreadsheet at their corresponding location. The spreadsheet multiplied these values by the entered wash volumes (mL) to find the regionally deposited drug mass. These values were converted to percent of nebulized dose and averaged across three runs of the same setup. Regional deposition percentages were the main numerical result of this study.

8.3 Experimental Results

Laboratory HPLC deposition data lacked significant difference among mouthpiece designs. All three mouthpiece designs produced similar tracheal filter deposition values of approximately 90% of the nebulized drug mass as shown in Table 8.2. Deposition values from this study matched well to the previous development study (See Table 7.3). Both mouthpiece and model deposition values were consistently extremely low at less than 1% nebulized dose.

The Control and Monitoring Unit functioned as intended during experimental tests. The direct connection, without leaks, of the system to the ASL 5000 enabled reliable detection of the simulated subject's inhalations.

8.4 Discussion

This study successfully created a device capable of use for human subjects testing whist completing the objective of laboratory benchtop testing of several mouthpiece designs. Main system components were produced following methods expected to be considered safe for human subject use of the device. In place of a human subject, this study developed 3D printed models which can be reused in future studies. Device features such as a protective sleeves and cable strain relief were incorporated to increase robustness.

Results from the HDS development study indicated the exiting aerosol had an MMAD of approximately 1 μm at the tubing outlet. Considering this small particle size, virtually no difference in MT loss and tracheal delivery among mouthpiece designs was not surprising. The lack of difference gives considerable freedom in the continued development of the HDS human interface. However, a major limitation of this study is the lack of human interaction with the

device interface during aerosol administration. It is expected that tongue positioning and salivation will be concerns regarding system function, drug deposition, and user comfort. This experiment did not have the ability to test either of these input variables, but future human factors studies could be developed to suggest a mouthpiece design considering salivation, tongue control, and comfort. Mouthpieces that act to prevent tongue movement with a physical barrier are not a new idea but are not implemented on commercial mainstream oral aerosol delivery systems (Dionisio et al. 2018). Seemingly the HDS systems, and other aerosol delivery systems, would benefit from a tongue control mechanism. The Subject 5 model used in this study more accurately matches human oral geometry than previously tested idealized models; however, it still lacks the capability to fully mimic a human subject's movement, saliva production, and heating input over the course of the system usage. During short treatment sessions of low-concern drugs, like albuterol, subject movements is not expected to be a major issue in willing adult subjects. However, subject tolerance and compliance with treatments over a longer duration or with high-concern drugs, like corticosteroids and antibiotics, warrants further investigation even with willing adult subjects.

Although future internal VCU studies could use the current system, external studies would need additional systems designed, built, and verified. For studies utilizing machines other than the ASL5000, nebulizer production timing can still be achieved with a simple input voltage signal during inhalation. The creation process steps and time estimates for a second HDS system, matching the developed system, are listed in Table 8.3. The production of an additional system, by an individual with previous experience on the LVMH or HDS system construction, would take approximately 26 hours of labor over a 7-day period with current construction techniques.

8.5 Tables

Table 8.1: HPLC washing details

Sample ID Number	Item	Wash Volume (mL)	Concentration Min – Max (µg/mL)	Information
1	Inside Nebulizer	100	10.8 – 13.0	Determines Amount Nebulized
2	Nebulizer Skirt	2	1.0 – 3.8	Commercial Device
3	Inlet Filter	10	1.5 – 2.8	Exhalation and Timing
4	Mixer Heater	10	0.5 – 0.7	Device Performance
5	Tubing	5	2.3 – 3.0	Transport Deposition
6	Mouthpiece	2.5	0.3 – 0.5	Inside and Outside within mouth
7	Model All	80	0.7 – 0.8	Two Pieces Combined
8	Blank	---	---	Mouth Upper Corner Deposition Out of Calibration Range
9	Filter 1	80	5.4 – 9.1	Filters 50/50 Water/Ethanol
10	Filter 2	20	0.3 – 0.8	Not Absolute Filter at System's Particle Size

Table 8.2: Drug deposition for mouthpiece designs

MP ID	SC	TB	TD
(% Nominal)	$\mu \pm \sigma$	$\mu \pm \sigma$	$\mu \pm \sigma$
Neb Skirt	0.6 ± 0.3	0.7 ± 0.5	0.9 ± 0.5
Inlet Filter	2.8 ±0.5	3.1 ± 1.3	3.5 ± 1.1
Mixer Heater	0.8 ±0.1	0.7 ± 0.1	0.9 ± 0.2
Tubing	1.9 ± 0.2	1.4 ± 0.3	1.8 ± 0.3
Mouthpiece	0.2 ± 0.0	0.2 ± 0.0	0.2 ± 0.0
Model	0.6 ± 0.1	0.6 ± 0.1	0.6 ± 0.1
Tracheal Filter	88.0 ± 6.5	88.2 ± 10.3	92.9 ± 4.7
Recovery	94.9 ± 6.5	94.8 ± 10.6	100.9 ± 6.4
Tracheal Filter Mass (µg)	605.9 ± 127.5	661.4 ± 18.5	671.9 ± 20.5
Nebulized Mass (µg)	681.4 ± 100.1	757.8 ±70.8	726.2 ± 22.2

Table 8.3: Time Estimates to build another system for third party testing.

Item	Item Time	Hands-on-time
Gather/Order Parts	4 days	2 hours
Print CMU Case	20 hours	2 hours
Assemble CMU	6 hours	6 hours
Make Cables/Connectors	3 hours	3 hours
3D Systems Outer Flow Path	4 days	1 hour
Disassemble SN:001 Heater	25 hours	1 hour
Assemble SN:003 Unit	2 days	3 hours
Pharmacy Verification	8 hours	8 hours
Total	*7 days*	*26 hours*

Note times are based on working speed of an individual with previous experience on the LVMH or HDS system construction.

8.6 Figures

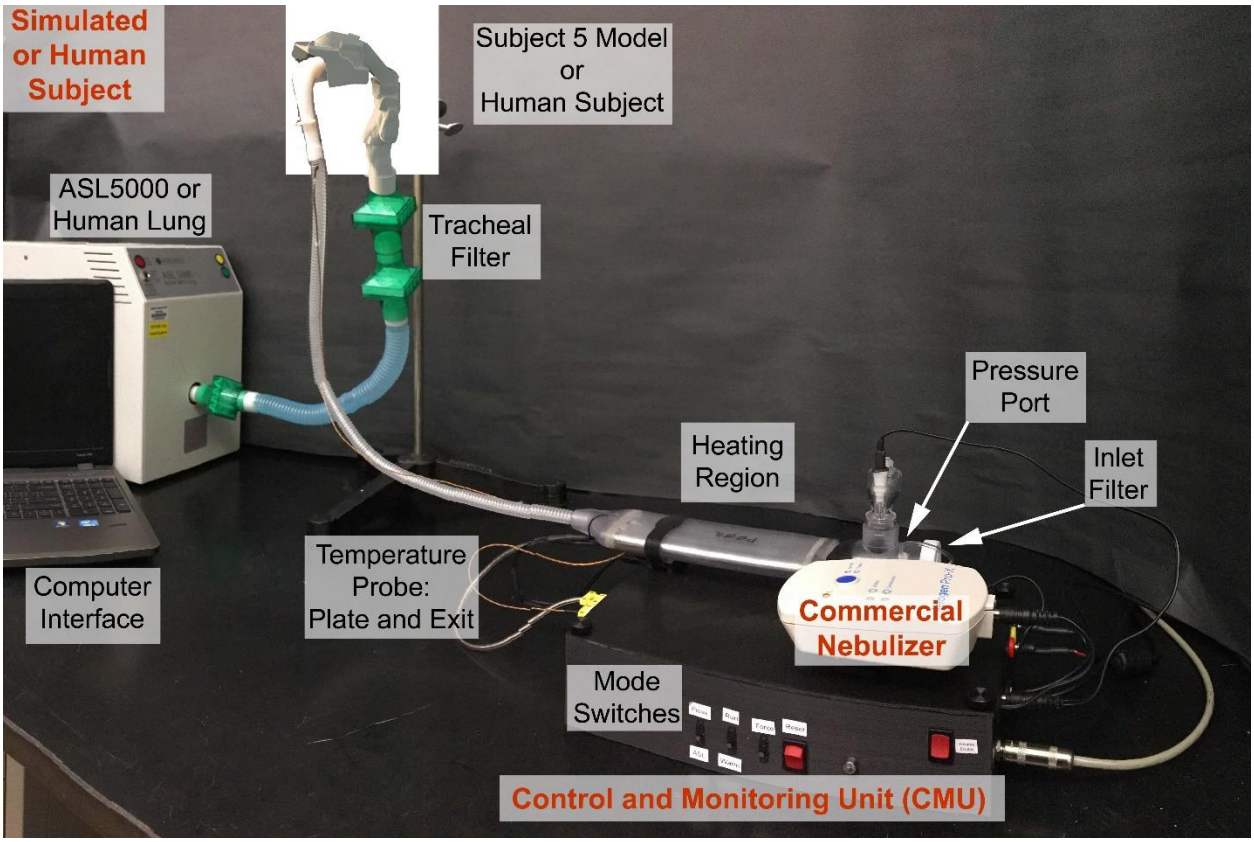

Figure 8.1: System setup overview with developed device that could be used in human subject testing.

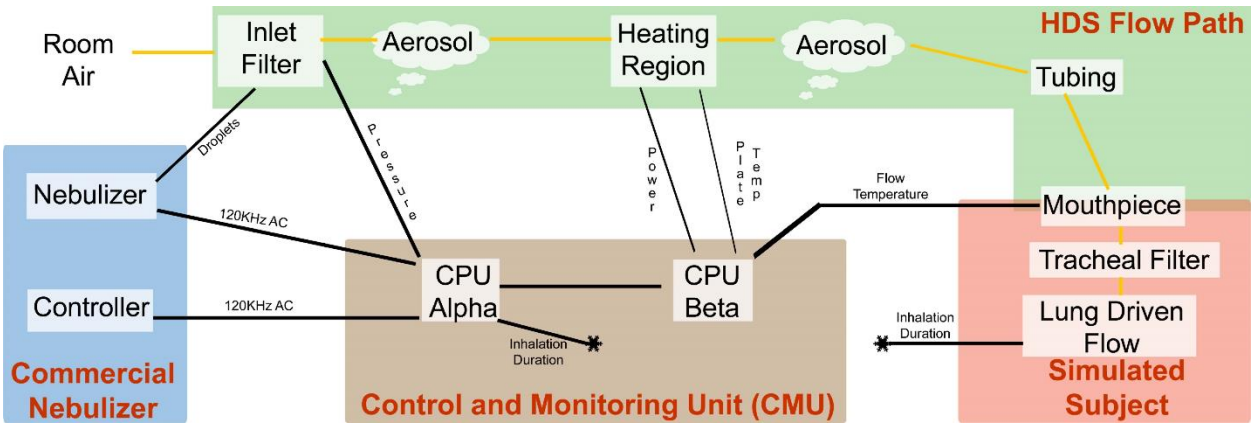

Figure 8.2: Experimental system setup diagram for HDS testing

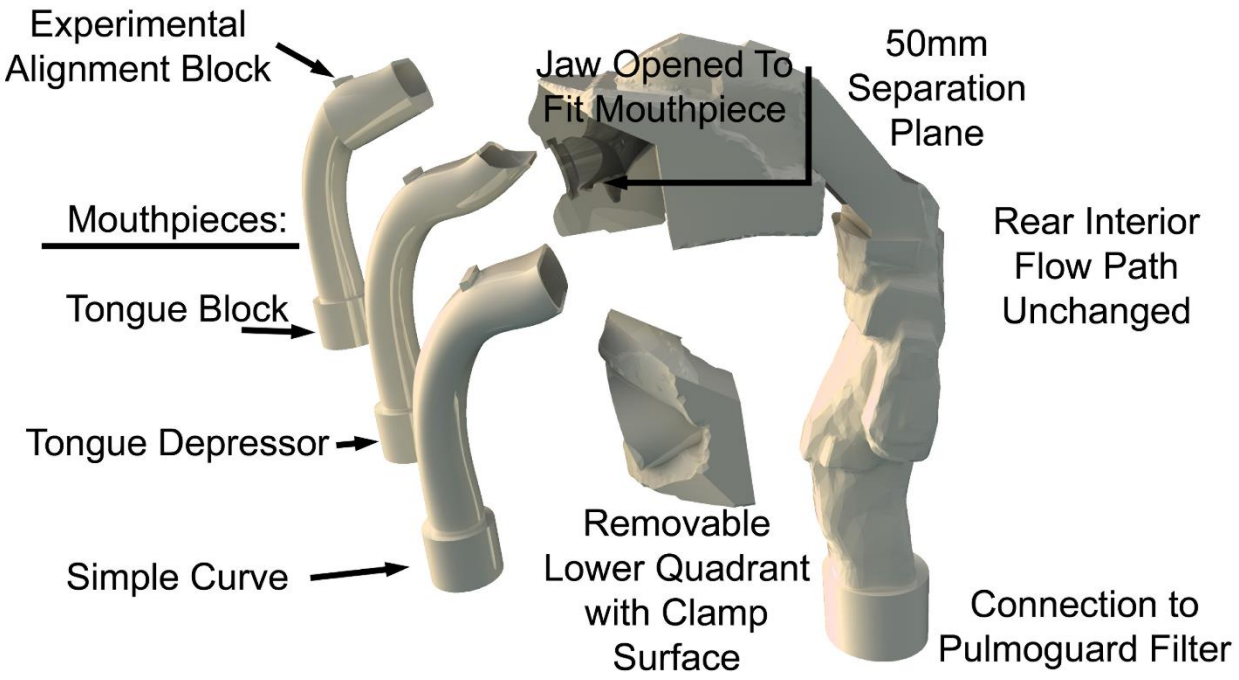

Figure 8.3: Exploded view of the Subject 5-10mm model and the three study mouthpieces.

a) Simple Curve b) Tongue Depressor c) Tongue Block

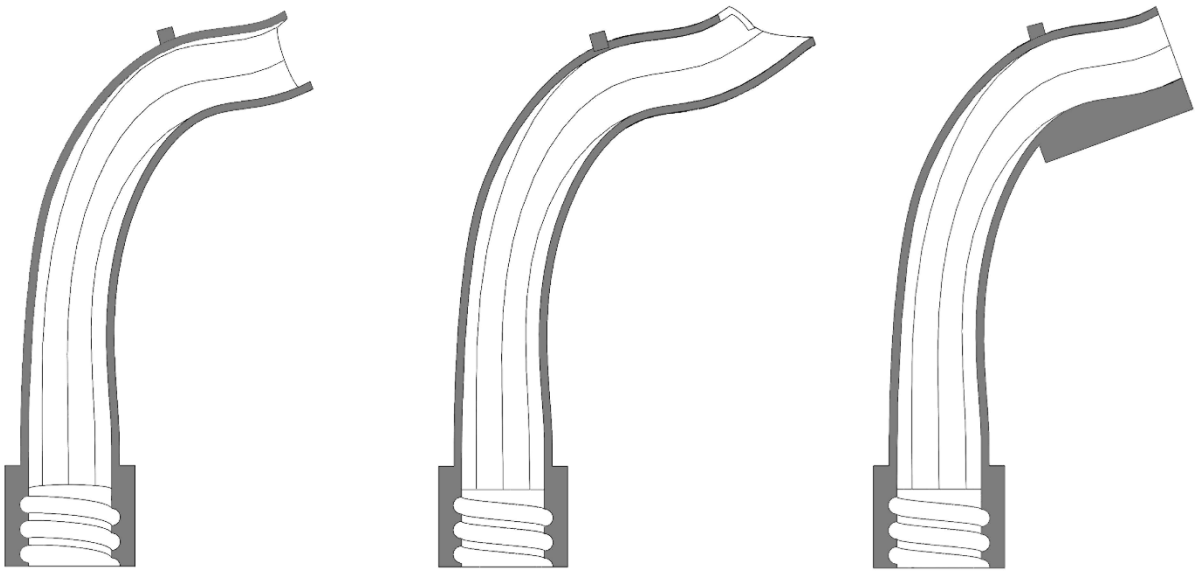

Figure 8.4: Midline cross-section showing interior flow pathways of the three study mouthpieces

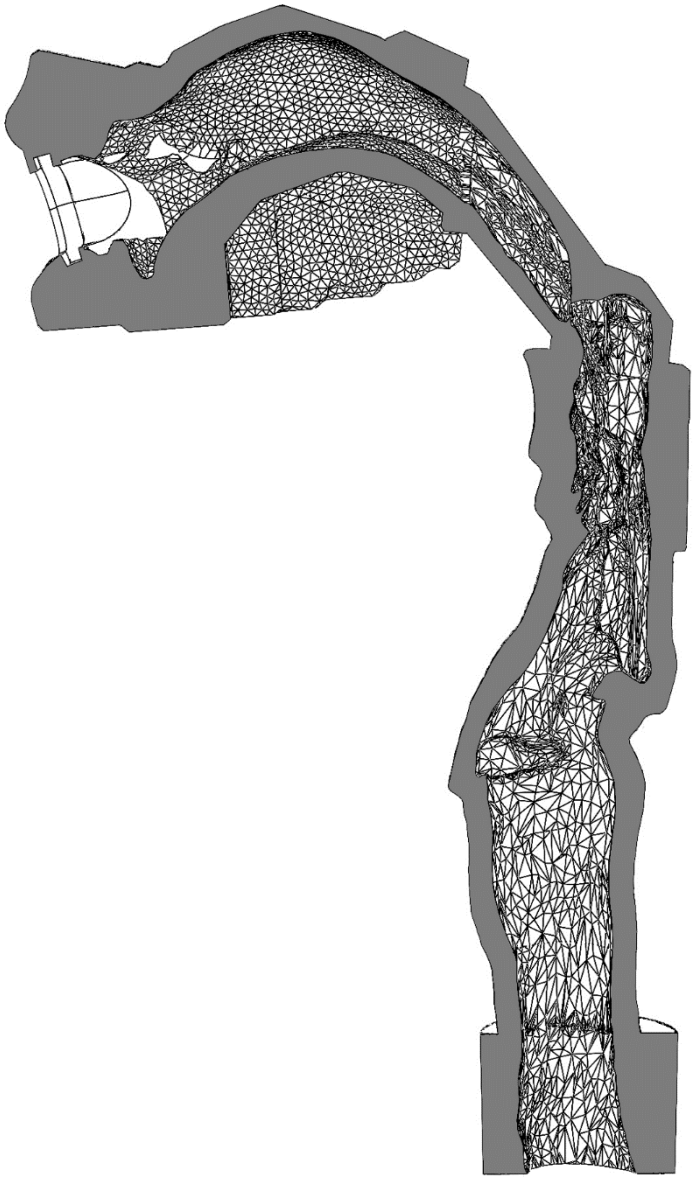

Figure 8.5: Midplane cross-section cutaway of Subject 5-10mm model

Chapter 9: Construction of an In-House Small-Particle Spray Dryer

9.1 Introduction/Rationale

The Aerosols In Medicine (AIM) laboratory evaluates novel dry powder inhalers (DPIs) loaded with Excipient Enhanced Growth (EEG) powders produced in a nebulizer-based, laboratory-scale spray dryer. The multi-stage powder production process (See Figure 9.1b) performed in collaboration with Dr. Hindle's laboratory produces batches of powder in quantities of a few hundred mg with median volume diameters of approximately 1µm (Bonasera 2021). Pharmaceutical powder production via a spray dyer is applicable to many drug substances and provides adjustable powder characteristics (Weers and Miller 2015). The manipulation and control of process variables generates engineered particles with tunable radial composition, improved bioavailability and efficacy, and enhanced aerosol dispersion characteristics (Vicente et al. 2013). The Buchi B-90 manipulations typically utilized at Virginia Commonwealth University (VCU) are changes to solution pump rate, nebulizer spray rate, drying air flowrate, and drying air temperature. Published data of novel DPI inhalers performance, utilizing EEG powder spray dried at VCU, indicated large benefits over commercially available delivery systems (Farkas et al. 2018). However, powders required substantial prescreening before use in the developed DPI devices due to batch-to-batch variability and a lack of knowledge connecting spray dryer input parameters with powder performance, especially with small-particle formulations. Device and powder development at VCU continues to utilize the Buchi B-90 for production of powders to test systems for high efficiency pharmaceutical delivery to the lungs (Howe et al. 2021). Ongoing work continues to investigate methods to achieve predictable, repeatable, and tunable high-performance powders from the commercial spray dryer.

Leveraging the AIM laboratory skill and resources, Longest et al. (2020) developed tandem Computational Fluid Dynamics (CFD) simulations of the Buchi B-90 and experimental tests to link spray dryer maximum instantaneous drying rate (κ_{max}) and the dispersibility of powders. This connection provided a method to predict device performance using CFD and therefore, suggest additional spray drying conditions to test. These CFD-suggested tests and additional experiments to modify the spray dryer configurations would benefit from access to an additional spray dryer system. However, the high cost and difficult reconfigurability of the Buchi B-90 limited access to an additional system. Redevelopment of the Buchi-B90 concepts created the VCU Small Particle Spray Dryer which provided a low-cost, open-source experimental platform for spray dryer investigations. The objective of this chapter was to build and document an in-house small-particle spray dryer capable of producing powders with similar characteristics and performance as the Buchi Nano Spray Dryer B-90. Key attributes of the VCU Small Particle Spray Dryer include: an operating temperature range of 35 – 120 °C, inlet humidity range of 0 – 100 % relative humidity, dryer gas flow rates of 80 – 160 liters per minute, and high efficiency capture of the spray dried powder.

9.2 Materials and Methods

Detailed measurements of the Buchi Nano Spray Dryer B-90 system flow path components were taken, and an evaluation of system functionality priorities was performed to develop design goals for the VCU Small Particle Spray Dryer. Constrained to a limited budget, an exploratory proof-of-concept system was created and functioned as expected. This prompted approval for additional funding and resources for the development of the initial prototype into a

suitably robust and versatile laboratory tool. The main tower, first developed for proof-of-concept testing, served as an adjustable platform for the integration of the various accompanying systems required for consistent production of spray-dried particles. This chapter on spray dryer construction encompasses the initial proof-of-concept version and the version used for a study on mesh head selection, currently in development by other AIM lab group members.

9.2.1 Drying Tower Frame

The drying tower frame was constructed with Series 20 T-slot extruded aluminum beams from 80/20 (Columbia City, Indiana, USA) allowing for high versatility in component positioning. Four 20x20x1700 mm vertical beams were placed at the corners of a 294x294 mm square and were aligned together at three separate horizontal locations by four 20x20x254mm beams forming level surfaces (See Figure 9.2). Connections between beams were made with 20 Series 2 Hole Inside Corner Brackets (Part # 14053) and 20 Series 5 Hole L Flat Plates (Part 20-4081). The lowest of these horizontal support divisions was approximately 80 mm from the base and served as the main platform holding the drying tower cylinder sealing mechanism as described in Section 9.2.4. The bottom of each vertical beam was tapped and then a height-adjustable foot was screwed into the base. These adjustable feet were used to level and stabilize the drying tower frame into position atop the laboratory workbench. Lastly the metal frame was electrically grounded via a wired connection to the laboratory building.

9.2.2 Air Intake System

Inlet Mixing Chamber

To effectively achieve a range of inlet air properties in the open loop spray dryer system, a plastic tub approximately 45x60x45 cm with a clear plastic lid was converted into a mixing chamber. The goal of this box was to mix ambient room air with additional dry air or water vapor, depending on the desired conditions, before entering the drying region. Dry air, supplied from the laboratory wall air with an additional three stage filtering and drying system (DryAire Model 6760, Germantown, Wisconsin, USA), was routed into the chamber through the sidewall with a brass through-wall connector and muffler. Water vapor was introduced into the chamber from an ultrasonic-nebulizer-based humidifier. Flexible tubing with a 1-inch inner diameter transported air from the inlet mixing chamber towards the drying region.

Inlet Heater and Power Source

Air from the Inlet Mixing Chamber required heating to reach the desired temperature of up to 120 °C before mixing with the aerosolized solution. A desirable heater would cause minimal flow resistance, quickly respond to input signals, and be capable of operating in a range of power outputs. Multiple heater configurations were investigated before selecting the custom solution of inserting a heat gun thermal unit into a section of metal pipe. This large-diameter, single-element heater configuration required no sudden directional changes in the flow and was capable of high flow rates with minimal backpressure. Air passed directly over the unit's multiple electrical heating coil wraps to increase temperature quickly when energized. The output power of the heating element was controlled via an adjustment dial on a 20-amp 0–130 VAC voltage transformer. Overall inlet temperature measurement was achieved with a

commercially available thermocouple and temperature controller switching the voltage to the heating element on/off to achieve the selected temperature.

Inlet Unifier

Directly before entering the main spray drying chamber, air passed through the Inlet Unifier. The main functional component of the 185 mm diameter Inlet Unifier was a piece of wool felt sandwiched between two 304 stainless-steel screens and inlaid into a rigid plate. This heat resistant combination dissipated the jet of air exiting the heater tube. The proof-of-concept system transition utilized a 3D-printed plastic cap to step from the smaller heater diameter to the larger chamber diameter. However, the use of plastic initially required a sharp reduction to the system's maximum inlet heating temperature to prevent thermally induced failure. This cap was subsequently replaced with a machined aluminum transition to ensure full temperature operational range capability.

Air Flow

Air circulation was provided by an ERWEKA VP1000 vacuum pump (Bättwil, Switzerland) regulated to move 120 liters per minute from the Inlet Mixing Chamber to the fume hood exhaust. Specifically, the pump was initially located with the regulated intake coming from the Inlet Mixing Chamber and the exhaust port connected to a flowmeter and then to the rest of the system (See Figure 9.1a). Correct flow rates required the regulation valve to be nearly fully open. The Sensirion SFM3000 flow meter (Stäfa ZH, Switzerland) was connected to a laboratory desktop computer for measurement readout. Subsequent advances of the system moved the vacuum pump downstream of the spray dryer (See Figure 9.3).

9.2.3 Drying Tower Cylinders

The main spray drying chamber of the VCU Small Particle Spray Dryer was constructed from two cylinders stacked together to provide a height of approximately 865 mm. Both cast acrylic cylindrical tubing sections (ePlastics, San Diego, California, USA) had an inner diameter of 171.5 mm and wall thickness of 6.35 mm. The upper cylinder had a 76.2 mm hole drilled through the wall 110 mm from the top surface. At this hole a second piece of 63.5 mm ID cast acrylic tubing was connected perpendicularly, allowing for insertion of the spray head apparatus into the spray tower. The lower cylinder was left unmodified for this experimental setup. Between the upper and lower cylinders, a square o-ring (dash number 261) and a 3D printed support ring provided sealed connection when fully assembled. Rubber surfaces on the Inlet Unifier and Lifting Mechanism provided sealed connections at the top and bottom of the Drying Tower Cylinders.

9.2.4 Lifting Mechanism

The Lifting Mechanism was designed to support the Drying Tower Cylinders and Electronic Collector systems during assembly and then to raise and provide sealing pressure against the stationary Inlet Unifier plate during operation. This movable platform consisted of a frame, roller guides, and a baseplate. The frame was assembled from sections of the same T-slot extruded aluminum as the Drying Tower Frame, and it rested on the lowest horizontal support dividers. Polyamide nylon rollers (093028, FATH GmBH, Splat, Germany) were connected to the lifter frame and positioned into the vertical T-slots of the Drying Tower Frame for linear travel. The plastic baseplate was connected to the upper surface of the moveable frame. This baseplate included connection ports for sensors, connections for air flow tubing, and housing for

collector system components. A lever-action clamp on each side of the baseplate was utilized to evenly apply lifting and clamping force against the Drying Tower horizontal support members. The original rubber-tipped clamping surfaces were replaced with 18-8 stainless steel M6 button cap bolts which provided smoother clamping-action and better final-height adjustment.

9.2.5 Electronic Collector System

The VCU Small Particle Spray Dryer used electrostatic precipitation to separate aerosolized powder from the airstream. This process utilized a positive, highly-charged outer cylinder with grounded center electrode to create an electric field (See Figure 9.1). In general, the electric field defected the particles (charged by the aerosolization and drying process) and left the air unchanged. However, the high voltage difference (~15 kVDC) between the outer and inner metals created corona discharges which further charged the powder particles and increased collection system capture efficiency.

Outer Positive High Voltage Cylinder

A 174 mm ID 319 mm tall stainless-steel cylinder's inner surface was polished and utilized as the collection surface. The outer surface except the lower inch was wrapped in electrically insulated heat resistant tape. A ring of copper contacts, attached to the lifter baseplate, contacted the lower outer surface to center the collection cylinder and electrically connect to a Spellman (Hauppauge, New York, USA) CZE1000R high voltage power supply. A cast acrylic cylinder with 222 mm outer diameter and 6.35 mm wall thickness was placed around the collection cylinder to prevent accidental contact with metal components. This plastic cylinder also provided sealing surfaces to the flow path drying tower cylinders and lifting baseplate.

Inner Grounded Center Stars

The inner electrode unit was connected to the high voltage power supply and building grounds. At the core was a 316 stainless-steel threaded rod (3/8-16) supporting evenly spaced metal star plates. The bottom end of the rod, ground down for electrical connection, was inserted through the lifter baseplate with lower spacer resting on an o-ring seal. Twenty-four plates each containing thirty-six evenly spaced spikes were cut from 0.004” thick metal stock using a water jet. A punch was used to create an approximately 8 mm hole at the center of each plate. This hole was sized such that the plates loosely screwed onto the threaded rod for easy assembly yet stayed electrically connected when assembled. Spacers placed between each spiked plate were created from a drilled and tapped 28.7 mm OD PTFE rod cut into 10 mm thick discs. The stack of plates was organized such that the sixteen larger (100 mm OD) plates were on the lower two-thirds and the eight smaller (89 mm OD) plates were at the top third with a nut at the very top. When energized, this collection system made corona discharge regions at the spikes, charged the surrounding aerosol, and deposited the aerosol on the outer cylinder.

9.2.6 Spray Head System

The spray head system was designed to provide stable and continuous aerosolization of the bulk solution through the entire spray drying duration. The system was comprised of four main components (peristaltic pump, temperature regulated liquid reservoir, spray head power source, and vibrating mesh head) each serving a specific function. The peristaltic pump pulled fluid from the thermal reservoir through the mesh head and back to the reservoir. The spray head power source forced a small amount of this fluid through the mesh head on each vibration cycle

in the form of droplets. The mesh head consisted of a metal plate, with a multitude of holes, adhered to a piezo element. Various commercial and custom mesh head designs were implemented into this system; however, the specifics and performance of these designs were not within the scope of this chapter. Nor were the multiple iterations of the temperature regulated liquid reservoir, also known as the FarkanCooler, within the scope of this chapter.

9.2.7 Operating the Spray Drying Run

Operation of a standard complete experimental spray dryer run with electronic collection and powder testing consisted of multiple steps spread out over approximately one week. The overall experimental process work flow is presented in Figure 9.1b. A detailed list of steps focused on nebulized production of powders was tabulated and presented in Table 9.3. Briefly, the process began with preparation of the spray solution into a pre-cooled state. Next, the spray head system was setup and primed. Then, the cleaned spray dryer components were assembled and the air flow system adjusted to correct operational parameters. After double checking electrical connections, the high voltage collector was powered on. The spray head system was then turned on, and the powder production lasted for 170 minutes. After the spray duration was complete, the spray head system, humidification system, and heating system were turned off, while leaving dry airflow till the system cooled slightly. After this cooling period, airflow was stopped and the spray dryer tower disassembled. The metal collection cylinder was scraped with a spatula to remove the powder. After weighing and consolidating the powder into a glass jar, the powder was left loosely covered in a dry room-temperature desiccator for 5 days. Powder was then removed from the desiccator, sealed in a glass jar, returned to the desiccator, and scheduled for dispersion testing.

9.2.8 Powder Dispersion Testing

Dispersion performance testing a utilized novel in-house Dry Powder Inhaler (DPI) devices (Howe et al. 2021), according to in-house laboratory standards, to obtain values for Mass Median Aerodynamic Diameter (MMAD) and regional deposition. Briefly, novel DPI key features included: small diameter inlet capillaries, aerosolization chamber, and outlet capillaries. The DPI connected to a gradually expanding nasal interface with single outlet. The D1-Single-v2 device aerosolization chamber was loaded with 10 mg of powder and then actuated three times. There was an approximate five second pause between each actuation of the device. The actuation air source was the miniFarkantimer set to a Q90 flow rate of 1.7 liters per minute and actuation time of 0.36 seconds to produce 10 mL pulses of air.

9.3 Resulting Device Functionality

The VCU Small Particle Spray Dryer system technical data and operational requirements presented in Table 9.1 were similar to the Buchi B-90 system. Listed operational space requirements of approximately two square meters reflect setup in the developmental laboratory, but are adjustable depending on organization of required accessories and working surfaces. Based on the steps presented in Table 9.2, construction of a second VCU Small Particle Spray Dryer would take approximately 50 hours of labor for an individual with previous experience on the system.

The VCU Small Particle Spray Dryer was able to reach and sustain operational performance goals in order to generate powders for experimental testing. Spray drying of an

EEG solution in a basic system configuration resulted in powder with a bulk density of 191 mg/cc. Laboratory standardized testing of this powder, in a novel DPI, resulted in 73% of the loaded dose to be emitted from the device. Additional experimental information and results are presented in Table 9.4.

9.4 Discussion

Selection of the VCU Small Particle Spray Dryer frame's construction method was done early in the design process to provide a foundation for the project. An extruded aluminum T-slot system was selected due to versatility, machinability, and the author's familiarity. Continued use of this construction method is recommended for both the current spray dryer and future laboratory scale prototyping projects. Design and construction methods should be re-evaluated to consider assembly labor-saving options if multiple copies of the system were to be created at the same time. The use of acrylic drying chamber cylinders, instead of glass, was mainly due to the lower cost and greater availability of acrylic than that of glass. The acrylic drying cylinders were less resistant to deformation at the heater interface, had lower thermal conductivity, and had a different static electricity dissipation. Deformation of the cylinders was slow and counteracted by adjustments to the lifter mechanism final position. Increased insulative properties of the acrylic might actually be beneficial to the uniform evaporation process by keeping radial heat loss through the chamber to a minimum. Additional studies have been proposed to further insulate the chamber and evaluate radial temperature profiles during operation. Although the exact interactions of the two materials and the charged particles were not measured, the small amounts of chamber deposition were considered acceptable for current operations.

Flow within the spray dryer system was driven by a regulated vacuum pump which pushed air through the drying region. The exhaust side of the vacuum pump was found to emit an aerosol which left a black residue on the flowmeter and connecting tubing. Partway through the prototyping stages, the vacuum pump placement was moved, which changed the configuration from a pushing flow to a pulling flow (See Figure 9.3). The pulling flow configuration, utilized going forward, meant the spray chamber was at a slightly lower than atmospheric pressure. In both configurations, the felt circle in the Inlet Unifier acted as a final filter before the air moved through the drying region. The use of felt, instead of the porous hard media used in the Buchi B-90, kept cost down and manufacturing simple. The felt did limit the rate of energy input by the heater due to burning risk; however, the system still met the 120 °C drying temperature goal with minimal risk.

The function of the VCU Small Particle Spray Dryer was to create dry powders for inhalation therapies. The created system functioned as intended, but more importantly provided an experimental platform for evaluation of the spray drying process. The powder aerosolization metrics, from a novel DPI device, agree with published values of powder produced on a Buchi B-90 spray dryer (Howe et al. 2021). The VCU Small Particle Spray Dryer could be utilized to supplement production rates but would best be utilized as a testing platform for future powder processing experiments.

9.5 Tables

Table 9.1: Small Particle Spray Device System Technical Data

Item	Required Value	Unit
Physical		
Dimensions (W x D x H) Main Tower	294 x 294 x 1800	mm
Dimensions (W x D x H) System Operation	2750 x 750 x 1800	mm
Weight	~39	kg
Exhaust Flow Rate	> 120	LPM
Electrical		
Connection Voltage	120	VAC
Frequency	60	Hz
System Amperage Draw	30	A
Number of Individual Electrical Outlets Required	12	- - -
Drying Process		
Heating Capacity	1680	Watts
Max Inlet Temperature	120	°C
Spray Rate Range	0.02 – 0.9	mL/min

Table 9.2: Time estimates to build another independent system with electronic collection method.

Task #	Item	Item Time (hrs)	Hands-On Time (hrs)
1	Cut & prepare ~16m of 8020 20x20 extruded aluminum into correct length for exoskeleton	2	2
2	Assemble tower frame with L brackets and corner braces	3	3
3	Assemble lifter frame structure and attach additional roller hardware	0.5	0.5
4	CNC Router cut lifter base plates from 1/4” thick plastic	2.5	2
5	CNC Router cut lower separator & upper plate from 11/16” and 15/16” thick plastic	2.5	1
6	Glue rubber gaskets to surfaces	24	1
7	Mount lifter base plate & lifters to the lifter frame	0.5	0.5
8	Cut & bend copper for outer electrode connections	1.5	1.5
9	Finish lifter subsystem by attaching accessories & connecters	0.75	0.75
10	Manufacture 24 plastic spacer bushings	2	2
11	Manufacture collector rod ends	1	1
12	Get 8 small and 16 large collector spike plates cut from Microseal Inc	1	1
13	Assemble collector center electrode	2	2
14	Polish stainless-steel collection cylinder	3	3
15	Wrap collection cylinder outer surface with tape	0.25	0.25
16	Create top aluminum cap on lathe & mill	3	3
17	Mount upper plate to tower frame	0.25	0.25
18	Cut 304 stainless-steel 30x30x0.0095 screen & F-13 x 1/8” felt circles for inlet unifier	0.25	0.25
19	Silicone & bolt inlet unifier plus top cap onto upper plate	24	0.25
20	Assemble heater core into pipe & connect to top cap	1	1
21	Cleanup & prepare plastic drying cylinder edges	0.5	0.5
22	Drill holes into side of upper cylinder for thermocouple & spray head cylinder	0.5	0.5
23	Cut profile into spray head cylinder & then cut to length	0.75	0.75
24	3D print spray head cylinder end cap pieces	10	0.5
25	Epoxy end cap & upper cylinder to spray head cylinder	24	0.25
26	Design, print, and cast middle rubber seal for main cylinders	72	3
27	Manufacture metal spray head positioning arm subsystem	2.5	2.5
28	3D print spray head mesh containment subsystem	3	1
29	Construct FarkanCooler	100	8
30	3D print humidity source inlet adapter	9	0.5
31	Construct & assemble Fishbowl subsystem	2	2
32	Cut to length & attach flow tubing to fishbowl, flow sensor, dryer, flow pumps, and exhaust,	0.25	0.25

33	Final assembly and checking of all components	2	2
34	Assemble temperature sensors and controllers	1	1
	Total 1-38	302.5	49

Note times are based on some previous experience on the VCU Spray Dryer system construction. Additionally, ordering and shipping times are not included in estimations.

Table 9.3: Start-up, shut-down, and electronic collection procedural order for a normal run of 170 minutes for initial experiments

Step	Item
1	Pre-make solution 12 hours minimum before spray and pre-cool
2	Assemble tower for spray configuration
3	Setup FarkanCooler and spray feed pump then turn off feed pump
4	Turn vacuum pump on and check flow rate
5	Setup, position, and turn on humidity source
6	Fully turn on house air to wall mounted dryer
7	Recheck air flow rate and water content
8	Adjust via pressure regulator and humidity strength dial to achieve correct water content
9	Turn on heater power source and ensure voltage regulator is at ~35%
10	Monitor tower temperature for 70°C setpoint
11	Ensure center ground and outer high voltage (HV) leads are connected
12	Turn on and enable the HV power supply
13	Power on the spray feed pump and spray head voltage signal
14	Observe normal spray plume pattern
15	Record start time and operating conditions
16	Monitor for duration of spray drying run time
17	Record stop time and operating conditions
18	Disconnect the feed tube from liquid reservoir
19	Once spray stops, turn off spray head voltage signal
20	Turn off FarkanCooler
21	Disable and turn off HV power supply
22	Turn off humidity source
23	Turn off heater and monitor temperature
24	Once inlet drops below 50°C, turn off vacuum pump
25	Turn off house air
26	Lower tower and place upper sections to side
27	Lift out collector cylinder and place on clean, pre-creased, aluminum foil
28	Use spatula to scrap circumferentially, from inner top to bottom, the powder onto the foil

29	Pour powder into a pre-cleaned, dried, and pre-weighted glass vial
30	Re-weigh vial to determine current total mass collected
31	Cover with Kimwipe and reweigh for baseline storage mass
32	Store in desiccator at 0% RH for 5 days
33	Flush spray loop with DI water
34	Rinse collector electrodes with DI water then spray with denatured alcohol and set to dry
35	Wipe residual powder from spray drying tower components
36	Empty and clean humidification source

Table 9.4: Experimental Testing Parameters and Results

Item	Quantity	Unit
Dryer Flow Rate	120	LPM
Inlet Water Content	10	g/m^3
Drying Temperature	70	°C
Spray Device	Aerogen Pro	- - -
Spray Rate	0.42	mL/min
Spray Time	240	minutes
Collected Mass	194.5	mg
Number of Actuations	3	
Pause Between Actuations	5	sec
Actuation Flow	1.7	L/sec
Actuation Time	0.036	sec
Actuation Volume	10	mL
Powder Bulk Density	191	mg/cc
MMAD out of interface excluding pre-separator	1.75 ± 0.07	µm
MMAD out of interface including pre-separator	1.92 ± 0.09	µm
Emitted from device	81.52 ± 2.65	% loaded
Emitted from interface	72.83 ± 3.75	% loaded
Recovery	85.90 ± 5.05	% loaded

9.6 Figures

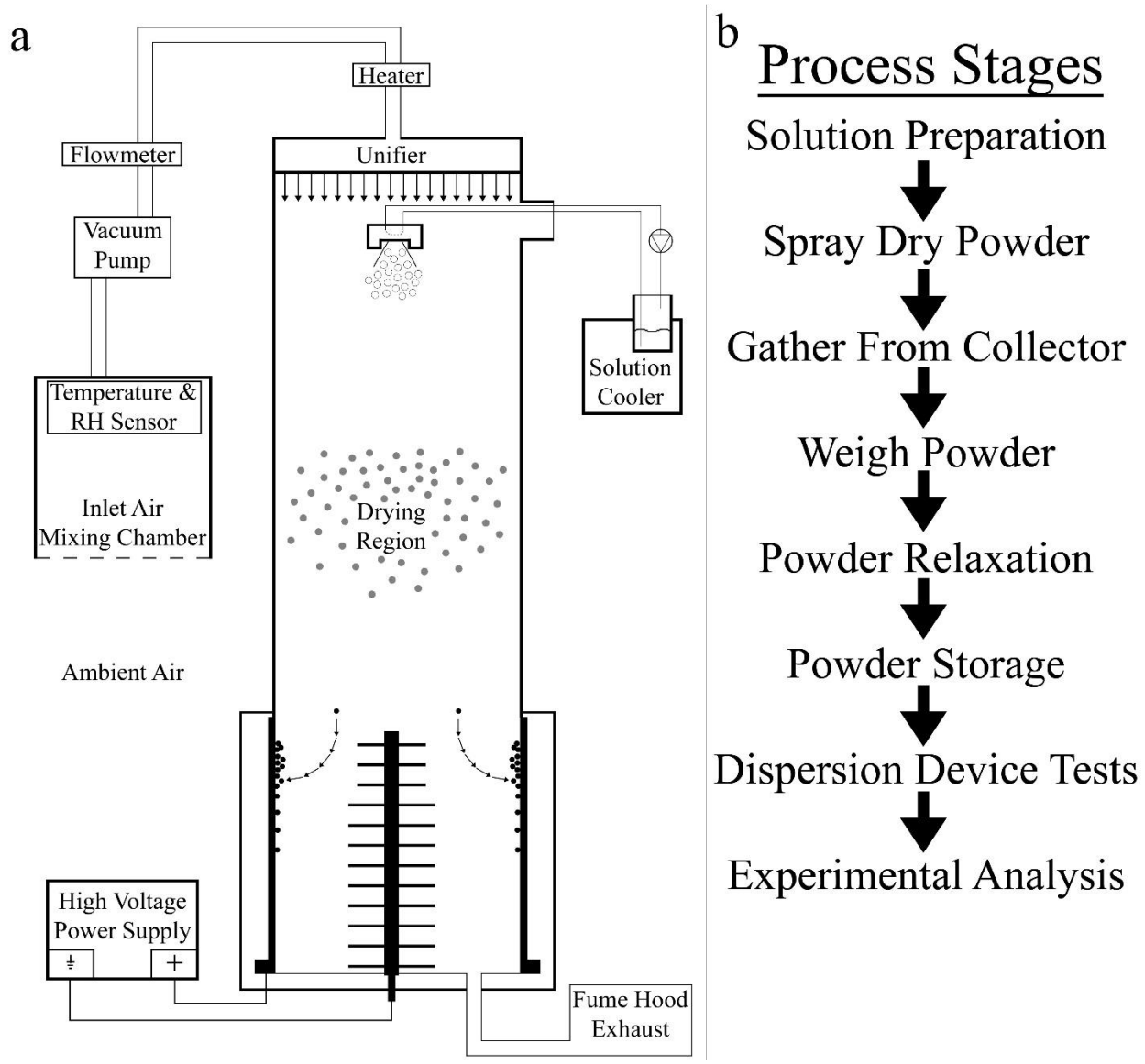

Figure 9.1: Diagram of **(a)** the VCU Small Particle Spray Dryer components mimicking the Buchi Nano Spray Dryer B-90 and **(b)** the overall process flow diagram for both systems

a b

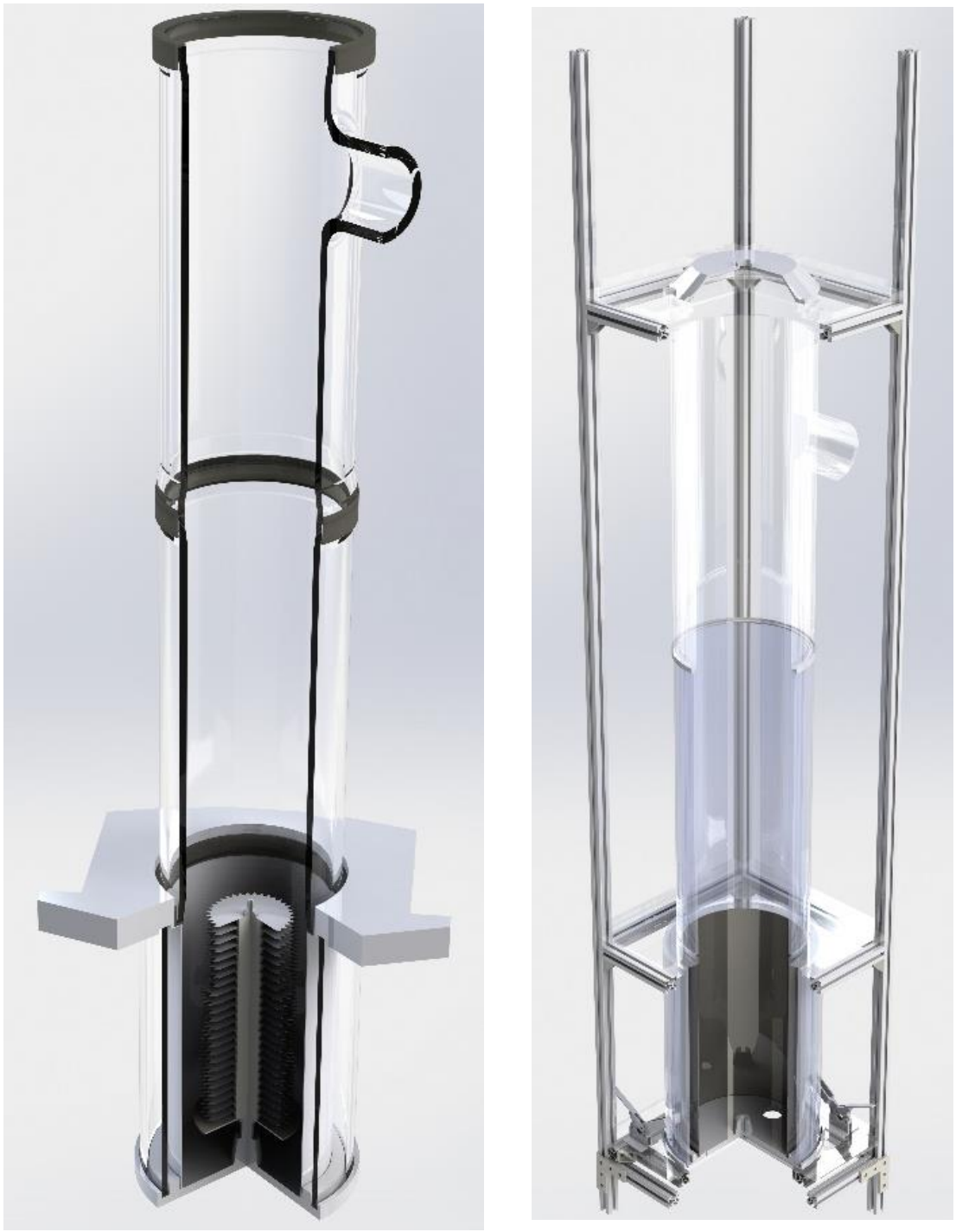

Figure 9.2: Cutaway views of **(a)** the Buchi Nano Spray Dryer B-90 tower and **(b)** the VCU Small Particle Spray Dryer tower with frame.

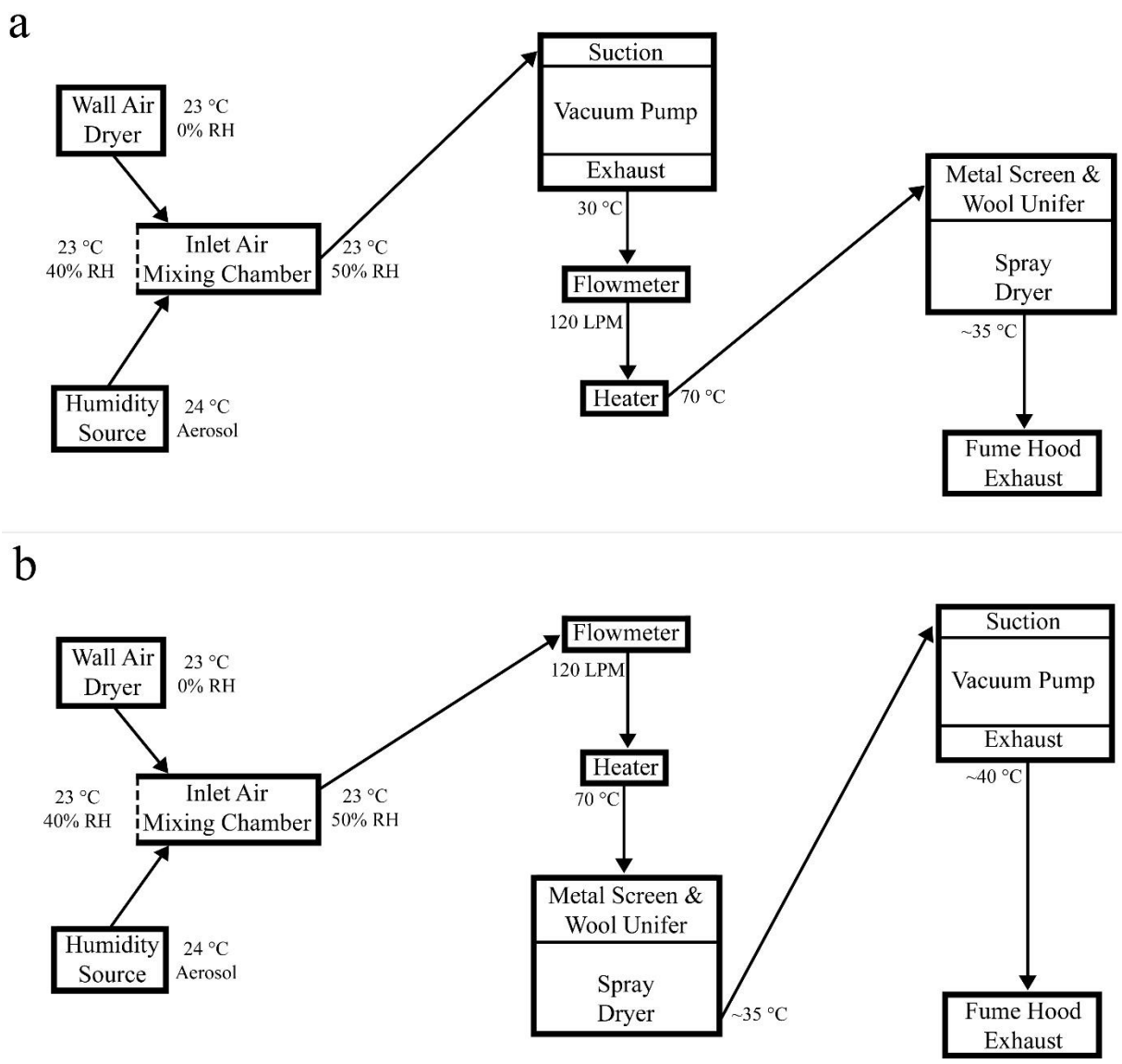

Figure 9.3: Air flow diagram of **(a)** push and **(b)** pull setups.

Chapter 10: Measuring and Controlling Spray Drying Operations

10.1 Introduction/Rationale

Process monitoring and product tracing are key aspects of quality control and experimental investigations. Supplemental software to the Buchi Nano Spray Dryer B-90 provides a method to manage the operational data collected during experiments. The VCU Small Particle Spray Dryer succeeded in producing high performance powders (See Table 9.4) but lacked ability to easily manage and trace the operational parameters. This inability is especially highlighted when compared to published and unpublished Computational Fluid Dynamics (CFD) simulations (Longest et al. 2020) which are able to measure system properties most anywhere within the simulation region with minimal post-processing. Additionally, the originally developed VCU Small Particle Spray Dryer was able to achieve the CFD-suggested drying conditions, but it lacked ability to quantify how precisely these conditions existed throughout the experimental run. The objective of this chapter was to develop, construct, and document, enhanced control and monitoring capabilities for an in-house small particle spray dryer. Key attributes of the system include: visual readouts of current system conditions, coordinated recording of system conditions, direct input of operation parameter goals, expansion room for additional sensors, and accessible programing for coding operational changes.

10.2 Materials and Methods

10.2.1 Inlet Air Water Content

The VCU Small Particle Spray Dryer utilized an open loop system configuration with room air as the drying gas (See Figure 10.1). Air, a general term for a mixture of gasses, has different properties depending on physical constraints and chemical composition ratio. This study's parameter of concern was the capacity to absorb water from the nebulized drug solution. This was dependent on the interconnected inlet air attributes of temperature, relative humidity (RH), and water vapor concentration. The water vapor concentration was measured in grams per cubic meter of air. For experimental planning and computational fluid dynamics, a calculation spreadsheet was previously created to organize test cases and associated values. This spreadsheet performed a set of calculations to output RH values of the inlet-mixing-chamber air, the drying-tower air, and the outlet air. These values were obtained from inputs of inlet-mixing-chamber water vapor concentration, inlet-mixing-chamber air temperature, drying-tower air temperature and flowrate, nebulizer flowrate, and spray solution liquid water mass fraction. Intermediate steps were: finding the vapor mass fraction (Y_v) (See Equation 3.1) and finding the saturated mass fraction ($Y_{v,sat}$) at each location. $Y_{v,sat}$ was determined from a version of the Antoine equation and ideal gas law

$$Y_{v,sat} = \frac{P_{sat} * R * T}{\rho} \qquad \text{(eq 10.1)}$$

with

$$P_{sat} = e^{A - \frac{B}{T - C}} \qquad \text{(eq 10.2)}$$

where P_{sat} is the saturation pressure of air, R is the gas constant of water vapor, T is the air temperature in Kelvin, ρ is the air density in kg/m^3, A = 23.196, B = 3816.4, and C = 46.13. The main output of the calculations, the resulting RH at each specific location, was then calculated as

a ratio of Y_v and $Y_{v,sat}$ (See Equation 3.2). During pre-control system experimental runs, the inlet-mixing-chamber air temperature was measured then entered into the spreadsheet to check to see how closely the experimental conditions matched the goal conditions. Adjustments to inlet conditions were then made, if deemed necessary. Reorganization of these equations to utilize the experimentally measured values of temperature and RH as inputs, and to output an inlet-air water vapor concentration value, was key for implementing an automated control system response.

10.2.2 Air Monitoring Progression

Bluetooth Sensors – First Stage

In the first stage of increased monitoring, Sensirion SHT31 Smart Gadget temperature and relative humidity devices were linked via Bluetooth to a handheld computer running the iOS-based sensor-manufacturer application. These sensors were configured to record data every ten seconds during the run and to capture changes during the experiment. Device output was considered for manual adjustments during setup, then left mainly as a monitor during the run, with occasional additional manual adjustments. Post run, the data was exported, saved, and organized with the other relevant run information. The SHT31 devices were located to measure temperature and relative humidity of the ambient air, the inlet-mixing-chamber air, and the post-production storage container air. This first stage mimicked the analog measurement and recording process of the original VCU Small Particle Spray Dryer of Chapter 9.

Pre-Collection Temperature Probe – Second Stage

The second stage of increased monitoring consisted of a 13-point temperature sensor device positioned just above the collector. This 3D printed apparatus was positioned within the

171.5mm diameter removable transition. This location was defined as the separating point of the drying region from the collection region (See Figure 10.2 a). The cross section of the bars holding the sensors was tear-drop shaped to minimize deposition. The 13 measurement points were placed in a cross pattern following a log scale positioning system equating to 0.032, 0.135, 0.321, 0.500, 0.679, 0.865, and 0.968 times the diameter of the removal transition. The bi-metallic joint of each of the thirteen 30-gauge PFA insulated K-type thermocouples (5SC-TT-K-30-36) from OMEGA Engineering Inc (Norwalk, CT, USA) was positioned just above the crossbars and epoxied into place. The molded connectors were cut off and the wire ends were hooked up to a Raspberry Pi 3+ running custom code. Thermocouple interface and signal interpretation was handled via Thermocouple Amplifier Breakout v2.0 Printed Circuit Boards (PCB)s developed by Adafruit Industries (New York, NY, USA) and a compact custom wiring harness on a prototyping breadboard (See Figure 10.2 b). To achieve the compact breadboard wiring, a 3D printed insulating divider cover was developed to prevent short-circuits of the MAX31855 Integrated Circuit (IC) based PCBs underside solder points and the connecting jumpers (See Figure 10.2 c). Communication to these PCBs was via Serial Peripheral Interface (SPI) protocol which shares power, ground, clock, and data lines, but requires individual chip-select pins. To provide an organized and consolidated set of chip-select pins, an expansion PCB was placed atop the Raspberry Pi. This Adafruit GPIO Expander Bonnet utilized a MCP23017 IC to provide sixteen additional General-Purpose Input Output (GPIO) pins accessible via the Inter-Integrated Circuit (I^2C) communication bus. The controlling code for this stage's temperature measurement apparatus was written in a Python script that, when executed, queried the sensor array approximately once per second for one minute. Each query was displayed on the connected monitor in a text-based pattern matching the actual sensor crossed layout (See Figure

10.3). This second stage performed monitoring of the interior temperature independent of collector mechanism without altering the operations of ongoing experimental studies.

Electronic Controlled – Third Stage

The third stage of increased system air monitoring incorporated parameter measurements into a feedback loop for system control by the onboard Raspberry Pi computer. This developed control system software version, dubbed Motz, focused on two parameters of the inlet air. The first focus was controlling the humidification aerosol production within the inlet-mixing-chamber to achieve a desired water vapor concentration. Temperature and relative humidity conditions of the mixing chamber air were measured using a Sensirion SCC30-DB PCB positioned at the intake tube entrance. This SHT30-DIS IC based PCB module, communicating via the I^2C bus to the Raspberry Pi, was signaled by the Motz control program to report a Single Shot High-Repeatability reading for each cycle of the control routine. Water vapor concentration calculations, based on received sensor data and algebraic manipulations of the same equations explained in Section 10.3.1, were handled by the software and returned a relative error percentage. The Motz version of the control system reacted to these calculated values by turning on or off the humidification aerosol production, in the inlet-mixing-chamber, at specific relative error values. Specifically, the on-board GPIO pin 23 was placed in a low state (off) or high state (on) which triggered circuitry to switch a relay. This relay routed power to the ultra-sonic nebulizer circuit board of the humidification system causing aerosolization into the inlet-mixing-chamber. This first focus of the third stage handled the inlet-mixing-chamber humidification requirement, without needing separate conversions of the sensor readouts and water vapor concentration goals.

The second focus of the Motz software was controlling the inlet heater power to achieve a desired drying-air temperature. Drying-air temperature was sensed via a K-type metal rod thermocouple placed between the Inlet Unifier and the Spray Head. Connection to the Raspberry Pi was achieved via the same PCB system as the pre-collector temperature probe. Based on a direct comparison of the measured temperature value to the setpoint, the on-board GPIO pin 24 was placed in a high/low state to activate/deactivate the heater relay. When activated, the heater relay completed the heater circuit allowing AC current flow from the voltage regulator through the heater element. This portion of the third stage not only controlled drying-air inlet temperature, but also provided a link and reference point for the pre-collection temperature probe measurements.

10.2.3 Nebulizer Spray Rate

In typical use of the Buchi B-90 and VCU Small Particle Spray Dryer, nebulizer liquid flows from a cooled bulk-storage reservoir (FarkanCooler) into the spray head. A portion of this fluid flow is nebulized, while the remainder flows back into the bulk-storage container. Two methods (flow and mass based) for the measurement of the nebulization rate were developed for utilization, depending on application.

Flow Based

In theory, a subtraction of the flow returning to the reservoir from the flow going into the spray head would equal the spray rate. Therefore, two Sensirion SLF3S-1300F flow meters were incorporated into the liquid flow path. Theses sensors communicate via the I^2C bus, but all have the same address; therefore, an Adafruit TCA9548A I2C Multiplexer PCB was utilized between

the sensors and controller. This Texas Instruments TCA9548A IC based PCB allowed for programmable connection of specific devices to the communication bus. The utilized SLF3S-1300F flow meters were known to be sensitive to flow spikes present in the spray dryer system setup; therefore, the manufacture-suggested flow-damping-kit tubing was implemented with a variable critical orifice. Additionally, a windowed-median filter was applied to the measured signal before subtraction was performed. This system allowed for direct utilization of nebulizer spray rate in other parts of the controlling program.

Mass Based

In theory, the only exit for mass from the nebulizer spray circuit as a whole was the spraying of liquid. Therefore, an electronic mass balance was placed under the bulk-storage cooling reservoir to track the decreasing system mass. This Reshy brand digital balance with increments of 0.01 g and a capacity of 5000 g was sufficient to capture the decreasing mass of the operating FarkanCooler. Mass was recorded separately from the electronic control system every minute for five minutes and then the average flow rate was calculated from the known solution density.

10.2.4 Data Output

Control system monitoring and data logging was included in the Motz software version. Parameter monitoring was provided via a regularly rewritten on-screen output, and a separate output file was recorded for logging. Display output and file storage of system parameters was the last item in the operation control period loop.

Screen Logging Output

A customizable text-based output to the Integrated Development Environment (IDE) that rewrote itself on each update, without saving, was implemented for monitoring of system parameters relevant for system development (See Figure 10.3). An update time of two seconds was chosen by setting the *log_screen_interval* value to 2.00 before running the control script. When activated, the screen logging code printed specified parameter labels and values organized into columns, and it also printed labeled values from the pre-collection temperature probe in a pattern matching the physical build. Code manipulations at approximately line 375 enabled changes to exact formatting and outputs.

Text-based Logfile Output

Data logging for post-run analysis was a tab-delimited text file in which each new line entry corresponded to a specific recording event. The gap of ten seconds between recording events was set using the *log_file_interval* variable. Creation and configuration of the logging file was coded at approximately lines 180 – 190 of the control script version Motz. The output file path name was specified to include system date and a user-defined identifier. The first couple of file content lines, containing general information and column headings, were also written in this setup code section. During each operation period loop requiring a data output, code around line 400 added a new line entry containing parameter values to the end of the file. Chosen output parameters included items such as the time (Unix epoch of January 1, 1970 00:00:00 UTC), the inlet air conditions, pre-collection temperature information, and the spray liquid reservoir temperature. Once the run was completed, this recorded data file was translated into a graphical format for visualization (See Figure 10.4).

10.2.5 Control System Verification

Operational verification of the VCU Small Particle Spray Dryer control system was done in stages and culminated with initiating several test cases with different spray conditions. During development, the control subsystems were tested independently, then integrated together. A long duration spray drying run, from system startup to shutdown and cleanup, was completed to test reaction of control system to environmental changes during a full-length experimental run. Several cases (See Table 10.3) were selected as targets for further research. Lastly, the ability of the control system to achieve the parameters of inlet-air water vapor concentration and drying-air temperature was tested by initiating and running a few minutes of each test case.

10.3 Results

The developed VCU Small Particle Spray Dryer with the Motz control system does not self-limit the range of parameter setpoints. However, not all possible parameter values were achievable due to both physical and computational limits; therefore, suggested limits on operating condition parameters are listed in Table 10.1. The procedural order to achieve a dried powder with the Motz control software (listed in Table 10.2) contained additional steps over the hand-controlled system process to setup the computer control and measurement systems. The mass-based method for determination of the nebulizer spray rate during experimental runs was successfully utilized and was recommended for immediate implementation. This system provided faster feedback than the previously utilized volume-based methods. Even faster measurements were achieved with the electronic flow sensors, but the cost of the speed increase

was a lack of consistently accurate information. Reliable spray rate measurements via the flow meters were not able to be achieved with the current peristaltic pumping mechanism setup. During the full-length experimental run, the python-based script (See Appendix 12.1.4) kept the inlet-air water vapor concentration and drying-air temperature constant. The graphical log of the full-length experimental run (See Figure 10.4) depicted this constant density input, while increases in box temperature led to decreases in box relative humidity requirements. Control system verification case outcomes were successful and tabulated in Table 10.3.

10.4 Discussion

The developed control and measuring system for the VCU Small Particle Spray Dryer was successfully implemented to provide a higher level of monitoring during powder production. Additionally, the system was developed with expandable capacity for future experimental needs. Major advantages of the developed system over the Buchi B90 were the reduced cost and increased operational flexibility. However, the commercial system provided clear advantages in robustness and ease-of-use in many areas. The following subsections explore the consequences of the implemented design choices.

Air Monitoring Inlet Mixing Box

The Motz version of the control software achieved the goal of a steady-predefined inlet-air water vapor concentration through control of relative humidity within the Inlet Mixing Chamber. However, an observable cyclic variability in relative humidity was introduced due to the relative-error on-off method of humidifier control. The range of variability was considered acceptable for this first control system version as it was predictable. Future versions could be

improved by refined humidification controls such as the inclusions of resistors for variable strength humidification and new algorithms for rate-of-change based control.

Air Monitoring Spray Region

The inclusion of recorded outputs in the control system allowed for the quantification of the temperature swings observed within the drying region during tests of previous systems. One reason for these swings was the use of the high thermal mass K-type metal rod thermocouple chosen to mimic the Buchi B-90 sensor and give a representative temperature across the flow field. Future systems could lessen the fluctuations through the use of a faster response time probe, enhanced control algorithms, or heater voltage control.

Connection of the pre-collection temperature probe through the expansion board required utilization of a smaller CPU heat sink which limited natural convective cooling. Fortunately, thermal issues were not found to be of great concern with the Motz version of the control script elevating CPU temperature to approximately 43°C under load. The huge expansion capability of the expansion bonnet, and possible additional stacked bonnets, was determined to out-weigh the possible need for forced-air cooling to run future software version.

Temperature sensors used in the spray region utilized a calibration offset in the code to account for sensor differences at expected system thermal equilibrium. These values were manually adjusted and checked sporadically during initial development and experimentation. Offset values were small and therefore minimal resources were spent on this topic. Future versions could implement a more stringent calibration process into the spray drying routine, if highly accurate values were desired. Additionally, the basic signal to temperature conversion routine could be replaced by the more computationally intensive NIST subroutine.

Nebulizer Spray Rate

Although the measurement systems were developed specifically for the VCU Small Particle Spray Dryer, both systems could be implemented on the Buchi-B90 unit. Even though the mass-based system lacked centrally integrated data logging, it should be utilized immediately for experimental runs where nebulizer spray rate is of importance. Reliable spray rate measurements from the electronic flow meters requires additional engineering to either remove the peristaltic pump or mitigate the current flow spikes. Given that the VCU Small Particle Spray Dryer does not currently implement variable spray rate nor flow rate mechanisms, the mass-based system functions sufficiently.

Data Output

The screen output format shown in Figure 10.3 was developed to display pertinent information needed during system software development. Much of the information constantly refreshed on the screen could be transitioned to the data logging file, thereby, leaving fewer values in the screen-based output. Reformatting of these pertinent values could enable the IDE software to graphically display a log during the experimental run.

The filename of the data output was chosen to only include the year, month, day, and identifier to limit the character length. However, data loss due to file overwriting occurs if user does not update the identifier for each new run of the script. A possible solution to this would be to additionally include the hour and minute of file creation in the filename. Another solution would be for the program to check to see if an identical filename already exists in the specified directory.

Control System Verification

The control system verification methods, a full operational length test case, and several test case startups, demonstrated system performance without detrimental errors. This lack of error was perhaps due to the operator's singular focus on the verification task without the hectic multi-person environment typically encountered during regular operations. Control system script fatal errors occurred at multiple points during non-control system verification testing; however, all errors encountered during experimentation were able to be remedied with minimal disruption to workflow. The developed code, version Motz, contained almost no error handling nor error monitoring. As an initial laboratory system, it was determined that only operating system file modification commands required error handling. Future software developers and system engineers could focus attention to modifying or implementing checksum algorithms, error returns, exit procedures, input verifications, output verification, and user interface warnings.

10.5 Tables

Table 10.1: Specific Operating/Measuring Ranges Recommendations

Item	Recommended Value	Unit
Air Flow Rate	< 140[a]	LPM
Temperature Mixing	< 85[b]	°C
Temperature Heating	< 140[c]	°C
Temperature Cooling	-2-22	°C
Temperature FarkanCooler	10-20	°C
Log Screen Interval	≥ 1	Second
Log File Interval	≥ 1	Second
Allowable Relative Error	≥ ± 2	%

[a] limited by use of single pump
[b] limited by Sensirion Inlet Temperature PCB operating spec
[c] limited by 3D printed spray head

Table 10.2: Start-up, shut-down, and electronic collection procedural order for a normal run of 170 minutes with Motz control system

Step	Item
1	Pre-make solution 12 hours minimum before spray and pre-cool
2	Assemble tower for spray configuration
3	Setup FarkanCooler atop mass balance
4	Setup spray feed pump prime the flow lines
5	Fill and position the humidity source
6	Power on the Raspberry Pi
7	Update Raspberry Pi current time
8	Open the Spray System Control version Motz Python script file
9	Check parameter set-points for correct value
10	Ensure correct output filename items
11	Fully turn on house air to wall mounted dryer
12	Turn vacuum pump on
13	Check flow rate and begin software recording
14	Turn on heater power source and ensure voltage regulator is at ~35%
15	Run the Python Control Script
16	Monitor and wait for inlet temperature to reach setpoint
17	Power on the spray feed pump and spray head voltage signal
18	Observe normal spray plume pattern
19	Ensure center ground and outer high voltage (HV) leads are connected
20	Turn on and enable the HV power supply
21	Record spray system mass at one-minute intervals and determine flow rate
22	Monitor for correct operation until end of spray duration
23	Disconnect the feed tube from liquid reservoir
24	Once spray stops, turn off spray head voltage signal
25	Turn off FarkanCooler
26	Disable and turn off HV power supply
27	Toggle the Control System End Switch

28	Turn off vacuum pump and end flow logging
29	Turn off house air
30	Lower tower and place upper sections to side
31	Lift out collector cylinder and place on clean, pre-creased, aluminum foil
32	Use spatula to scrap circumferentially, from inner top to bottom, the powder onto the foil
33	Pour powder into a pre-cleaned, dried, and pre-weighted glass vial
34	Reweigh vial to determine current total mass collected
35	Cover with Kimwipe and reweigh for baseline storage mass
36	Store in desiccator at 0% RH for 5 days
37	Flush spray loop with DI water
38	Rinse collector electrodes with DI water then spray with denatured alcohol and set to dry
39	Wipe residual powder from spray drying tower components
40	Empty and clean humidification source
41	Transfer data from Raspberry Pi
42	Shutdown Raspberry Pi then turn off power

Table 10.3: Cases for testing control system reaction to additional parameters

Case	Water Vapor Concentration (g/m^3)[a]	Drying Air Temperature (°C)	Corresponding Inlet Box RH at 24 °C (%)	Successfully Achieved (Yes/No)
0	10	70	46	Yes
1	7	60	33	Yes
2	5	60	23	Yes
3	7	50	33	Yes
[a] concentration of water vapor in air measured as grams of water per meter cubed of air				

10.6 Figures

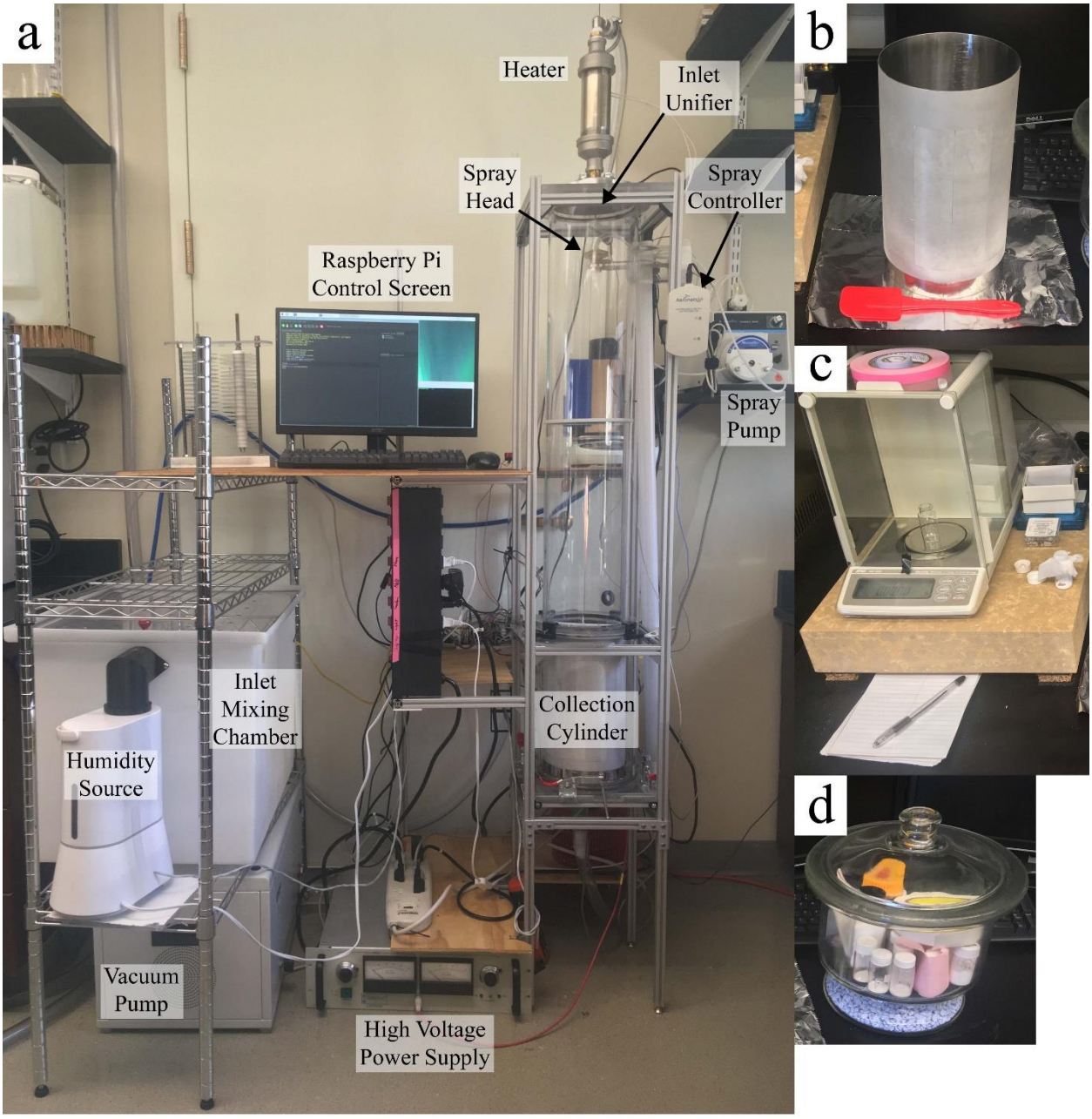

Figure 10.1: General system setup pictures of **(a)** spray dryer unit, **(b)** collection cylinder on collection foil, **(c)** mass balance with covered vial, and **(d)** storage desiccator

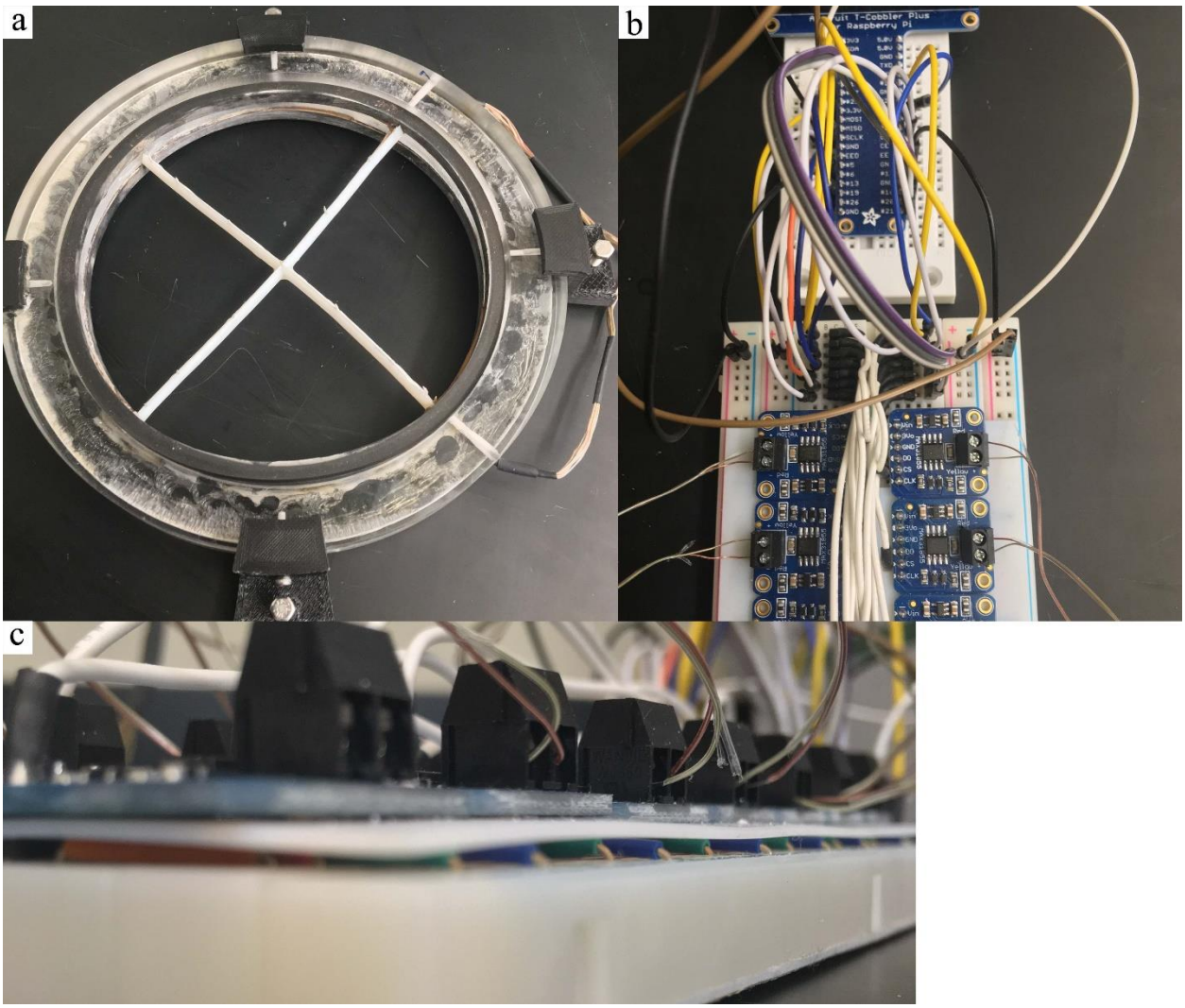

Figure 10.2: Pre-collector temperature measurement apparatus.

(a) sensor cross installed within spacer ring, **(b)** thermocouple breakout breadboard, and **(c)** 3D printed cover preventing short circuits

```
BoxTcel                          BoxRhoDryAir                     BoxPsat                 YvBoxSat
23.720912489509416                1.1892333187081123               2908.371794072519       0.01785021712362792
BoxAirBulkDensityActualgperm3    BoxAirBulkDensityGoalgperm3      BoxABDRelError
9.852987304199308                 10                               -1.4701269580069187
YvBoxActual                      YvBoxGoal                        YvBoxRelError
0.008285159143457907              0.008408778868442063             -1.470126958006922
BoxRH                            RHBoxGoal                        BoxRHRelError
46.414892805371174                47.107431860375286               -1.4701269580069065
humidity_strength                PressurePa
humidity_strength                 1092.25
TTOP                             TTOPgoal                         TTOPPRelError
69.75                             70                               -0.35714285714285715
TPOST                            RoomTcel                         RoomRH                  last_loop_duration
37.5                              23.560692759594104               34.338902876325626      0.1344139575958252
Bulk Liquid Temp
4.5
TA1                                                 TB1
        TA2                                 TB2
                TA3                 TB3
                        TC
                TB4                 TA4
        TB5                                 TA5
 TB6                                                TA6
38.25                                                34.5
         43.5                                    42.0
                  44.0                 42.25
                          39.5
                  42.5                 41.25
         44.25                                   42.75
 38.75                                                38.0
TAVG              40.88461538461539
last logged to screen at  1636566688.052194
last logged to file at  1636566680.7823944
```

Figure 10.3: Graphic of the VCU Small Particle Spray Dryer control system (version Motz) screen output feature

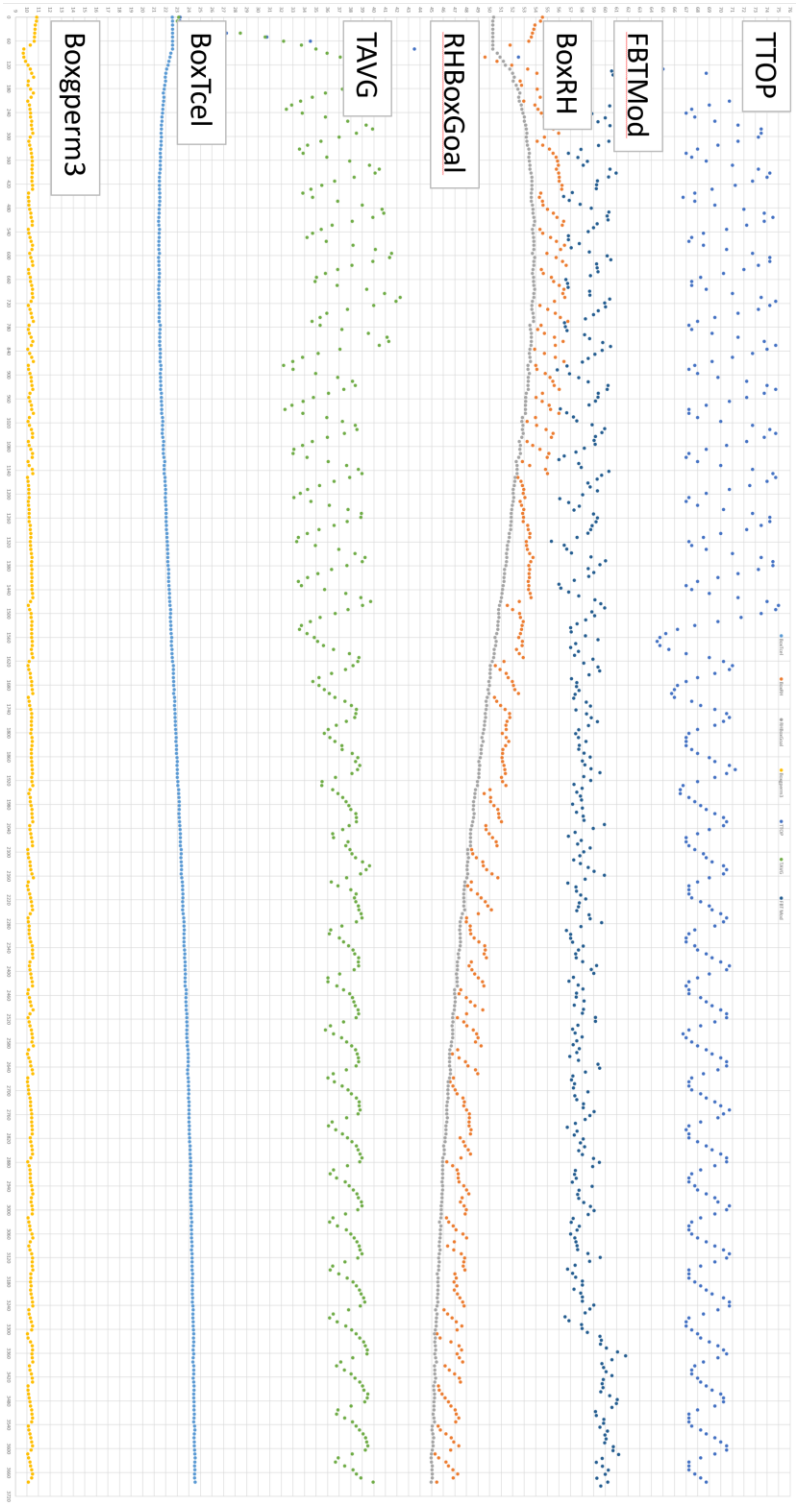

Figure 10.4: Representative graphical data output derived from the text-based logfile of the control system code

Chapter 11: Conclusions and Future Work

This dissertation focused on vibrating mesh nebulizers for production of pharmaceutical aerosols targeting the lungs. A systematic device development approach interweaving computer simulation, mechanical design, and pharmaceutical testing supported the completion of this research scope. The developed systems enabled high efficiency targeted delivery of medication and opened the door to more impactful use of current inhaled medicines and previously too costly medicines. Research on these systems added several contributions to the field of aerosol drug delivery and to the research capabilities at VCU. However, potential for additional development and research are still numerous in this growing field.

Nebulized Aerosol Delivery During Continuous Flow Respiratory Support

This dissertation successfully implemented a combination of previously and newly developed technologies to deliver therapeutic aerosol during high flow nasal cannula therapy at high efficiency. Application of developed technology opens the door for new inhalation treatments and efficacy improvement of current treatment protocols. This dissertation specifically contributed the hardware and software integration to detect and utilize the inhalation effort of a spontaneously breathing adult subject during therapy.

Extension to new topics and advanced functions

The patented technology applied in the initial human subject tests should be explored further in continuation of testing and expansion into new topics. Exploration of the Heated Dryer System illustrates one area of expansion for this technology. Electronic control and monitoring of aerosol therapies has the potential to greatly increase the efficacy of treatments. Suggestions

for the future of this system can be split into the two categories of those specific to laboratory testing and of those for advanced function. Before a human subject radiolabeled laboratory study, procedures for dynamic drug nebulization duration should be established. Duration-change and execution criteria must be well documented and could be either computer algorithm initiated or experimenter initiated. For example, the duration could be changed from 1000 milliseconds to a percentage of the subject's inhalation duration. Total drug nebulizer duration was already tracked in some code versions and treatment time could be linked to this parameter. Radiolabeled human subject laboratory studies could also incorporate an additional layer of protection against fugitive aerosol emission and spread. This could be as simple as a cloth facemask or a more advanced approach such as the use of a modified medical facemask. Unpublished development of a modified PerformaTrak™ facemask for use with the LVMH device could possibly filter exiting air and measure breathing flowrate of the subject. Suggested advanced functions for incorporation into future devices would help with both efficiency and device usability. Removal of the Aeroneb Solo skirt or direct integration of a mesh nebulizer would likely give a slight increase in efficiency. Utilization of nebulizers with greater ability to nebulize viscous or low-ion solutions would broaden the drug application range for the LVMH. For all nebulizer designs, reliability of the aerosol production is key for consistent performance. Modifications to the nebulizer driving signal, such as a high amplitude lower frequency burst, at the start of production might increase reliability of the Aeroneb Solo aerosol production. Lastly, incorporation of an internal airflow source and self-cleaning options similar to the Fisher & Paykel Airvo 2 system should be explored.

Nebulized Aerosol Delivery With Inhalation Based Flow

This dissertation presented a stand-alone high efficiency delivery system for therapeutic aerosols via the oral route. The adult population already has several options for stand-alone oral delivery of prescription medications. However, this new device is important because initial tests, conducted in this dissertation, suggest that the unit's deep lung delivery efficiency far exceeds commercially available devices. Future high-resource treatment facilities could utilize this technology to develop enhanced treatment regiments.

Topic outlook and system improvements

The developed main hardware and software technology was focused on oral delivery, but the system concept is applicable to multiple scenarios of forced cyclic flow. The first and foremost next application of this system is the testing of EEG aerosols. Minimal, if any, device hardware or software modifications would likely be needed for direct usage of the current system in short-term delivery studies of radiolabeled aerosol in human subjects. However, device usage scenarios requiring delivery times longer than a couple minutes need to incorporate additional saliva management techniques such as a recessed area at the device exit to collect excess saliva. This device technology could readily be applied to electronic ventilator-based ventilation drug delivery situations. The developed system already includes the software coding and input port for receiving a voltage signal from an inhalation-driving device and then triggering nebulization synchronized to the input signal. However, the application to ventilator-based drug delivery would require new hardware to adapt to the specific flow pathways. Since human subject testing at VCU remains a challenge, the Heated Dryer System should be modified for continued benchtop applications. Recent work from the Corcoran laboratory in Pittsburgh, Pennsylvania,

and Fromen laboratory in Newark, Delaware, continue to improve the realism of models for testing when human subject studies are unavailable. Continued major advancement of the developed system might require collaboration with research organizations outside of Virginia Commonwealth University.

Dry Powder Production

This dissertation presented a re-creation of the Buchi Nano Spray Dryer B-90 technology to produce dry powders with primary particle sizes near 1 μm. The uniqueness of the developed system lies in the lower cost and increased adaptability for particle engineering experiments. The powders produced by this system and utilized in the novel inhalers developed at VCU are of interest because the combined systems are capable of achieving such high estimated lung dosages.

Although the developed system was successful, additional improvements and features for the VCU Small Particle Spray Dryer are easily envisioned. The usability of the system would be greatly enhanced by molded and cast-in-place silicone sealing rings without sacrificing experimental versatility. A new lifter mechanism which allows single hand actuation would also help system usability. However, the simplicity of the current system allows good experimental versatility for testing additional powder collection methods. A potential new lifter mechanism should have separate systems for sealing of the pre-collection temperature sensor up to the inlet unifier and for sealing of the powder collection system. Although not necessary, separate sealing mechanisms make the exploration of new collection systems easier by allowing straight forward integration. Exploration of new collection systems, such as using high porosity membranes and increased water content control, has begun; but thus far has been inconclusive. Additional post-

production testing equipment and handling procedures may shed light onto the major post-production factors influencing the powder particle and the powder bulk characteristics.

Future control system software should consider additional features to improve experimental versatility. Advance system control, via additional buttons or switches, could allow ability to change setpoint parameters during the run, to change calibration values, and to log the time of external events. An ability to change setpoints during the run could lead to control system reactions to parameters such as pre-collection temperature, outlet temperature and relative humidity, spray liquid bulk temperature, and ambient conditions. Updates to the control system should not overlook the information logging features of the control system. Future experimenters should re-evaluate current need and purpose of the screen-based on-line monitoring as a visual tool, and then adjust the output accordingly.

Closing Remarks

It has been a privilege to have been involved with activities at the VCU engineering program for so many years. During my time here at VCU I have seen many changes, expansions, and even a name change from School of Engineering to College of Engineering. Several new facilities have opened, including the East Hall, the Institute for Engineering and Medicine wing, the Biotech spaces, and the Engineering Research Building. Yet, VCU Engineering still holds onto the thing that brought me here originally. It provides research opportunities for those who seek to get involved.

The Aerosols in Medicine laboratory has been my engineering home for the later years of my time at VCU. The research topics being investigated here are interesting, complex, and useful for society as a whole. I am especially excited for the continued laboratory research in the realm

of dry powder inhaler delivery of Excipient Enhanced Growth pharmaceutical formulations and in the realm of combined pharmaceutical aerosol delivery with respiratory support. I believe both of these technological platforms have the potential to be highly beneficial to society if commercialized and mass produced. Through the research and development of these topics, I have learned new skills in aerosol science, laboratory experimentation, and computer aided design while applying and refining my skills, first learned many years ago, in computational thinking and exploratory experimentation. As I graduate and transition away from academics into industry, I am excited about both my future endeavors and the continued research prospects of the work I have completed for my degree.

Chapter 12: Appendix

12.1 Computer Codes

12.1.1 LVMH Human Subjects Safety Trial – Brown Box Code

The following Arduino code to run the Brown Box Build (BBB) of the LVMH was used in the Human Safety Trial experiments and can be utilized for additional testing with the ASL5000. The controls the LVMH based on the sensed breathing profile of a subject connected to the system. Additional control code schemes were written for the BBB for experimental development, and more details can be found in the file archieve Appendix 12.3. Supporting h and cpp files were originally sourced from GitHub posts. These library files are required for code operation and are included here with my comments for clarity.

Control Board Main File

```
/************************************************************
 *  BBB1_CS_D18_v1
 *
 *  Heating turned on or off at start of loop based on temp controller
 *
 *  Switch case statement to trigger drug from ASL or Pressure input
 *
 *  PRESSURE INPUT MODE
 *  *Critical pressure relative to sensed Max and Min pressures (decimal form of % generally set
at 50%)
 *  with a reset every x.xxx seconds (cPressResetMills) to sensor value generally 20
 *  *When sensed pressure crosses below critical pressure, gap then produce aerosol for target
length
 *
 *  ASL INPUT MODE
 *  *ASL digital out set to produce 5V ttl constant signal on inhale
 *  *On 5V inhale signal, gap then produce aerosol for target length
 *  *This code only allows for production after ASL start - for prestart production use updated
timer code
 *    -possible method for this would make the drug nebulizer normally producing and then ASL to
signal humidity neb
 *
 *  SERIAL TRANSFER most items removed because monitor unit gathers data
 *
*    Last Updated 5th Feb 2020
*
 ************************************************************/

#include <Wire.h>
#include "SDP3x.h"

// variables for device as builts
const int ledHardPin = LED_BUILTIN; // the number of the LED pin hardwired on board
const int relay1Pin = 4; // Nebulizer - NC saline NO drug
```

```
const int relay2Pin = 7; // LED Neb Status - NC saline NO drug
const int relay3Pin = 8; // Not Used in BB_B1
const int relay4Pin = 12;// Heater Power - NC none, 24V+ at Common, NO heater
const int LEDinhalePin = 3; // Inhale LED illuminate HIGH

// variables for heating
const int heatcallPin = 11;
int heatcallState = LOW;

// variables for breath determination mode
const int breathmodePin = 9;
int breathmodeState = LOW; // LOW ==> Pressure Triggers ---- HIGH ==> ASL Triggers

// variables for ASL breath profile
const int ASLinhalePin = 6;
int ASLinhaleState = LOW; // LOW ==> ASL Exhale ---- HIGH ==> ASL Inhale

// variables for breath point determination
float difPressure;
float difTemperature;
float cPress;
float cPressMaxSpan;
float cPressMinSpan;
float cPressMaxLast;
float cPressMinLast;
float difPressureMid;
float MMweighttemp;
float MMweight;
float MMweightp;
int patExhaleState = 1;
unsigned long cPressMaxSpanWrite;
unsigned long cPressMinSpanWrite;
unsigned long cPressMaxLastWrite;
unsigned long cPressMinLastWrite;
unsigned long difPressureMidWrite;
int cPressSpanMillis;
int cPressLastMillis;
int difPressureMidMillis;

// variables for millis time keeping and drug production
unsigned long exhaleEND;
int iterationA = 0;
int iterationB = 0;
unsigned long targetINTdrug;
unsigned long breathSTART;
unsigned long drugSTART;
unsigned long currentMillis;

int delayTimePRESS;
int delayTimeASL;

/*************************************************************/

void setup()
{
  // initialize digital pins as outputs
  pinMode(relay1Pin, OUTPUT);
  pinMode(relay2Pin, OUTPUT);
  pinMode(relay3Pin, OUTPUT);
  pinMode(relay4Pin, OUTPUT);
  pinMode(ledHardPin, OUTPUT);
  pinMode(LEDinhalePin, OUTPUT);

  // initialize digital pins as inputs
  pinMode(heatcallPin, INPUT);
  pinMode(breathmodePin, INPUT);
  pinMode(ASLinhalePin, INPUT);
  pinMode(A4, INPUT);
  pinMode(A5, INPUT);

  // initialize counters and timers
```

```
  delayTimePRESS = 250;   //milliseconds trigger to production PRESSURE MODE
  delayTimeASL = 100;     //milliseconds trigger to production ASL MODE
  targetINTdrug = 200;    //milliseconds aerosol production length
  cPress = 150;           //arbitrary start value for critical pressure point
  cPressMaxSpan = 1;     //arbitrary start value for critical max pressure point of Span
  cPressMinSpan = 600;   //arbitrary start value for critical min pressure point of Span
  cPressMaxLast = 160;   //arbitrary start value for critical max pressure point of Last
  cPressMinLast = 140;   //arbitrary start value for critical min pressure point of Last
  MMweight = 0.5;         //Preset % between max and min to place critical trigger
  MMweightp = 1-MMweight;//and calculated complement point (MMweight = 0 to 1 ==> min to max)
  cPressSpanMillis = 30000;     //milliseconds between max/min pressure resets (system change
responce time)
  cPressLastMillis = 20002;     //milliseconds behind to search for the determination of reset
values
  difPressureMidMillis = cPressLastMillis/2;  // implies that cPressLastMillis must be even by
int definition

  //Pressure sensor Setup
  Wire.begin();
  Serial.begin(9600);
  difPressure = 145.0;
  difTemperature = 12;
}

/*****************************************************************/

void loop()
{
// Read temp controller status and put relay in proper position
heatcallState = digitalRead(heatcallPin);
  if (heatcallState == HIGH) {
    digitalWrite(relay4Pin, HIGH);
  }
  else {
    digitalWrite(relay4Pin, LOW);
  }

// Read breath sensing mode switch and save into breathmodeState value
breathmodeState = digitalRead(breathmodePin);

switch (breathmodeState){ //change between Pressure Sensor and ASL
  case LOW: // use the Pressure Sensor for triggering nebulizers

     //Read pressure sensor
     //Set cPressMaxMinSpan AND cPressMaxMinLast values if needed
     //Set a dif pressure mid value at a central time point
     //Reset cPressMaxMinSpan and cPressMaxMinLast value if needed
     //Set cPress value based on MMweight percent and cPressMaxMinSpan
     //Compare diffPressure and cPress to determine if exhale
     //Read and export true breath cycle from ASL for analysis

      // Read (and print) differential pressure value of sensor
      difPressure = SDP3x.getPressureDiff();
      Serial.print(difPressure);
      Serial.print("\t");

      // Set cPressMaxMinSpan AND cPressMaxMinLast values if needed
      if (difPressure > cPressMaxSpan) {
        cPressMaxSpan = difPressure;
        cPressMaxSpanWrite = millis();
      }
      if (difPressure < cPressMinSpan) {
        cPressMinSpan = difPressure;
        cPressMinSpanWrite = millis();
      }
      if (difPressure > cPressMaxLast) {
        cPressMaxLast = difPressure;
        cPressMaxLastWrite = millis();
      }
      if (difPressure < cPressMinLast) {
        cPressMinLast = difPressure;
```

```
        cPressMinLastWrite = millis();
      }

      // Set a dif pressure mid value at a central time point
      if ((millis() - difPressureMidWrite) >= difPressureMidMillis){
        difPressureMid = difPressure;
        difPressureMidWrite = millis();
      }

      // Reset cPressMaxMinSpan value if needed
      if ((millis() - cPressMaxSpanWrite) >= cPressSpanMillis){
        cPressMaxSpan = cPressMaxLast;
        cPressMaxSpanWrite = millis();
      }
      if ((millis() - cPressMinSpanWrite) >= cPressSpanMillis){
        cPressMinSpan = cPressMinLast;
        cPressMinSpanWrite = millis();
      }

      // Reset cPressMaxMinLast value if needed
      if ((millis() - cPressMaxLastWrite) >= cPressLastMillis){
        cPressMaxLast = (difPressure + difPressureMid)/2;
        cPressMaxLastWrite = millis();
      }
      if ((millis() - cPressMinLastWrite) >= cPressLastMillis){
        cPressMinLast = (difPressure + difPressureMid)/2;
        cPressMinLastWrite = millis();
      }

      // Set cPress value based on MMweight percent and cPressMaxMinSpan
      cPress = cPressMaxSpan*MMweight + cPressMinSpan*MMweightp;
      Serial.print(cPress);
      Serial.print("\t");

      // Compare diffPressure and cPress to determine if exhale
      if (difPressure> cPress) {
        digitalWrite(LEDinhalePin, LOW);
        patExhaleState = 1;
      }
      else {
        digitalWrite(LEDinhalePin, HIGH);
        patExhaleState = 0;
      }

      // Read and export true breath cycle from ASL for analysis
      ASLinhaleState = digitalRead(ASLinhalePin);
      Serial.print(ASLinhaleState);
      Serial.print("\t");

    /************************************************/

    // once patExhaleState drops to 0 have a gap then drug for length of time
    if (patExhaleState == 0) {
      currentMillis=millis();
      if (iterationA == 0) { // do first time through only
        exhaleEND = currentMillis;
//        Serial.print("0\t");//Exhaling Ends
        iterationA = iterationA + 1; // prevent first time rewrite
      }
      else {
        if (currentMillis - exhaleEND >= delayTimePRESS) {
          if (iterationB == 0) { // do first time through only
            digitalWrite(relay1Pin, HIGH);
            drugSTART = millis();
            digitalWrite(relay2Pin, HIGH);
//            Serial.print("10\t"); // Inhaling Drug Production Starts
            iterationB = iterationB + 1;
          }
          else {
            if (currentMillis - drugSTART <= targetINTdrug) {
              digitalWrite(relay1Pin, HIGH);
```

```
              digitalWrite(relay2Pin, HIGH);
//              Serial.print("10\t"); // Inhaling Drug Production
            }
            else {
              digitalWrite(relay1Pin, LOW);
              digitalWrite(relay2Pin, LOW);
//              Serial.print("7\t"); // Inhaling Saline Production
            }
          }
        }
        else {
          digitalWrite(relay1Pin, LOW);
          digitalWrite(relay2Pin, LOW);
//          Serial.print("3\t"); // Inhaling Delay Gap
          iterationB = 0;
        }
      }
    }
    else {
      currentMillis=millis();
      digitalWrite(relay1Pin, LOW);
      digitalWrite(relay2Pin, LOW);
//      Serial.print("0\t"); // Exhaling
      iterationA = 0;
    }


//    // Print time values and pressure points
    Serial.print(currentMillis);
    Serial.print("\t");
    Serial.println();
    delay(1);
    break;

  case HIGH: // use the ASL for triggering nebulizers

    // Read status of ASL breath cycle by reading ASLinhalePin and save into ASLinhaleState
    ASLinhaleState = digitalRead(ASLinhalePin);
//    Serial.print(ASLinhaleState);
//    Serial.print("\t");
    currentMillis=millis();
    digitalWrite(LEDinhalePin, ASLinhaleState*-1+1);
//    Serial.print(ASLinhaleState*-1+1);
//    Serial.print("\t");

    /************************************************/

    //once ASLinhaleState rises to HIGH have gap then drug for length of time
    if (ASLinhaleState == HIGH) {
      if (iterationA == 0) { // do first time through only
        breathSTART = currentMillis;
//        Serial.print("3\t"); // Inhaling Delay Gap Starts
        iterationA = iterationA + 1; // prevent first time rewrite
      }
      else {
        if (currentMillis - breathSTART >= delayTimeASL) {
          if (iterationB == 0) { // do first time through only
            digitalWrite(relay1Pin, HIGH);
            drugSTART = millis();
            digitalWrite(relay2Pin, HIGH);
//            Serial.print("10\t"); // Inhaling Drug Pruduction Starts
            iterationB = iterationB + 1;
          }
          else {
            if (currentMillis - drugSTART <= targetINTdrug) {
              digitalWrite(relay1Pin, HIGH);
              digitalWrite(relay2Pin, HIGH);
//              Serial.print("10\t"); // Inhaling Drug Production
            }
            else {
              digitalWrite(relay1Pin, LOW);
```

```
              digitalWrite(relay2Pin, LOW);
//              Serial.print("7\t"); // Inhaling Saline Production
            }
          }
        }
        else {
          digitalWrite(relay1Pin, LOW);
          digitalWrite(relay2Pin, LOW);
//          Serial.print("3\t"); // Inhaling Delay Gap
          iterationB = 0;
        }
      }
    }
    else {
      digitalWrite(relay1Pin, LOW);
      digitalWrite(relay2Pin, LOW);
//      Serial.print("0\t"); // Exhaling
      iterationA = 0;
    }

    delay(1);
    break;
  }

  //Serial.println(); // New line of serial output to signify new loop through the code
}
```

Control Board Supporting .h File

```
#ifndef SDP3X_H
        #define SDP3X_H

        // convert two 8 bit values to one word
        #define BIU16(data, start) (((uint16_t)(data)[start]) << 8 | ((data)[start + 1]))

        // data length of result from I2C
        #define COMMAND_DATA_LENGTH 2
        #define RESULT_DATA_LENGTH 6

        #define DEFAULT_SDP3X_I2C_ADDRESS  0x21
        #define DEFAULT_SDP8XX_I2C_ADDRESS 0x25

        // triggered mode with 50ms conversion time
        typedef enum {
           SDP_MEASUREMENT_COMMAND_0 = 0x36,
           SDP_MEASUREMENT_COMMAND_1 = 0x2F
        } SDP3xCommands;

        class SDP3xClass
        {
          public:
//              SDP3xClass() : mI2CAddress(DEFAULT_SDP3X_I2C_ADDRESS) {}
      SDP3xClass() : mI2CAddress(DEFAULT_SDP8XX_I2C_ADDRESS) {}
              void setI2CAddress(uint8_t i2cAddress);

              uint8_t readSensor(uint8_t* readData, uint8_t size);
              float getPressureDiff(void);
              float getTemperature(void);

          private:
              uint8_t mI2CAddress;
        };

        extern SDP3xClass SDP3x;

#endif
```

Control Board Supporting. cpp File

```
#include <inttypes.h>
#include <Wire.h>
#include "Arduino.h"
#include "SDP3x.h"

#define SDP_DEBUG

#ifdef SDP_DEBUG
#define DEBUG_PRINT(label, value) \
  Serial.print(" ["); \
  Serial.print(label); Serial.print(" = "); Serial.print(value); \
  Serial.print("] ");

#else
#define DEBUG_PRINT(label, value)
#endif
/*****************************************************************************
 * Global Functions
 *****************************************************************************/

 /*****************************************************************************
  * setI2CAddress
  *  Changes I2C address
  *
  * @param i2cAddress - the I2C address to use
*****************************************************************************/
 void SDP3xClass::setI2CAddress(uint8_t i2cAddress)
 {
   mI2CAddress = i2cAddress;
 }

/*********************************************************
 * getPressureDiff
 *  Gets the current Pressure Differential from the sensor.
 *
 * @return float - The Pressure in Pascal
 *********************************************************/
float SDP3xClass::getPressureDiff(void)
{
  int16_t dp_ticks;
  int16_t dp_scale;
  uint8_t readData[RESULT_DATA_LENGTH] = { 0 };

  readSensor(readData, RESULT_DATA_LENGTH);
  // merge chars to one word
  dp_ticks = BIU16(readData, 0);
  dp_scale = 60;

  return dp_ticks/(float)dp_scale;
}

/*********************************************************
 * getTemperature
 *  Gets the current Temperature from the sensor.
 *
 * @return float - The Temperature
 *********************************************************/
float SDP3xClass::getTemperature(void)
{
  int16_t  temperature_ticks;
  uint8_t readData[RESULT_DATA_LENGTH] = { 0 };

  readSensor(readData, RESULT_DATA_LENGTH);  // merge chars to one word
  temperature_ticks = BIU16(readData, 3); // temperature starts @ 4th byte
  float t_scale = 200.0;
  return temperature_ticks/t_scale;
}
```

```
/*****************************************************************************
 * readSensor
 *  Gets RAW sensor data
 *
 * @param readData - a data buffer to store data into
 * @param size     - the size of said data buffer
 * @return uint8_t - number of bytes read
 *****************************************************************************/
uint8_t SDP3xClass::readSensor(uint8_t* readData, uint8_t size)
{
  uint8_t rxByteCount=0;

  uint8_t txData[COMMAND_DATA_LENGTH] =
    {SDP_MEASUREMENT_COMMAND_0, SDP_MEASUREMENT_COMMAND_1};

  Wire.beginTransmission(mI2CAddress);
  Wire.write(txData, COMMAND_DATA_LENGTH);
  Wire.endTransmission();

  delay(50);  // wait for data conversion in sensor

  // 2 bytes DP, 1 byte CRC, 2 bytes T, 1 byte CRC
  Wire.requestFrom((uint8_t)mI2CAddress, size);
  rxByteCount = 0;
  while (Wire.available()) { // wait till all arrive
      readData[rxByteCount] = Wire.read();
      rxByteCount++;
  }
  return rxByteCount;
}

SDP3xClass SDP3x;
```

Log Board Main File

```
/*************************************************************************
BBB1_Log_D18_v2

Inputs from the other board of:
ASL State, Nebulizer state, Patient state
Ground, Vin

On First ASL HIGH loop it resets values for clean count

Last Updated 5th Feb 2020

 *************************************************************************/

int serialmonitor = 0;
int resetCheck = 0;

const int PATstatePin = 8;
const int ASLstatePin = 2;
const int NEBstatePin = 7;
unsigned long currentMillis;

int PATstate = 0;
int lastPATstate = 0;
int ASLstate = 0;
int lastASLstate = 0;
int NEBstate = 0;
int lastNEBstate = 0;

int ASLFlagNumber = 0;
int PATFlagNumber = 0;
int NEBFlagNumber = 0;
int breathAFlagNumber = 0;
int breathPFlagNumber = 0;
int drugFlagNumber = 0;

void setup() {
  Serial.begin(9600);
  pinMode(ASLstatePin, INPUT);
  pinMode(NEBstatePin, INPUT);
  pinMode(PATstatePin, INPUT);
}

void loop() {
  currentMillis = millis();
  ASLstate = digitalRead(ASLstatePin);
  NEBstate = digitalRead(NEBstatePin);
  PATstate = digitalRead(PATstatePin);

if (serialmonitor == 1){
    Serial.print(currentMillis);
    Serial.println();
    Serial.print("\t");
    Serial.print(ASLstate);
    Serial.print("\t");
    Serial.print(NEBstate);
}

// compare ASL State with previous ASL State
if (ASLstate != lastASLstate){
  Serial.println();
  Serial.print(ASLstatePin);
  Serial.print("\t");
  Serial.print(currentMillis);
  Serial.print("\t");

  // reset values if first time
  if (resetCheck == 0){
    ASLFlagNumber = 0;
```

```
    PATFlagNumber = 0;
    NEBFlagNumber = 0;
    breathAFlagNumber = 0;
    breathPFlagNumber = 1;    // 1 not 0 due to the fact that environment will be running and
unit "will" have sensed the breath
    drugFlagNumber = 0;
    resetCheck = 1;
  }
  ASLFlagNumber ++;
  Serial.print(ASLFlagNumber);
  Serial.print("\t");
  lastASLstate = ASLstate;
  if (ASLstate == HIGH){
    breathAFlagNumber ++;
    Serial.print (breathAFlagNumber);
    Serial.print ("\t InASL");
  }
  else{
    Serial.print (breathAFlagNumber);
    Serial.print ("\t ExASL");
  }
}
else {

}

// compare Nebulizer State with previous Nebulizer State
if (NEBstate != lastNEBstate){
  Serial.println();
  Serial.print(NEBstatePin);
  Serial.print("\t");
  Serial.print(currentMillis);
  Serial.print("\t");
  NEBFlagNumber ++;
  Serial.print(NEBFlagNumber);
  Serial.print("\t");
  lastNEBstate = NEBstate;
  if (NEBstate == HIGH){
    drugFlagNumber ++;
    Serial.print (drugFlagNumber);
    Serial.print ("\t");
    Serial.print (breathAFlagNumber);
    Serial.print ("\t Drug");
  }
  else{
    Serial.print (drugFlagNumber);
    Serial.print ("\t");
    Serial.print (breathAFlagNumber);
    Serial.print("\t Humi");
  }
}
else {

}

// compare Exhale State with previous Exhale State
if (PATstate != lastPATstate){
  Serial.println();
  Serial.print(PATstatePin);
  Serial.print("\t");
  Serial.print(currentMillis);
  Serial.print("\t");
  PATFlagNumber++;
  Serial.print(PATFlagNumber);
  Serial.print("\t");
  lastPATstate = PATstate;
  if (PATstate == HIGH){
    breathPFlagNumber ++;
    Serial.print (breathAFlagNumber);
    Serial.print ("\t");
    Serial.print (breathPFlagNumber);
```

```
    Serial.print ("\t InPat");
  }
  else{
    Serial.print (breathAFlagNumber);
    Serial.print ("\t");
    Serial.print (breathPFlagNumber);
    Serial.print("\t ExPat");
  }
}
else {

}

  delay(1);        // delay in between reads for stability
}
```

12.1.2 Heated Dryer System

Controller codes and system information for the HDS system: This section is split into three sub-sections to explain the device pinout, device output, and specific controller code. This system contained two Arduino Uno microcontrollers, identified as Alpha and Beta, which controlled the main system operation and the heating operation respectively.

HDS Device Pinout

Pin	Alpha	Beta	I/O	Associated Variable Description
0	RX	RX	Input	
1	TX	TX	Output	
2	ModeASLPressurePin	ModeASLPressurePin	Input	ModeASLPressureState
3	ModeWarmRunPin	ModeWarmRunPin	Input	ModeWarmRunState
4	relay1Pin	relay1Pin	Output	
5	ASLPin	ASLPin	Input	ASLState
6	FlowPin	FlowPin	Output | Input	FlowState
7	relay2Pin	relay2Pin	Output	
8	relay3Pin	relay3Pin	Output	
9	hpsInlet	TSplateCS	Output	
10	----	TSexitCS	Output	
11	----	TSauxCS	Output	
12	SPIpressureMISO	MasterInSlaveOut	I/O	Standard Arduino Uno Configuration
13	SPIpressureCLK	Clock	I/O	

HDS Device Output

Each Arduino had a continuous serial output log during experimental runs. The following charts correspond to the tab delimited output data and are part of the upper column labels used in excel to organize the data. Additional run information and data analyses were also inserted into the first seven rows of the excel spreadsheets.

Alpha Board

Time Stamp Hours	Time Stamp Min	Time Stamp Sec	Program State	Start Millis	ASL State	Press Value	Neb State	IA	IB	IC	Drug Total	End Millis

Beta Board

Time Stamp Hours	Time Stamp Min	Time Stamp Sec	Program State	Start Millis	T Plate	T Exit	Delay Time	TSP plate actual	T Offset	Inhale Time	End Millis

HDS Controller Code

Alpha Board Main File

```
/*************************************************
  HDSalphaB4v1
  This is program for the Heated Dryer System Alpha Board

  Main task is the nebulizer control of system.
  During ASL mode the program....
  During Pressure Mode the program takes input from pressure
  sensors and experimenter input of subject specific
  parameters to determine starting/stopping of the nebulizer.

  Program base is the HDSalphaB3v1 code

  First Saved 20 June 2020
  Last Updated 07 Jan 2021


 *************************************************/

#include <SPI.h>
#include "Honeywell_pressure_sensors.h"
```

```
// subject specific items/quanities/variables
//int ModeCodeFunctionState = LOW; // LOW --> B3 mode of unknown values ||| HIGH --> B4 mode of
preknown values
int ModeCodeFunctionState = HIGH; // LOW --> B3 mode of unknown values ||| HIGH --> B4 mode of
preknown values
float subjectInhaleLengthSeconds = 2.325; // subject's average inhalation duration measured (sec)
float subjectMainInhalePressure = -55; // subject's

unsigned long setDrugIntervalASL = 1000;
unsigned long setDrugIntervalPressure = subjectInhaleLengthSeconds*1000/3;

// variables for device as builts, mode selection, SPI Pressure Sensor Communications
const int ModeASLPressurePin = 2;
int ModeASLPressureState = LOW; // LOW --> ASL Mode ||| HIGH --> Pressure Mode
const int ModeWarmRunPin = 3;
int ModeWarmRunState = LOW; // LOW --> Warmup Mode ||| HIGH --> Run Mode
const int relay1Pin = 4; //
const int ASLPin = 5; // input from ASL to determine flow
int ASLState = LOW; // LOW --> Exhaling state ||| HIGH --> Inhaling state
const int FlowPin = 6;
int FlowState = LOW; // LOW --> Exhale Mode ||| HIGH --> Inhale Mode
const int relay2Pin = 7; //
const int relay3Pin = 8; // Drug Neb Relay
HPS hpsInlet(9); // Pin 9 HPS sensor chip select pin
// Pin 10
// Pin 11
// Pin 12 SPI Master In Slave Out (MISO --> standard Arduino Uno Configuration
// Pin 13 SPI Clock --> standard Arduino Uno Configuration

// variables for breath point determination
float inletPressure;
float inletPressureOffset;
float cPress;
float cPressForceful;

// variables for millis time keeping, drug production, and logging
unsigned long currentMillis;
unsigned long breathStart;
unsigned long drugStart;
unsigned long drugEnd;
unsigned long drugTotal;
int drugEndUpdate;
int iterationA;
int iterationB;
int iterationC;
int iterationD;
unsigned long targetDrugIntervalASL;
unsigned long targetDrugIntervalPressure;
unsigned long modDrugInterval;
unsigned long drugDelayTimeASL;
unsigned long drugDelayTimePress;
int programState;
int nebState;
int delayTimeWarm = 49;
int delayTimeRun = 9;

void setup() {
// initialize digital pins as outputs
pinMode(relay1Pin, OUTPUT);
pinMode(relay2Pin, OUTPUT);
pinMode(relay3Pin, OUTPUT);
//pinMode(relay4Pin, OUTPUT);
pinMode(FlowPin, OUTPUT);

// initialize digital pins as inputs
pinMode(ModeASLPressurePin, INPUT);
pinMode(ModeWarmRunPin, INPUT);
pinMode(ASLPin, INPUT);

//initialize values
```

```
inletPressureOffset = 4; // calibration value to bring base pressure to zero
inletPressure = 850; // arbitary starting inlet pressure value in units of pascals
cPress = -10; // critical pressure value for determining breath flow start in units of pascals
cPressForceful = -30; // critical pressure value for determining forceful flow in units of
pascals
iterationA = 0;
iterationB = 0;
iterationC = 0;
iterationD = 0;
targetDrugIntervalASL = 1000; //very high number to ensure production entire length of breath
targetDrugIntervalPressure = 300; // low number after which the drug production is determined by
pressure
modDrugInterval = 0;
drugDelayTimeASL = 100; // milli seconds after FlowState before drug allowed to start in ASL mode
(to simulate pressure gap)
//drugDelayTimePressure = 10; // pressure mode delay is imposed by the negativity of the cPress
value

Serial.begin(115200);
SPI.begin();
SPI.beginTransaction(SPISettings(800000, MSBFIRST, SPI_MODE0));
delay(100);
}

void loop() {
currentMillis = millis();
// Read Device Switch Positions
ModeASLPressureState = digitalRead(ModeASLPressurePin);
ModeWarmRunState = digitalRead(ModeWarmRunPin);
ASLState = digitalRead(ASLPin);

// Follow Code Control of Either B3 or B4
switch (ModeCodeFunctionState){
/*************************************************************************/
case LOW: // Code Control of B3 Concept
// Act on current information to produce control nebulizer and send information to other board
switch (ModeWarmRunState){ //change between warmup and usage control modes
  /*************************************************************************/
  case LOW: // no drug production but log rest of system
  // Warm Up Mode

  switch (ModeASLPressureState){ // change between ASL and pressure determiniation of Flow State
    /************************************************/
    case LOW:
    // ASL Determination Mode

    // Set Flow State Value from ASL Input
    FlowState = ASLState;
    digitalWrite(FlowPin,FlowState); // sends info to beta board

    // Set program state for Serial Monitor
    programState = 1;
    break;
    /************************************************/
    case HIGH:
    // Pressure Determination Mode

    // Set Flow State Value from Pressure Sensor Value
    inletPressure = hpsInlet.getPressurePa() + inletPressureOffset; // Get inlet Pressure value
plus zero point correction
    if (inletPressure < cPress){
      FlowState = HIGH;
    }
    else {
      FlowState = LOW;
    }
    digitalWrite(FlowPin,FlowState); // sends info to beta board

    // Set program state for Serial Monitor
    programState = 2;
    break;
```

```
    /*************************************************/
  }

  // Warm up delay to limit Serial Monitor Output
  delay(delayTimeWarm);

  break;
  /*****************************************************************************/
  case HIGH: // drug production at correct time during inhalations
  // Run Mode

  switch (ModeASLPressureState){ // change between ASL and pressure determiniation of Flow State
    /*************************************************/
    case LOW:
    // ASL Determination Mode

    // Set Flow State Value from ASL Input
    FlowState = ASLState;
    digitalWrite(FlowPin,FlowState); // sends info to beta board

    /************************/
    // Once FlowState rises to HIGH, have a gap then produce drug for predetermined length of
time
    if (FlowState == HIGH) { // flow towards outlet so nebulize at correct time
      if (iterationA == 0) { // do first time flow is towards outlet only
        breathStart = currentMillis;
//        Serial.print("3\t"); // Inhaling Delay Gap Starts
        iterationA = iterationA + 1; // prevent first time rewrite
      }
      else { // not the first time at flow state of high
        if (currentMillis - breathStart >= drugDelayTimeASL) { // time is after the drugDelayTime
          if (iterationB == 0) { // do first time time is after the delay only
            digitalWrite(relay3Pin, HIGH);
            drugStart = millis();
            nebState = 1;
//            Serial.print("10\t"); // Inhaling Drug Production Started
            iterationB = iterationB + 1;
          }
          else { // not the first time at time after the drugDelayTime
            if (currentMillis - drugStart <= targetDrugIntervalASL) { // time is before the
targetDrugIntervalASL length
              digitalWrite(relay3Pin, HIGH);
              nebState = 1;
//              Serial.print("10\t"); // Inhaling Drug Production Continues
            }
            else { // time is after the targetDrugIntervalASL length
                digitalWrite(relay3Pin, LOW);
                nebState = 0;
//                Serial.print("7\t"); // Inhaling Saline Production Occuring
            }
          }
        }
        else { // time is before the drugDelayTime
          digitalWrite(relay3Pin, LOW);
          nebState = 0;
//          Serial.print("3\t"); // Inhaling Saline during Delay Gap
          iterationB = 0;
        }
      }
    }
    else { // flow away from outlet so prevent nebulization
      digitalWrite(relay3Pin, LOW);
      nebState = 0;
//      Serial.print("0\t"); // Exhaling
      iterationA = 0;
    }
    /************************/

    // Set program state and values for Serial Monitor
    programState = 3;
    // determine pressure value for logging
```

```
      // possibly just a NaN value assigned
    inletPressure = 800;

    break;
    /*************************************************/
    case HIGH:
    // Pressure Determination Mode

    /************************/
    // Set Flow State Value from Pressure Sensor Value
    inletPressure = hpsInlet.getPressurePa() + inletPressureOffset; // Get inlet Pressure value +
a slight zero point correction
    if (inletPressure < cPress){
      FlowState = HIGH;
    }
    else {
      FlowState = LOW;
    }
    digitalWrite(FlowPin,FlowState); // sends info to beta board

    /************************/
    // Once FlowState rises to HIGH, (have no gap and produce drug for predetermined length of
time before pressure control)
    if (FlowState == HIGH) { // flow towards outlet so nebulize at
      if (iterationA == 0) { // do first time flow is towards outlet only
        digitalWrite(relay3Pin, HIGH);
        drugStart = millis();
        nebState = 1;
        breathStart = currentMillis;
        iterationA = iterationA + 1; // prevent first time rewrite
      }
      else { // not the first time flow towards outlet
        if (currentMillis - drugStart >= targetDrugIntervalPressure) { // time is after the goal
time so use pressure as control
          if (inletPressure < cPressForceful){ // forcefull inhalation still occurring so keep
nebulization going
            // && interationB == 0 (use counter to prevent a restarting after stopping
            digitalWrite(relay3Pin, HIGH);
            nebState = 1;
          }
          else { // forcefull inhation not occuring so stop nebulization
            digitalWrite(relay3Pin, LOW);
            nebState = 0;
            iterationB = iterationB + 1;
          }
        }
        else { // time is within the targetDrugIntervalPress goal time so keep nebulization going
          digitalWrite(relay3Pin, HIGH);
          nebState = 1;
        }
      }
    }
    else { // flow away from outlet so prevent nebulization and reset iteration counters
      digitalWrite(relay3Pin, LOW);
      nebState = 0;
      iterationA = 0;
      iterationB = 0;
    }

    /************************/

    // Set program state for Serial Monitor
    programState = 4;

    break;
    /*************************************************/
  }

  // Running delay to limit Serial Monitor Output
  delay(delayTimeRun);
```

```
  /*****************************************************************************/
  delay(1);

Serial.print(programState);
Serial.print("\t");
Serial.print(currentMillis);
Serial.print("\t");
Serial.print(ASLState);
Serial.print("\t");
Serial.print(inletPressure);
Serial.print("\t");
Serial.print(FlowState);
Serial.print("\t");
Serial.print(nebState);
Serial.print("\t");
Serial.print(iterationA);
Serial.print("\t");
Serial.print(iterationB);
Serial.print("\t");
Serial.print(millis());
Serial.println();
break;
}
// end of switch ModeWarmRunState B3
break;

/*****************************************************************************/


case HIGH: // Code Control of B4 Concept
// Determine Start and Stop Criteria
//*******
//float subjectInhaleLengthSeconds = 3.1; // subject's average inhalation duration measured in
seconds
//float subjectMainInhalePressure = -55; // subject's
//setDrugIntervalASL = 1000;
//setDrugIntervalPressure = subjectInhaleLengthSeconds*1000/3;
//*******

// Act on current information to produce control nebulizer and send information to other board

switch (ModeWarmRunState){ //change between warmup and useage control modes
  /*****************************************************************************/
  case LOW: // no drug production but log rest of system
  // Warm Up Mode

  switch (ModeASLPressureState){ // change between ASL and pressure determiniation of Flow State
    /*************************************************/
    case LOW:
    // ASL Determination Mode

    // Set Flow State Value from ASL Input
    FlowState = ASLState;
    digitalWrite(FlowPin,FlowState); // sends info to beta board

    // Set program state for Serial Monitor
    programState = 1;

    break;
    /*************************************************/
    case HIGH:
    // Pressure Determination Mode

    // Set Flow State Value from Pressure Sensor Value
    inletPressure = hpsInlet.getPressurePa() + inletPressureOffset; // Get inlet Pressure value
plus zero point correction
    if (inletPressure < cPress){
      FlowState = HIGH;
    }
    else {
      FlowState = LOW;
```

```
    }
    digitalWrite(FlowPin,FlowState); // sends info to beta board

    // Set program state for Serial Monitor
    programState = 2;

    break;
    /*************************************************/
  }

  // Warm up delay to limit Serial Monitor Output
  delay(delayTimeWarm);

  break;
  /*****************************************************************************/
  case HIGH: // drug production at correct time during inhalations
  // Run Mode

  switch (ModeASLPressureState){ // change between ASL and pressure determiniation of Flow State
    /*************************************************/
    case LOW:
    // ASL Determination Mode

    // Set Flow State Value from ASL Input
    FlowState = ASLState;
    digitalWrite(FlowPin,FlowState); // sends info to beta board

    /************************/
    // Once FlowState rises to HIGH, have a gap then produce drug for predetermined length of
time
    if (FlowState == HIGH) { // flow towards outlet so nebulize at correct time
      if (iterationA == 0) { // do first time flow is towards outlet only
        breathStart = currentMillis;
//        Serial.print("3\t"); // Inhaling Delay Gap Starts
        iterationA = iterationA + 1; // prevent first time rewrite
      }
      else { // not the first time at flow state of high
        if (currentMillis - breathStart >= drugDelayTimeASL) { // time is after the drugDelayTime
          if (iterationB == 0) { // do first time after the delay only
            digitalWrite(relay3Pin, HIGH);
            drugStart = millis();
            nebState = 1;
//            Serial.print("10\t"); // Inhaling Drug Production Started
            iterationB = iterationB + 1;
          }
          else { // not the first time at time after the drugDelayTime
            if (currentMillis - drugStart <= targetDrugIntervalASL) { // time is before the
targetDrugIntervalASL length
              digitalWrite(relay3Pin, HIGH);
              nebState = 1;
//              Serial.print("10\t"); // Inhaling Drug Production Continues
            }
            else { // time is after the targetDrugIntervalASL length
                digitalWrite(relay3Pin, LOW);
                nebState = 0;
                if (iterationD == 0){ // just first time after the target interval length
                  drugEnd = millis();
                  drugEndUpdate = 1;
                  iterationD = iterationD + 1; // prevent going into it again
                  //iterationC = 0; // nebulization ended due to the time elapsing
                }
//              Serial.print("7\t"); // Inhaling Saline Production Occuring
            }
          }
        }
        else { // time is before the drugDelayTime
          digitalWrite(relay3Pin, LOW);
          nebState = 0;
//          Serial.print("3\t"); // Inhaling Saline during Delay Gap
          iterationB = 0;
        }
```

```
      }
    }
    else { // flow away from outlet so prevent nebulization
      digitalWrite(relay3Pin, LOW);
      nebState = 0;
//      Serial.print("0\t"); // Exhaling
      iterationA = 0;
      iterationD = 0;
    }
    /************************/

// Update the total drug run time if there is a new drugEndvalue
  if (drugEndUpdate == 1) { // if a new value has been set
    drugTotal = drugTotal + (drugEnd - drugStart);
    drugEndUpdate = 0;
  }


    // Set program state and values for Serial Monitor
    programState = 3;
    // determine pressure value for logging
      // possibly just a NaN value assigned
    inletPressure = 800;

    break;
    /*****************************************************/
    case HIGH:
    // Pressure Determination Mode

    /************************/
    // Set Flow State Value from Pressure Sensor Value
    inletPressure = hpsInlet.getPressurePa() + inletPressureOffset; // Get inlet Pressure value +
a zeropoint correction
    if (inletPressure < cPress){
      FlowState = HIGH;
    }
    else {
      FlowState = LOW;
    }
    digitalWrite(FlowPin,FlowState); // sends info to beta board

    /************************/
    // Once FlowState rises to HIGH, (have no gap and produce drug for predetermined length of
time remove pressure control)
    if (FlowState == HIGH) { // flow towards outlet so nebulize at
      if (iterationA == 0) { // do first time flow is towards outlet only
        digitalWrite(relay3Pin, HIGH);
        drugStart = millis();
        nebState = 1;
        breathStart = currentMillis;
        iterationA = iterationA + 1; // prevent first time rewrite
        iterationC = iterationC + 1; // an increase of iterationC from zero means that
nebulization has started
      }
      else { // not the first time flow towards outlet
        if (currentMillis - drugStart >= setDrugIntervalPressure) { // time is after the goal
time so stop neb
          digitalWrite(relay3Pin, LOW);
          nebState = 0;
          if (iterationB == 0) { // do first time after the setDrugIntervalPressureTime
            drugEnd = millis();
            drugEndUpdate = 1;
            iterationC = 0; // iterationC equal to zero means that nebulization has been stopped
by time duration
          }
          iterationB = iterationB + 1;
        }
        else { // time is within the setDrugIntervalPressure goal time so keep nebulization going
          digitalWrite(relay3Pin, HIGH);
          nebState = 1;
        }
```

```
      }
    }
    else { // flow away from outlet so prevent nebulization and reset iteration counters
      digitalWrite(relay3Pin, LOW);
      nebState = 0;
      if (iterationC != 0) { // would mean that the setDrugIntervalPressure time was not reached
before flow reversed
            drugEnd = millis();
            drugEndUpdate = 1;
            iterationC = 0;
          }
      iterationA = 0;
      iterationB = 0;
    }

    /************************/

    // Set program state for Serial Monitor
    programState = 4;

    break;
    /************************************************/
  }
  // Update the total drug run time if there is a new drugEndvalue
  if (drugEndUpdate == 1) { // if a new value has been set
    drugTotal = drugTotal + (drugEnd - drugStart);
    drugEndUpdate = 0;
  }

  // Running delay to limit Serial Monitor Output
  delay(delayTimeRun);

  break;
  /*****************************************************************************/
  delay(1);
  break;
}

Serial.print(programState);
Serial.print("\t");
Serial.print(currentMillis);
Serial.print("\t");
Serial.print(ASLState);
Serial.print("\t");
Serial.print(inletPressure);
Serial.print("\t");
Serial.print(FlowState);
Serial.print("\t");
Serial.print(nebState);
Serial.print("\t");
Serial.print(iterationA);
Serial.print("\t");
Serial.print(iterationB);
Serial.print("\t");
Serial.print(iterationC);
Serial.print("\t");
Serial.print(drugTotal);
Serial.print("\t");
Serial.print(millis());
Serial.println();

// end of switch ModeWarmRunState B4
break;

}
// end of switch ModeCodeFunctionState
}
// end of void loop
```

Alpha Board Supporting .h File

```
/*
        Arduino library for Honeywell pressure sensors
        Currently just supporting SPI sensors. I2c and Analog to come.
        Fletcher Bach - Dec. 2016
        MIT License

 Heavily updated and modified by Ben Spence - Oct 2020
*/

#ifndef HPS_h
#define HPS_h

#include "Arduino.h"

class HPS {
public:
        HPS(int pin);
        float getPressureCount();
  float getPressurePa();
  float transferFunctionPa(uint16_t);
private:
        int _pin;
        float transferFunctionPSI(uint16_t);
};

#endif
```

Alpha Board Supporting. cpp File

```
/*
        Arduino library for Honeywell pressure sensors
        SPI Models supported, I2C and Analog support to come
        Fletcher Bach - Dec. 2016
        MIT license

  Heavily updated and modified by Ben Spence - Oct 2020
*/

#include "Arduino.h"
#include "Honeywell_pressure_sensors.h"
#include <SPI.h>

HPS::HPS(int pin) {
    pinMode(pin, OUTPUT);
    digitalWrite(pin, HIGH);
    _pin = pin;
}

float HPS::getPressureCount() {
    int whichChip = _pin;

    byte firstByte;
    byte secondByte;

    // select sensor by bringing Slave Select pin LOW
    digitalWrite(whichChip, LOW);

    // query for two bytes
    firstByte = SPI.transfer(0x00);
    secondByte = SPI.transfer(0x00);

    // de-select sensor by bringing Slave Select pin HIGH
    digitalWrite(whichChip, HIGH);

    // bitshifting the first byte 8 bits to the left and combine to second
    uint16_t bothBytes = (firstByte << 8) | secondByte;

    return (bothBytes);
}

float HPS::getPressurePa() {
    int whichChip = _pin;

    byte firstByte;
    byte secondByte;

    // asserting this sensor by bringing CS pin low
    digitalWrite(whichChip, LOW);

    // here we're asking for our two bytes
    firstByte = SPI.transfer(0x00);
    secondByte = SPI.transfer(0x00);

    // de-asserting this sensor by bringing CS pin high
    digitalWrite(whichChip, HIGH);

    // bitshifting the first byte 8 bits to the left and combine with second
    uint16_t bothBytes = (firstByte << 8) | secondByte;

    // Transfer counts to engineering units based on correct device specs

//    //Values from Data Sheet for SSCDLNN040MGSA5
//    float outputMax = 14745.0; // 90% of 2e14 counts = 0.9*16384
//    float outputMin = 1638.0; //10% of 2e14 counts = 0.1*16384
//    float pressureMax = 4000.0; // 40mbar = 4000Pa
//    float pressureMin = 0.0;
//    float pascalOutput = 0;
```

```
    //Values from Data Sheet for SSCDLNN060MDSA5
    float outputMax = 14745.0; // 90% of 2e14 counts = 0.9*16384
    float outputMin = 1638.0; //10% of 2e14 counts = 0.1*16384
    float pressureMax = 6000.0; // 60mbar = 6000Pa
    float pressureMin = -6000.0; // 60mbar = 6000Pa
    float pascalOutput = 0.0; // initialize value

    pascalOutput = ((bothBytes - outputMin) * (pressureMax - pressureMin) / (outputMax -
outputMin))+pressureMin;

    return pascalOutput;
}

float HPS::transferFunctionPSI(uint16_t dataIn) {
    //Values from Data Sheet for SSCDLNN040MGSA5
    float outputMax = 14745.0; // 90% of 2e14 counts = 0.9*16384
    float outputMin = 1638.0; //10% of 2e14 counts = 0.1*16384
    float pressureMax = 30.0; // max 30 psi (from sensor's data sheet)
    float pressureMin = 0.0;
    float pressureOutput = 0.0;

    // transfer function: using sensor output to solve for pressure
    pressureOutput = ((dataIn - outputMin) * (pressureMax - pressureMin) / (outputMax -
outputMin))+pressureMin;

    return (pressureOutput);
}

float HPS::transferFunctionPa(uint16_t dataIn) {
//    //Values from Data Sheet for SSCDLNN040MGSA5
//    float outputMax = 14745.0; // 90% of 2e14 counts = 0.9*16384
//    float outputMin = 1638.0; //10% of 2e14 counts = 0.1*16384
//    float pressureMax = 4000.0; // 40mbar = 4000Pa
//    float pressureMin = 0.0;
//    float pressure = 0.0;

    //Values from Data Sheet for SSCDLNN060MDSA5
    float outputMax = 14745.0; // 90% of 2e14 counts
    float outputMin = 1638.0; //10% of 2e14 counts
    float pressureMax = 6000.0; // 60mbar = 6000Pa
    float pressureMin = -6000.0;
    float pressure = 0.0;

    // transfer function: using sensor output to solve for pressure
    pressure = ((dataIn - outputMin) * (pressureMax - pressureMin) / (outputMax -
outputMin))+pressureMin;

    return (pressure);
}
```

Beta Board Main File

```
/*************************************************
  HDSbetaB4v1
  This is program for the Heated Dryer System Beta Board

  Main task is the temperature control of system. Program
  takes input from Alpha Board and temperature sensors to
  manipulate the voltage applied to the heating elements.

  Temperature sensor code modeled from the example code of
  Adafruit Thermocouple Sensor w/MAX31855K

  Utilizes a moving heat plate setpoint based on outlet temp

  Program base is the HDSbetaB3v2 code

  First Saved 20 June 2020
  Last Updated 15 Dec 2020

*************************************************/

#include <SPI.h>
#include "Adafruit_MAX31855.h"

// variables for device as builts, mode selections, SPI Temperature Sensor Communications
const int ModeASLPressurePin = 2;
int ModeASLPressureState = LOW; // LOW --> ASL Mode ||| HIGH --> Pressure Mode
const int ModeWarmRunPin = 3;
int ModeWarmRunState = LOW; // LOW --> Warmup Mode ||| HIGH --> Run Mode
const int relay1Pin = 4; // Heat voltage
const int ASLPin = 5; // input from ASL for reference
const int FlowPin = 6;
int FlowState = LOW; // LOW --> Exhale Mode ||| HIGH --> Inhale Mode
const int relay2Pin = 7; // Heat enable
const int relay3Pin = 8; //
#define TSplateCS   9 // SPI chip select pin of the heating plate sensor
#define TSexitCS   10 // SPI chip select pin of the exit of the system sensor
#define TSauxCS   11 // SPI chip select pin of the auxiliary sensor
Adafruit_MAX31855 thermocouplePlate(TSplateCS);
Adafruit_MAX31855 thermocoupleExit(TSexitCS);
Adafruit_MAX31855 thermocoupleAux(TSauxCS);

// const int relay4Pin = 12;// Removed due to SPI interface
// Pin 12 SPI Master In Slave Out (MISO --> standard Arduino Uno Configuration
// Pin 13 SPI Clock --> standard Arduino Uno Configuration

// variable for millis time keeping
unsigned long currentMillis;
int delayTimeWarm = 200;
int delayTimeRun = 50;
unsigned long lastSPReset = 0;
int SPResetDuration = 20000; // 30 second duration for rest
int SPSearchWait = 1000; // 14 second wait before searching/logging starts
unsigned long lastExhalationMillis = 0;

//variables for temperature control parameters
double TplateC;
double TexitC;
double TauxC;
float TSPplateWarm = 75; //35 for general function testing if needed
float TSPplateExhale = 78;
float TSPplateExhaleHalfPowerDelta = 1;
float TSPplateInhaleMax = 95;
float TSPexitInhale = 30;

float TexitObservedMin = 21;
float TexitObservedMax = 21;
float TexitObserved = 21; // comes from TexitC value but only after the SPSearchWait length of
time
```

```
float TSPplateExhaleExitDelta = 0;
float TexitObservedDeltaSP = 0;


void setup() {
// initialize digital pins as outputs
pinMode(relay1Pin, OUTPUT);
pinMode(relay2Pin, OUTPUT);
pinMode(relay3Pin, OUTPUT);
//pinMode(relay4Pin, OUTPUT);


// initialize digital pins as inputs
pinMode(ModeASLPressurePin, INPUT);
pinMode(ModeWarmRunPin, INPUT);
pinMode(ASLPin, INPUT);
pinMode(FlowPin, INPUT);


Serial.begin(115200);

delay(100);
}


void loop() {
currentMillis = millis();
// Read Device Switch Positions
ModeASLPressureState = digitalRead(ModeASLPressurePin);
ModeWarmRunState = digitalRead(ModeWarmRunPin);
FlowState = digitalRead(FlowPin);
// Read Device Temperatures
TplateC = thermocouplePlate.readCelsius();
TexitC = thermocoupleExit.readCelsius();

// Act on current information to control the system temperatures
switch (ModeWarmRunState){ //change between warmup and usage control modes based on device switch
position
  /*****************************************************************************/
  case LOW: //heating of metal plate with monitoring and set points based on metal plate
  // Warm Up Mode
  // FlowState does not matter for the control process

  if (TplateC < TSPplateWarm){// plate below setpoint --> activate full power heating
    digitalWrite(relay1Pin, HIGH); // switch to 24v power
    digitalWrite(relay2Pin, HIGH); // activate heating

    // Output to Serial Monitor
    Serial.print("WFP\t");
    Serial.print(currentMillis);
    Serial.print("\t");
    Serial.print(TplateC);
    Serial.print("\t");
    Serial.print(TexitC);
  }
  else { // plate at or above setpoint --> deactivate heating
    digitalWrite(relay2Pin, LOW); //deactivate heating when at or above setpoint
    digitalWrite(relay1Pin, LOW); // switch to 12v power

    // Output to Serial Monitor
    Serial.print("WNP\t");
    Serial.print(currentMillis);
    Serial.print("\t");
    Serial.print(TplateC);
    Serial.print("\t");
    Serial.print(TexitC);

  }

  Serial.print("\t");
  Serial.print(delayTimeWarm);
```

```
  delay(delayTimeWarm); // delay during warmup to minimize serial output
  break;

  /*****************************************************************************/
  case HIGH: //heating of metal plate with monitoring and set points based on flow status
  // Run Mode
  // FlowState matters for the control process

  switch (FlowState){ // change between exhale and inhale states based on information from alpha
board
    /*************************************************/
    case LOW: // Exhaling therefore bad information on the far sensors use plate as control
    // Exhaling Mode
    // Far sensor at the mouthpiece is currently defined as exit sensor

    if (TplateC < (TSPplateExhale+TSPplateExhaleExitDelta-TSPplateExhaleHalfPowerDelta)){
      digitalWrite(relay1Pin, HIGH); // switch to 24v power
      digitalWrite(relay2Pin, HIGH); // activate heating

      // Output to Serial Monitor
      Serial.print("REF\t");
      Serial.print(currentMillis);
      Serial.print("\t");
      Serial.print(TplateC);
      Serial.print("\t");
      Serial.print(TexitC);

    }
    else{ if(TplateC >= (TSPplateExhale+TSPplateExhaleExitDelta-TSPplateExhaleHalfPowerDelta)&&
TplateC <= (TSPplateExhale+TSPplateExhaleExitDelta+TSPplateExhaleHalfPowerDelta)){
      digitalWrite(relay1Pin, LOW); // switch to 12v power
      digitalWrite(relay2Pin, HIGH); // activate low power heating when at setpoint range

      // Output to Serial Monitor
      Serial.print("REH\t");
      Serial.print(currentMillis);
      Serial.print("\t");
      Serial.print(TplateC);
      Serial.print("\t");
      Serial.print(TexitC);

      }
      else{ // over the set point --> no heating required
        digitalWrite(relay1Pin, LOW); // switch to 12v power
        digitalWrite(relay2Pin, LOW); // deactivate heating when above setpoint range

        // Output to Serial Monitor
        Serial.print("REN\t");
        Serial.print(currentMillis);
        Serial.print("\t");
        Serial.print(TplateC);
        Serial.print("\t");
        Serial.print(TexitC);

      }
    }

    // Set a time of the most recent exhalation loop to be used later in inhalation loops
    lastExhalationMillis = currentMillis;

    break;
    /*************************************************/
    case HIGH: // Inhaling therefore good infomartion on the far sensor so use these to control
plate
    // Inhaling Mode
    // Far sensor at the mouthpiece is currently defined as exit sensor

    //// Calculate values based on gathered information

    // Check if current temperature is an Observed value
    if (currentMillis - lastExhalationMillis >= SPSearchWait) {
```

```
      TexitObserved = TexitC;
        // Check if current Observed value is a new min or max
        if (TexitObserved > 15 && TexitObserved < 150) { // prevents nan values and outlier
values from influencing
          if (TexitObserved > TexitObservedMax) {
            TexitObservedMax = TexitObserved;
          }
          if (TexitObserved < TexitObservedMin) {
            TexitObservedMin = TexitObserved;
          }
        }
    }

    // Check if time to update the set point values and update if time (reset timer when update
happens)
    if (currentMillis - lastSPReset >= SPResetDuration) {
      //if statement to check has enough time elapsed since previous reset
      TexitObservedDeltaSP = (0.5*(TexitObservedMax-TexitObservedMin));
      TSPplateExhaleExitDelta = TexitObservedDeltaSP;
      TexitObservedMin = TexitObserved;
      TexitObservedMax = TexitObserved;
      lastSPReset = currentMillis;
    }

    //// Act on calculated and gathered information to decide heater power
    if (TplateC <= TSPplateInhaleMax){ // plate is at or below maximum plate set point

      if (TexitC <= TSPexitInhale) {
        digitalWrite(relay1Pin, HIGH); // switch to 24v power
        digitalWrite(relay2Pin, HIGH); // activate heating when at or below inhale exit set point

        // Output to Serial Monitor
        Serial.print("RIF\t");
        Serial.print(currentMillis);
        Serial.print("\t");
        Serial.print(TplateC);
        Serial.print("\t");
        Serial.print(TexitC);

      }
      else{
        digitalWrite(relay1Pin, LOW); // switch to 12v power
        digitalWrite(relay2Pin, LOW); // deactivate heating when above inhale exit set point

        // Output to Serial Monitor
        Serial.print("RIS\t");
        Serial.print(currentMillis);
        Serial.print("\t");
        Serial.print(TplateC);
        Serial.print("\t");
        Serial.print(TexitC);

      }
    }
    else{ // plate is above maximum plate set point
      digitalWrite(relay1Pin, LOW); // switch to 12v power
      digitalWrite(relay2Pin, LOW); // deactivate heating when above maximum plate set point

      // Output to Serial Monitor
      Serial.print("RIM\t");
      Serial.print(currentMillis);
      Serial.print("\t");
      Serial.print(TplateC);
      Serial.print("\t");
      Serial.print(TexitC);

    }

    break;
    /************************************************/
```

```
  }
  /*****************************************************************************/
  Serial.print("\t");
  Serial.print(delayTimeRun);
  delay(delayTimeRun); // delay during Run to minimize serial output
  break;
}


Serial.print("\t");
Serial.print(TSPplateExhale+TSPplateExhaleExitDelta);
Serial.print("\t");
Serial.print(TSPplateExhaleExitDelta);
Serial.print("\t");
Serial.print(TexitObservedDeltaSP);
Serial.print("\t");
Serial.print(TexitObservedMin);
Serial.print("\t");
Serial.print(TexitObservedMax);
Serial.print("\t");
Serial.print(currentMillis - lastExhalationMillis);
Serial.print("\t");
Serial.print(millis());
Serial.println();

}
```

12.1.3 ASL Routine Creation

The code below contains the concepts of the Mathematica Notebook file used to create the pseudo-randomized breath patterns. For brevity and understanding multiple code lines of input/output have been modified, removed, or shortened. Location of full codes, additional code capabilities, and additional explanation on usage, can be found in the archival database (See Appendix 12.3)

Mathematica Notebook Summary for Creation of Breath Profile

N2L Project Section
HDS Project Section
Case 7.2 TCAM Pattern --> Trapezoidal Conscious Adult Mouth breathing with 900mL Vt and randomized I:E of 1:1.3 - 1:8
Pattern Creation

```
IEvector= Range[1.8,1.25,-0.1]
 {1.8,1.7,1.6,1.5,1.4,1.3}
Vtidal = 900;
bl=6;
bln30=bl*0.7;
bln20=bl*0.8;
bln10=bl*0.9;
bl=bl*1.0;
blp10=bl*1.1;
blp20=bl*1.2;
blp30=bl*1.3;
blvector={bln30,bln20,bln10,bl,blp10,blp20,blp30}
tlongestvec=Range[0,blp30,1/512];
 {4.2,4.8,5.4,6.,6.6,7.2,7.8}
Shapetpoints={{1/8,5/8,2/8},{1/8,4/8,3/8}}
 {{1/8,5/8,1/4},{1/8,1/2,3/8}}
intmat=ConstantArray[0,{Length[blvector],Length[IEvector]}];
extmat= ConstantArray[0,{Length[blvector],Length[IEvector]}];
infmat= ConstantArray[0,{Length[blvector],Length[IEvector]}];
exfmat= ConstantArray[0,{Length[blvector],Length[IEvector]}];
tottmat= ConstantArray[0,{Length[blvector],Length[IEvector]}];
ttensor= ConstantArray[0,{Length[blvector],Length[IEvector]}];
Shapeten=ConstantArray[0,{Length[blvector],Length[IEvector],9}];
m30timeten=ConstantArray[0,{Length[blvector],Length[IEvector],2}];
m30delivten=ConstantArray[0,{Length[blvector],Length[IEvector]}];
m30firstten=ConstantArray[0,{Length[blvector],Length[IEvector]}];
```

```
m30secondten=ConstantArray[0,{Length[blvector],Length[IEvector]}];
Shapetpoints[[2,3]]
Length[Shapeten[[1,1]]]
 3/8
 9
For[i=1,i<1+Length[blvector],i++,
 For[j=1,j<1+Length[IEvector],j++,
  intmat[[i,j]]=blvector[[i]]/(IEvector[[j]]+1);
  extmat[[i,j]]=blvector[[i]]/(IEvector[[j]]+1)*IEvector[[j]];
  infmat[[i,j]]=1/(intmat[[i,j]]*2);
  exfmat[[i,j]]=1/(extmat[[i,j]]*2);
  tottmat[[i,j]]=intmat[[i,j]]+extmat[[i,j]];
  ttensor[[i,j]]=Range[0,tottmat[[i,j]],1/512];
  For[k=1,k<=Length[Shapeten[[1,1]]],k++,
   Which[
    k==1,Shapeten[[i,j,k]]=Solve[Vtidal/1000*60==xx/2*(intmat[[i,j]]+Shapetpoints[[1,2]]*intmat[[i,j]]),xx][[1,1,2]],
    k==2,Shapeten[[i,j,k]]=Solve[Vtidal/1000*60==xx/2*(extmat[[i,j]]+Shapetpoints[[2,2]]*extmat[[i,j]]),xx][[1,1,2]],
    k==3,Shapeten[[i,j,k]]=Shapetpoints[[1,1]]*intmat[[i,j]],
    k==4,Shapeten[[i,j,k]]=(Shapetpoints[[1,1]]+Shapetpoints[[1,2]])*intmat[[i,j]],
    k==5,Shapeten[[i,j,k]]=Shapetpoints[[1,3]]*intmat[[i,j]],
    k==6,Shapeten[[i,j,k]]=Shapetpoints[[2,1]]*extmat[[i,j]],
    k==7,Shapeten[[i,j,k]]=intmat[[i,j]]+Shapetpoints[[2,1]]*extmat[[i,j]],
    k==8,Shapeten[[i,j,k]]=intmat[[i,j]]+(Shapetpoints[[2,1]]+Shapetpoints[[2,2]])*extmat[[i,j]],
    k==9,Shapeten[[i,j,k]]=Shapetpoints[[2,3]]*extmat[[i,j]],
    True,1
    ]
   ]
  ]
 ]
Shapeten
TCAMTIEten=ttensor;
For[i=1,i<1+Length[blvector],i++,
  For[j=1,j<1+Length[IEvector],j++,
    For[k=1,k<(Length[ttensor[[i,j]]]+1),k++,
     Which[
       ttensor[[i,j,k]]<Shapeten[[i,j,3]],
       TCAMTIEten[[i,j,k]]=-Shapeten[[i,j,1]]/Shapeten[[i,j,3]]*ttensor[[i,j,k]]
       (* above from y=mx+b with b=0 and m= rise of Qmax from Shapeten[[1]] divided by run of length of time from
Shapeten[[3]] with x=time from ttensor*),
       ttensor[[i,j,k]]>=Shapeten[[i,j,3]]&& ttensor[[i,j,k]]<Shapeten[[i,j,4]],
       TCAMTIEten[[i,j,k]]=-Shapeten[[i,j,1]],
       ttensor[[i,j,k]]>= Shapeten[[i,j,4]]&&ttensor[[i,j,k]]<intmat[[i,j]],
       TCAMTIEten[[i,j,k]]=(Shapeten[[i,j,1]]/Shapeten[[i,j,5]])*(ttensor[[i,j,k]]-Shapeten[[i,j,4]])-Shapeten[[i,j,1]]
       (* above from point slope y-y1=m(x-x1) to y=m(x-x1)+y1*),
       ttensor[[i,j,k]]>=intmat[[i,j]]&&ttensor[[i,j,k]]<Shapeten[[i,j,7]],
       TCAMTIEten[[i,j,k]]=Shapeten[[i,j,2]]/Shapeten[[i,j,6]]*(ttensor[[i,j,k]]-intmat[[i,j]]),
       (* above from exrampup,-1,*)
       ttensor[[i,j,k]]>=Shapeten[[i,j,7]]&&ttensor[[i,j,k]]<Shapeten[[i,j,8]],
       TCAMTIEten[[i,j,k]]=Shapeten[[i,j,2]]
       (*above from exhaling steady maxflow*),
       ttensor[[i,j,k]]>= Shapeten[[i,j,8]],
       TCAMTIEten[[i,j,k]]=(-Shapeten[[i,j,2]]/Shapeten[[i,j,9]])(ttensor[[i,j,k]]-(Shapeten[[i,j,8]]))+Shapeten[[i,j,2]],
       (* above from exrampdown*)
```

```
      True,
      TCAMTIEten[[i,j,k]]=1
      (* above from catch all others statement*)
      ];
     ];
    m30timeten[[i,j]]=MinMax[Nearest[TCAMTIEten[[i,j]]-> ttensor[[i,j]],-5,2]];(* m30 changed to minus 5 as guess
of forcefull breathing*)
    m30firstten[[i,j]]=m30timeten[[i,j,1]];
    m30secondten[[i,j]]=m30timeten[[i,j,2]];
    m30delivten[[i,j]]=m30timeten[[i,j,2]]-m30timeten[[i,j,1]];
    ];
  ];
```

Numerical Checking of Pattern

General Pattern Check

```
MatrixForm[intmat]
({
  {1.5, 1.55556, 1.61538, 1.68, 1.75, 1.82609},
  {1.71429, 1.77778, 1.84615, 1.92, 2., 2.08696},
  {1.92857, 2., 2.07692, 2.16, 2.25, 2.34783},
  {2.14286, 2.22222, 2.30769, 2.4, 2.5, 2.6087},
  {2.35714, 2.44444, 2.53846, 2.64, 2.75, 2.86957},
  {2.57143, 2.66667, 2.76923, 2.88, 3., 3.13043},
  {2.78571, 2.88889, 3., 3.12, 3.25, 3.3913}
 })
MatrixForm[extmat]
({
  {2.7, 2.64444, 2.58462, 2.52, 2.45, 2.37391},
  {3.08571, 3.02222, 2.95385, 2.88, 2.8, 2.71304},
  {3.47143, 3.4, 3.32308, 3.24, 3.15, 3.05217},
  {3.85714, 3.77778, 3.69231, 3.6, 3.5, 3.3913},
  {4.24286, 4.15556, 4.06154, 3.96, 3.85, 3.73043},
  {4.62857, 4.53333, 4.43077, 4.32, 4.2, 4.06957},
  {5.01429, 4.91111, 4.8, 4.68, 4.55, 4.4087}
 })
MatrixForm[tottmat]
({
  {4.2, 4.2, 4.2, 4.2, 4.2, 4.2},
  {4.8, 4.8, 4.8, 4.8, 4.8, 4.8},
  {5.4, 5.4, 5.4, 5.4, 5.4, 5.4},
  {6., 6., 6., 6., 6., 6.},
  {6.6, 6.6, 6.6, 6.6, 6.6, 6.6},
  {7.2, 7.2, 7.2, 7.2, 7.2, 7.2},
  {7.8, 7.8, 7.8, 7.8, 7.8, 7.8}
 })
MatrixForm[Shapeten]
({
  {({
    {44.3077},
    {26.6667},
    {0.1875},
    {1.125},
    {0.375},
```

```
    {0.3375},
    {1.8375},
    {3.1875},
    {1.0125}
~~~~~~~~~~~~~~~~~~~~~~~~~~
    {19.5976},
    {16.3314},
    {0.423913},
    {2.54348},
    {0.847826},
    {0.551087},
    {3.94239},
    {6.14674},
    {1.65326}
   })}
 })
Total[intmat,2]/42
 2.36358

 Mean[Mean[intmat]]
 2.36358
```

Minus Point Pattern Check

Graphical Check of Pattern

```
ListPlot[Join[TCAMTIEten[[1]],TCAMTIEten[[2]],TCAMTIEten[[3]],TCAMTIEten[[4]],TCAMTIEten[[5]],TCAM
TIEten[[6]],TCAMTIEten[[7]]]]
```

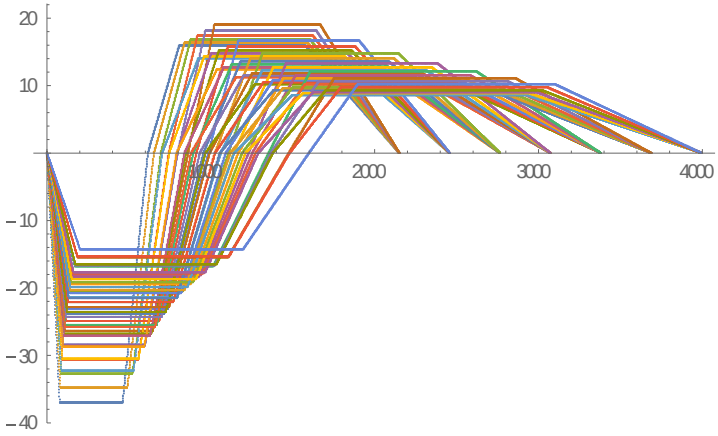

Exporting Files

```
 SetDirectory["J:/Lab_Research/HeatedDryerSystem/HDS_Profile_Creation/HDS_TCAM_Pattern"]
J:\Lab_Research\HeatedDryerSystem\HDS_Profile_Creation\HDS_TCAM_Pattern
```

Main Pattern File Creation

```
(* Only need to run to get the waveform for specific breaths. Not needed for re-creation of orders *)

Export["TCAM_IE11.in",TCAMTIEten[[1,1]],"List"];
~~~~~~~~~~~~~~~~~~~~~~~~~~
Export["TCAM_IE76.in",TCAMTIEten[[7,6]],"List"];
```

```
breathnamesIE=List[
  "C:\Program Files (x86)\ASL Software 3.6\vars\HDS_Study\HDS_TCAM_Pattern\TCAM_IE11.vr3","C:\Program
Files (x86)\ASL Software 3.6\vars\HDS_Study\HDS_TCAM_Pattern\TCAM_IE76.vr3"];
 numberbreathsIE=60;
 breathorderIErecreate=RandomInteger[{1,Dimensions[tottmat][[1]]*Dimensions[tottmat][[2]]},numberbreathsIE]
(* Creates new order each run *)
{1,7,9,9,15,37,11,32,13,3,9,26,30,31,41,9,4,38,40,31,34,14,23,21,39,11,6,39,5,42,5,24,15,32,26,6,40,10,25,5,25,4,4
2,28,31,6,35,3,11,15,15,15,23,42,40,20,29,32,6,7}
(* Random String from 70 breath testing *)
breathorderIE={17,31,7,15,10,23,3,28,11,2,5,32,28,8,19,33,22,4,19,23,12,30,16,24,35,11,5,35,37,21,9,30,21,32,6,6
,26,17,1,15,11,6,2,27,35,32,19,9,28,36,26,8,13,17,32,21,29,37,18,12};
 scriptfileIE=ConstantArray[1,{Length[breathorderIE]+4,2}];
 scriptfileIE[[1]]={1,
  "C:\Program Files (x86)\ASL Software 3.6\vars\HDS_Study\HDS_TCAM_Pattern\TCAM_Zero_Flow.vr3"};
scriptfileIE[[2]]={10,
  "C:\Program Files (x86)\ASL Software 3.6\vars\HDS_Study\HDS_TCAM_Pattern\TCAM_IE46.vr3"};
scriptfileIE[[Length[breathorderIE]+3]]={1,
  "C:\Program Files (x86)\ASL Software 3.6\vars\HDS_Study\HDS_TCAM_Pattern\TCAM_IE46.vr3"};
scriptfileIE[[Length[breathorderIE]+4]]={100,
  "C:\Program Files (x86)\ASL Software 3.6\vars\HDS_Study\HDS_TCAM_Pattern\TCAM_Zero_Flow.vr3"};
 For[i=1,i<=(Length[breathorderIE]),i++,
 scriptfileIE[[i+2,2]]=breathnamesIE[[breathorderIE[[i]]]];
 ]
 Export["TCAM_IE_71breath.sct",scriptfileIE,"Table"]
 TCAM_IE_71breath.sct
```

Supporting Patterns File Creation

Still Have to Create the “vr3” files and the “XXX_Zero_Flow” file

Normal files use function_residual_capacity of 0.2200 and reverse use 1.3000

vr3 Zero_Flow file text

vr3 Zero_Flow file exports

```
 Export["TCAM_Zero_Flow.vr3",vr3fileinfoZeroFlow,"Text"]
 TCAM_Zero_Flow.vr3
```

vr3 Main Pattern file text

```
 vr3fileinfoBase46={
  "
    (lung_model)   function_residual_capacity          (float)   function_residual_capacity          =          0.2200
    (spont_breath)          spont_breath_input_file_name     (string)  spont_breath_input_file_name     =
          SR8D23~1.IN
    (spont_breath)          spont_breath_file_directory      (string)  spont_breath_file_directory      =
          C:\Program Files (x86)\ASL Software 3.6\vars\HDS_Study\HDS_SRAM_Pattern\
    (spont_breath)          breath_file_time_increment       (float)   breath_file_time_increment       =
          0.0019531          (seconds)
  "
  };
```

vr3 Main Pattern file manipulation and export

spont_breath_input_file_name change

```
 Export["TCAM_IE11.vr3",StringReplace[vr3fileinfoBase46,"SR8D23~1"->"TCAM_IE11"],"Text"];
Text"];
Export["TCAM_IE76.vr3",StringReplace[vr3fileinfoBase46,"SR8D23~1"->"TCAM_IE76"],"Text"];
```

12.1.4 Spray Dryer Control Codes

The code below contains the concepts of the VCU Small Particle Spray Dryer control code version Motz. Code is written in the Python language but is presented as a representation of actual code which has been edited for easier reading. This is not directly portable to the Raspberry Pi but exact code can be found in the archive (See Appendix 12.3). This program was developed for functionality over robustness and therefore has limited error handling. Some of the referenced libraries, none of which I wrote, have error handling built into them. However, I did not utilize these features in this version.

```
#Main Control Code For Spray Dryer System
#Handles inlet air properties, heating, pre-collector temperature, and logging
#Requires input of setpoints and log_file_location
#Code testing on Python 3.7
#Dev by oldschoolhip - Ben Spence
#First Dev 12th March 2021
#Updated 10th November 2021


# Get reference libraries section
        import adafruit_max31855
        import adafruit_mcp230xx.mcp23017
        from busio import SPI
        from digitalio import DigitalInOut
        from digitalio import Direction
        import board
        import math
        import time
        import smbus


# General variable initialization, naming, and definitions section
        #Communication parameters
        spi = SPI(clock=board.SCK, MISO=board.MISO, MOSI=board.MOSI)
        bus = smbus.SMBus(1)

        i2cBonnet = board.I2C() #setup the bonnet expansion PCB
        mcpBonnet = adafruit_mcp230xx.mcp23017.MCP23017(i2cBonnet)


        #Expansion Multiplexor setups
        TCAADDRtrh = 0x70
        TCAADDRliquid = 0x71

        def tcaTRHselect(i):
            dataforwrite = 1 << i #bit shifting the input argument
            bus.write_i2c_block_data(TCAADDRtrh, 0x00, [dataforwrite])

        def tcaLIQUIDselect(i):
            dataforwrite = 1 << i #bit shifting the input argument
            bus.write_i2c_block_data(TCAADDRliquid, 0x00, [dataforwrite])
```

```
        # Operation Switches
        Operation_Exit_Switch = DigitalInOut(board.D21)
        Operation_Exit_Switch.direction = Direction.INPUT
        #Operation_Exit_Switch.value returns False when grounded and True when 3.3V
        #When it goes True the program exits
        flag_mode_sensorcalibration = 1


#Top inlet and outlet items
        #Define chip select pins, corresponding sensors, and calibration offset
        csTOP = mcpBonnet.get_pin(15) #assign the bonnet pin to the sensor
        csTOP.switch_to_output(value=False) #assign pin to output and
        sensorTOP = adafruit_max31855.MAX31855(spi,csTOP)
        TTOPoffset = 0.0
        TTOPgoal = 70

        csPOST = DigitalInOut(board.D20)
        csPOST.switch_to_output(value=False)
        sensorPOST = adafruit_max31855.MAX31855(spi,csPOST)
        TPOSToffset = 0.0

        #Define the air flow items and heater element items
        heat_relay = DigitalInOut(board.D24)
        heat_relay.direction = Direction.OUTPUT
        heat_relay.value = False
        SDP3PressFlowAddress = 0x21
        bus.write_i2c_block_data(0x21, 0x36, [0x15]) #read continuous differential pressure averaging mode


        #Inlet humidity control definitions
        BoxTRHsensor = (0) #specific SD and SL pin set on multiplexor the sensor is connected
        RoomTRHsensor = (1) #specific SD and SL pin set on multiplexor the sensor is connected

        PsatA = 23.196
        PsatB = 3816.44
        PsatC = 46.13
        AirConstantR = 287 #J/kg*K
        WaterVaporConstantR = 461.5 #J/kg*K
        BoxPressure = 101325 #Pascals

        BoxWaterContentGoalgperm3 = 10 #g/m^3
        BoxWaterContentGoal = BoxWaterContentGoalgperm3/1000 #kg/m^3


        #Define the atomizer unit relay pin
        humidity_relay = DigitalInOut(board.D23)
        humidity_relay.direction = Direction.OUTPUT
        humidity_relay.value = False

        #Define Spray Liquid Items
        csLiquidT = mcpBonnet.get_pin(8)
        csLiquidT.switch_to_output(value=False)
        sensorLiquidT = adafruit_max31855.MAX31855(spi,csLiquidT)


# Pre-Collector Cross Sensors
        # Define chip select pins, corresponding sensors, and calibration offset
        # See lab notebook page 139 for naming convention diagram

        csA1 = mcpBonnet.get_pin(1)
        ……
        csA6 = mcpBonnet.get_pin(6)
        csC = mcpBonnet.get_pin(7)
        csB1 = mcpBonnet.get_pin(9)
        ……
        csB6 = mcpBonnet.get_pin(14)

        csA1.switch_to_output(value=False)
        ……
        csB6.switch_to_output(value=False)
```

```
        sensorA1 = adafruit_max31855.MAX31855(spi,csA1)
        ..............
        sensorB6 = adafruit_max31855.MAX31855(spi,csB6)

        # calculated in Dryer 5th October 2021
        TA1offset = -0.25
        ..............
        TB6offset = 0.0


#Logging items
        #items for log timing
        loop_start_time = 0.0
        last_start_time = 0.0
        last_loop_duration = 0.0
        flag_log_screen = 0.0
        log_screen_timestamp_p1 = 0.0
        log_screen_interval = 2.000 #python uses seconds
        flag_log_file = 0.0
        log_file_timestamp_p1 = 0.0
        log_file_interval = 10.000

        #create/overwrite the logfile object
        log_filedate = time.strftime("%Y", time.localtime())+"_"+time.strftime("%m", time.localtime())+"_"+time.strftime("%d",
        time.localtime())
        log_fileID = "_CAPSs"
        log_fileextra = "_Pi"
        log_filepath = "SysControlOutput/"+log_filedate+log_fileID+log_fileextra+".txt"
        logfile = open(log_filepath,'w')
        try:
            logfile.write("intro_text_with_goal_settings_and_other_information\n")
            logfile.write("loop_start_time\tBoxTcel\tBoxRH\tRHBoxGoal\tBoxgperm3\tTTOP\tTAVG\ tTPOST\tLiquidT\n")
        finally:
            logfile.close()


# ~~~~~~~~~~~~~~~~~~~~~~~~~~~~~~~~~~~~~~~~~~~~~~~~~~~~~~~~~~~~~~~~~~~~~~~~~~~~
# Loop through code for control of system sensor calibration

while flag_mode_sensorcalibration == 1:
    #run calibration items
    print("Calibration Period Started and Running")
    time.sleep(1.5)

    #Check button to see if a re-calibration period is wanted
    #Tell calibration settings
    print("offsets at")
    #check status of flag_mode_sensorcalibration pin
    flag_mode_sensorcalibration = 0

else: print("Calibration Period Ended")


# ~~~~~~~~~~~~~~~~~~~~~~~~~~~~~~~~~~~~~~~~~~~~~~~~~~~~~~~~~~~~~~~~~~~~~~~~~~~~
# Loop through code for control of system operation

while Operation_Exit_Switch.value == False:
    last_start_time = loop_start_time
    loop_start_time = time.time()
    last_loop_duration = loop_start_time - last_start_time

    #Top inlet temperature control section
    #prevent heater power if no or not enough flow
    #leave this to manual switch on the unit for now
    #check the airflow anyways
    rawPRESSUREsensordata = bus.read_i2c_block_data(0x21, 0x00, 9)
    rawPRESSUREfloatingpoint = (rawPRESSUREsensordata[0] << 8)|rawPRESSUREsensordata[1]
    PressurePa = rawPRESSUREfloatingpoint/60
```

```
#check temperature then react to temperature
TTOP = sensorTOP.temperature + TTOPoffset
TTOPRelError = (TTOP - TTOPgoal) / TTOPgoal * 100

if TTOP < TTOPgoal:
    heat_relay.value = True
else:
    heat_relay.value = False


#Inlet box humidity control section
#check temperature and RH inside box
#calculate water content
#calculate error of water content, temperature, and RH
#react to error

#T&RH check
tcaTRHselect(BoxTRHsensor) #select the correct sensor
bus.write_i2c_block_data(0x44, 0x24, [0x00]) #ask for a single shot high repeatability measurement
#meaning ~12.5ms measurement duration
time.sleep(0.020) #give sensor time to do measurement datasheet says max 15ms required for measurement
#read back data that is 6 bytes long (2 T, 1 CRC, 2 RH, 1 CRC)
BoxTRHsensordata = bus.read_i2c_block_data(0x44, 0x00, 6)
BoxTcel = (((BoxTRHsensordata[0]*256.0) + BoxTRHsensordata[1])/65535.0)*175 - 45
BoxRH = (((BoxTRHsensordata[3]*256.0) + BoxTRHsensordata[4])/65535.0)*100
#ignore the CRC bytes at this point

    #calculate actual water vapor content and the actual RH goal to achieve this based on actual temperature
BoxRhoDryAir = BoxPressure / (AirConstantR*(BoxTcel+273.15)) #kg/m^3
BoxPsat = math.exp(PsatA-PsatB/((BoxTcel+273.15)-PsatC))
YvBoxSat = BoxPsat / (BoxRhoDryAir*WaterVaporConstantR*(BoxTcel+273.15)) #unit ratio
YvBoxActual = BoxRH/100*YvBoxSat #unit ratio mass water/(mass of water plus mass of air) === mass water/total mass
BoxWaterContentActual = YvBoxActual*BoxRhoDryAir #kg/m^3
BoxWaterContentActualgperm3 = BoxWaterContentActual*1000 #g/m^3

YvBoxGoal = BoxWaterContentGoal/BoxRhoDryAir #calculate the goal ratio and RH to acheive BoxWaterContentGoal
RHBoxGoal = YvBoxGoal/YvBoxSat*100 #this is the goal RH based on actual box temperature to obtain correct box water content in
    g/m^3

#calculate error of water content and thereby also RH assuming box stays at constant temperature
YvBoxRelError = (YvBoxActual - YvBoxGoal) / YvBoxGoal * 100
BoxABDRelError = (BoxWaterContentActualgperm3 - BoxWaterContentGoalgperm3) / BoxWaterContentGoalgperm3 * 100
BoxRHRelError = (BoxRH - RHBoxGoal) / RHBoxGoal * 100

#react to error with a couple levels of strength
if BoxABDRelError > 5: #way over the mark
    humidity_relay.value = False #turn off the humidity relay
    #humidity_strength = 0 #turn the power all the way up

elif BoxABDRelError < -5: #way under the mark
    humidity_relay.value = True #turn on the humidity relay
    #humidity_strength = 100 #turn up the power all the way

elif BoxABDRelError <= 5 and BoxABDRelError > 2.5: #little over the mark
    humidity_relay.value = True #turn on the humidity relay
    #humidity_strength = 25 #but keep power lower

elif BoxABDRelError >= -5 and BoxABDRelError < -2.5: #little under the mark
    humidity_relay.value = True #turn on the humidity relay
    #humidity_strength = 75 #but keep power higher

elif BoxABDRelError <= 2.5 and BoxABDRelError >= -2.5: #near the mark
    humidity_relay.value = True #turn on the humidity relay
    #humidity_strength = 50 #keep power middle of the road

else:
    humidity_relay.value = True #default to humidity
    #humidity_strength = 10
```

```
# Check temperature of spray liquid bulk container
#Get temperature value for sensor
LiquidT = sensorLiquidT.temperature

# Check temperature at collector start section
#Get temperature value for each sensor
TA1 = sensorA1.temperature + TA1offset
            ..............
TB6 = sensorB6.temperature + TB6offset

TAVG = (TA1+TA2+TA3+TA4+TA5+TA6+TC+TB1+TB2+TB3+TB4+TB5+TB6)/13

# Check Temperature and Humidity at System Outlet section
#Do as a sanity check and secondary spray rate measurement
#would want to place a filter membrane over the sensor element
#currently just checking temperature with k type probe
TPOST = sensorPOST.temperature + TPOSToffset

#Check room temperature and humidity
tcaTRHselect(RoomTRHsensor) #select the correct sensor
bus.write_i2c_block_data(0x44, 0x24, [0x00]) #ask for a single shot high repeatability measurement
#meaning ~12.5ms measurement duration
time.sleep(0.020) #give sensor time to do measurement datasheet says max 15ms required for measurement
#read back data that is 6 bytes long (2 T, 1 CRC, 2 RH, 1 CRC)
RoomTRHsensordata = bus.read_i2c_block_data(0x44, 0x00, 6)
RoomTcel = (((RoomTRHsensordata[0]*256.0) + RoomTRHsensordata[1])/65535.0)*175 - 45
RoomRH = (((RoomTRHsensordata[3]*256.0) + RoomTRHsensordata[4])/65535.0)*100
#ignore the CRC bytes at this point

# Check if logging needs to happen and if so update the flag
if (time.time() - log_screen_timestamp_p1) >= log_screen_interval : flag_log_screen = 1
if (time.time() - log_file_timestamp_p1) >= log_file_interval : flag_log_file = 1

# Output to screen section
#if flag_log_screen is high write data to screen

if flag_log_screen == 1 :
    #Print Inlet Box Items
    print("BoxTcel\t\t\t\tBoxRhoDryAir\t\t\tBoxPsat\t\t\tYvBoxSat")
    print(BoxTcel,"\t\t",BoxRhoDryAir,"\t\t",BoxPsat,"\t",YvBoxSat)
    print("BoxWaterContentActualgperm3\tBoxWaterContentGoalgperm3\tBoxABDRelError")
    print(BoxWaterContentActualgperm3,"\t\t",BoxWaterContentGoalgperm3,"\t\t\t\t",BoxABDRelError)
    print("YvBoxActual\t\t\tYvBoxGoal\t\t\tYvBoxRelError")
    print(YvBoxActual,"\t\t",YvBoxGoal,"\t\t",YvBoxRelError)
    print("BoxRH\t\t\t\tRHBoxGoal\t\t\tBoxRHRelError")
    print(BoxRH,"\t\t",RHBoxGoal,"\t\t",BoxRHRelError)
    print("humidity_strength\t\tPressurePa")

    #print(humidity_strength,"\t\t\t\t",PressurePa)
    print("humidity_strength\t\t",PressurePa)

    #Print Upper Section Items
    print("TTOP\t\t\t\tTTOPgoal\t\t\tTTOPPRelError")
    print(TTOP,"\t\t\t\t",TTOPgoal,"\t\t\t\t",TTOPRelError)

    #Print Outlet Items
    print("TPOST\t\t\t\tRoomTcel\t\t\tRoomRH\t\t\tlast_loop_duration")
    print(TPOST,"\t\t\t\t",RoomTcel,"\t\t",RoomRH,"\t",last_loop_duration)

    #Print Liquid Items
    print("Bulk Liquid Temp")
    print(LiquidT)

    #Print pre-collector temperature values in pattern
    print("TA1\t\t\t\t\t\tTB1\n \tTA2\t\t\t\tTB2\n \t\tTA3\t\tTB3\n \t\t\tTC\n \t\tTB4\t\tTA4\n \tTB5\t\t\t\tTA5\n TB6\t\t\t\t\t\tTA6")
    print(TA1,"\t\t\t\t\t\t",TB1,"\n\t",TA2,"\t\t\t\t",TB2,"\n\t\t",TA3,"\t\t",TB3,"\n\t\t\t",
                TC,"\n\t\t",TB4,"\t\t",TA4,"\n\t",TB5,"\t\t\t\t",TA5,"\n",TB6,"\t\t\t\t\t\t",TA6)
    print("TAVG\t\t",TAVG)
```

```
        #Acknowledge logging by resetting timer and flag
        log_screen_timestamp_p1 = time.time() #equals the current time
        print("last logged to screen at ", log_screen_timestamp_p1)
        print("last logged to file at ", log_file_timestamp_p1)
        flag_log_screen = 0

    # Output to file section
    #if flag_log_file is high write data to file
    if flag_log_file == 1 :
        #create entry
        entryA = str(loop_start_time)+"\t"+str(BoxTcel)+"\t"+str(BoxRH)+"\t"+str(RHBoxGoal) +"\t"
        entryB = str(BoxWaterContentActualgperm3)+"\t"+str(TTOP)+"\t"+str(TAVG) +"\t"+str(TPOST)+"\t"
        entryC = str(LiquidT)+"\n"
        entryTotal = entryA + entryB +entryC

        #print items into the file by appending
        logfile = open(log_filepath,'a')
        try:
            logfile.write(entryTotal)
        finally:
            logfile.close()

        #Acknowledge logging by resetting timer and flag
        log_file_timestamp_p1 = time.time() #equals the current time
        print("last logged to file at ", log_file_timestamp_p1)
        flag_log_file = 0

else: print("Operation Period Ended")

# ~~~~~~~~~~~~~~~~~~~~~~~~~~~~~~~~~~~~~~~~~~~~~~~~~~~~~~~~~~~~~~~~~~~~~~~~~~~~~~~~~~~~~~~
# End of file items and garbage collection

# Stop the flow pressure reading sensor
bus.write_i2c_block_data(0x21, 0x3F, [0xF9])
print("sensor stopped")

# Turn off all relay/output
humidity_relay.value = False
heat_relay.value = False
print("relays off")

# End of file
```

12.2 Data Gathering, Parsing, and Preprocessing Procedure of LVMH and HDS Tests

12.2.1 File Naming Structures

Each experimental run creates multiple files in multiple locations. This section explains the naming convention used in the saving and analyzing of the files. These specific items are for the LVMH synchronization tests, however the LVMH human safety study and HDS test had similar naming conventions.

Data Collection

SLCC3A2ir					
SLC	C3	A	2	i	r
Experimental Study Identifier	*Breathing Pattern and Trigger Identifier*	*Model or Subject Identifier*	*Run Number*	*Data Source*	*Status Identifier*
Streamlined Cannula Study	Case 3 Variable DNI Pressure Trigger	Model A	#	Inlet Flow Data	Raw form without processing
Additional Options					
N2L	C1-5	O, A, B, …	1-n	i, m, d, a, b	r, ---

ASL5000 Files

DNI_IE46.vr3				
DNI	_IE	4	6	.vr3
Breath Pattern Identifier	*Indicate Variable I:E Ratio*	*Breath Length Option*	*I:E Ratio Option*	*File Type Function*
Deep Nasal Inhalation	I:E Ratio	4 = Middle	6 = Last	Simulation Parameter File
Additional Options				
DNIR, SRAM, SRAMR, TCAM, TCAMR		1-7	1-6	.in, out

12.2.2 Flow Sensor Setup

Use of multiple SFM3000 sensors requires each sensor matching imbedded GUI to be setup individually via the following steps for sensors labeled A and B. If additional units are to be connected simply iterate the first two steps.

- Plug Unit A into computer and open new software instance
- Unplug Unit A from computer
- Plug Unit B into computer and open new software instance
- Unplug Unit B from computer
- Plug all units into computer
- “Run” and “Stop” each instance (note incorrect units will appear)
- “Run” and “Stop” each instance a second time (correct units auto-populate)
- Update csv file locations for all instances
- Update all instances to absolute timing and correct interval (20ms for LVMH)

12.2.3 Bulk Data Edits in Notepad++

- Place files in folders/subfolders
- In Notepad++ do a Search and Replace with “Find in Files”
- Set upper directory level and select check in subfolders
- Run with Find what “ and Replace with (no text)
- Run with Find what : and Replace with ,
- Run with Find what / and Replace with ,
- Run with Find what (Text of Old Header) Replace with (Text of New Header)

12.2.4 Excel Organization of Arduino Serial Outputs

Data from Arduino board serial outputs were saved as a text stream in sequential order. The following steps are taken, after bulk data edits in Notepad++, to organize and present the data for post-processing analysis. Multiple methods are described due to the different controllers within each Control and Monitoring Unit and the purpose of each experiment.

LVMH Synchronization Study Nebulizer Board Output

Minimal processing was required for this output stream and was performed independently of the Monitoring Board output organization. In this case, an additional column was added for the graphing time. This value was calculated and a graph of the sensed and critical pressure throughout this time created.

LVMH Synchronization Study Monitoring Board Output

Large amount of post processing was required for this output stream but was performed independently of the Nebulizer Board output. The main goal of this analysis was the determination of how close the *predicted-inhalation-start-time* matched the *actual-inhalation-start-time* of the ASL5000 breath pattern. Briefly, the process involved aligning and linking drug delivery to the known ASL5000 breaths, then calculating a time differential. The steps of this process are listed below:

- Insert header template information into rows 1-7 of spreadsheet
- Select all data and use excel Sort feature to organize by Item Flag (4, 5, 6 → DRUG, ASL, PAT)
- Move data to correct column grouping labeled in the header template

- Re-sort each column grouping to have inhalation events then exhalation events, both sub-organized by time, earliest first
- Calculate the run normalized time for each event based on the first ASL5000 breath inhalation event time
- Calculate each drug production event's time differential value
- Calculate a run time differential value based on the average value of the central 60 breaths for comparison among the different experimental setups

LVMH Human Safety Study Nebulizer Board Output

Processing of the Human Safety Study Nebulizer board was similar to the Synchronization Study, but required additional attention due to the unique and spontaneous breathing pattern. A run normalized time zero point was established and an additional column was added with the normalized time value for each output event of the nebulizer board. Both the sensor recorded differential pressure and the device calculated critical pressure were plotted versus normalized time. The plot aspect ratio was then dramatically increased such that individual data points on ~50 millisecond intervals were distinguishable for the entire several minute time period. Visually traversing this plot, the subject's breath timing information was determined by a transcription of the normalized time values of each *inhalation-start* and *exhalation-start* event. Qualitative notes on the events were also taken during this sensor log review. The device-determined critical pressure value was included in the plot to assist with quick visual alignment; however, breath event timings were based solely on information from the sensor recorded differential pressure values.

LVMH Human Safety Study Monitoring Board Output

The Monitoring Board required large amount of post processing and was performed with the breath information determined from the Nebulizer Board output. The two main goals of this analysis were to determine wholistic breathing pattern metrics and to quantify drug nebulization algorithm functionality. Briefly, the process involved calculating metrics for each of the previously determined breaths and then classifying the system operation for each breath. The steps of this process are listed below:

- Insert header template information into rows 1-7 of spreadsheet
- Select all data and use excel Sort feature to organize by Item Flag
- Move data to correct column grouping labeled in the header template
- Re-sort each column grouping to have inhalation events then exhalation events, sub-organized by time, earliest first
- Calculate for each breath the associated value of I:E and Breath Frequency
- Link each nebulization event to corresponding inhalation events based on temporal distance from *inhalation-start* and device operation
- For each breath classify associated nebulization events into categories of Correct Delivery, Missed Delivery, Multiple Delivery, or No Delivery
- For each breath, count number of nebulization events within each category

HDS Study Boards

Intense data analysis of the operational data streams from the HDS study boards was limited to developmental stages. Most experimental runs were simply live monitored for correct

operational performance. For developmental evaluation, the Beta board data was processed for graphical representation. Most data points were already formatted for direct plotting on a dual y-axis chart with minor adjustments to axis bounds. However, the character-based output of device state was converted to a numerical-based format allowing for plotting.

12.3 Digital Files Storage within Longest Database

A file repository has been created on the laboratory server which contains the digital information related to projects presented in this dissertation. This repository is divided into four sections by the three overall objective topics plus a general laboratory section. The purpose of this is to organize relevant dissertation information and identify the version created for experimentation. Therefore, neither intermediate versions nor work not directly related to dissertation objectives are included in the repository. However, no guarantee is made that files will function properly when opened from the repository due to file path changes, software license issues, or software versioning issues. If this occurs, access the file from within the complete main data backup or original file path.

The file repository location is:

W:\Longest Group\Member_Folders\spencebm\spencebm_database

Intermediate steps and non-dissertation items are located in two locations:

J:\Lab_Research

D:\spencebm

Chapter 13: Administration Support Appendix

13.1 Journal Publication List

Dutta, R., B. Spence, X. Wei, S. Dhapare, M. Hindle and P. W. Longest (2020). "CFD Guided Optimization of Nose-to-Lung Aerosol Delivery in Adults: Effects of Inhalation Waveforms and Synchronized Aerosol Delivery." Pharm Res 37(10): 199.

Longest, P. W., Spence, B. M., Hindle, M. 2019. Devices for Improved Delivery of Nebulized Pharmaceutical Aerosols to the Lungs. *Journal of Aerosol Medicine and Pulmonary Drug Delivery* [2.9]. DOI: 10.1089/jamp.2018.1508

Spence, B. M., Longest, P. W., Wei, X., Dhapare, S., Hindle, M. 2019. Development of a high flow nasal cannula (HFNC) and pharmaceutical aerosol combination device. *Journal of Aerosol Medicine and Pulmonary Drug Delivery* [2.9]. DOI: 10.1089/jamp.2018.1488

Longest, P. W., Spence, B. M., Holbrook, L. T., Mossi, K. M, Son, Y.-J., Hindle, M. 2012. Production of inhalable submicrometer and nanoparticle aerosols from conventional mesh nebulizers for improved respiratory drug delivery. *Journal of Aerosol Science* 51:66-80.

13.2 Conference Proceedings

Spence, B., Momin, M., Hindle, M., Longest, P. Development of A Heated Dryer System (HDS) for High-Efficiency Excipient Enhanced Growth (EEG) Delivery of Nebulized Medications during Oral Inhalation. International Society for Aerosols in Medicine 23rd ISAM Congress 2021.

Spence, B., DeWilde, C., Priday, A., Syed, A., Dhapare, S., Wei, X., Longest, P. W., Hindle, M. Implementation of a Combination Device for High Efficiency Aerosol Delivery and High Flow Nasal Cannula Therapy in Adult Human Subjects. Respiratory Drug Delivery 2020.

Spence, B., Momin, M., Dhapare, S., Wei, X., Longest, P. W., Hindle, M., Synchronizing High Efficiency Aerosol Delivery with Inhalation During High Flow Nasal Cannula Therapy. Respiratory Drug Delivery 2020.

Hindle, M., Wei, X., Spence, B. M., Golshahi L., Longest, P. W., 2018. Aerosol Therapy During Non-invasive Ventilation: Challenges and Opportunities. *Respiratory Drug Delivery*. 1:137-148.

Dhapare, S., Spence, B., Boc ST., Wei, X., Bass, K., Longest, P., Hindle, M., Breath-synchronized Delivery of Aerosols to Infants Using a Very Low Volume Mixer-heater. Respiratory Drug Delivery 2018. Volume 2, 2018: 643-646.

Spence, B. M., Wei, X., Hindle, M., Longest, P., Optimization of a Combination Device for high efficiency aerosol delivery and High Flow Nasal Cannula therapy. Respiratory Drug Delivery 2018. Volume 2, 2018: 669-674.

Dhapare, S., Boc, ST., Spence, B., Bass, K., Longest, P., Hindle M., Overcoming the Challenges of Aerosol Delivery to Infants During Non-invasive Ventilation. RDD Asia 2018, Volume 1, 2018: 93-102

Boc, S., Spence, B., Bass, K. Longest, P., Hindle, M. "High-efficiency delivery of aerosols via an infant nasal cannula". RDD Europe 2017 (Editors: Dalby RN, Peart J, Suman JD, Young PM, and Traini D), Volume 2, 2017: 385-388.

Boc, S., Spence, B., Wei. X., Bass, K., Longest, P., Hindle, M. Improved Nose-to-Lung (N2L) Aerosol Delivery in an In Vitro Airway Model. International Society for Aerosols in Medicine 21st ISAM Congress 2017.

Spence, B., Wei. X., Hindle, M., Longest, P. Development and Characterization of a Mixer-Heater System for Testing Excipient Enhanced Growth Aerosol Delivery in Human Subjects. International Society for Aerosols in Medicine 21st ISAM Congress 2017.

13.3 Intellectual Property

P.W. Longest, M. Hindle, B. Spence, S. Dhapare, X. Wei, "Combination devices, systems, and methods for humidification of the airways and high efficiency delivery of pharmaceutical aerosols". (US201862659985P) 2018

List of References

Anderson, S. D. and C. M. Smith (1991). "Osmotic challenges in the assessment of bronchial hyperresponsiveness." Am Rev Respir Dis **991**(143): 543-546.

Ari, A. and J. B. Fink (2012). "Inhalation therapy in patients receiving mechanical ventilation: an update." Journal of Aerosol Medicine and Pulmonary Drug Delivery **25**(6): 319-332.

ASTM_International (2004). F1690-96 standard specification for humidifiers for medical use, West Conshohocken, PA: American Society for Testing Materials.

Bass, K., S. Boc, M. Hindle, K. Dodson and W. Longest (2019). "High-Efficiency Nose-to-Lung Aerosol Delivery in an Infant: Development of a Validated Computational Fluid Dynamics Method." Journal of Aerosol Medicine and Pulmonary Drug Delivery **32**(3): 132-148.

Benchetrit, G. (2000). "Breathing pattern in humans: diversity and individuality." Respiration Physiology **122**(2-3): 123-129.

Bennett, G., M. Joyce, E. F. Fernandez and R. MacLoughlin (2019). "Comparison of aerosol delivery across combinations of drug delivery interfaces with and without concurrent high-flow nasal therapy." Intensive Care Medicine Experimental **7**.

Bennett, G., M. Joyce, L. Sweeney and R. MacLoughlin (2018). "In Vitro Determination of the Main Effects in the Design of High-Flow Nasal Therapy Systems with Respect to Aerosol Performance." Pulmonary Therapy **https://doi.org/10.1007/s41030-018-0054-x**: 1-14.

Bennett, W. D., M. Xie, K. Zeman, H. Hurd and S. Donaldson (2015). "Heterogeneity of Particle Deposition by Pixel Analysis of 2D Gamma Scintigraphy Images." Journal of Aerosol Medicine and Pulmonary Drug Delivery **28**(3): 211-218.

Biswas, R., N. A. Hanania and A. Sabharwal (2017). "Factors Determining In Vitro Lung Deposition of Albuterol Aerosol Delivered by Ventolin Metered-Dose Inhaler." Journal of Aerosol Medicine and Pulmonary Drug Delivery **30**(4): 256-266.

Boc, S., B. Spence, K. Bass, P. W. Longest and M. Hindle (2017). "Improved Nose-to-Lung (N2l) Aerosol Delivery in an in Vitro Infant Airway Model." Journal of Aerosol Medicine and Pulmonary Drug Delivery **30**(3): 32-33.

Bonasera, S. (2021). Formulation, Characterization and Pharmacokinetic Modelling of Excipient Enhanced Growth Spray-Dried Inhalation Powders. Doctor of Philosophy, Virginia Commonwealth University.

Corcoran, T. E. (2015). "Imaging in Aerosol Medicine." Respiratory Care **60**(6): 850-855.

Corcoran, T. E., J. E. Godovchik, K. H. Donn, D. R. Busick, J. Goralski, L. W. Locke, M. R. Markovetz, M. M. Myerburg, A. Muthukrishnan and L. Weber (2017). "Overnight delivery of hypertonic saline by nasal cannula aerosol for cystic fibrosis." Pediatric pulmonology **52**(9): 1142-1149.

Crowe, C., M. Sommerfeld and Y. Tsuji (1998). Multiphase Flows with Drops and Bubbles. Boca Raton, CRC Press.

Dailey, P. A., R. Harwood, K. Walsh, J. B. Fink, T. Thayer, G. Gagnon and A. Ari (2018). "Aerosol delivery through adult high flow nasal cannula with heliox and oxygen." Respiratory Care **62**(9): 1186-1192.

Daviskas, E. and S. D. Anderson (2006). "Hyperosmolar agents and clearance of mucus in the diseased airway." Journal Of Aerosol Medicine-Deposition Clearance And Effects In The Lung **19**(1): 100-109.

Demers, R. R., C. Burciaga and M. Sousa (2016). "The Respirgard II 303 breathing circuit filter is NOT an "absolute filter"." Respiratory Care **61**(12): 1710-1711.
Dhand, R. (2007). "Inhalation therapy in invasive and noninvasive mechanical ventilation." Current Opinion in Critical Care **13**(1): 27-38.
Dhand, R. (2012). "Aerosol therapy in patients receiving noninvasive positive pressure ventilation." Journal of Aerosol Medicine and Pulmonary Drug Delivery **25**(2): 63-78.
Dhapare, S., S. Boc, B. Spence, K. Bass, P. W. Longest and M. Hindle (2018). "Overcoming the Challenges of Aerosol Delivery to Infants During Non-invasive Ventilation." Respiratory Drug Delivery 2018 **Volume 1, 2018: 93-102**: 93-102.
DiBlasi, R. M. (2015). "Clinical controversies in aerosol therapy for infants and children." Respiratory Care **60**(6): 894-916.
Dionisio, G. H., D. O. dos Santos, L. Perossi, M. H. de Paula, H. C. D. de Souza and A. C. Gastaldi (2018). "The Influence of Different Mouthpieces on Impulse Oscillometry Results." Respiratory Care **63**(5): 565-572.
Ditcham, W., J. Murdzoska, G. C. Zhang, C. Roller, D. von Hollen, K. Nikander and S. G. Devadason (2014). "Lung Deposition of Tc-99m-Radiolabeled Albuterol Delivered through a Pressurized Metered Dose Inhaler and Spacer with Facemask or Mouthpiece in Children with Asthma." Journal of Aerosol Medicine and Pulmonary Drug Delivery **27**: S63-S75.
Dugernier, J., M. Hesse, T. Jumetz, E. Bialais, J. Roeseler, V. Depoortere, J.-B. Michotte, X. Wittebole, S. Ehrmann and P.-F. Laterre (2017). "Aerosol delivery with two nebulizers through high-flow nasal cannula: A randomized cross-over single-photon emission computed tomography study." Journal of Aerosol Medicine and Pulmonary Drug Delivery **30**(5): 349-358.
Dugernier, J., M. Hesse, R. Vanbever, V. Depoortere, J. Roeseler, J.-B. Michotte, P.-F. Laterre, F. Jamar and G. Reychler (2017). "SPECT-CT Comparison of Lung Deposition using a System combining a Vibrating-mesh Nebulizer with a Valved Holding Chamber and a Conventional Jet Nebulizer: a Randomized Cross-over Study." Pharmaceutical Research **34**: 290-300.
El Taoum, K. K., J. X. Xi, J. Kim and A. Berlinski (2015). "In Vitro Evaluation of Aerosols Delivered via the Nasal Route." Respiratory Care **60**(7): 1015-1025.
Eschenbacher, W. L., H. A. Boushey and D. Sheppard (1984). "Alteration in osmolarity of inhaled aerosols cause bronchoconstriction and cough, but absence of a permeant anion causes cough alone." The American review of respiratory disease **129**(2): 211-215.
Farkas, D., M. Hindle and P. W. Longest (2018). "Development of an Inline Dry Power Inhaler That Requires Low Air Volume." Journal of Aerosol Medicine and Pulmonary Drug Delivery **31**(4): 255-265.
Farkas, D., M. Hindle and P. W. Longest (2018). "Efficient Nose-to-Lung Aerosol Delivery with an Inline DPI Requiring Low Actuation Air Volume." Pharmaceutical research **35**(10): 194.
Finlay, W. H. (1998). "Estimating the type of hygroscopic behavior exhibited by aqueous droplets." Journal of Aerosol Medicine **11**(4): 221-229.
Finlay, W. H. (2001). The mechanics of inhaled pharmaceutical aerosols : an introduction. San Diego, Academic Press.
Fok, T. F., S. Monkman, M. Dolovich, S. Gray, G. Coates, B. Paes, F. Rashid, M. Newhouse and H. Kirpalani (1996). "Efficiency of aerosol medication delivery from a metered dose inhaler versus jet nebulizer in infants with bronchopulmonary dysplasia." Pediatric Pulmonology **21**(5): 301-309.
Geller, D. E. (2009). "Aerosol antibiotics in cystic fibrosis." Respiratory Care **54**(5): 658-670.

Golshahi, L., P. W. Longest, M. Azimi, A. Syed and M. Hindle (2014). "Intermittent Aerosol Delivery to the Lungs During High-Flow Nasal Cannula Therapy." Respiratory Care **59**(10): 1476-1486.
Golshahi, L., P. W. Longest, M. Azimi, A. Syed and M. Hindle (2014). "Intermittent aerosol delivery to the lungs during high flow nasal cannula therapy." Respiratory Care **59**(10): 1476-1486.
Golshahi, L., G. Tian, M. Azimi, Y.-J. Son, R. L. Walenga, P. W. Longest and M. Hindle (2013). "The use of condensational growth methods for efficient drug delivery to the lungs during noninvasive ventilation high flow therapy." Pharmaceutical Research **30**: 2917-2930.
Golshahi, L., G. Tian, M. Azimi, Y. J. Son, R. Walenga, P. W. Longest and M. Hindle (2013). "The use of condensational growth methods for efficient drug delivery to the lungs during noninvasive ventilation high flow therapy." Pharmaceutical Research **30**(11): 2917-2930.
Golshahi, L., R. L. Walenga, P. W. Longest and M. Hindle (2014). "Development of a Transient Flow Aerosol Mixer-Heater System for Lung Delivery of Nasally Administered Aerosols Using a Nasal Cannula." Aerosol Science and Technology **48**(10): 1009-1021.
Guilmette, R. A., J. D. Wicks and R. K. Wolff (1989). "Morphometry of human nasal airways in vivo using Magnetic Resonance Imaging." Journal of Aerosol Medicine **2**(4): 365-377.
Haq, I., S. Gopalakaje, A. C. Fenton, M. C. McKean, C. J. O'Brien and M. Brodlie (2014). "The evidence for high flow nasal cannula devices in infants." Paediatric Respiratory Reviews **15**(2): 124-134.
Hess, D. R. (2007). "The mask of noninvasive ventilation: Principles of design and effects on aerosol delivery." Journal of Aerosol Medicine **20**: S85-S99.
Hess, D. R. (2015). "Aerosol therapy during noninvasive ventilation or high-flow nasal cannula." Respiratory Care **60**(6): 880-893.
Higgins, R., W. Cookson, D. Lane, S. John, G. McCarthy and S. McCarthy (1987). "Cardiac arrhythmias caused by nebulised beta-agonist therapy." The Lancet **330**(8563): 863-864.
Hindle, M. and P. W. Longest (2012). "Condensational growth of combination drug-excipient submicrometer particles for targeted high-efficiency pulmonary delivery: evaluation of formulation and delivery device." Journal of Pharmacy and Pharmacology **64**(9): 1254-1263.
Hindle, M. and P. W. Longest (2013). "Quantitative analysis and design of a spray aerosol inhaler. Part 2: Improvements in mouthpiece performance." Journal of Aerosol Medicine and Pulmonary Drug Delivery **26**(5): 237-247.
Hinds, W. C. (1999). Aerosol technology : properties, behavior, and measurement of airborne particles. New York, Wiley.
Hosseini, S. (2021). Evaluation of Regional Extrathoracic Deposition of Low- and High-Momentum Aerosol Using Anatomically-Correct In Vitro Airway Models. Doctor of Philosophy, Virginia Commonwealth University.
Howe, C., M. A. M. Momin, D. R. Farkas, S. Bonasera, M. Hindle and P. W. Longest (2021). "Advancement of the Infant Air-Jet Dry Powder Inhaler (DPI): Evaluation of Different Positive-Pressure Air Sources and Flow Rates." Pharmaceutical Research **38**(9): 1615-1632.
ICRP (1994). Human Respiratory Tract Model for Radiological Protection. New York, Elsevier Science Ltd.
Küng, M., S. W. Croley and B. A. Phillips (1987). "Systemic cardiovascular and metabolic effects associated with the inhalation of an increased dose of albuterol: influence of mouth rinsing and gargling." Chest **91**(3): 382-387.

Lee, J. H., K. J. Rehder, L. Williford, I. M. Cheifetz and D. A. Turner (2013). "Use of high flow nasal cannula in critically ill infants, children, and adults: a critical review of the literature." Intensive Care Medicine **39**(2): 247-257.
Lindemann, J., R. Leiacker, G. Rettinger and T. Keck (2002). "Nasal mucosal temperature during respiration." Clinical Otolaryngology & Allied Sciences **27**(3): 135-139.
Longest, P. W., M. Azimi, L. Golshahi and M. Hindle (2014). "Improving aerosol drug delivery during invasive mechanical ventilation with redesigned components." Respiratory Care **59**(5): 686-698.
Longest, P. W., D. Farkas, A. Hassan and M. Hindle (2020). "Computational Fluid Dynamics (CFD) Simulations of Spray Drying: Linking Drying Parameters with Experimental Aerosolization Performance." Pharmaceutical Research **37**(6).
Longest, P. W., L. Golshahi, S. R. B. Behara, G. Tian, D. R. Farkas and M. Hindle (2015). "Efficient Nose-to-Lung (N2L) Aerosol Delivery with a Dry Powder Inhaler." Journal of Aerosol Medicine and Pulmonary Drug Delivery **28**(3): 189-201.
Longest, P. W., L. Golshahi and M. Hindle (2013). "Improving Pharmaceutical Aerosol Delivery During Noninvasive Ventilation: Effects of Streamlined Components." Annals of Biomedical Engineering **41**(6): 1217-1232.
Longest, P. W. and M. Hindle (2009). "Evaluation of the Respimat Soft Mist inhaler using a concurrent CFD and in vitro approach." Journal of Aerosol Medicine and Pulmonary Drug Delivery **22**(2): 99-112.
Longest, P. W. and M. Hindle (2009). "Quantitative analysis and design of a spray aerosol inhaler. Part 1: Effects of dilution air inlets and flow paths." Journal of Aerosol Medicine and Pulmonary Drug Delivery **22**(3): 271-283.
Longest, P. W. and M. Hindle (2009). "Quantitative Analysis and Design of a Spray Aerosol Inhaler. Part 1: Effects of Dilution Air Inlets and Flow Paths." Journal of Aerosol Medicine and Pulmonary Drug Delivery **22**(3): 271-283.
Longest, P. W. and M. Hindle (2010). "CFD simulations of enhanced condensational growth (ECG) applied to respiratory drug delivery with comparisons to in vitro data." Journal of Aerosol Science **41**: 805-820.
Longest, P. W. and M. Hindle (2011). "Numerical model to characterize the size increase of combination drug and hygroscopic excipient nanoparticle aerosols." Aerosol Science and Technology **45**: 884-899.
Longest, P. W. and M. Hindle (2012). "Condensational growth of combination drug-excipient submicrometer particles for targeted high efficiency pulmonary delivery: comparison of CFD predictions with experimental results." Pharm Res **29**(3): 707-721.
Longest, P. W. and M. Hindle (2012). "Condensational growth of combination drug-excipient submicrometer particles: Comparison of CFD predictions with experimental results." Pharmaceutical Research **29**(3): 707-721.
Longest, P. W., M. Hindle, S. Das Choudhuri and J. Xi (2008). "Comparison of ambient and spray aerosol deposition in a standard induction port and more realistic mouth-throat geometry." Journal of Aerosol Science **39**(7): 572-591.
Longest, P. W., B. M. Spence, L. T. Holbrook, K. M. Mossi, Y.-J. Son and M. Hindle (2012). "Production of inhalable submicrometer aerosols from conventional mesh nebulizers for improved respiratory drug delivery." Journal of Aerosol Science **51**: 66-80.
Longest, P. W., G. Tian, R. Delvadia and M. Hindle (2012). "Development of a stochastic individual path (SIP) model for predicting the deposition of pharmaceutical aerosols: Effects of

turbulence, polydisperse aerosol size, and evaluation of multiple lung lobes." Aerosol Science and Technology **46**(12): 1271-1285.
Longest, P. W., G. Tian, X. Li, Y.-J. Son and M. Hindle (2012). "Performance of combination drug and hygroscopic excipient submicrometer particles from a softmist inhaler in a characteristic model of the airways." Annals of Biomedical Engineering **40**(12): 2596-2610.
Longest, P. W., R. L. Walenga, Y.-J. Son and M. Hindle (2013). "High efficiency generation and delivery of aerosols through nasal cannula during noninvasive ventilation." Journal of Aerosol Medicine and Pulmonary Drug Delivery **26**(5): 266-279.
Longest, P. W. and J. Xi (2007). "Effectiveness of direct Lagrangian tracking models for simulating nanoparticle deposition in the upper airways." Aerosol Science and Technology **41**(4): 380-397.
Longest, P. W. and J. Xi (2008). "Condensational growth may contribute to the enhanced deposition of cigarette smoke particles in the upper respiratory tract." Aerosol Science and Technology **42**: 579-602.
Longest, W., B. Spence and M. Hindle (2019). "Devices for Improved Delivery of Nebulized Pharmaceutical Aerosols to the Lungs." Journal of Aerosol Medicine and Pulmonary Drug Delivery **32**(5): 317-339.
Lowry, R. H., A. M. Wood and T. W. Higenbottam (1988). "Effects of pH and osmolarity on aerosol-induced cough in normal volunteers." Clinical Science **74**(4): 373-376.
Nikander, K., I. Prince, S. Coughlin, S. Warren and G. Taylor (2010). "Mode of Breathing-Tidal or Slow and Deep-through the I-neb Adaptive Aerosol Delivery (AAD) System Affects Lung Deposition of Tc-99m-DTPA." Journal of Aerosol Medicine and Pulmonary Drug Delivery **23**: S37-S43.
Nishimura, M. (2015). "High-flow nasal cannula oxygen therapy in adults." Journal of Intensive Care **3**(1): 15.
Perry, S. A., K. C. Kesser, D. E. Geller, D. M. Selhorst, J. K. Rendle and J. H. Hertzog (2013). "Influences of Cannula Size and Flow Rate on Aerosol Drug Delivery Through the Vapotherm Humidified High-Flow Nasal Cannula System." Pediatric Critical Care Medicine **14**(5): E250-E256.
Pitance, L., L. Vecellio, T. Leal, G. Reychler, H. Reychler and G. Liistro (2010). "Delivery Efficacy of a Vibrating Mesh Nebulizer and a Jet Nebulizer under Different Configurations." Journal of Aerosol Medicine and Pulmonary Drug Delivery **23**(6): 389-396.
Reminiac, F., L. Vecellio, N. Heuze-Vourc'h, A. Petitcollin, R. Respaud, M. Cabrera, D. Le Pennec, P. Diot and S. Ehrmann (2016). "Aerosol therapy in adults receiving high flow nasal cannula oxygen therapy." Journal of Aerosol Medicine and Pulmonary Drug Delivery **doi:10.1089/jamp.2015.1219**.
Restrepo, R. D. and B. K. Walsh (2012). "Humidification during invasive and noninvasive mechanical ventilation: 2012." Respiratory Care **57**(5): 782-788.
Sarhan, R. M., A. A. Elberry, N. S. Abdelwahab, H. Rabea, M. N. Salem and M. E. A. Abdelrahim (2019). "Effect of Oxygen Flow on Aerosol Delivery From a Nebulizer With a Holding Chamber." Respiratory Care **64**(12): 1508-1515.
Spence, B., C. DeWilde, A. Priday, A. Syed, S. Dhapare, X. Wei, P. Longest and M. Hindle (2020). "Implementation of a Combination Device for High Efficiency Aerosol Delivery and High-Flow Hasal Cannula Therapy in Adult Human Subjects." Respiratory Drug Delivery 2020 **3**: 723-728.

Spence, B., M. Momin, S. Dhapare, X. Wei, P. Longest and M. Hindle (2020). "Synchronizing High Efficiency Aerosol Delivery with Inhalation During High Flow Nasal Cannula Therapy." Respiratory Drug Delivery 2020 **3**: 717-722.
Spence, B., M. Momin, M. Hindle and P. Longest (2021). "Development of A Heated Dryer System (HDS) for High-Efficiency Excipient Enhanced Growth (EEG) Delivery of Nebulized Medications during Oral Inhalation
Abstracts: International Society for Aerosols in Medicine e.V. 23rd ISAM Congress Boise, ID May 22-26, 2021." Journal of Aerosol Medicine and Pulmonary Drug Delivery **34**(5).
Spence, B. M., W. Longest, X. Y. Wei, S. Dhapare and M. Hindle (2019). "Development of a High-Flow Nasal Cannula and Pharmaceutical Aerosol Combination Device." Journal of Aerosol Medicine and Pulmonary Drug Delivery **32**(4): 224-241.
Sunbul, F., J. B. Fink, R. Harwood, M. M. Sheard, R. D. Zimmerman and A. Ari (2014). "Comparison of HFNC, bubble CPAP and SiPAP on aerosol delviery in neonates: An in-vitro study." Pediatric Pulmonology **DOI 10.1002/ppul.23123**.
Tian, G., M. Hindle and P. W. Longest (2014). "Targeted lung delivery of nasally administered aerosols." Aerosol Science and Technology **48**(4): 434-449.
Tian, G., P. W. Longest, X. Li and M. Hindle (2013). "Targeting aerosol deposition to and within the lung airways using excipient enhanced growth." Journal of Aerosol Medicine and Pulmonary Drug Delivery **26**(5): 248-265.
Tobin, M. J., T. S. Chadha, G. Jenouri, S. J. Birch, H. B. Gazeroglu and M. A. Sackner (1983). "Breathing Patterns .1. Normal Subjects." Chest **84**(2): 202-205.
Tobin, M. J., M. J. Mador, S. M. Guenther, R. F. Lodato and M. A. Sackner (1988). "Variability of Resting Respiratory Drive and Timing in Healthy-Subjects." Journal of Applied Physiology **65**(1): 309-317.
Vicente, J., J. Pinto, J. Menezes and F. Gaspar (2013). "Fundamental analysis of particle formation in spray drying." Powder Technology **247**: 1-7.
Vinchurkar, S. and P. W. Longest (2008). "Evaluation of hexahedral, prismatic and hybrid mesh styles for simulating respiratory aerosol dynamics." Computers and Fluids **37**(3): 317-331.
Walenga, R. L., P. W. Longest, A. Kaviratna and M. Hindle (2017). "Aerosol drug delivery during noninvasive positive pressure ventilation: Effects of intersubject variability and excipient enhanced growth." Journal of Aerosol Medicine and Pulmonary Drug Delivery **30**(3): 190-205.
Walenga, R. L., G. Tian, M. Hindle, J. Yelverton, K. Dodson and P. W. Longest (2014). "Variability in nose-to-lung aerosol delivery." Journal of Aerosol Science **78**: 11-29.
Ward, J. J. (2013). "High-flow oxygen administration by nasal cannula for adult and perinatal patients." Respiratory Care **58**(1): 98-120.
Weers, J. G. and D. P. Miller (2015). "Formulation Design of Dry Powders for Inhalation." Journal of Pharmaceutical Sciences **104**(10): 3259-3288.
Wilcox, D. C. (1998). Turbulence Modeling for CFD, 2nd Ed. California, DCW Industries, Inc.
Zeman, K. L., J. Rojas Balcazar, F. Fuller, K. H. Donn, R. C. Boucher, W. D. Bennett and S. H. Donaldson (2017). "A trans-nasal aerosol delivery device for efficient pulmonary deposition." Journal of Aerosol Medicine and Pulmonary Drug Delivery **30**(4): 223-229.

This page intentionally left blank.